พิร์โรลิดินิลเพปไทด์นิวคลีอิกแอซิดที่มีตัวเชื่อมเป็นกรดบีตาอะมิโนที่มีออกซีเทน

นายภัทรเกียรติ แสนคงสุข

วิทยานิพนธ์นี้เป็นส่วนหนึ่งของการศึกษาตามหลักสูตรปริญญาวิทยาศาสตรมหาบัณฑิต
สาขาวิชาเคมี ภาควิชาเคมี
คณะวิทยาศาสตร์ จุฬาลงกรณ์มหาวิทยาลัย
ปีการศึกษา 2559

PYRROLIDINYL PEPTIDE NUCLEIC ACID WITH AN OXETANE-CONTAINING β-AMINO ACID LINKER

Mr. Pattarakiat Seankongsuk

A Thesis Submitted in Partial Fulfillment of the Requirements
for the Degree of Master of Science Program in Chemistry
Department of Chemistry
Faculty of Science
Chulalongkorn University
Academic Year 2016

Thesis Title	PYRROLIDINYL PEPTIDE NUCLEIC ACID WITH AN OXETANE-CONTAINING β-AMINO ACID LINKER
By	Mr. Pattarakiat Seankongsuk
Field of Study	Chemistry
Thesis Advisor	Professor Tirayut Vilaivan, D.Phil.
Thesis Co-Advisor	Assistant Professor Panuwat Padungros, Ph.D.

Accepted by the Faculty of Science, Chulalongkorn University in Partial Fulfillment of the Requirements for the Master's Degree

.....Dean of the Faculty of Science
(Associate Professor Polkit Sangvanich, Ph.D.)

THESIS COMMITTEE

.....Chairman
(Associate Professor Vudhichai Parasuk, Ph.D.)

.....Thesis Advisor
(Professor Tirayut Vilaivan, D.Phil.)

.....Thesis Co-Advisor
(Assistant Professor Panuwat Padungros, Ph.D.)

.....Examiner
(Associate Professor Voravee Hoven, Ph.D.)

.....External Examiner
(Assistant Professor Chaturong Suparpprom, Ph.D.)

ภัทรเกียรติ แสนคงสุข : พิร์โรลิดินิลเพปไทด์นิวคลีอิกแอซิดที่มีตัวเชื่อมเป็นกรดบีตาอะมิโนที่มีออกซีเทน (PYRROLIDINYL PEPTIDE NUCLEIC ACID WITH AN OXETANE-CONTAINING β-AMINO ACID LINKER) อ.ที่ปรึกษาวิทยานิพนธ์หลัก: ศ. ดร. ธีรยุทธ วิไลวัลย์, อ.ที่ปรึกษาวิทยานิพนธ์ร่วม: ผศ. ดร. ภาณุวัฒน์ ผดุงรส, หน้า.

เพปไทด์นิวคลีอิกแอซิด (PNA) เป็นสารเลียนแบบนิวคลีอิกแอซิดที่แสดงสมบัติการจับยึดได้อย่างดีเยี่ยมกับ DNA และ RNA คู่สม โดยการจับยึดระหว่าง PNA-DNA หรือ PNA-RNA มีความแข็งแรงสูงกว่าการจับยึดกันเองระหว่างกรดนิวคลีอิกในธรรมชาติด้วยกันเอง และมีความจำเพาะเจาะจงในการจับยึดเป็นไปตามกฎของวัตสัน-คริก เนื่องจากโครงสร้างของ PNA ที่เป็นเพปไทด์จึงทำให้ PNA มีสมบัติที่แตกต่างจากนิวคลีอิกในธรรมชาติซึ่งรวมไปถึงความเสถียรที่สูงทั้งในเชิงเคมีและชีวภาพ จากสมบัติที่กล่าวมาทั้งหมดทำให้มีการนำเอา PNA มาประยุกต์ใช้อย่างแพร่หลายทั้งในแง่ของการตรวจวินิจฉัย การรักษาโรค รวมทั้งการใช้งานทางด้านชีวภาพและวัสดุศาสตร์ ที่ผ่านมาได้มีการศึกษาเกี่ยวกับ PNA อย่างกว้างขวาง ในบรรดา PNA ชนิดใหม่เหล่านี้ พิร์โรลิดินิลเพปไทด์นิวคลีอิกแอซิดซึ่งเป็นพีเอ็นเอที่มีคอนฟอร์เมชั่นถูกจำกัด โดยมีโครงสร้างหลักเป็นเพปไทด์ที่ประกอบไปด้วยองค์ประกอบสำคัญ 2 ส่วน คือ โพรลีนที่ถูกดัดแปรด้วยนิวคลีโอเบส กับไซคลิกบีตาอะมิโนแอซิดเช่น (1*S*,2*S*)-2-aminocyclopentanecarboxylic acid (acpc) เป็น PNA ระบบหนึ่งที่โดดเด่น เนื่องจากแสดงการจับยึดกับ DNA คู่สมได้มีเสถียรภาพและความจำเพาะเจาะจงในการจับยึดกับดีเอ็นเอที่สูงกว่า PNA ต้นแบบ และการเปลี่ยนส่วนของ 2-aminocyclopentanecarboxylic acid ไปเป็น (1*S*,2*S*)-2-aminocyclobutanecarboxylic acid (acbc) จะทำให้ได้ acbcPNA ซึ่งมีเสถียรภาพในการจับยึดกับ DNA สูงยิ่งขึ้นไปอีก ในงานวิจัยนี้จึงเสนอ PNA ชนิดใหม่ที่อาศัยโครงสร้างหลักของ acbcPNA โดยมีการแทนที่เมทิลีนคาร์บอนในวงแหวนไซโคบิวเทนด้วยออกซิเจนอะตอม เกิดเป็นพิร์โรลิดินิลพีเอ็นเอที่มีออกซีเทนในโครงสร้างหลัก เพื่อเพิ่มการละลายน้ำของ PNA และลดความไม่จำเพาะเจาะจงในการจับยึดกับโมเลกุลไม่ชอบน้ำ โดยคาดหมายว่าจะไม่ส่งผลกระทบต่อความสามารถในการจับยึดกับ DNA ทั้งในแง่เสถียรภาพและความจำเพาะเจาะจง ในการสังเคราะห์ PNA ชนิดใหม่ จำเป็นต้องพัฒนาวิธีการสังเคราะห์ *N*-Fmoc-protected (2*S*,3*S*)-3-aminooxetane-2-carboxylic acid [Fmoc-(2*S*,3*S*)-*epi*-oxetin] ซึ่งเป็นองค์ประกอบหลักสำคัญ โมเลกุลเป้าหมายนี้สามารถเตรียมได้ผ่านปฏิกิริยาทั้งหมด 11 ขั้นตอน โดยเริ่มต้นจาก (*Z*)-but-2-ene-1,4-diol ที่มีปฏิกิริยา Jorgensen organocatalytic epoxidation เป็นปฏิกิริยาสำคัญในการกำหนดสเตอริโอเคมีบนสารเป้าหมายซึ่งขั้นนี้ได้เคร้ลอิพอกไซด์ที่มี %ee สูงถึง 91-95% จากนั้นจึงสร้างวงออกซีเทนโดยการเปิดวงอีพอกไซด์แบบเลือกจำเพาะด้วยเอไซด์ ตามด้วยการทำโทซิลเลชั่นแบบเลือกจำเพาะ และการปิดวงภายใต้สภาวะที่เป็นเบส ขั้นตอนที่เหลือเป็นการปรับเปลี่ยนหมู่ฟังก์ชันและหมู่ปกป้องจนได้สารเป้าหมายสามารถคิดร้อยละผลผลิตได้เป็น 5.1% โดยที่สารเป้าหมายมี %ee สูงถึง 94% สารประกอบออกซีเทนอะมิโนแอซิดและพิร์โรลิดินิลพีเอ็นเอโมโนเมอร์ถูกใช้ในการสังเคราะห์ aocPNA ที่มีลำดับเบสเป็น GTAGATCACT ด้วยวิธีการสังเคราะห์บนวัฏภาคของแข็งโดยอาศัยหมู่ปกป้อง Fmoc อย่างไรก็ตามการสังเคราะห์ aocPNA มีความท้าทายเนื่องจากเกิดการสลายตัวของ aocPNA ภายใต้สภาวะที่เป็นเบสและกรดซึ่งใช้ในการปลดหมู่ปกป้องออกจากนิวคลีโอเบสและปลด aocPNA ออกจากวัฏภาคของแข็ง จากการติดตามด้วยเทคนิคแมสสเปกโทรเมทรีและ NMR ของแบบจำลองของออกซีเทนเพปไทด์เสนอแนะว่าการสลายตัวในสภาวะที่เป็นกรดเริ่มจากการเปิดวงออกซีเทนและจึงเกิดการแตกออกของพันธะเอไมด์ที่เชื่อมต่อระหว่างวงออกซีเทนและวงโพรลีน หลังจากการปรับสภาวะที่เหมาะสมในการปลดหมู่ปกป้องและปลด aocPNA ออกจากวัฏภาคของแข็งสามารถสังเคราะห์ aocPNA ได้สำเร็จแม้จะมีร้อยละผลได้ค่อนข้างต่ำ (1.2-1.3%) นอกจากนี้ aocPNA แสดงความสามารถในการจับยึดกับ DNA และ RNA คู่สมอย่างจำเพาะเจาะจงได้ แม้ว่าจะมีประสิทธิภาพในการจับยึดที่ด้อยกว่า acbcPNA และพิร์โรลิดินิลพีเอ็นเอชนิดอื่นๆ จากการคำนวณทางคอมพิวเตอร์เสนอแนะคำอธิบายว่าเกิดจากการที่มุมทอร์ชันนัลระหว่างหมู่คาร์บอนิลและเอไมด์บนวงออกซีเทนแตกต่างจากมุมทอร์ชันนัลที่เหมาะสมในการจับยึดระหว่างสายของ PNA กับ DNA ค่อนข้างมาก

ภาควิชา เคมี	ลายมือชื่อนิสิต .....
สาขาวิชา เคมี	ลายมือชื่อ อ.ที่ปรึกษาหลัก .....
ปีการศึกษา 2559	ลายมือชื่อ อ.ที่ปรึกษาร่วม .....

5772096123 : MAJOR CHEMISTRY

KEYWORDS: PEPTIDE NUCLEIC ACID (PNA) / DNA RECOGNITION / FOLDAMERS / OXETANE / AMINO ACIDS

PATTARAKIAT SEANKONGSUK: PYRROLIDINYL PEPTIDE NUCLEIC ACID WITH AN OXETANE-CONTAINING β-AMINO ACID LINKER. ADVISOR: PROF. TIRAYUT VILAIVAN, D.Phil., CO-ADVISOR: ASST. PROF. PANUWAT PADUNGROS, Ph.D., pp.

Peptide Nucleic Acid (PNA) is a nucleic acid mimic that exhibits excellent binding properties with complementary DNA and RNA. The PNA-DNA or PNA-RNA binding is stronger than the self-binding between natural nucleic acids, although the Watson-Crick base pairing is still strictly obeyed. The peptide-like structure of PNA contributed to its several distinct properties from natural nucleic acids including the higher chemical and biological stability. These aforementioned properties makes PNA useful in several applications such as diagnosis, therapeutic and other purposes such as tools in biological and materials sciences. Several variants of PNA is known to date. Among these, the conformationally constrained pyrrolidinyl peptide nucleic acid containing a dipeptide backbone derived from nucleobase-modified proline and a cyclic β-amino acid such as (1*S*,2*S*)-2-aminocyclopentanecarboxylic acid (acpc) is a notable PNA system since it show even higher binding affinity and sequence specificity to complementary DNA when compared to the original PNA. Changing the 2-aminocyclopentanecarboxylic acid spacer to (1*S*,2*S*)-2-aminocyclobutanecarboxylic acid (acbc) increased the DNA binding affinity of the resulting acbcPNA even further. Here in, a novel PNA was proposed based on the structure of acbcPNA by replacement of a methylene carbon atom in the cyclobutane ring with an oxygen atom to become an oxetane-containing pyrrolidinyl PNA in order to improve the solubility and reduce non-specific binding, without compromising the binding affinity and specificity. Towards this goal, there is a need to develop an efficient synthetic method for *N*-Fmoc-protected (2*S*,3*S*)-3-aminooxetane-2-carboxylic acid [Fmoc-(2*S*,3*S*)-*epi*-oxetin] required as a key building block. The compound was prepared via a 11 step-sequence reaction starting from the commercially available (*Z*)-but-2-ene-1,4-diol. A key reaction to introduce stereochemistry on target molecule is Jorgensen organocatalytic epoxidation to generate a chiral epoxide in 91-95% ee. The oxetane ring was formed following regioselective epoxide ring opening with azide, selective monotosylation and cyclization under basic conditions. The remaining steps involve functional group interconversion and protecting group manipulation, which afforded the desired target in 5.1% overall yield with 94% ee. The oxetane amino acid and pyrrolidinyl PNA monomers were used for synthesis of aocPNA carrying a GTAGATCACT sequence *via* Fmoc solid phase peptide synthesis (Fmoc-SPSS). The synthesis of aocPNA posed some unexpected challenges since it is susceptible to degradation under basic and acidic conditions, which is required for nucleobase deprotection and cleavage of aocPNA from the solid support. Based on mass spectrometry data and model NMR experiments, the decomposition under acidic conditions most likely began with hydrolysis of oxetane following by fragmentation of the amide bond connecting the oxetane and the proline moieties. Even if the nucleobase deprotection and cleavage conditions were carefully optimized, aocPNAs were obtain in low isolated yield (1.2-1.3%). In addition, aocPNA exhibits DNA and RNA binding capability in sequence specific fashion. However, the binding affinity was lower than acbcPNA and other pyrrolidinyl PNAs. Computational calculation suggested that the torsional angle between carbonyl and amide substituents on the oxetane amino acid is substantially different from the optimal value required for the PNA-DNA duplex.

Department: Chemistry	Student's Signature .....
Field of Study: Chemistry	Advisor's Signature .....
Academic Year: 2016	Co-Advisor's Signature .....

ACKNOWLEDGEMENTS

Firstly, I would like to sincerely thank and express my deepest gratitude to my advisor Professor Dr.Tirayut Vilaivan and co-advisor Assistant Professor Dr. Panuwat Padungros for their supervision, not only on my research but also for integrative knowledge and being influential on my logical and critical thinking skills. Their guidance and encouragement helped me understanding and solving problems on my research topic and writing this thesis. I am also grateful to thesis examiners: Associate Professor Dr. Vudhichai Parasuk, Associate Professor Dr. Voravee Hoven and Assistant Professor Dr. Chaturong Suparpprom for their valuable comments and suggestions. Moreover, I would like to express my thankfulness to National Science and Technology Development Agency (NSTDA) for the financial support of my study and research through the Junior Science Talent Project (JSTP) research grant (JSTP-06-57-06E). I am also grateful to Graduate School, Chulalongkorn University for the Overseas Research Experience Scholarship for Graduate Student for providing me the opportunity to have research experience abroad at Division of Chemistry and Biological Chemistry (CBC), School of Physical and Mathematical Sciences (SPMS), Nanyang Technological University (NTU) under guidance of Associate Professor Roderick Wayland Bates. During the 4 month research internship period at NTU, I have learned a lot of things. I would also like to thank Associate Professor Dr. Viwat Vchirawongkwin for the help with computational simulation. In addition, I would like to thank members of TV research group and my friends for their stimulating discussion, friendship and advices. Finally, I am deeply indebted to my family for moral supports throughout the research and my life in general.

CONTENTS

Page

Page

Page

Page

List of Figures

List of Tables

List of Abbreviations and Symbols

$[\alpha]_D$	specific rotation
2,4-DNP	2,4-dinitrophenylhydrazine
2-ADP	2-aminoethyl diphenylborinate
A	adenine
Abq	AB quartet
Ac	acetyl
acbc	2-aminocyclobutanecarboxylic acid
acbcPNA	pyrrolidinyl PNA with 2-aminocyclobutanecarboxylic acid spacer
achcPNA	pyrrolidinyl PNA with 2-aminocyclohexanecarboxylic acid spacer
AcOH	acetic acid
acpc	2-aminocyclopentanecarboxylic acid
acpcPNA	pyrrolidinyl PNA with 2-aminocyclopentanecarboxylic acid spacer
aeg	*N*-2-aminoethylglycine
aegPNA	*N*-2-aminoethylglycyl PNA
aocPNA	pyrrolidinyl PNA with (2*S*,3*S*)-3-aminooxetane-2-carboxylic acid spacer
atfcPNA	pyrrolidinyl PNA with 3-aminotetrahydrofuran-2-carboxylic acid spacer
ATR	attenuated total reflection
Bn	benzyl
Boc	*tert*-butoxycarbonyl
Boc_2O	di-*tert*-butyl dicarbonate

BOP	benzotriazol-1-yloxy tris(dimethylamino)phosphonium hexafluorophosphate
br	broad signal
Bz	benzoyl
c	concentration
C	cytosine
Cbz	carbobenzyloxy
CCA	α-cyano-4-hydroxycinnamic acid
δ	chemical shift
d	doublet
DAIB	diacetoxy iodobenzene
DBU	1,8-diazabicycloundec-7-ene
Dcom	complementary DNA
dd	doublet of doublet
DIBAL-H	diisobutylaluminum hydride
DIEA	*N*,*N*-diisopropylethylamine
DMAP	4-dimethylaminopyridine
DMDO	dimethyldioxirane
DMF	*N*,*N*-dimethylformamide
DMSO	dimethylsulfoxide
DMSO-d_6	deuterated dimethylsulfoxide
DNA	deoxyribonucleic acid
DsmC	DNA with single mismatch C
DsmG	DNA with single mismatch G
DsmT	DNA with single mismatch T
dt	doublet of triplet
ε	extinction coefficient

EDTA	ethylenediaminetetraacetic acid
equiv.	equivalent
ESI	electrospray ionization
Fmoc	9-fluorenylmethoxycarbonyl
FmocOSu	*N*-(9-fluorenylmethoxycarbonyloxy) succinimide
Fmoc-SPPS	Fmoc solid phase peptide synthesis
G	guanine
HATU	*O*-(7-azabenzotriazol-1-yl)-*N*,*N*,*N*',*N*'-tetramethyluronium hexafluorophosphate
HOAt	1-hydroxy-7-azabenzotriazole
HPLC	high performance liquid chromatography
Ibu	isobutyryl
J	coupling constant
m	multiplet
m/z	mass-to-charge ratio
MALDI-TOF	matrix assisted laser desorption ionization-time of flight
mCPBA	*meta*-chloroperoxybenzoic acid
MD	molecular dynamics
MeCN	acetonitrile
MS	mass spectrometry
NGP	neighboring group participation
ν_{max}	maximum frequency
NMR	nuclear magnetic resonance
O/N	overnight
OD	optical density
PCC	pyridinium chlorochromate
Pfp	pentafluorophenyl

Piv	pivaloyl
PNA	peptide nucleic acid or polyamide nucleic acid
ppm	part per million
q	quartet
Rcom	complementary RNA
Red-Al	sodium bis(2-methoxyethoxy)aluminumhydride
R_f	retention factor
RNA	ribonucleic acid
rt	room temperature
s	singlet
T	thymine
TBAHS	tetrabutyl ammonium hydrogen sulfate
TBHP	*tert*-butylhydroperoxide
TEA	triethylamine
Temp	temperature
TEMPO	(2,2,6,6-tetramethylpiperidine-1-yl)oxyl
TFA	trifluoroacetic acid
THF	tetrahydrofuran
TIPS	triisopropylsilane
TLC	thin layer chromatography
T_m	melting temperature
TMS	trimethylsilyl
t_R	retention time
Tr	trityl
Ts	*para*-toluenesulfonyl
UV	ultraviolet
UV-vis	ultraviolet-visible

Chapter 1

Introduction

1.1. Peptide Nucleic Acid (PNA)

Peptide nucleic acid (PNA) was first introduced as nucleic acid mimic in 1900s by Nielsen's research group.[1] The deoxyribose phosphate backbone of natural DNA is replaced by *N*-2-aminoethylglycine (aeg) backbone in PNA. Thus the seminal PNA designed by Nielsen and coworkers is now commonly referred to as aegPNA (Figure 1.1).

PNA shows strong binding affinity with DNA/RNA and also bind with natural nucleic acids according to the Watson-Crick base pairing rules. The higher stability between DNA-PNA duplex arises from the absence of negative charge on the polyamide backbone of PNA. This leads to no electrical repulsion between PNA and DNA/RNA strands in hybrid form, compared to negative charge repulsion of phosphate group in the case of double strands DNA. Despite the increased duplex stability, the mismatch discrimination in DNA or RNA targeted by PNA is significantly better than either DNA or RNA. Moreover, the unnatural polyamide structure of PNA offers additional advantages in term of chemical and enzymatic stabilities towards proteases and nucleases.[1-2] From these aforementioned characteristics, PNA has been applied in various practical uses especially diagnostic and clinical purposes including application of biotechnology and material science.[3-4]

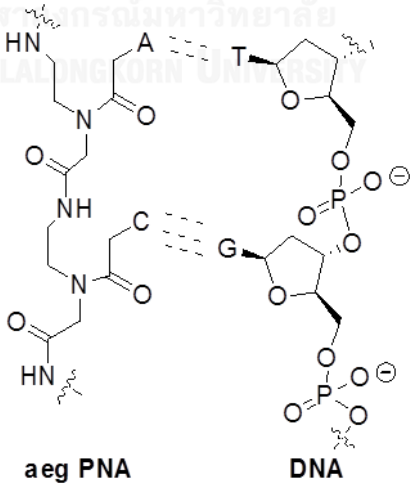

Figure 1.1 Binding between aegPNA and natural DNA according to Watson-Crick base pairing rules

Since early 2000s, Vilaivan and coworkers has been developing novel conformationally constrained PNA systems, namely pyrrolidinyl PNAs (Figure 1.2). This pyrrolidinyl PNAs basic skeleton comprises of nucleobase-modified proline amino acid and cyclic β-amino acid, which acts as a spacer between nucleobase moieties in analogous way to the phosphate group in DNA/RNA. Vilaivan's research group has systematically studied the effect of stereochemistry of the pyrrolidine ring, as well as stereochemistry and ring-size of the cyclic β-amino acid spacers toward DNA binding properties of pyrrolidinyl PNAs and found that they play crucial roles. With (1*S*,2*S*)-2-aminocyclopentane carboxylic acid (acpc) spacer, only (2'*R*,4'*R*) and (2'*R*,4'*S*) isomers of acpcPNA can bind to DNA. Next, the stereochemistry of the pyrrolidine ring was fixed as (2'*R*,4'*R*), and the spacer part was varied, with different ring-size including four-, five-, and six-membered ring while the stereochemistry of the spacer was fixed as (1*S*,2*S*), resulting in acbcPNA, acpcPNA, and achcPNA respectively.[5-7]

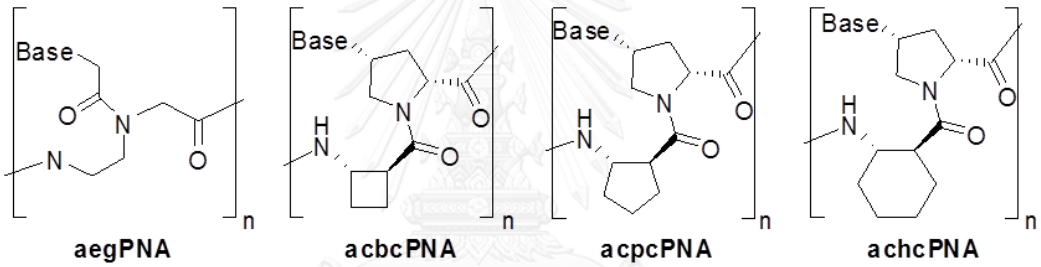

aegPNA : *N*-(2-aminoethyl)glycine PNA

acbcPNA : pyrrolidinyl PNA with (1*S*,2*S*)-2-aminocyclobutanecarboxylic acid spacer

acpcPNA : pyrrolidinyl PNA with (1*S*,2*S*)-2-aminocyclopentanecarboxylic acid spacer

achcPNA : pyrrolidinyl PNA with (1*S*,2*S*)-2-aminocyclohexanecarboxylic acid spacer

Figure 1.2 Structure of the original aegPNA and conformationally constrained pyrrolidinyl PNAs

A representative of PNA in this class is acpcPNA, which carries (1*S*,2*S*)-2-aminocyclopentane carboxylic acid as spacer. It exhibits greater affinity and sequence specificity in binding to DNA than the original aegPNA. This could attribute to the conformational restriction in the pyrrolidinyl PNA structures, which resulted in limitation of conformational flexibility. Thus upon binding with DNA, the pyrrolidinyl PNAs experience less entropic lost due to the conformational change from single-stranded PNA to PNA-DNA duplex. Furthermore, acpcPNA binds to DNA only in antiparallel orientation like natural DNA. Enhancement of DNA binding affinity with retention of specificity was observed with the four-membered ring spacer (acbcPNA) when compared to acpcPNA. By contrast, achcPNA carrying a six-membered ring spacer totally lost its DNA binding ability. In-depth analysis by computational calculation of structures of

pyrrolidinyl PNA-DNA duplexes suggested that the optimal torsional angle between the amino and carboxyl groups of the spacer should be close to 99°. The native torsional angle of achc oligomers is approximately 60° based on crystallographic data, which is largely different to the calculation value. On the other hand, the torsional angle of acbc oligomers is 95°, which is closer to the optimal value than that of acpc oligomers as shown in Figure 1.3. This explains why acbcPNA exhibits the highest binding affinity to DNA comparing to other prrolidinyl PNAs.[8]

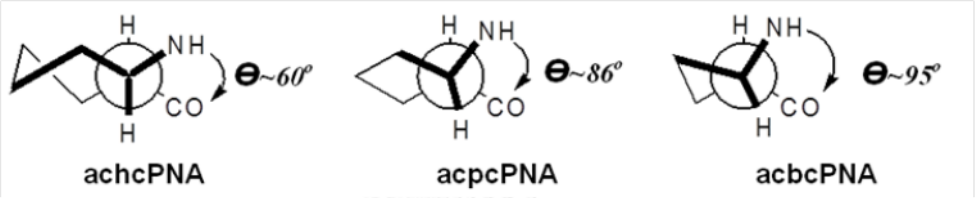

Figure 1.3 Torsional angle of achcPNA, acpcPNA and acbcPNA[8]

Despite great potential applications of PNAs, their practical uses are still limited due to poor water solubility and non-specific interaction to hydrophobic materials. To overcome this obstacle, Ly and coworkers demonstrated the synthesis of hydrophilic PNA, namely $^{R\text{-}MP}\gamma$PNA as shown in Figure 1.4. The addition of polar diethylene glycol unit to the backbone of the original aegPNA improves water solubility of PNA and also reduces non-specific interaction to non-targeted DNA, while the DNA binding affinity and specificity remained the same.[9]

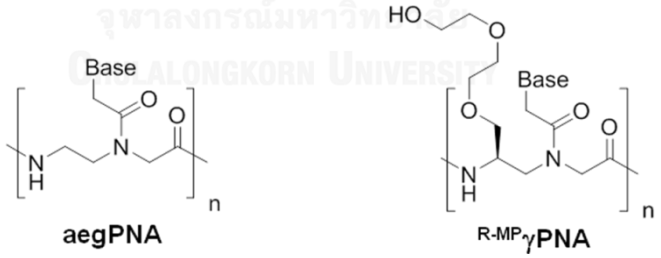

Figure 1.4 Comparison between structure of the original aegPNA and $^{R\text{-}MP}\gamma$PNA by Ly and coworkers[9]

In an attempt to increase hydrophilicity of acpcPNA, pyrrolidinyl PNA with 3-aminotetrahydrofuran-2-carboxylic acid spacer (atfcPNA, Figure 1.5) was recently introduced. The spacer was modified from acpcPNA by replacing a methylene group in the cyclopentane ring with an oxygen atom to form a tetrahydrofuran ring. However, atfcPNA exhibits only marginal improvement in solubility while the binding affinity and sequence specificity towards DNA and RNA binding are essentially the same as acpcPNA.[10]

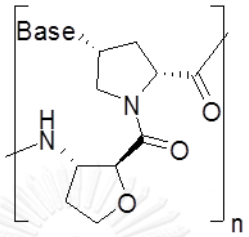

Figure 1.5 Structure of pyrrolidinyl PNA with (1*S*,2*S*)-3-aminotetrahydrofuran-2-carboxylic acid spacer (atfcPNA)

In this research, we are interested in development of a novel conformationally constrained pyrrolidinyl PNA by replacing the cyclobutane ring of acbcPNA with an oxetane ring in order to increase hydrophilicity of the resulting PNA (Figure 1.6). In order to compare the effect from core structure of spacer, in this work, the novel PNA has designed to retain stereochemistry on PNA structure like acbcPNA, acpcPNA and atfaPNA.[8, 10] Due to the structural similarity with acbcPNA, we expect that aocPNA will maintain strong binding affinity and sequence specificity towards DNA and RNA. In addition, the presence of the oxetane ring should increase water solubility, which is beneficial for PNA study that required high sample concentration such as NMR spectroscopy.

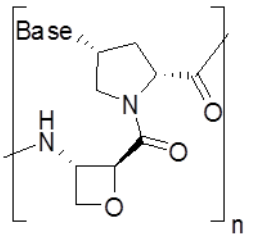

Figure 1.6 Structure of aocPNA, which is the target molecule of this research

1.2. *trans*-3-Amino-oxetane-2-carboxylic acid (*epi*-oxetin)

The structure of PNA was divided into 2 parts including nucleobases-modified D-proline and a cyclic β-amino acid containing oxetane ring. The *trans*-3-amino-oxetane-2-carboxylic acid is naturally occurring and is known as *epi*-oxetin.[11] Since the chemistry of the nucleobases-modified D-proline has already been solved in previous other works,[12] only the oxetane amino acid moiety is the synthetic focus in the present work. The aocPNA will be synthesized *via* Fmoc solid phase peptide synthesis (Fmoc-SPPS). The precursor required is therefore the Fmoc-protected *epi*-oxetin monomer with (2*S*,3*S*) configuration (Figure 1.7).

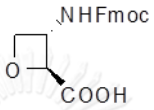

Figure 1.7 Structure of Fmoc-protected (2*S*,3*S*)-*epi*-oxetin required as the key building block for aocPNA

In 1997, Bach and coworkers reported a synthesis of oxetin by a 4-step reaction sequence that provided a mixture of racemic of *cis*-oxetin (**6c** and **6d**) in up to 14% yield (Figure 1.8).[11] Photocycloaddition between butyl glyoxylate (**1**) and Boc-protected enamine **2** yielded racemic mixture of **3a** and **3b**.[11] Subsequent debenzylation by catalytic hydrogenolysis in the presence of Pd/C afforded racemic **4a** and **4b**.[11] Acid treatment of Boc-protected **4a** and **4b** followed by saponification of the ester provided racemic oxetin **6c** and **6d** in good yield.[11] Bach's strategy presents a concise method to prepare oxetin within only 4 steps and relatively high overall yield. However, the obvious drawbacks are the *cis*-oxetin selectivity of the reaction, and the low yield of the photocycloaddition step, thus this is not a method of choice for synthesis of enantiomerically pure *epi*-oxetin.[11]

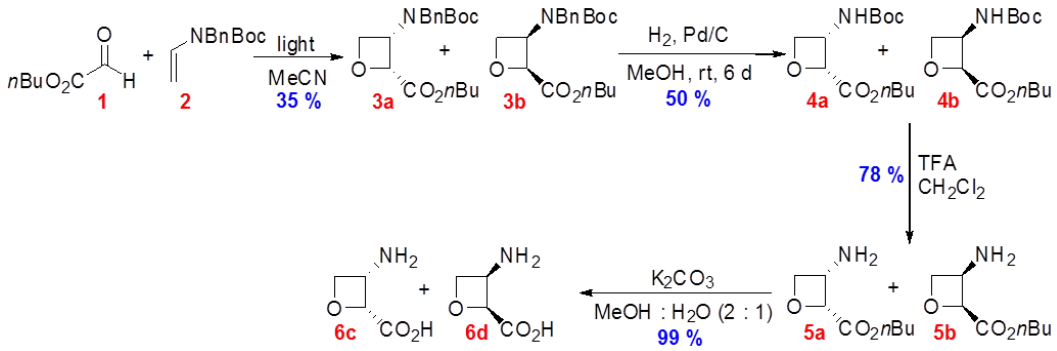

Figure 1.8 Synthesis of racemic oxetin **6a** และ **6b** starting from **1** and **2** by Batch and coworkers

In 1984, Ōmura and coworkers reported the isolation of (2*R*,3*S*) oxetin (**6c**) from Streptomyces sp. OM-2317. It exhibits potent anti-biotic properties to Bacillus subtilis and Piricularia oryzae. All four possible stereoisomers of oxetin were later synthesized by Ōmura's group in order to study their structure-activity relationship.[13] The Ōmura's 15-step synthesis of (2*S*,3*S*)-*epi*-oxetin starting from D-glucose afforded (2*S*,3*S*)-*epi*-oxetin in 1.2% overall yield. Selective protection of D-glucose **7** with acetone using sulfuric acid as a catalyst was performed to give **8** followed by benzylation of the remaining hydroxyl group with benzyl bromide to yield **9**.[14] Selective deprotection of one of the acetonide group under mildly acidic condition furnished diol **10**, which was subjected to oxidative cleavage with sodium metaperiodate to provide aldehyde intermediate **11** [13] as shown in Figure 1.9.

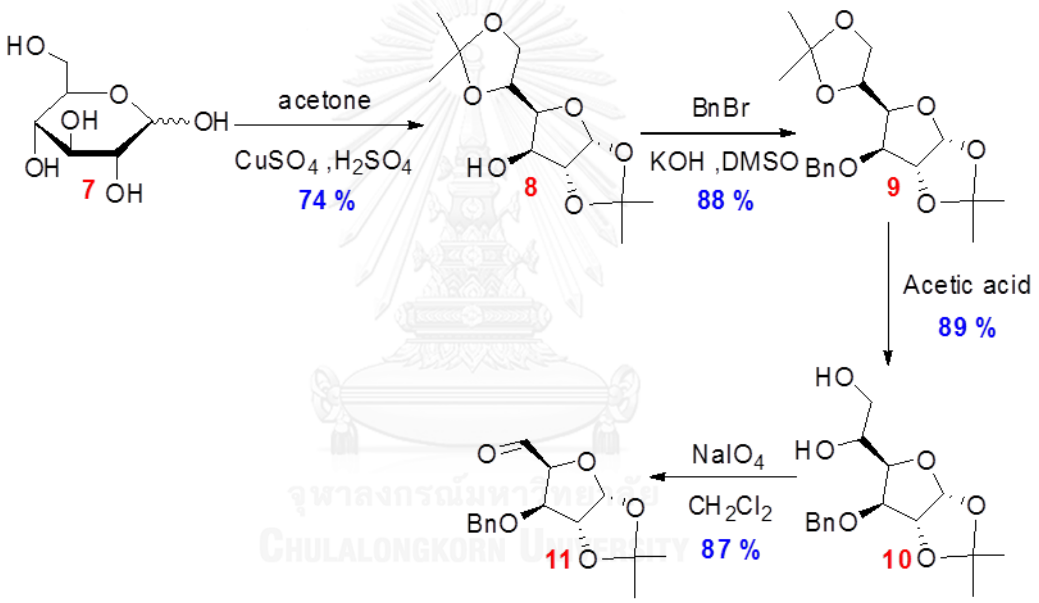

Figure 1.9 Synthesis of aldehyde intermediate **11** from D-glucose **7**

Wittig reaction between aldehyde **11** and a stabilized phosphorus ylide **12** generated a mixture of *cis*- and *trans*-olefinic ester **13** and **14** in 11:9 ratio. By column chromatography, these two geometrical isomers were separated. Subsequent reduction of the ester group of **14** with diisobutylaluminum hydride (DIBAL-H) yielded *trans*-allylic alcohol **15**. The intermediate **15** was added to epoxidation by mCPBA to produce a mixture of epoxyalcohols **16a** and **16b** in 3:1 ratio. The two diastereomers were separable by column chromatography. Thus, the intermediate **16a** was isolated and treated with sodium azide (NaN_3) to open the epoxide ring yielding the azide intermediate **17** [13] as shown in Figure 1.10.

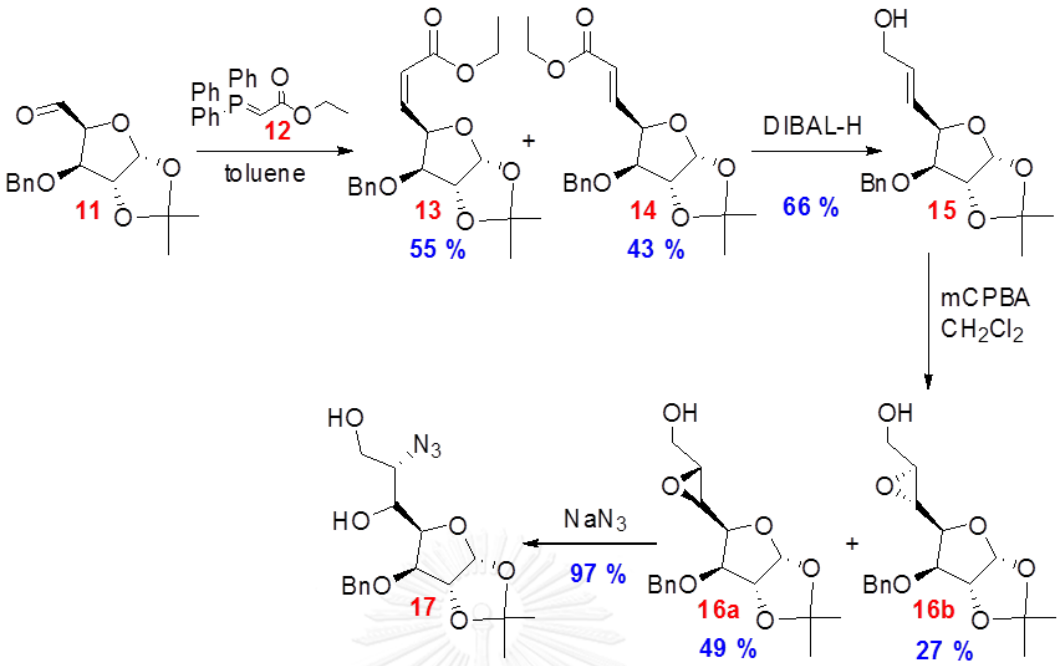

Figure 1.10 Synthesis of **17** from **11**

Key steps for the installation of the oxetane ring in the intermediate **19** involve selective activation of the primary alcohol followed by cyclization (Figure 1.11). First, the primary alcohol of **17** was activated with *p*-toluenesulfonyl chloride (TsCl) to give **18**, which underwent cyclization in the presence of potassium *tert*-butoxide (^{t}BuOK) to form the oxetane ring. Finally, functional group interconvesion of azide **19** by hydrogenation, followed by protection with benzyl chloroformate gave the intermediate **20** which was eventually deprotected to obtain **21** [13] as shown in Figure 1.11.

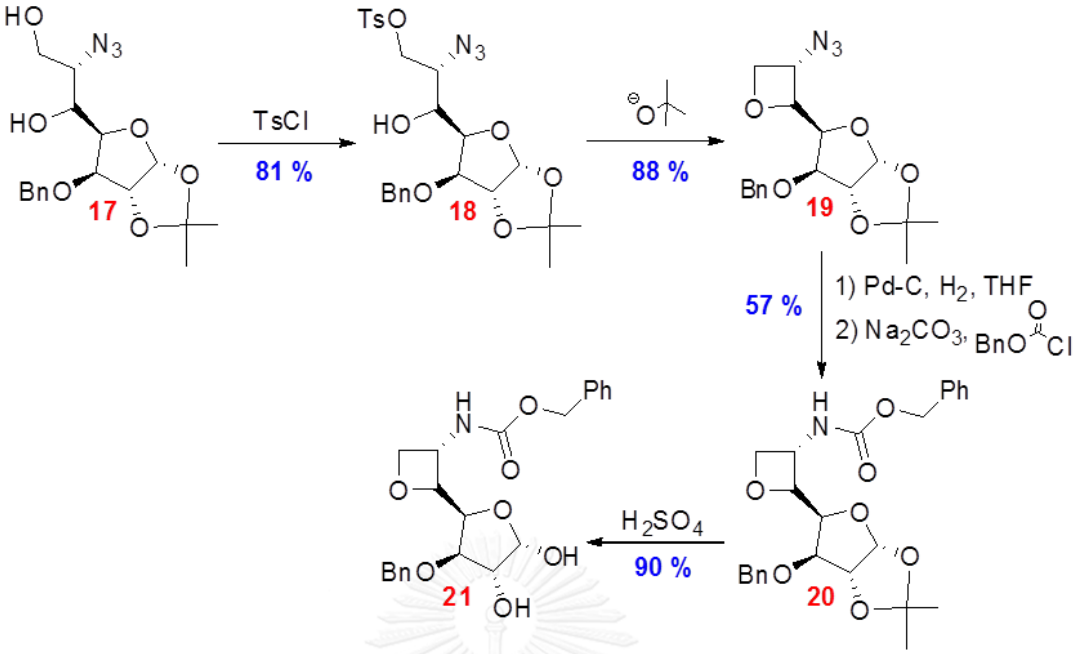

Figure 1.11 Synthesis of **21** from **17**

Next, the intermediate **21** was reduced with sodium borohydride ($NaBH_4$) to generate tetraol **22**, which was subjected to an oxidative cleavage to yield protected-*epi*-oxetin **23**. Finally, deprotection of the benzyloxycarbonyl (Cbz) group under hydrogenation produced the desired (2*S*,3*S*)-*epi*-oxetin (**6a**)[13] as shown in Figure 1.12.

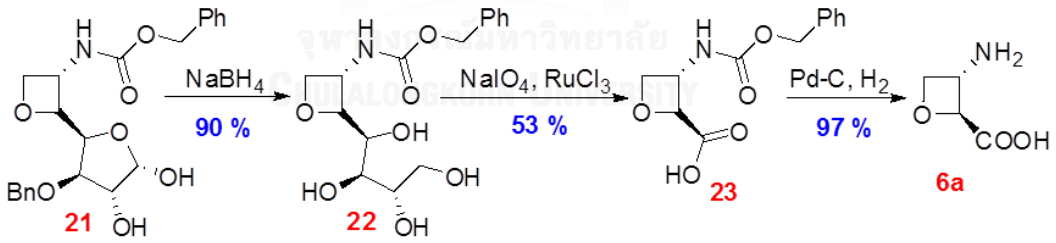

Figure 1.12 Synthesis of **6a** from **21**

A more recent synthesis of (2*S*,3*S*)-*epi*-oxetin (**6a**) was also reported by Blauvelt and Howell in 2008 (Figure 1.13).[15] Trityl protection of L-serine **24** precursor to **25** was carried out and followed by lactonization using benzotriazol-1-yloxy tris(dimethylamino)phosphonium hexafluorophosphate (BOP) as a coupling reagent to generate lactone **26**. Then, methylenation of **26** with dimethyltitanocene (Cp_2TiMe_2) gave the oxetane intermediate **27**, which was epoxidized by dimethyldioxirane (DMDO) to obtain diastereomeric epoxides **28a**:**28b** in 2:1 ratio.

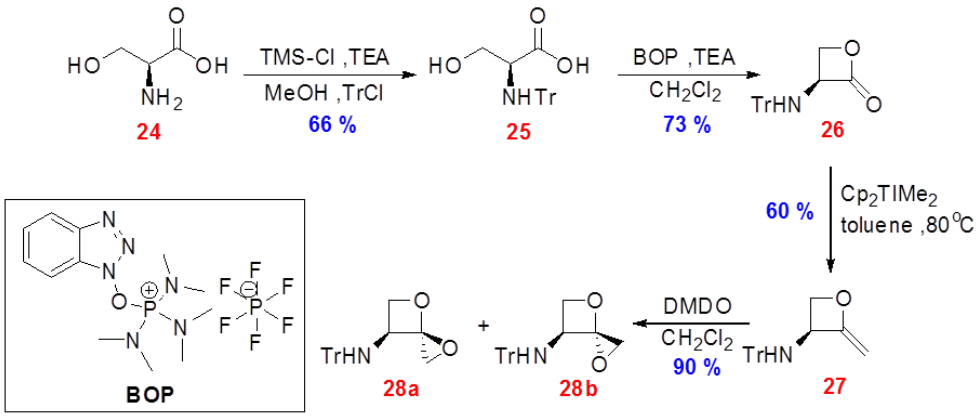

Figure 1.13 Synthesis of diastereomeric mixture between **28a** and **28b** from L-serine **24**

The diastereomeric mixture of epoxide **28a** and **28b** was reduced to the corresponding alcohols with DIBAL-H at -78 °C. Successful separation of alcohol **29a** and **29b** was achieved at this step and provided enantiopure **29a** in 48% yield. The remaining steps were straightforward functional group manipulation, beginning with acylation with acetic anhydride (Ac_2O) and switching the trityl protecting group to *tert*-butyloxycarbonyl (Boc) protection to generate **31a**. Deacetylation of **31a** to obtain **32a** followed by oxidation afforded the carboxylic acid **33a**. Finally, Boc deprotection of **33a** by TFA treatment resulted in (2*S*,3*S*)-*epi*-oxetin (**6a**)[15] as shown in Figure 1.14.

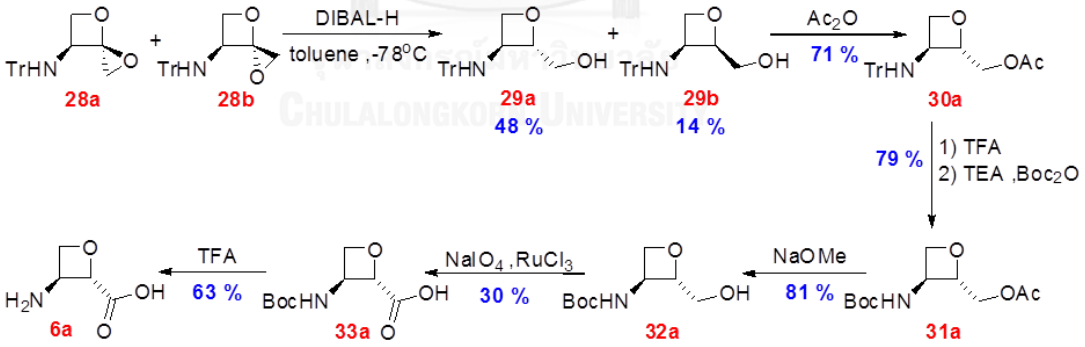

Figure 1.14 Synthesis of **6a** from diastereomeric mixture between **28a** and **28b**

Very recently, Aitken and coworkers adopted Bach's procedure to synthesize all four stereoisomers of oxetin *via* a 5 step reaction sequence.[16] The photocycloaddition between **1** and **34** provided mixture of four stereoisomers **35a**, **35b**, **35c** and **35d** which could be separated into *cis*- and *trans*-isomers as racemic mixture. The *trans*-racemate **35c** and **35d** was *N*-formylated and hydrolyzed to give the racemic amino acid **33**. Chiral auxiliary **36** was installed to provide the diastereomeric mixture of **37a** and **37b** which were chromatographically separated. After

hydrolysis, pure enantiomer of Boc-protected (2*S*,3*S*)-*epi*-oxetin **33a** was obtained. Lastly, Boc deprotection provided *epi*-oxetin **6a** in almost quantitative yield as shown in Figure 1.15.

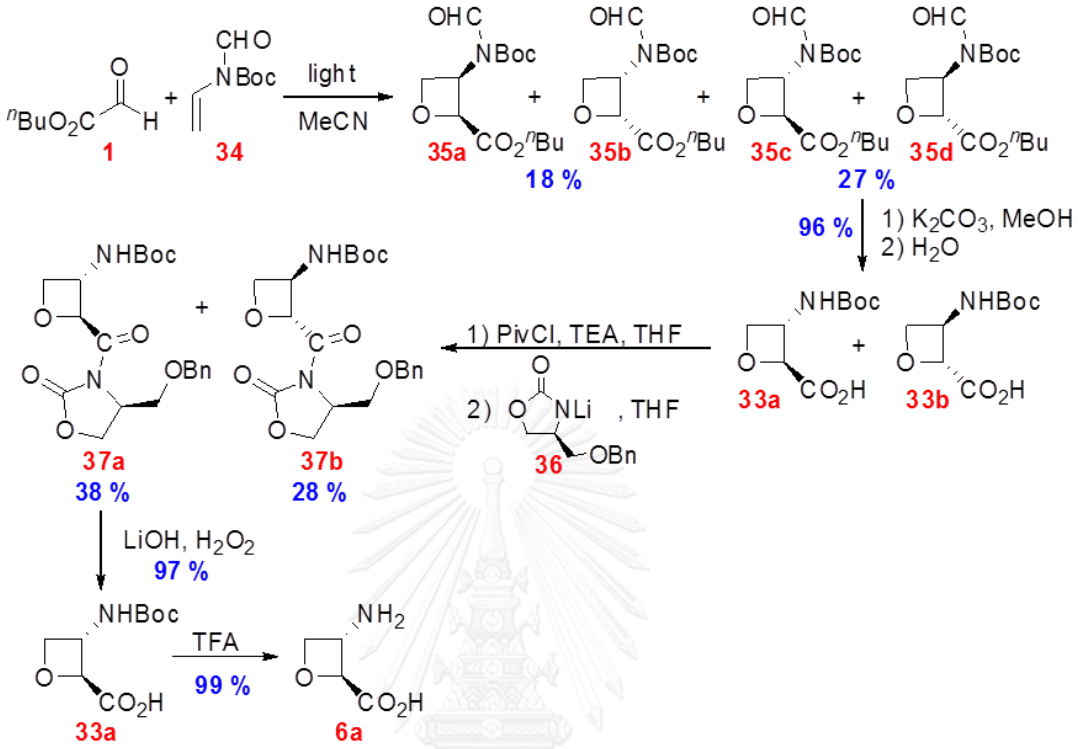

Figure 1.15 Synthesis of (2*S*,3*S*)-*epi*-oxetin (**6a**) from compound **1** and **34**

The disadvantage of Bach and Aitken syntheses is that the reaction is non-stereoselective and all stereoisomers are generated and required tedious separation. For Blauvelt and Howell's procedure, apart from low overall yield, their synthetic strategy depends on highly reactive and costly reagents such as DIBAL-H and Cp_2TiMe_2. Moreover, the DMDO epoxidation of **27** also provided diastereomeric mixture of **28a** and **28b**. While Ōmura's route is considerably long synthetic scheme comprises of 15-step reaction sequence, however, this synthetic strategy uses common reagents and reactions that are more simple to carry out such as Wittig olefination, epoxidation, and oxidative cleavage.

To find a more practical route to synthesize Fmoc-protected (2*S*,3*S*)-*epi*-oxetin, we proposed a concise approach to synthesize Fmoc-protected (2*S*,3*S*)-*epi*-oxetin following Omura's approach,[13] but the number of reaction has shortened by replacing the glucose-derived epoxide **16a** (Figure 1.15) with a more simple chiral epoxide (**50a**) obtained by asymmetric epoxidation. Regioselective ring opening of epoxide **50a** with nitrogen nucleophile following cyclization should generate the desired oxetane core structure **53a**. After that a few steps of functional group conversion should gain desired Fmoc-protected (2*S*,3*S*)-*epi*-oxetin **55a**. This synthetic method is

expected to reduce complexity from multiple steps reaction of Ōmura[13] and difficulty of sensitive reaction of Blauvelt and Howell,[15] as well as to provide only the desired (2*S*,3*S*)-isomer of *epi*-oxetin.

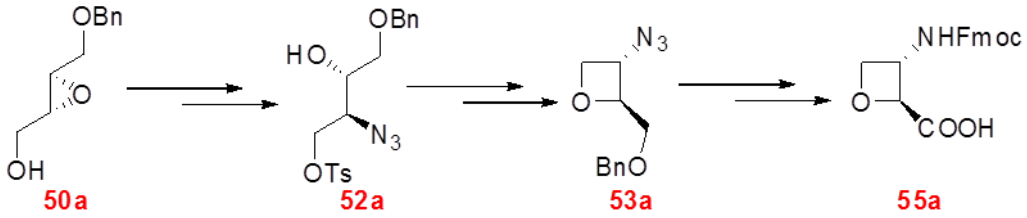

Figure 1.16 Synthetic plan of Fmoc-protected (2*S*,3*S*)-*epi*-oxetin (**55a**)

1.3. Objective of the work

1.3.1. To develop a concise and efficient synthetic method for (2*S*,3*S*)-3-(((9*H*-fluoren-9-yl)methoxy)carbonylamino)oxetane-2-carboxylic acid

1.3.2. To synthesize a novel pyrrolidinyl PNA with (2*S*,3*S*)-3-aminooxetane-2-carboxylic acid spacer (aocPNA)

1.3.3. To evaluate binding affinity and sequence specificity of aocPNA towards DNA/RNA

Chapter 2
Experimental section

2.1. General procedure

2.1.1. Tools and Instruments

All reactions were performed in clean and oven dried glasswares. Solvents were removed on a Büchi Rotavapor R 200 with Büchi Vacuum pump V 700 or water aspirator. Molecular sieve was activated by heating with heating mantle under vacuum (Vacuubrand pump model RZ2). Dried solvents for moisture sensitive reaction were prepared by drying over activated 4 Å molecular sieve. Thin layer chromatography (TLC), using for monitoring the reaction, was silica gel 60 F254 0.2 mm pre-coated aluminium plates and purchased from Merck D.C. Spots on TLC were observed by visualization under 254 nm UV light or dipping in one of following stains: ceric molybdate, 2,4-dinitrophenylhydrazine (2,4-DNP), ninhydrin or aqueous potassium permanganate ($KMnO_4$). Silica gel 70-230 mesh was used in purification by column chromatography.

Melting points were measured on an electrothermal melting point apparatus model 9100. Optical rotations ($[\alpha]^D$) were obtained on a Jasco P-1010 Polarimeter using sodium light (D line, 589.3 nm). Functional group determinations were acquired by Nicolet 6700 infrared (IR) spectroscopy. Structural elucidations were performed by nuclear magnetic resonance (NMR) on Varian Mercury-400 plus or Bruker Avance 400 operating at 400 MHz for ^{1}H NMR and 100 MHz for ^{13}C NMR. Exact masses of all new compounds were indicated by high resolution mass spectroscopy (HRMS) operating on micrOTOf (Bruker) spectrometer (Department of Chemistry, Faculty of Science, Mahidol University).

Enantioselectivities were determined by chiral high performance liquid chromatography (chiral HPLC) using Waters Delta 600 controller system, a gradient pump, Waters 2996 photodiode array detector (D2 lamp) and 100 μL manual sample loop (Rheodyne 7725), column: OJ-H HPLC (DAICEL), 250 x 4.6 mm, 5 μm particle size. Signals and data were processed by the base Empower software. The enantioselectivities were expressed in term of %enantiomeric excess (%ee). The same HPLC machine, including controller system, pump, detector, sample loop and processing software, was used together with a column ACE 5 A71197, C18-AR, 150 x 4.6 mm, 5 μm particle size for separation or Vertisep UPS, 50 x 4.6 mm, 3 μm particle size for analysis of novel PNA. HPLC fractions were collected manually by observation on real-time HPLC chromatogram. The frozen combined fractions were evaporated by Freeze dryer (Labcoco).

Molecular weight of the novel PNAs were measured using Matrix-assisted Laser Desorption/Ionization Time-of-Flight (MALDI-TOF) mass spectrometry (Bruker Daltonik GmbH,

Breman, Germany) in linear positive mode and solution of α-cyano-4-hydroxycinnamic acid (CCA) in 1% trifluoroacetic acid (v/v) and 50% (v/v) acetonitrile in water as matrix. Thermal denaturation was measured in term of melting temperature (T_m) on CARY 100 Bio UV-Visible spectrophotometer (Varian).

2.1.2. Chemicals

All reagent grade chemicals for synthesis were purchased from Fluka, Acros, Merck or Sigma-Aldrich. Unless otherwise stated, analytical grade organic solvents from Burdick&Jackson and RCI Labscan were used in performing the reaction. Laboratory grade solvents from RCI Labscan were used for column chromatography and thin layer chromatography. HPLC grade solvents for all HPLC experiments were purchased from Merck and Scharlau. DNA and RNA oligonucleotides for evaluation the binding properties of aocPNA were purchased from Bio Basic Inc (Canada). Milli-Q water was obtained from ultrapure water system with Millipak® 40 filter unit 0.22 μm, Millipore (USA).

2.2. Synthesis of (*E*)-4-(benzyloxy)but-2-en-1-ol (42)

In this work, three methods to synthesize compound **42** were proposed in order to study the most convenient and suitable way to obtain **42**.

2.2.1. Synthesis of (*E*)-4-(benzyloxy)but-2-en-1-ol (42) starting from (*Z*)-but-2-ene-1,4-diol (38)

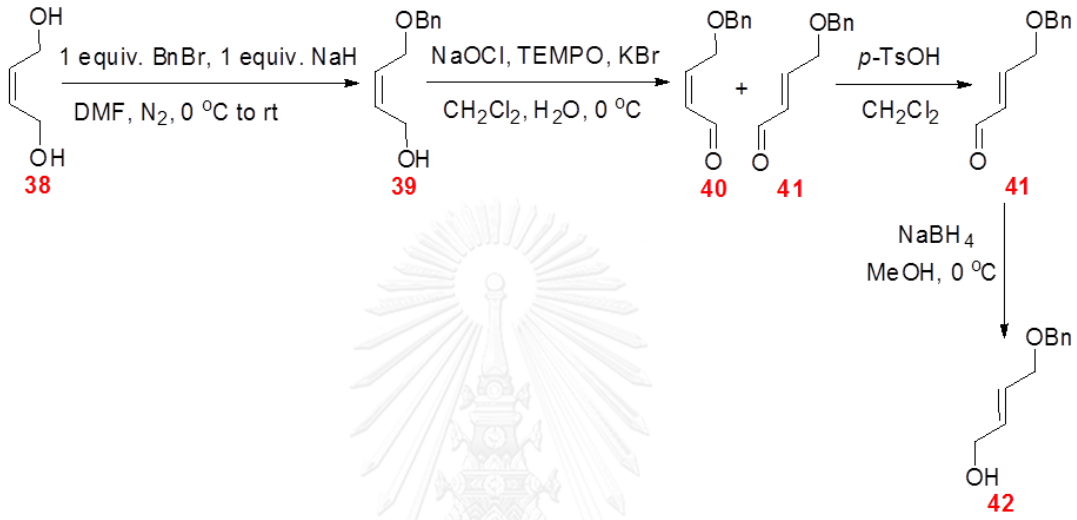

Figure 2.1 Synthesis of **42** from **38**

Benzylation of (*Z*)-but-2-ene-1,4-diol (**38**)[17]

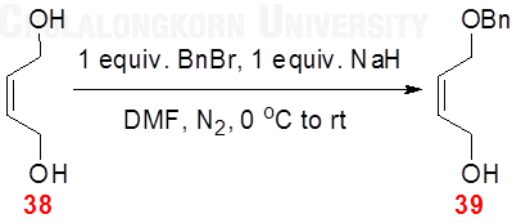

cis-2-Betene-1,4-diol **38** (1.60 mL, 20 mmol) was added dropwise into a suspension of 60% sodium hydride in mineral oil (0.8697 g, 12 mmol of sodium hydride) in *N*,*N*-dimethylformamide (DMF, 20 mL) in 2-neck round bottom flask under nitrogen atmosphere in an ice bath. The solution was kept under nitrogen atmosphere while stirring at 0 °C for 2 hours. After that, benzyl bromide (2.40 mL, 20 mmol) was added dropwise at 0 °C. The reaction mixture was left under nitrogen atmosphere and allowed to warm up to ambient temperature for 19 hours. The reaction was monitored by TLC analysis (hexanes:ethyl acetate 3:1; ceric molybdate,

R_f = 0.14). After completion, the solution was poured into ice and extracted with diethyl ether (Et_2O, 3×40 mL). The combined organic layer was washed with water 4 times, dried over sodium sulfate (Na_2SO_4) anhydrous and evaporated. Finally, the crude product was purified by column chromatography on silica gel using hexanes:ethyl acetate 17:3 as an isocratic mobile phase to obtain (*Z*)-4-(benzyloxy)but-2-en-1-ol (**39**) as yellow liquid in 1.7257 g (48% yield). ^{1}H NMR (400 MHz, $CDCl_3$) δ (ppm) 7.39 – 7.27 (m, 5H, -C_6H_5), 5.86 – 5.70 (m, 2H, -*H*C=C*H*-), 4.53 (s, 2H, -O-CH_2-Ph), 4.17 (d, *J* = 6.2 Hz, 2H, -CH_2-OH), 4.09 (d, *J* = 5.9 Hz, 2H, -CH_2-O-Bn).

Oxidation of (*Z*)-4-(benzyloxy)but-2-en-1-ol (**39**) to aldehyde

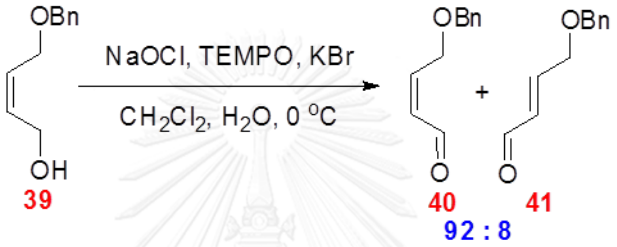

Compound **39** (1.7257 g, 9.7 mmol) of and (2,2,6,6-tetramethylpiperidin-1-yl)oxyl (TEMPO, 0.0186 g, 0.1 mmol) were dissolved in dichloromethane (CH_2Cl_2, 24 mL). Water (37 mL) and potassium bromide (KBr, 0.3116 g, 2.62 mmol) and 0.81 M sodium hypochlorite in water (NaOCl, 28 mL, 29.1 mmol) were subsequently added. Next, sodium hydrogen carbonate ($NaHCO_3$) was added to control pH range around 8-9**.** The reaction was stirred vigorously at 0 °C for 10 minutes and monitored by TLC (hexanes:ethyl acetate 3:1; 2,4-DNP, R_f = 0.40). After completion of the reaction, the organic phase was separated and remaining aqueous phase was extracted with CH_2Cl_2 (2×40 mL). The combined organic layer was dried over Na_2SO_4 anhydrous and evaporated under reduced pressure to obtain a mixture between (*Z*)-4-(benzyloxy)but-2-enal (**40**) and (*E*)-4-(benzyloxy)but-2-enal (**41**) in 92:8 ratio (indicated by ^{1}H NMR analysis) as yellow liquid in 1.5982 g (94% yield). ^{1}H NMR (400 MHz, $CDCl_3$) δ 10.05 (d, *J* = 6.8 Hz, 1H, -C(O)*H*), 7.39 – 7.27 (m, 5H, -C_6H_5), 6.64 (dt, *J* = 11.2, 5.5 Hz, 1H, -*H*C=CH-CHO), 6.10 – 6.02 (m, 1H, -HC=C*H*-CHO), 4.59 (s, 2H, -O-CH_2-Ph), 4.52 (dd, *J* = 5.3, 1.5 Hz, 2H, -CH_2-O-Bn).

Isomerization of (*Z*)-4-(benzyloxy)but-2-enal (**40**) to (*E*)-4-(benzyloxy)but-2-enal (**41**)[18]

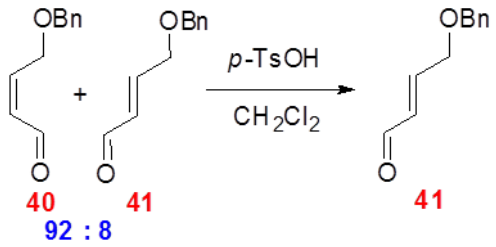

p-toluenesulfonic acid monohydrate (*p*-TsOH·H_2O, 26.7 mg, 0.14 mmol) was added to a solution of the mixture between aldehydes **40** and **41** (1.5982 g, 9.07 mmol) in CH_2Cl_2 (27 mL). The reaction mixture was stirred for 30 minutes and monitored by ^{1}H NMR. After completion, 5 mL of saturated $NaHCO_3$ in water was added and stirred for 5 minutes. The organic phase was separated and evaporated to obtain (*E*)-4-(benzyloxy)-but-2-enal (**41**) as yellow liquid in 1.5442 g (97% yield). ^{1}H NMR (400 MHz, $CDCl_3$) δ 9.58 (d, *J* = 7.9 Hz, 1H, -C(O)*H*), 7.41 – 7.28 (m, 5H, C_6H_5), 6.85 (dt, *J* = 15.7, 4.0 Hz, 1H, -*H*C=CH-CHO), 6.41 (dd, *J* = 15.7, 7.9 Hz, 1H, -HC=C*H*-CHO), 4.59 (s, 2H, -O-CH_2-Ph), 4.32 – 4.26 (m, 2H, -CH_2-O-Bn).

NaBH4 reduction of (*E*)-4-(benzyloxy)-but-2-enal (**41**)[19]

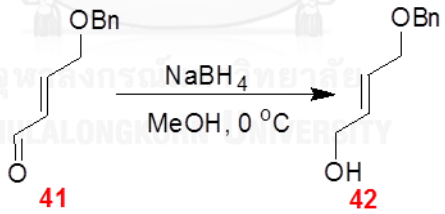

$NaBH_4$ (0.2814 g, 7.4 mmol) was slowly added to a solution of aldehyde **41** (1.2395 g, 7.0 mmol) in methanol (MeOH, 14 mL) at 0 °C. The reaction mixture was stirred at 0 °C for 30 minutes and monitored by TLC (hexanes:ethyl acetate 3:1; ceric molybdate, R_f = 0.18). After the completion, a few mLs of water and citric acid were added to neutralize the solution. The crude product, obtained by evaporation of the solvents under reduced pressure, was purified by column chromatography on silica gel using hexanes:ethyl acetate 3:1 as an isocratic mobile phase to obtain (*E*)-4-(benzyloxy)but-2-en-1-ol (**42**) as yellow liquid in 0.9749 g (78% yield). ^{1}H NMR (400 MHz, $CDCl_3$) δ 7.41 – 7.29 (m, 5H, C_6H_5), 5.99 – 5.84 (m, 2H, -*H*C=C*H*-), 4.56 (s, 2H, -O-CH_2-Ph), 4.19 (dd, *J* = 5.0, 1.0 Hz, 2H, -CH_2-OH), 4.07 (dd, *J* = 5.4, 0.9 Hz, 2H, -CH_2-O-Bn).

2.2.2. Synthesis of (*E*)-4-(benzyloxy)but-2-en-1-ol (42) from but-2-yne-1,4-diol (43)

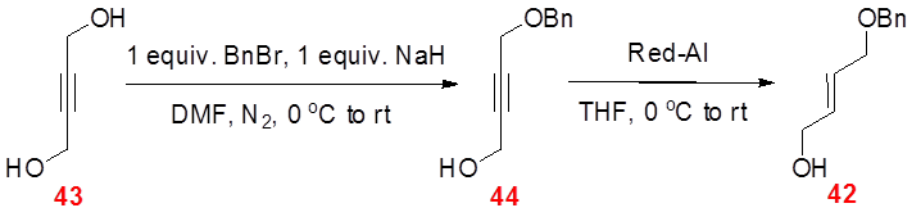

Figure 2.2 Synthesis of **42** from **43**

Benzylation of but-2-yne-1,4-diol (**43**)

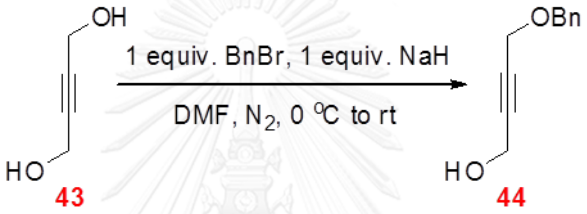

Following the same protocol for Benzylation of (*Z*)-but-2-ene-1,4-diol (**38**) using 1,4-butynediol **43** (1.7281 g, 20 mmol), 60% sodium hydride in mineral oil (0.8500 g, 12 mmol of sodium hydride), and benzyl bromide (2.40 mL, 20 mmol) in anhydrous DMF (5 mL) to obtain 4-(benzyloxy)but-2-yn-1-ol (**44**) as yellow liquid in 0.8487 g (24% yield, hexanes:ethyl acetate 3:1; ceric molybdate, R_f = 0.15). ^{1}H NMR (400 MHz, $CDCl_3$) δ 7.38 – 7.27 (m, 5H, C_6H_5), 4.60 (s, 2H, -O-CH_2-Ph), 4.32 (s, 2H, -CH_2-OH), 4.21 (s, 2H, -CH_2-O-Bn).

Alkyne reduction of 4-(benzyloxy)but-2-yn-1-ol (**44**)[20]

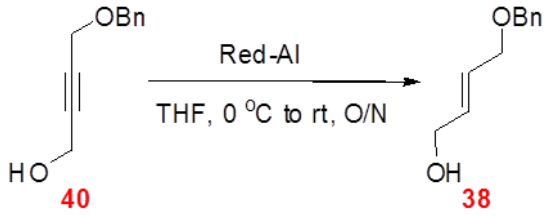

Sodium bis(2-methoxyethoxy)aluminumhydride (Red-Al, 2.40 mL, 20 mmol) was added to a solution of compound **44** (0.8487 g, 4.82 mmol) in distilled tetrahydrofuran (THF, 15 mL) under nitrogen atmosphere at 0 °C. The reaction was stirred at 0 °C for 20 hours and monitored by TLC (hexanes:ethyl acetate 3:1; $KMnO_4$, R_f = 0.14). After completion of the reaction, water (5 mL) was added to quench remaining Red-Al followed by addition of 10% w/v sodium hydroxide (NaOH) in water (15 mL). The reaction mixture was extracted with ethyl acetate (3×25 mL). The combined organic phase was dried over Na_2SO_4 anhydrous, evaporated and purified by column chromatography on silica gel using gradient mobile phase starting from hexanes:ethyl acetate 17:3 to 1:1 to obtain (*E*)-4-(benzyloxy)but-2-en-1-ol (**42**) as yellow liquid in 0.4382 g (51% yield). ^{1}H NMR (400 MHz, $CDCl_3$) δ 7.31 – 7.19 (m, 5H, C_6H_5), 5.89 – 5.73 (m, 2H, -*H*C=C*H*-), 4.46 (s, 2H, -O-CH_2-Ph), 4.09 (d, *J* = 4.9 Hz, 2H, -CH_2-OH), 3.97 (d, *J* = 5.4 Hz, 2H, -CH_2-O-Bn).

2.2.3. Synthesis of (*E*)-4-(benzyloxy)but-2-en-1-ol (42) from benzyl glycidyl ether (45)

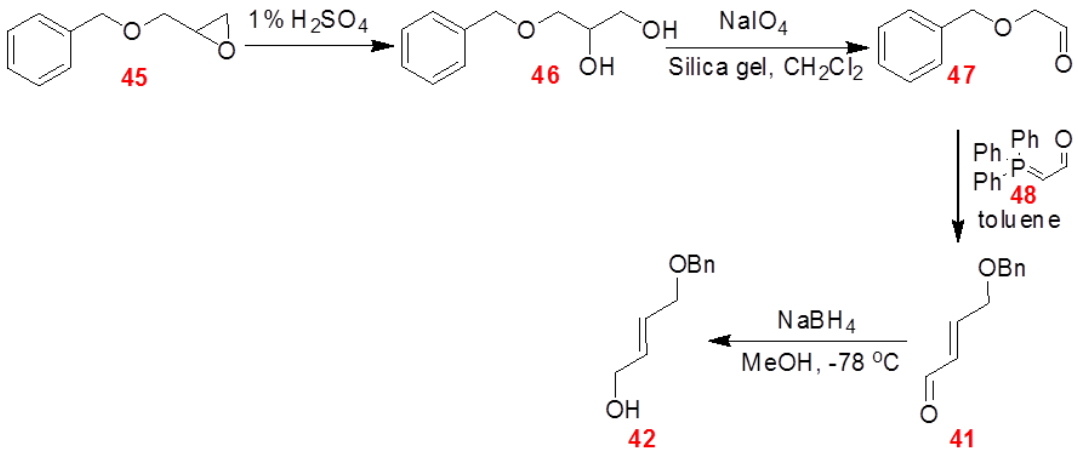

Figure 2.3 Synthesis of **42** from **45**

Epoxide ring opening of benzyl glycidyl ether (**45**)[21]

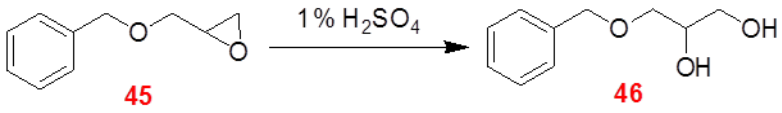

Benzyl glycidyl ether (**45**, 3.05 mL, 20 mmol) was dissolved in 1% v/v sulfuric acid (H_2SO_4) in water (50 mL). The reaction was completed after stirring at ambient temperature for 4 hours as indicated by TLC analysis (hexanes:ethyl acetate 3:2; UV light, R_f = 0.14). Sodium chloride (NaCl) was added until the solution became saturated with NaCl. After that, the solution was extracted with ethyl acetate (3×50 mL) and the combined organic phase was dried over Na_2SO_4 anhydrous and evaporated under reduced pressure to obtain 3-(benzyloxy)propane-1,2-diol (**46**) as yellow liquid in 3.5656 g (98% yield). ^{1}H NMR (400 MHz, $CDCl_3$) δ 7.41 – 7.27 (m, 1H, C_6H_5), 4.55 (s, 1H, -O-CH_2-Ph), 3.95 – 3.85 (m, 1H, -O-CH_2-CH(OH)-CH_2-OH), 3.75 – 3.49 (m, 4H, -O-CH_2-CH(OH)-CH_2-OH).

Periodate oxidation of 3-(benzyloxy)propane-1,2-diol (**46**)

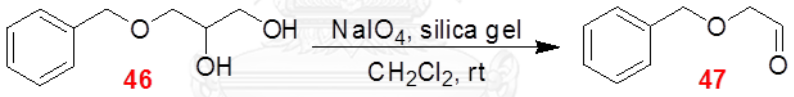

Sodium periodate ($NaIO_4$) pre-adsorbed on silica gel was prepared by adding 0.65 M $NaIO_4$ in water into suspension of silica gel (40 g) in CH_2Cl_2 (150 mL).[22] Then, diol **46** (3.5656 g, 19.6 mmol) in CH_2Cl_2 (25 mL) was added dropwise into the prepared $NaIO_4$ suspension. The reaction was stirred at ambient temperature for 90 minutes and monitored by TLC (hexanes:ethyl acetate 1:1; UV light and 2,4-DNP, R_f = 0.50). After completion of the reaction, the $NaIO_4$-supported silica gel was filtered off and the filtrate was washed with saturated $NaHCO_3$ solution. Organic phase was evaporated under reduced pressure to gain a crude reaction product. Finally, the crude product was purified by short column chromatography using ethyl acetate as eluent to obtain 2-(benzyloxy)acetaldehyde (**47**) as yellow liquid in 2.8153 g (96% yield). ^{1}H NMR (400 MHz, $CDCl_3$) δ 9.73 (s, 1H, -C(O)H), 7.44 – 7.29 (m, 5H, C_6H_5), 4.63 (s, 2H, -O-CH_2-Ph), 4.10 (s, 2H, -O-CH_2-CHO).

Wittig reaction of 2-(benzyloxy)acetaldehyde (**47**) with phosphorus ylide **48**

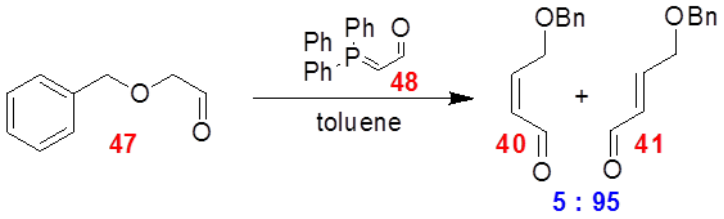

Aldehyde **47** (2.8153 g, 18.8 mmol) and ylide **48** (6.2765 g, 20.6 mmol) were dissolved together in toluene (80 mL). The reaction was stirred at room temperature for 24 hours and monitored by TLC (hexanes:ethyl acetate 3:1; 2,4-DNP, R_f = 0.31). After completion of the reaction, the solvent from reaction mixture was evaporated and triphenylphosphine oxide (by-product from the reaction) was precipitated in hexanes at -20 $^{\circ}$C and filtered off. The filtrate was evaporated and purified by column chromatography on silica gel using gradient mobile phase starting from pure hexanes to hexanes:ethyl acetate 9:1 to obtain a mixture between (*Z*)-4-(benzyloxy)but-2-enal (**40**) and (*E*)-4-(benzyloxy)but-2-enal (**41**) in 5:95 ratio (indicated by ^{1}H NMR analysis) as yellow liquid in 2.7096 g (82% yield). ^{1}H NMR (400 MHz, $CDCl_3$) δ 9.59 (d, *J* = 7.9 Hz, 1H, -C(O)*H*), 7.46 – 7.28 (m, 5H, C_6H_5), 6.85 (dt, *J* = 15.8, 4.0 Hz, 1H, -*H*C=CH-CHO), 6.41 (dd, *J* = 15.8, 7.9 Hz, 1H, 1H, -HC=C*H*-CHO), 4.60 (s, 2H, -O-CH_2-Ph), 4.29 (dd, *J* = 3.8, 1.7 Hz, 2H, -CH_2-O-Bn).

$NaBH_4$ reduction of (*E*)-4-(benzyloxy)but-2-enal (**41**) at -78 °C[19]

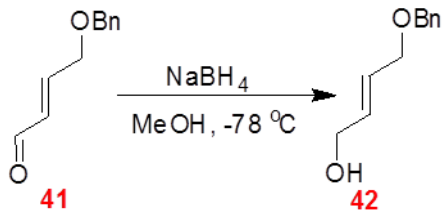

$NaBH_4$ (0.5162 g, 13.6 mmol) was added to a solution of aldehyde **41** (2.4290 g, 13.6 mmol) in MeOH (25 mL) in dry ice bath (-78 °C). The reaction mixture was stirred at -78 °C for 30 minutes. After the reaction was completed as monitored by TLC (hexanes:ethyl acetate 3:1; ceric molybdate, R_f = 0.16), a few mLs of water and citric acid were added to neutralize the solution. The crude product, obtained after solvent evaporation, was purified by column chromatography on silica gel using hexanes:ethyl acetate 3:1 as an isocratic mobile phase to obtain (*E*)-4-(benzyloxy)but-2-en-1-ol (**42**) as yellow liquid in 0.9981 g (41% yield). ^{1}H NMR (400 MHz, $CDCl_3$) δ 7.39 – 7.27 (m, 1H, C_6H_5), 5.98 – 5.79 (m, 1H, -*H*C=C*H*-), 4.53 (s, 1H, -O-CH_2-Ph), 4.17 (d, *J* = 4.0 Hz, 1H, -CH_2-OH), 4.04 (d, *J* = 4.5 Hz, 1H, -CH_2-O-Bn).

$NaBH_4$ reduction of (*E*)-4-(benzyloxy)but-2-enal (**41**) at room temperature[19]

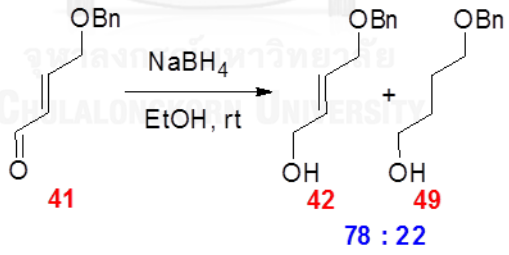

$NaBH_4$ (0.3291 g, 8.9 mmol) was added to a solution of aldehyde **41** (1.5442 g, 8.76 mmol) in ethanol (EtOH, 20 mL). The reaction mixture was stirred for 24 hours at ambient temperature and monitored by TLC (hexanes:ethyl acetate 3:1; ceric molybdate, R_f = 0.14). After the completion, a few mLs of water and citric acid were added to neutralize the solution, followed by solvent evaporation. Water was added and extracted with CH_2Cl_2 (3×20 mL). The combined organic layer was dried over Na_2SO_4 anhydrous, evaporated and purified by column chromatography on silica gel using gradient mobile phase starting from hexanes:ethyl acetate 9:1 to 1:1 to obtain a mixture between (*E*)-4-(benzyloxy)but-2-en-1-ol (**42**) and 4-(benzyloxy)butan-1-

ol (**49**) in 78:22 ratio (indicated by ^{1}H NMR analysis) as yellow liquid in 0.8880 g. (44% yield of compound **42** was calculated by ignoring the proportion of **49**) ^{1}H NMR (400 MHz, $CDCl_3$) δ 7.41 – 7.26 (m, 5H, C_6H_5), 5.97 – 5.80 (m, 2H, -*H*C=C*H*-),), 4.53 (s, 2H, -O-CH_2-Ph), 4.16 (d, *J* = 4.0 Hz, 2H, -CH_2-OH), 4.04 (d, *J* = 5.2 Hz, 2H, -CH_2-O-Bn).

2.3. Preliminary testing on racemic model for synthesis of 3-(((9*H*-fluoren-9-yl)methoxy)carbonylamino)oxetane-2-carboxylic acid (55)

After the synthesis of the starting material **42** was accomplished, then, preliminary testing in order to confirm the possibility to obtain the target molecule **55** from the proposed pathway was evaluated.

2.3.1. Racemic model synthesis of 3-(((9*H*-fluoren-9-yl)methoxy)carbonylamino)oxetane-2-carboxylic acid (55)

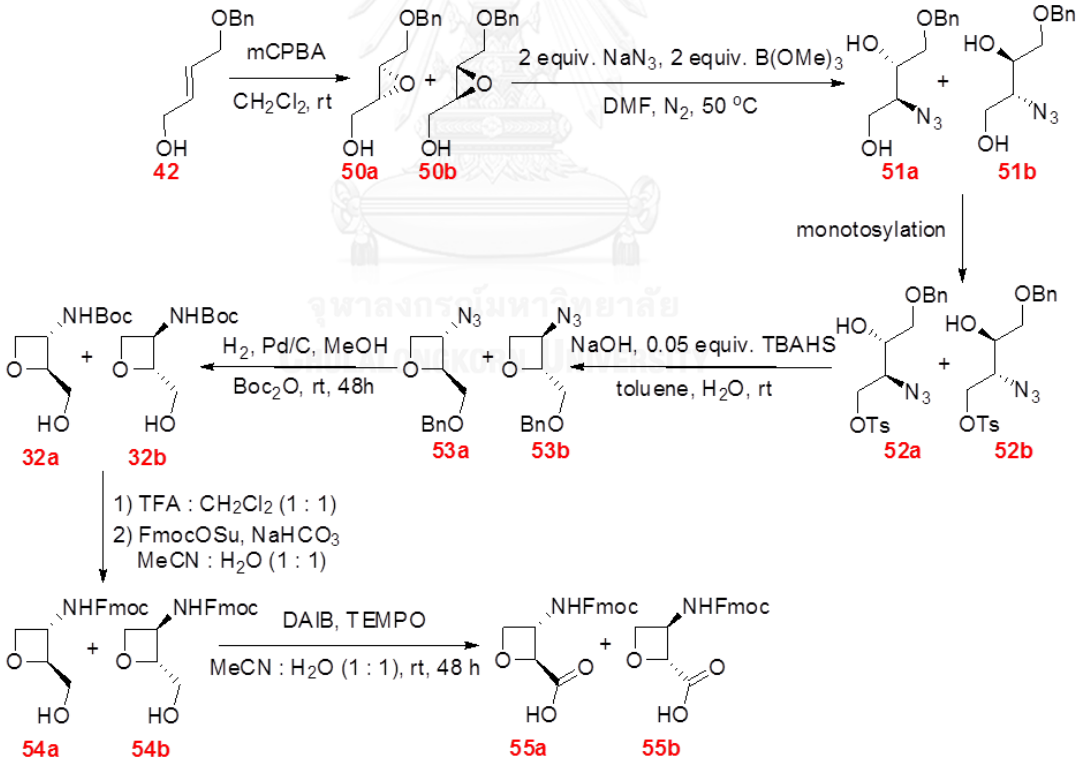

Figure 2.4 Synthesis of racemic **55** from **42**

Epoxidation of (*E*)-4-(benzyloxy)but-2-en-1-ol (**42**) with *m*-chloroperbenzoic acid (mCPBA)

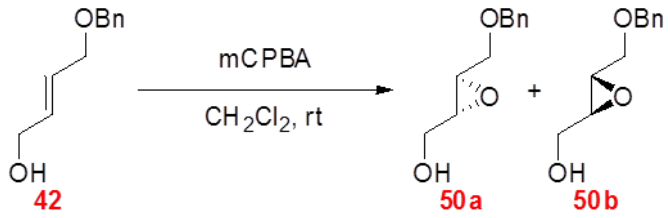

A solution of alkene **42** (1.8775 g, 10.6 mmol) in CH_2Cl_2 (60 mL) was treated with 70% w/w mCPBA (2.6158 g, 10.6 mmol). After 3 hours, the reaction was completed as monitored by TLC (hexanes:ethyl acetate 1:1; ceric molybdate, R_f = 0.28). Calcium hydroxide ($Ca(OH)_2$, 2.2649 g, 30.7 mmol) was added into the solution and the reaction was stirred for another 30 minutes. The precipitated calcium salt was removed by filtration and the filtrate was evaporated to obtain racemic (3-(benzyloxymethyl)oxiran-2-yl)methanol (**50**) as yellow liquid in 2.0135 g (98% yield). IR (ATR): 3413, 2916, 2859, 1458, 1253, 1096 cm^{-1}. ^{1}H NMR (400 MHz, $CDCl_3$): δ 7.41 – 7.29 (m, 5H, C_6H_5), 4.60 (ABq, *J* = 11.9 Hz, 2H, -O-C*H*$_2$-Ph), 3.95 (dd, *J* = 12.7, 2.2 Hz, 1H, -C*H*H-OBn), 3.79 (dd, *J* = 11.5, 3.0 Hz, 1H, -C*H*H-OH), 3.67 (dd, *J* = 12.7, 4.0 Hz, 1H, -CH*H*-OBn), 3.55 (dd, *J* = 11.5, 5.5 Hz, 1H, -CH*H*-OH), 3.26 (dt, *J* = 5.4, 2.7 Hz, 1H, epoxide proton), 3.12 (dt, *J* = 4.5, 2.4 Hz, 1H, epoxide proton), 2.01(br s, 1H, CH_2-O*H*). ^{13}C NMR (100 MHz, $CDCl_3$) δ 137.83, 128.46, 127.82, 127.77, 73.40, 69.68, 61.21, 55.77, 54.30.

Ring opening of racemic (3-(benzyloxymethyl)oxiran-2-yl)methanol (**50a** and **50b**) by sodium azide[23]

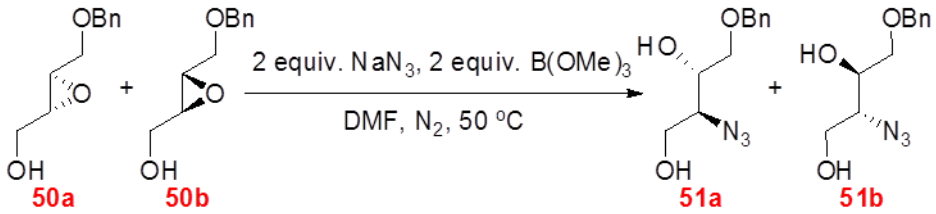

A solution of racemic **50** (0.3581 g, 1.84 mmol) and sodium azide (NaN_3, 0.2400 g, 3.69 mmol) in dried DMF was treated with trimethyl borate ($B(OMe)_3$, 0.41 mL, 3.69 mmol). The reaction was kept under nitrogen atmosphere while stirring at 50 °C for 5 hours and monitored by TLC (CH_2Cl_2:acetone 9:1; ceric molybdate, R_f = 0.30). After completion of the reaction, the reaction was cooled to 0 °C, followed by addition of saturated $NaHCO_3$ in water (20 mL), stirring

for another 30 minutes at 0 °C and extracted with ethyl acetate (3×20 mL). The combined organic phase was washed with water 4 times and saturated $NaHCO_3$ solution once, dried over Na_2SO_4 anhydrous and evaporated under reduced pressure to obtain racemic 2-azido-4-(benzyloxy)butane-1,3-diol (**51a** and **51b**) as yellow liquid in 0.3909 g (90% yield). IR (ATR): 3375, 2919, 2861, 2101, 1451, 1069 cm^{-1}. ^1H NMR (400 MHz, $CDCl_3$): δ 7.33 – 7.19 (m, 5H, C_6H_5), 4.50 (s, 2H, -O-CH_2-Ph), 3.85 – 3.45 (m, 6H, -CH_2-OBn, -C(OH)*H*-CH_2-OBn, -CH_2-OH and -C(N_3)*H*-CH_2-OH), 2.53 (s, 2H, -CH2-O*H* and -C(O*H*)H-CH_2-OBn). ^{13}C NMR (100 MHz, $CDCl_3$) δ 137.42, 128.58, 128.08, 127.92, 73.65, 70.97, 70.76, 63.96, 62.76.

Monotosylation of racemic 2-azido-4-(benzyloxy)butane-1,3-diol (**51a** and **51b**)

In this research, monotosylation of racemic 2-azido-4-(benzyloxy)butane-1,3-diol (**51a** and **51b**) was compared under two different conditions.

Tosylation of racemic 2-azido-4-(benzyloxy)butane-1,3-diol (**51a** and **51b**) *via* Standard condition

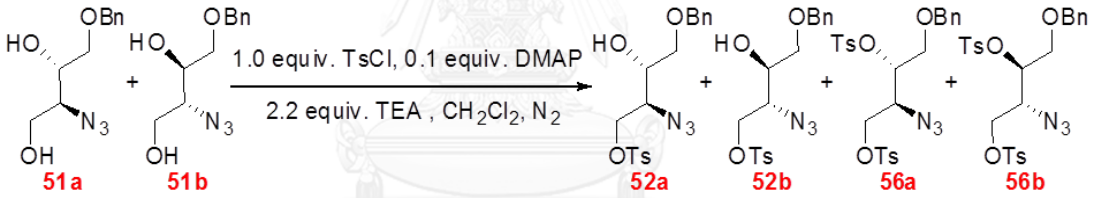

Racemic **51** was azeotropically dried by co-evaporation with toluene to reduce water content. After that compound **51** (0.2390 g, 1.0 mmol) was dissolved in dried and distilled CH_2Cl_2 (5 mL) under nitrogen atmosphere. Triethylamine (TEA, 0.25 mL, 3.63 mmol) and 4-dimethylaminopyridine (DMAP, 20.8 mg, 0.17 mmol) were added at 0 °C. Then, a solution of TsCl (0.3321 g, 1.73 mmol) in distilled CH_2Cl_2 (4 mL) was added dropwise into the reaction mixture. The reaction was stirred under nitrogen atmosphere at 0 °C and was allowed to warm up to room temperature for 24 hours. After the reaction was completed as indicated by TLC (hexanes:ethyl acetate 1:1; ceric molybdate, R_f = 0.45 and 0.55), water was added and the mixture was extracted wih ethyl acetate (3×10 mL). The organic layer was evaporated under reduced pressure and purified by column chromatography on silica gel using hexanes:ethyl acetate 4:1 as isocratic mobile phase to recover starting material **51** in 21% and obtain racemic-2-azido-4-(benzyloxy)-3-hydroxybutyl 4-methylbenzenesulfonate (**52**) as yellow liquid in 0.1491 g (38% yield, hexanes:ethyl acetate 1:1; ceric molybdate, R_f = 0.45) and racemic-2-azido-4-

(benzyloxy)butane-1,3-diyl bis(4-methylbenzenesulfonate) (ditosylated compound **56**) as colorless liquid in 0.0687 g (13% yield, hexanes:ethyl acetate 1:1; ceric molybdate, R_f = 0.55).

Racemic **52**: IR (ATR): 3441, 2931, 2865, 2093, 1459, 1361, 1172 cm^{-1}. ^{1}H NMR (400 MHz, $CDCl_3$) δ 7.84 (d, *J* = 8.3 Hz, 2H, -C_6H_2-CH_3), 7.42 – 7.29 (m, 7H, -C_6H_5 and -C_6H_2-CH_3), 4.57 (s, 2H, -O-CH_2-Ph), 4.44 (dd, *J* = 10.6, 2.9 Hz, 1H, -CH*H*-OTs), 4.16 (dd, *J* = 10.6, 7.4 Hz, 1H, -*CH*H-OTs), 3.76 (td, *J* = 7.7, 2.8 Hz, 1H, -C(OH)*H*-CH_2-OBn), 3.70 – 3.65 (m, 1H, -C(N_3)*H*-CH_2-OTs), 3.63 – 3.59 (m, 2H, -CH_2-OBn), 2.47 (s, 3H, -C_6H_4-CH_3). ^{13}C NMR (100 MHz, $CDCl_3$) δ 145.13, 137.30, 132.69, 129.94, 128.59, 128.10, 128.02, 127.89, 73.62, 70.21, 69.53 (2 carbons), 61.61, 21.66.

Racemic **56**: IR (ATR): 3050-2850, 2101, 1356, 1167 cm^{-1}. ^{1}H NMR (400 MHz, $CDCl_3$) δ 7.67 (t, *J* = 8.8 Hz, 4H, -C_6H_2-CH_3 on both Ts), 7.30 – 7.19 (m, 7H, -C_6H_5 and -C_6H_2-CH_3), 7.15 – 7.10 (m, 2H, -C_6H_2-CH_3), 4.51 – 4.37 (m, 1H, -C(OTs)*H*-CH_2-OBn), 4.33 (s, 2H, -O-CH_2-Ph), 4.13 (dd, *J* = 10.6, 3.2 Hz, 1H, -C(N_3)H-C*H*H-OTs), 3.97 – 3.91 (m, 1H, -C(N_3)*H*-CH_2-OTs), 3.84 (dd, *J* = 10.5, 8.1 Hz, 1H, -C(N_3)H-CH*H*-OTs), 3.52 (d, *J* = 4.2 Hz, 2H, -CH_2-OBn), 2.37 (s, 6H, -C_6H_4-CH_3 on both Ts). ^{13}C NMR (100 MHz, $CDCl_3$) δ 145.46, 145.26, 137.04, 133.10, 132.46, 130.00, 129.98, 128.48, 128.02, 127.99, 127.89, 127.77, 77.76, 73.56, 68.26, 67.65, 60.20, 21.71, 21.68. HRMS (ESI+): m/z calcd for $C_{25}H_{27}N_3O_7S_2Na$ [M + Na^+], 568.1188; found, 568.1238.

Tosylation of racemic 2-azido-4-(benzyloxy)butane-1,3-diol (**51a** and **51b**) *via* borinate complex

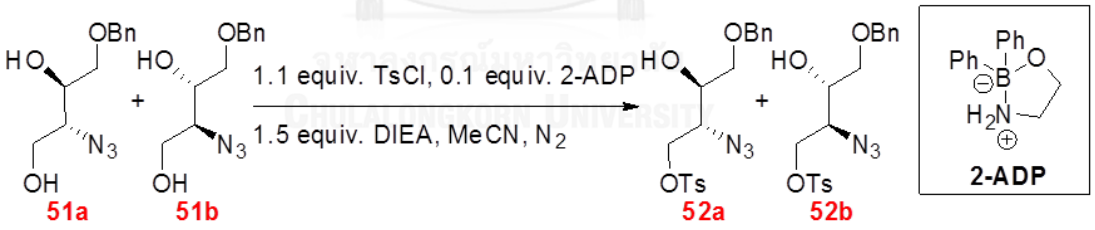

Racemic **51** was azeotropically dried by co-evaporation with toluene to reduce water content. After that racemic **51** (0.4745 g, 2.0 mmol), 2-aminoethyl diphenylborinate (2-ADP, 0.0463 g, 0.2 mmol), 0.4423 g (2.3 mmol) of TsCl and finely ground 4 Å molecular sieve (0.0572 g, 10%wt of racemic **47**) were added into distilled acetonitrile (10 mL) under nitrogen atmosphere at 0 °C. Then, *N*,*N*-diisopropylethylamine (DIEA, 0.52 mL, 3.0 mmol) was added dropwise. The reaction was kept under nitrogen atmosphere while stirring at 0 °C, and was allowed to warm up to room temperature for 6 days. After the reaction was completed as indicated by TLC (hexanes:ethyl acetate 1:1; ceric molybdate, R_f = 0.45). The reaction was quenched with water and extracted with ethyl acetate (3×20 mL). The combined organic phase was dried over Na_2SO_4

anhydrous, evaporated under reduced pressure and purified by column chromatography on silica gel using gradient mobile phase starting from hexanes:ethyl acetate 4:1 to 3:1 to obtained racemic mixture of 2-azido-4-(benzyloxy)-3-hydroxybutyl 4-methylbenzenesulfonate (**52)** as yellow liquid in 0.4754 g (61% yield, hexanes:ethyl acetate 1:1; ceric molybdate, R_f = 0.46). ^{1}H NMR result was the same as the product obtained from the DMAP condition above.

Cyclization of racemic 2-azido-4-(benzyloxy)-3-hydroxybutyl 4-methylbenzenesulfonate (**52a** and **52b**) to oxetane

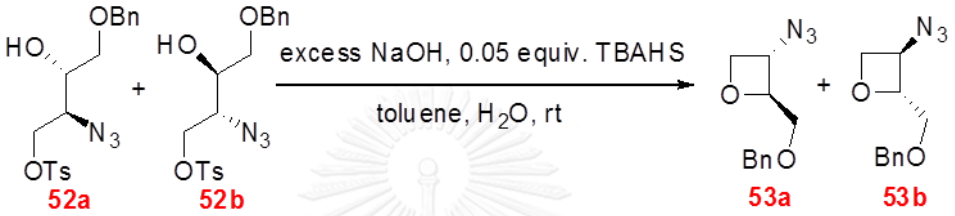

A solution of racemate **52** (0.2108 g, 0.54 mmol) in toluene (1.0 mL) was added dropwise into a suspension of tetrabutyl ammonium hydrogen sulfate (TBAHS, 18.3 mg, 0.054 mmol), finely ground NaOH (0.8744 g, 21.5 mmol), and water (150 μL) in toluene (2.4 mL). The reaction mixture was stirred at ambient temperature for 20 minutes and monitored by TLC (hexanes:ethyl acetate 3:1; ceric molybdate, R_f = 0.42). After completion of the reaction, the precipitated NaOH was removed by filtration and the filtrate was washed with water 3 times. The organic layer was dried over Na_2SO_4 anhydrous, evaporated under reduced pressure and purified by column chromatography on silica gel using hexanes:ethyl acetate 17:3 as isocratic elution to obtain racemic mixture of 3-azido-2-(benzyloxy-methyl)oxetane (**53**) as yellow liquid in 0.0840 g (70% yield). IR (ATR): 3100-3000, 3000-2800, 2093 cm^{-1}. ^{1}H NMR (400 MHz, $CDCl_3$) δ 7.44 – 7.30 (m, 5H, -C_6H_5), 4.85 – 4.80 (m, 1H, oxetane proton), 4.77 – 4.67 (m, 2H, oxetane protons), 4.65 – 4.59 (m, 1H, oxetane proton), 4.57 – 4.49 (m, 2H, -O-CH_2-Ph), 3.69 (d, *J* = 3.3 Hz, 2H, -CH_2-OBn). ^{13}C NMR (100 MHz, $CDCl_3$) δ 137.84, 128.49, 127.84, 127.71, 86.74, 73.77, 73.53, 70.42, 55.53. HRMS (ESI+): m/z calcd for $C_{11}H_{13}N_3O_2Na$ [M + Na^+], 242.0905; found, 242.0904.

Reduction Boc-protection and debenzylation of racemic 3-azido-2-(benzyloxy-methyl)oxetane (**53a** and **53b**)

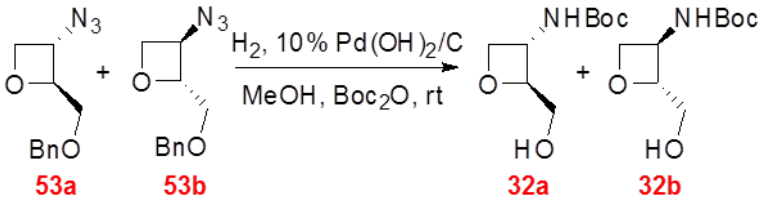

Di-*tert*-butyl dicarbonate (Boc_2O, 0.7618 g, 3.48 mmol and 10% $Pd(OH)_2/C$ (0.1280 g, 20%wt of racemic **53**) were added into a solution of racemic **53** (0.6365 g, 2.90 mmol) in MeOH (3 mL). The reaction was kept under hydrogen atmosphere while stirring at ambient temperature for 7 days and monitored by TLC (ethyl acetate; ninhydrin, R_f = 0.48). After the completion, the $Pd(OH)_2/C$ catalyst was removed by filtration and the solution was evaporated to obtain racemic mixture of *tert*-butyl-2-(hydroxymethyl)oxetan-3-ylcarbamate (**32a** and **32b**) as yellow liquid in 0.5226 g (89% yield). IR (ATR): 3309, 3000-2800, 1681, 1529, 1168 cm^{-1}. ^{1}H NMR (400 MHz, $CDCl_3$) δ 5.25 (br s, 1H, -N*H*-Boc), 4.73 – 4.57 (m, 3H, oxetane protons C*H*-CH_2OH, C*H*NH and C*H*HO), 4.44 (t, *J* = 6.3 Hz, 1H, oxetane proton CH*H*O), 3.83 – 3.65 (m, 2H, -CH_2-OH), 1.45 (s, 9H, -C(O)O-C(CH_3)$_3$). ^{13}C NMR (100 MHz, $CDCl_3$) δ 155.14, 89.82, 80.47, 74.26, 63.53, 47.23, 28.31.

Fmoc protection of racemic *tert*-butyl-2-(hydroxymethyl)oxetan-3-ylcarbamate (**32a** and **32b**)

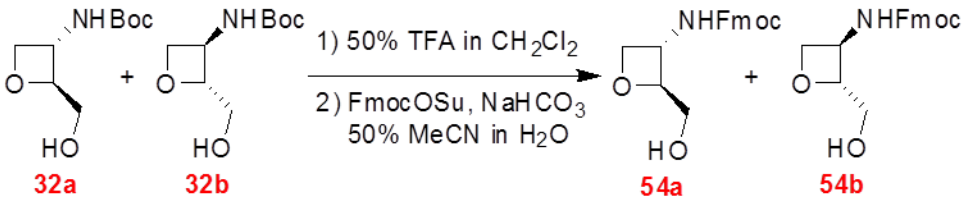

Racemic **32** (0.1053 g, 0.52 mmol) was dissolved in 50% v/v trifluoroacetic acid (TFA) in CH_2Cl_2 (1 mL) and stirred for 10 minutes. The reaction was monitored by TLC (ethyl acetate; ninhydrin, R_f = 0). After completion of the Boc deprotection, the solvent was removed by flushing with nitrogen gas. Then, the crude reaction was dissolved in 50% v/v acetonitrile in water (1 mL), containing $NaHCO_3$ (0.9280 g, 1.04 mmol). *N*-(9-fluorenylmethoxycarbonyloxy)succinimide (FmocOSu, 0.1781 g, 0.52 mmol) were added. The reaction was stirred at ambient temperature for 24 hours and monitored by TLC (hexanes:ethyl acetate 2:3; UV light, R_f = 0.10). After

completion of the reaction, the mixture was added with water, followed by addition of NaCl until the solution was saturated and extracted with ethyl acetate (3×5 mL). The combined organic phase was dried over Na_2SO_4 anhydrous and evaporated. The crude reaction was purified by stirring in Et_2O and filtration to obtain racemic mixture of (9*H*-fluoren-9-yl)methyl-2-(hydroxymethyl)oxetan-3-ylcarbamate (**54a** and **54b**) as white solid in 0.0644 g (38% yield). ^{1}H NMR (400 MHz, $CDCl_3$) δ 7.77 (d, *J* = 7.4 Hz, 2H, Fmoc aromatic C*H*), 7.57 (d, *J* = 7.2 Hz, 2H, Fmoc aromatic C*H*), 7.41 (t, *J* = 7.3 Hz, 2H, Fmoc aromatic C*H*), 7.32 (t, *J* = 7.2 Hz, 2H, Fmoc aromatic C*H*), 5.19 (br s, 1H, -N*H*-Fmoc), 4.76 – 4.60 and 4.51 – 4.38 (m, 6H, oxetane protons and Fmoc aliphatic CH_2), 4.20 (t, *J* = 5.5 Hz, 1H, Fmoc aliphatic C*H*), 3.76 (dd, *J* = 32.3, 12.6 Hz, 1H, -CH_2OH).

Oxidation to carboxylic acid of racemic (9*H*-fluoren-9-yl)methyl-2-(hydroxymethyl)oxetan-3-ylcarbamate (**54a** and **54b**)

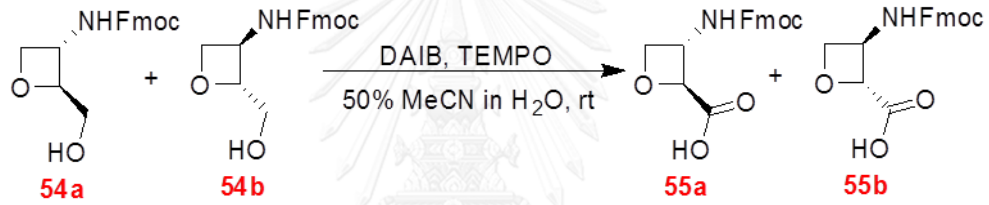

Diacetoxy iodobenzene (DAIB, 0.1401 g, 0.435 mmol) and TEMPO (0.0081 g, 0.05 mmol) were added into a solution of racemic **54** (0.0644 g, 0.198 mmol) in 50% v/v acetonitrile in water (3 mL). The reaction was stirred at ambient temperature for 24 hours. By TLC analysis (ethyl acetate:MeOH 9:1 with a few drops of acetic acid), 4 spots, R_f = 0, 0.21, 0.57 and 0.69, were observed under UV light, in which racemic **54** (R_f = 0.57) was still present. More DAIB and TEMPO were added and the reaction was left for longer periods. The addition of both reagents and extension of the reaction time were continued until the spot of racemic **54** (R_f = 0.57) was not observed. The total amounts of DAIB and TEMPO used in this reaction were 0.6260 g (1.94 mmol) and 0.0234 (0.15 mmol), respectively. Then, the reaction was made basic by addition of saturated $NaHCO_3$ solution and extracted with ethyl acetate (3×5 mL). The aqueous phase was acidified by 2 N HCl solution and extracted with ethyl acetate (3×5 mL). The combined organic phase was dried over Na_2SO_4 anhydrous, evaporated and purified by preparative TLC using ethyl acetate:MeOH 9:1. Unfortunately, no desired products could be isolated.

2.3.2. Alternation procedure for solution in synthesis of racemic 3-(((*9H*-fluoren-9-yl)methoxy)carbonylamino)oxetane-2-carboxylic acid (55a and 55b)

Due to the problem on oxidation of compound **54** to generate target **55** on (2.3.1), an alternative route was proposed by reordering the last 2 steps, i.e. by conducting oxidation of **32** before Fmoc protection of **33** to obtain the target **55**.

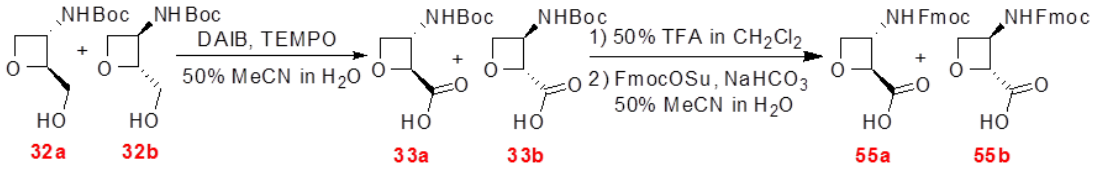

Figure 2.5 Synthesis of racemic **55** from racemate **32** through intermediate **33**

Oxidation of racemic *tert*-butyl-2-(hydroxymethyl)oxetan-3-ylcarbamate (**32a** and **32b**) to carboxylic acid

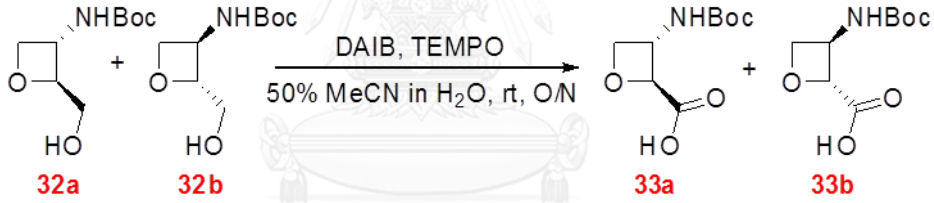

DAIB (1.6795 g, 5.41 mmol) and TEMPO (0.0906 g, 0.56 mmol) were added in a solution of racemic **32** (0.4582 g, 2.25 mmol) in 50% v/v acetonitrile in water (7 mL). The reaction was stirred at room temperature for 24 hours and monitored by TLC (hexanes:ethyl acetate 1:3; ninhydrin, R_f = 0.10). After completion of the reaction, the reaction was made basic by addition of saturated $NaHCO_3$ solution and extracted with Et_2O (3×5 mL). The aqueous phase was acidified by sodium hydrogen sulfate ($NaHSO_4$) and extracted with ethyl acetate (3×5 mL). The combined organic phase was dried over Na_2SO_4 anhydrous and evaporated under reduced pressure to obtain racemic 3-(*tert*-butoxycarbonylamino)oxetane-2-carboxylic acid (**33**) as yellow liquid in 0.3777 g (77% maximum yield). ^{1}H NMR (400 MHz, $CDCl_3$) δ 5.33 (br s, 1H, -N*H*-Boc), 5.07 (d, *J* = 6.9 Hz, 1H, oxetane proton C*H*CO_2H), 4.81 – 4.72 (m, 1H, oxetane proton CH*H*O), 4.71 – 4.61 (m, 1H, oxetane proton C*H*NH), 4.55 (t, *J* = 6.8 Hz, 1H, oxetane proton C*H*HO), 1.47 (s, 9H, -C(O)O-C(CH_3)$_3$).

Boc deprotection and Fmoc protection of racemic 3-(*tert*-butoxycarbonylamino)oxetane-2-carboxylic acid (**33a** and **33b**)

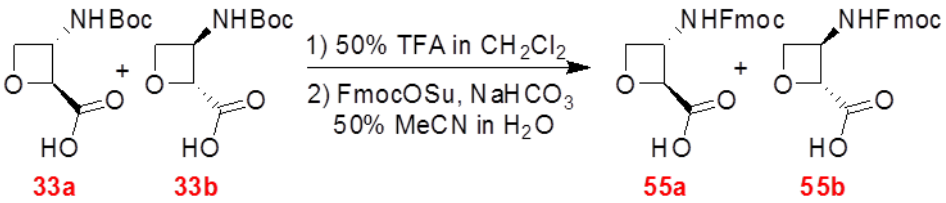

Racemic **33** (0.2492 g, 1.15 mmol) was dissolved in 50% v/v TFA in CH_2Cl_2 (2 mL) and stirred for 15 minutes. The reaction was monitored by TLC (ethyl acetate; ninhydrin, R_f = 0). After the completion of Boc deprotection, the solvent was removed by flushing with nitrogen gas. Then, the crude reaction product was dissolved in a solution of $NaHCO_3$ (0.2717 g, 3.23 mmol) in 50% v/v acetonitrile in water (8 mL). FmocOSu (0.3840 g, 1.15 mmol) was added. The mixture was stirred at ambient temperature for 20 hours and monitored, MeOH:CH_2Cl_2 3:17 with single develop; UV light, R_f = 0.10). After completion, saturated aqueous $NaHCO_3$ was added into the mixture, then, the solution was washed with Et_2O, resulting in precipitation of a white solid in the aqueous phase. The solid was filtered off, washed with 2M HCl followed by water, and dried in a desiccator to obtain racemic-3-(((9*H*-fluoren-9-yl)methoxy)carbonylamino)oxetane-2-carboxylic acid (**55a** and **55b**) with some unknown contaminants as white solid in 0.3077 g (79 %maximum yield). ^{1}H NMR (400 MHz, DMSO-d_6) δ 8.25 (d, *J* = 7.7 Hz, 1H, -N*H*-Fmoc), 7.87 (d, *J* = 7.3 Hz, 2H, Fmoc aromatic C*H*), 7.72 – 7.60 (m, 2H, Fmoc aromatic C*H*), 7.40 (t, *J* = 7.4 Hz, 2H, Fmoc aromatic C*H*), 7.32 (t, *J* = 7.0 Hz, 2H, Fmoc aromatic C*H*), 4.90 (d, *J* = 5.8 Hz, 1H, oxetane proton C*H*CO_2H), 4.62 – 4.50 (m, 2H, oxetane protons C*H*NH and C*H*HO), 4.41 – 4.29 (m, 3H, oxetane proton CH*H*O and Fmoc aliphatic CH_2), 4.28 – 4.15 (m, 1H, Fmoc aliphatic C*H*).

2.4. Synthesis of ((2*R*,3*R*)-3-(benzyloxymethyl)oxiran-2-yl)methanol (50a) *via* stereo selective epoxidation

A key intermediate to control stereochemistry on our proposed enantioselective synthesis of **55a** was epoxide **50a**. In this research, three stereoselective epoxidations were studied to optimize the enantioselectivity expecting to reach at least 90 %ee and gram quantities of the epoxide intermediate **50a**.

2.4.1. Sharpless epoxidation[24]

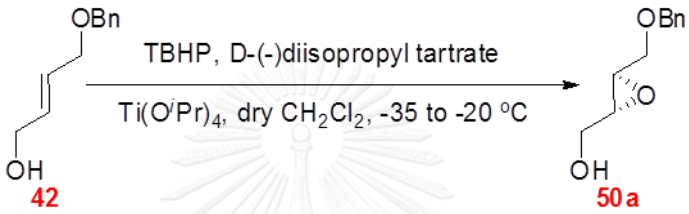

Finely ground 4 Å molecular sieve (0.06 g per 1 mmol of alkene **42**) and distilled CH_2Cl_2 (11 mL per 1 mmol of alkene **42**) were mixed in a round bottom flask under nitrogen atmosphere at -40 °C. Catalytic pre-formation was furnished by adding titanium (IV) isopropoxide and D-(-)diisopropyl tartrate. The solution was stirred for 30 minutes at -40 to -30 °C before adding the alkene **42** through a syringe and leaving the reaction for another 45 minutes. After that solution of 5.5 M *tert*-butylhydroperoxide (TBHP) in nonane (0.46 or 0.70 mL per 1 mmol of alkene **42**) was added dropwise. The reaction was stirred under nitrogen atmosphere at -35 to -20 °C for 19 hours (see exact quantities in Table 2.1). By TLC analysis using hexanes:ethyl acetate 1:1 as mobile phase and ceric molybdate stain as dipping agent, 4 spots including R_f = 0, 0.29, 0.46 and 0.59 were observed. None of these corresponded to compound **42** (R_f = 0.39). After completion of the reaction, water (1 mL per 1 mmol of alkene **42**) was added and the reaction was stirred at 0 °C for 10 minutes. After that saturated solutions of NaCl and NaOH (7 mL per 1 mmol of alkene **42**) was added, then the reaction was stirred at ambient temperature for 10 minutes. Organic phase was separated and aqueous phase was extracted with Et_2O 3 times. The white solid in combined organic phase was removed by vacuum filtration. After that the organic solution was evaporated under reduced pressure and purified by column chromatography on silica gel using gradient mobile phase starting from hexanes:ethyl acetate 9:1 to 3:2 to obtain ((2*R*,3*R*)-3-(benzyloxymethyl)oxiran-2-yl)methanol (**50a**) as yellow liquid which was characterized by ^{1}H NMR and ^{13}C NMR and indicated enantioselectivity in term of % enantiomeric excess (%ee) by chiral column HPLC (column:OJ-H chiral column, mobile phase:15% ^{i}PrOH in *n*-hexane, flow

rate:0.6 mL/min @ 210 nm, t_R major:36.21 min, t_R minor:41.68 min). The results and conditions were illustrated in Table 2.1.

Table 2.1 Conditions and results of Sharpless epoxidation

entry	amount of **42** g (mmol)	TBHP mL (mmol)	D-(-)diisopropyl tatrate mL (mmol)	Ti(O^iPr)$_4$ mL (mmol)	amount of product **50a** g (mmol)	%yield	%ee[b]
1	1.3501 (7.58)	3.45 (15.16)	0.60 (2.8)	0.56 (1.89)	1.1490 (5.91)	78	66
2[a]	1.3479 (4.92)	3.44 (18.92)	2.38 (11.4)	2.24 (7.57)	0.4941 (2.54)	52[c]	40

Note

[a] starting material **42** with contramination of 4-(benzyloxy)butan-1-ol (**49**) in ratio **42**:**49** = 68:32

[b] observation of %ee by chiral HPLC (column:OJ-H chiral column, mobile phase:15% ^{i}PrOH in *n*-hexane, flow rate:0.6 mL/min @ 210 nm, t_R major:36.21 min, t_R minor:41.68 min)

[c] calculation of % yield by focusing on the proportion of **42** which was 4.92 mmol from 7.57 mmol

2.4.2. Shi epoxidation

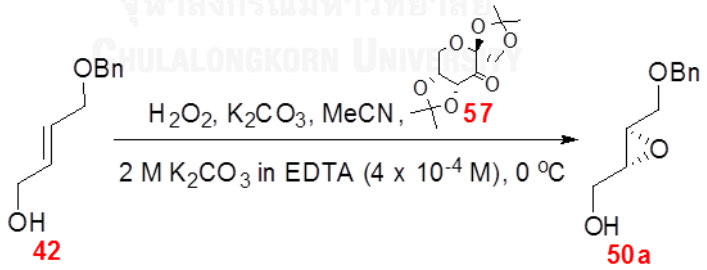

Solution of 2 M potassium carbonate (K_2CO_3) in 0.4 mM ethylenediaminetetraacetic acid (EDTA) in water (1.5 mL per 1 mmol of alkene **42**) was added into a solution of alkene **42** and compound **57** in acetonitrile (1.5 mL per 1 mmol of alkene **42**). Then, 30% w/v hydrogen peroxide (H_2O_2) in water was added dropwise at 0 °C. The reaction was stirred at 0 °C for 24 hours and monitored by TLC using hexanes:ethyl acetate 1:1 as mobile phase and ceric molybdate stain as dipping agent. Two spots, including R_f = 0 and 0.27, were observed and none of these corresponded to the starting material **42** (R_f = 0.37). After that water was added and the solution

was extracted with ethyl acetate 3 times. The combined organic phase was washed with 1 M sodium thiosulfate ($Na_2S_2O_3$) twice, dried over Na_2SO_4 anhydrous, evaporated under reduced pressure and purified by column chromatography on silica gel using gradient mobile phase starting from hexanes:ethyl acetate 9:1 to 13:7 to obtain (3-(benzyloxymethyl)oxiran-2-yl)methanol (**50**, hexanes:ethyl acetate 1:1; ceric molybdate, R_f = 0.27) as yellow liquid which was characterized by ^{1}H NMR, ^{13}C NMR and IR. Chiral HPLC analysis (column:OJ-H chiral column, mobile phase:15% ^{i}PrOH in *n*-hexane, flow rate:0.6 mL/min @ 210 nm, t_R major:36.21 min, t_R minor:41.68 min) and $[\alpha]_D^{23}$ (c 0.5, $CHCl_3$) indicated that the epoxide obtained was a racemic mixture. The results and conditions were illustrated in Table 2.2.

Table 2.2 Conditions of Shi epoxidation

entry	amount of **42** g (mmol)	30% w/v H_2O_2 mL (mmol)	amount of **57** g (mmol)	amount of product **50a** g (mmol)	%yield
1[b]	0.1797 (1.0)	0.45 (4.0)	0.0789 (0.31)	0.0100 (0.05)	5
2[c]	0.1791 (1.0)	4.55 (40.0)	0.0830 (0.32)	0.1306 (0.67)	67

Note

[a] measurement of $[\alpha]_D^{23}$ at 0° (c 0.5, $CHCl_3$)

[b] The starting material **42** (R_f = 0.37) was still observed by TLC analysis after leaving the reaction for 24 h. (recovered in 0.1361g calculating to 76% recovery)

[c] chiral HPLC (column:OJ-H chiral column, mobile phase:15% ^{i}PrOH in *n*-hexane, flow rate:0.6 mL/min @ 210 nm, t_R major:36.21 min, t_R minor:41.68 min) indicated 0 %ee

2.4.3. Jorgensen epoxidation[25]

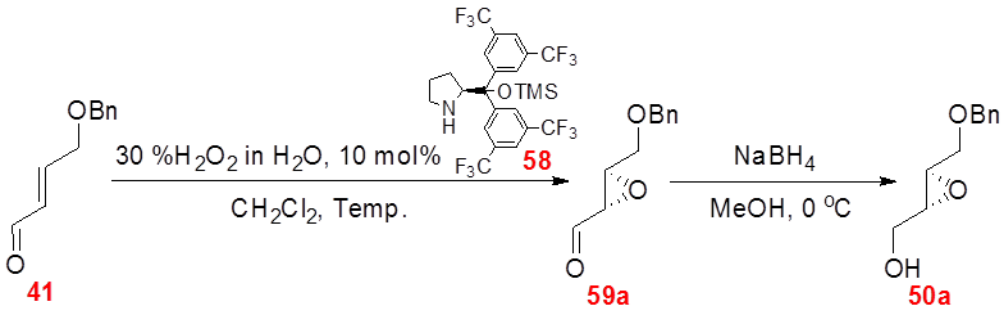

Solution of 30% w/v hydrogen peroxide (H_2O_2) was added dropwise into a solution of compounds **41** and **58** (see exact quantities in Table 2.2) in CH_2Cl_2 (2 mL per 1 mmol of alkene **41)**. The reaction was stirred at controlled temperature for 5 hours to be completed as

monitored by TLC analysis using hexanes:ethyl acetate 3:1 as mobile phase and 2,4-DNP stain as dipping agent. Two spots at R_f = 0 and 0.47 were observed. None of which corresponded to the starting aldehyde **41** (R_f = 0.28). After that, the organic phase was separated and the aqueous phase was re-extracted with CH_2Cl_2 (1 mL per 1 mmol of compound **41**). The combined organic phase was diluted with MeOH (2 mL per 1 mmol of compound **41**). Then, $NaBH_4$ was added into the solution at 0 $^{\circ}$C. The reaction was left for 30 minutes and monitored by TLC using hexanes:ethyl acetate 1:1 as mobile phase. Two spots, R_f = 0.22 and 0.74, were observed under UV light. Both of these spots were not active to 2,4-DNP, indicating a complete reaction. A few mL of water and citric acid were added to neutralize the solution. The solution was evaporated under reduced pressure and dissolved again in CH_2Cl_2 to precipitate remaining salts. Fitlration to collect the filtrate and solvent evaporation were performed. The crude product was purified by column chromatography using gradient mobile phase starting from hexanes:ethyl acetate 9:1 to 13:7 to obtain ((2*R*,3*R*)-3-(benzyloxymethyl)oxiran-2-yl)methanol (**50a**) as yellow liquid which was characterized by ^{1}H NMR and ^{13}C NMR and indicated enantioselectivity in term of % enantiomeric excess (%ee) by chiral column HPLC (column:OJ-H chiral column, mobile phase:15% ^{i}PrOH in *n*-hexane, flow rate:0.6 mL/min @ 210 nm, t_R major:36.21 min, t_R minor:41.68 min) and $[\alpha]_D^{23}$ (c 0.5, $CHCl_3$). The results and conditions are illustrated in Table 2.3.

Table 2.3 Conditions and results of Jorgensen epoxidation

entry	**41** g (mmol)	30% w/v H_2O_2 mL (mmol)	**58** g (mmol)	$NaBH_4$ g (mmol)	**50a** g (mmol)	Temp. ($^{\circ}$C)	%yield	specific rotation at 23 $^{\circ}$C[a]	%ee[c]
1	0.1775 (1.01)	1.50 (13.0)	0.0581 (0.10)	0.0431 (1.14)	0.1072 (0.55)	rt	55	+18.01	92
2	0.1779 (1.01)	1.50 (13.0)	0.0590 (0.10)	0.0392 (1.04)	0.1087 (0.56)	10-20	56	+17.48[b]	94
3	1.0325 (5.86)	8.70 (76.2)	0.3474 (0.58)	0.2230 (5.89)	0.5518 (2.84)	10-20	48	+17.70	95
4	0.7102 (4.0)	0.60 mL (5.2)	0.2300 (0.38)	0.1529 (4.04)	0.5391 (2.78)	10-20	69	+17.70	91

Note

[a] c = 0.5 g/100 mL in chloroform

[b] specific rotation at 22 $^{\circ}$C

[c] observation of %ee by chiral HPLC (column:OJ-H chiral column, mobile phase:15% ^{i}PrOH in *n*-hexane, flow rate:0.6 mL/min @ 210 nm, t_R major:36.21 min, t_R minor:41.68 min)

IR (thin film): 3415, 2921, 2863, 1456, 1280, 1106 cm^{-1}. ^{1}H NMR (400 MHz, $CDCl_3$) δ 7.48 – 7.26 (m, 5H, C_6H_5), 4.60 (ABq, *J* = 11.9 Hz, 2H, -O-CH_2-Ph), 3.95 (dd, *J* = 12.7, 1.8 Hz, 1H, -CH*H*-OBn), 3.79 (dd, *J* = 11.5, 3.0 Hz, 1H, -CH*H*-OH), 3.67 (dd, *J* = 12.5, 3.4 Hz, 1H, -*CH*H-OBn), 3.55 (dd, *J* = 11.5, 5.5 Hz, 1H, -*CH*H-OH), 3.26 (dt, *J* = 5.4, 2.7 Hz, 1H, epoxide proton), 3.12 (dt, *J* = 4.5, 2.4 Hz, 1H, epoxide proton). ^{13}C NMR (100 MHz, $CDCl_3$) δ 137.82, 128.46, 127.83, 127.78, 73.40, 69.67, 61.20, 55.77, 54.30. HRMS (ESI+): m/z calcd for $C_{11}H_{14}O_3Na$ [M + Na^+], 217.0841; found, 217.0838.

2.5. Synthesis of (2*S*,3*S*)-3-(((9*H*-fluoren-9-yl)methoxy)carbonylamino)oxetane-2-carboxylic acid (55a) starting from ((2*R*,3*R*)-3-(benzyloxymethyl)oxiran-2-yl)methanol (50a)

After the key intermediate ((2*R*,3*R*)-3-(benzyloxymethyl)oxiran-2-yl)methanol **50a** was synthesized in enantioenriched form. Synthesis of enantiomerically enriched (2*S*,3*S*)-3-(((9*H*-fluoren-9-yl)methoxy)-carbonylamino)oxetane-2-carboxylic acid (**55a**) was accomplished following the procedure described in the racemic model (Figures 2.4 and 2.5) as shown in Figure 2.6.

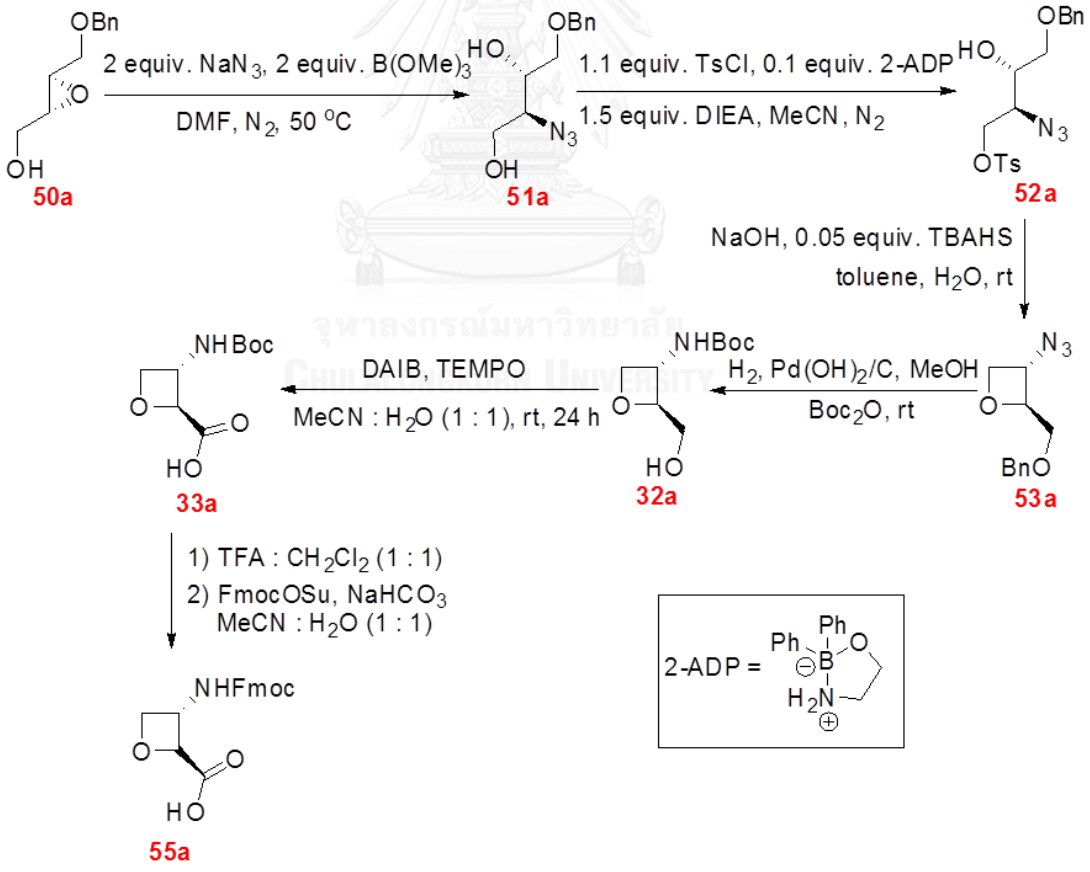

Figure 2.6 Improved pathway to synthesize **55a** starting from **50a**

Azide ring opening of ((2*R*,3*R*)-3-(benzyloxymethyl)oxiran-2-yl)methanol (**50a**)[23]

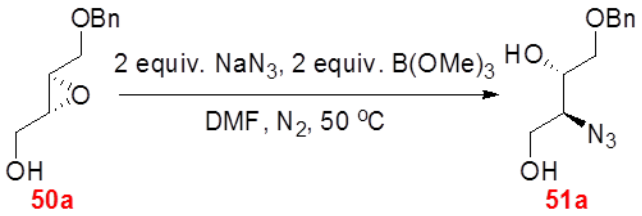

Following the same protocol for ring opening of racemic (3-(benzyloxymethyl)oxiran-2-yl)methanol (**50a** and **50b**) by sodium azide using epoxide **50a** (1.0234 g, 5.27 mmol**,** 91**%** ee), NaN_3 (0.6853 g, 10.54 mmol), and $B(OMe)_3$ (1.18 mL, 10.54 mmol) in anhydrous DMF (5 mL) to obtain (2*S*,3*S*)-2-azido-4-(benzyloxy)butane-1,3-diol (**51a**) as yellow liquid in 1.1371 g (91% yield, CH_2Cl_2:acetone 9:1; ceric molybdate, R_f = 0.26). $[\alpha]_D^{23}$ +22.4° (c 1.0, $CHCl_3$). IR (thin film): 3404, 2921, 2866, 2096, 1453, 1074 cm^{-1}. ^{1}H NMR (400 MHz, $CDCl_3$) δ 7.38 – 7.18 (m, 5H, C_6H_5), 4.50 (s, 2H -O-CH_2-Ph), 3.91 – 3.43 (m, 6H, -CH_2-OBn, -C(OH)*H*-CH_2-OBn, -CH_2-OH and -C(N_3)*H*-CH_2-OH). ^{13}C NMR (100 MHz, $CDCl_3$) δ 137.41, 128.59, 128.08, 127.94, 73.64, 70.96, 70.75, 63.94, 62.76. HRMS (ESI+): m/z calcd for $C_{11}H_{15}N_3O_3Na$ [M + Na^+], 260.1011; found, 260.1016.

Tosylation of (2*S*,3*S*)-2-azido-4-(benzyloxy)butane-1,3-diol (**51a**) *via* borinate complex

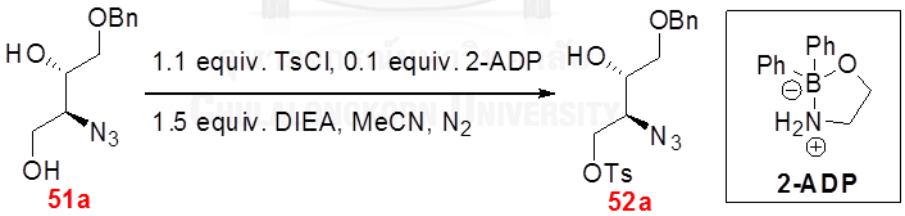

Following the same protocol for tosylation of racemic 2-azido-4-(benzyloxy)butane-1,3-diol (**51a** and **51b**) *via* borinate complex using **51a** (0.5657 g, 2.39 mmol), 2-ADP (0.0535 g, 0.24 mmol), TsCl (0.5262 g, 2.75 mmol), DIEA (0.63 mL, 3.59 mmol), and finely ground 4 Å molecular sieve (0.0619 g, 10%wt of compound **51a**) in distilled acetonitrile (10 mL) to obtain (2*S*,3*S*)-2-azido-4-(benzyloxy)-3-hydroxybutyl 4-methylbenzenesulfonate (**52a)** as yellow liquid in 0.5830 g (62% yield, hexanes:ethyl acetate 1:1; ceric molybdate, R_f = 0.46). $[\alpha]_D^{22}$ +23.9° (c 1.0, $CHCl_3$). IR (thin film): 3519, 2923, 2860, 2099, 1453, 1361, 1173 cm^{-1}. ^{1}H NMR (400 MHz, $CDCl_3$) δ 7.74 (d, *J* = 8.2 Hz, 2H, -$C_6H_2H_2$-CH_3), 7.32 – 7.21 (m, 7H, -C_6H_5 and -$C_6H_2H_2$-CH_3), 4.47 (s, 2H, -O-CH_2-Ph), 4.34 (dd, *J* = 10.6, 2.8 Hz, 1H, -CH*H*-OTs), 4.06 (dd, *J* = 10.6, 7.4 Hz, 1H, -C*H*H-OTs), 3.65 (td, *J* = 7.7, 2.7 Hz, 1H, -C(OH)*H*-CH_2-OBn), 3.61 – 3.54 (m, 1H, -C(N_3)*H*-CH_2-OTs), 3.53 – 3.50 (m, 2H, -CH_2-OBn), 2.37

(s, 3H, -C_6H_4-CH_3). ^{13}C NMR (100 MHz, $CDCl_3$) δ 145.14, 137.29, 132.67, 129.95, 128.59, 128.10, 128.02, 127.89, 73.61, 70.19, 69.55, 69.53, 61.60, 21.66. HRMS (ESI+): m/z calcd for $C_{18}H_{21}N_3O_5SNa$ [M + Na^+], 414.1100; found, 414.1091.

Cyclization of (2*S*,3*S*)-2-azido-4-(benzyloxy)-3-hydroxybutyl 4-methylbenzenesulfonate (**52a**) to oxetane

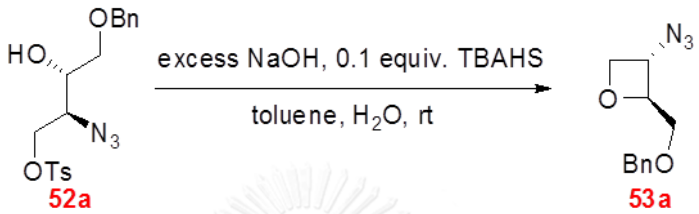

Following the same protocol for cyclization of racemic 2-azido-4-(benzyloxy)-3-hydroxybutyl 4-methylbenzenesulfonate (**52a** and **52b**) to oxetane using compound **52a** (1.3543 g, 3.46 mmol), tetrabutyl ammonium hydrogen sulfate (0.1258 g, 0.35 mmol), finely ground NaOH (5.6721 g, 21.5 mmol), and water (300 μL) in toluene (35 mL) to obtain (2*S*,3*S*)-3-azido-2-(benzyloxy-methyl)oxetane (**53a**) as yellow liquid in 0.5198 g (69% yield, hexanes:ethyl acetate 3:1; ceric molybdate, R_f = 0.42). $[\alpha]_D^{22}$ +49.0° (c 1.0, $CHCl_3$). IR (thin film): 3100-3000, 3000-2800, 2102 cm^{-1}. ^{1}H NMR (400 MHz, $CDCl_3$) δ 7.43 – 7.30 (m, 5H, -C_6H_5), 4.82 (m, 1H, oxetane proton), 4.77 – 4.66 (m, 2H, oxetane protons), 4.64 – 4.60 (m, 1H, oxetane proton), 4.58 – 4.51 (m, 2H, -O-CH_2-Ph), 3.69 (dd, *J* = 3.5, 0.9 Hz, 2H, -CH_2-OBn). ^{13}C NMR (100 MHz, $CDCl_3$) δ 137.84, 128.49, 127.84, 127.71, 86.75, 73.76, 73.54, 70.42, 55.53. HRMS (ESI+): m/z calcd for $C_{11}H_{13}N_3O_2Na$ [M + Na^+], 242.0905; found, 242.0901.

Reduction, Boc-protection and debenzylation of (2*S*,3*S*)-3-azido-2-(benzyloxy-methyl)oxetane (**53a**)

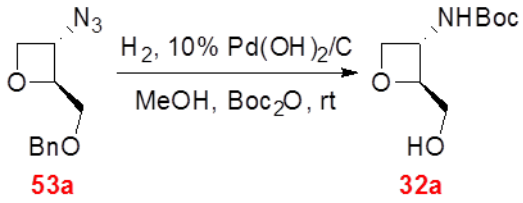

Following the same protocol for reduction Boc-protection and debenzylation of racemic 3-azido-2-(benzyloxy-methyl)oxetane (**53a** and **53b**) using oxetane **53a** (0.4998 g, 2.28 mmol), Boc_2O (0.5451 g, 2.5 mmol), and 10% $Pd(OH)_2/C$ (0.1008 g, 20%wt of compound **53a**) in MeOH (3 mL) to obtain *tert*-butyl (2*S*,3*S*)-2-(hydroxymethyl)oxetan-3-ylcarbamate (**32a**) as yellow liquid in 0.3751 g (81% yield, ethyl acetate; ninhydrin, R_f = 0.44). $[\alpha]_D^{22}$ –5° (*c* 0.5, $CHCl_3$). IR (ATR): 3328, 3000-2800, 1688, 1529, 1166 cm^{-1}. ^1H NMR (400 MHz, $CDCl_3$) δ 5.20 (br s, 1H, -N*H*-Boc), 4.73 – 4.57 (m, 3H, oxetane protons C*H*-CH_2OH, *CH*NH and *CH*HO), 4.44 (t, *J* = 6.4 Hz, 1H, oxetane proton CH*H*O), 3.86 – 3.70 (m, 2H, -C*H*$_2$-OH), 1.46 (s, 9H, -C(O)O-C(CH_3)$_3$). ^{13}C NMR (100 MHz, $CDCl_3$) δ 155.11, 89.79, 80.49, 74.22, 63.57, 47.30, 28.31. HRMS (ESI+): m/z calcd for $C_9H_{17}NO_4Na$ [M + Na^+], 226.1055; found, 226.1051.

Oxidation of *tert*-butyl (2*S*,3*S*)-2-(hydroxymethyl)oxetan-3-ylcarbamate (**32a**) to carboxylic acid

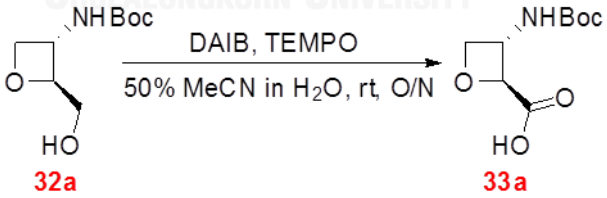

Following the same protocol for oxidation of racemic *tert*-butyl (2*S*,3*S*)-2-(hydroxymethyl)oxetan-3-ylcarbamate (**32a** and **32b**) to carboxylic acid using compound **32a** (0.1537 g, 0.76 mmol), DAIB (0.5453 g, 1.69 mmol), and TEMPO (0.0320 g, 0.20 mmol) in 50% v/v acetonitrile in water (4 mL) to obtain (2*S*,3*S*)-3-(*tert*-butoxycarbonylamino)oxetane-2-carboxylic acid (**33a**) as yellow liquid in 0.1422 g (87% yield, hexanes:ethyl acetate 1:3; ninhydrin, R_f = 0.10). $[\alpha]_D^{22}$ -18.1° (c 1.0, $CHCl_3$). IR (ATR): 3325, 3000-2800, 1713, 1688, 1524, 1158 cm^{-1}. ^1H NMR (400 MHz, $CDCl_3$) δ 5.60 (br s, 1H, -N*H*-Boc), 5.09 (d, *J* = 5.5 Hz, 1H, oxetane proton C*H*CO_2H), 4.84 –

4.78 (m, 1H, oxetane proton CH*H*O), 4.78 – 4.70 (m, 1H, oxetane proton C*H*NH), 4.59 (t, *J* = 6.0 Hz, 1H, oxetane proton C*H*HO), 1.48 (s, 9H, -C(O)O-C(C*H*$_3$)$_3$). ^{13}C NMR (100 MHz, $CDCl_3$) δ 171.47, 156.10, 84.03, 82.09, 73.78, 49.21, 28.23. HRMS (ESI+): m/z calcd for $C_9H_{15}NO_5Na$ [M + Na^+], 240.0848; found, 240.0843.

Fmoc protection of (2*S*,3*S*)-3-(*tert*-butoxycarbonylamino)oxetane-2-carboxylic acid (**33a**)

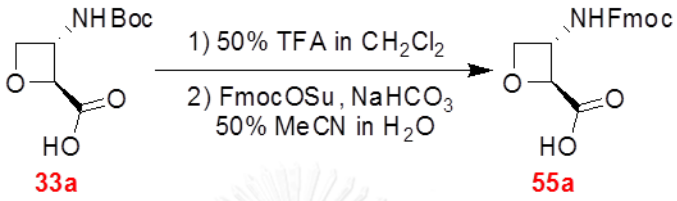

Following the same protocol for Boc deprotection and Fmoc protection of racemic 3-(*tert*-butoxycarbonylamino)oxetane-2-carboxylic acid (**33a** and **33b**); 1) Boc deprotection step: using Boc-acid **33a** (0.1322 g, 0.52 mmol) in 50% v/v TFA in CH_2Cl_2 (2 mL). 2) Fmoc protection: FmocOSu (0.1748 g, 0.52 mmol) and $NaHCO_3$ (0.1255 g, 1.49 mmol) in 50% v/v acetonitrile in water (8 mL) to obtain (2S,3S)-3-(((9*H*-fluoren-9-yl)methoxy)carbonylamino)oxetane-2-carboxylic acid (**55a**) as white solid in 0.1131 g (64% yield, MeOH:CH_2Cl_2 3:17 with single develop; UV light, R_f = 0.10). Mp: 142-144 °C $[\alpha]_D^{22}$ +19.8° (c 0.5,DMSO). IR (ATR): 3325, 3100-3000, 3000-2800, 1696, 1530, 1256 cm^{-1}. ^{1}H NMR (400 MHz, DMSO-d_6) δ 8.25 (d, *J* = 6.9 Hz, 1H, -N*H*-Fmoc), 7.90 (d, *J* = 7.5 Hz, 2H, Fmoc aromatic C*H*), 7.75 – 7.65 (m, 2H Fmoc aromatic C*H*), 7.43 (t, *J* = 7.4 Hz, 2H, Fmoc aromatic C*H*), 7.34 (t, *J* = 7.3 Hz, 2H, Fmoc aromatic C*H*), 4.93 (d, *J* = 5.3 Hz, 1H, oxetane proton C*H*CO_2H), 4.65 – 4.55 (m, 2H, oxetane protons C*H*NH and C*H*HO), 4.45 – 4.28 (m, 3H, oxetane proton CH*H*O and Fmoc aliphatic CH_2), 4.24 (t, *J* = 6.3 Hz, 1H, Fmoc aliphatic C*H*). ^{13}C NMR (100 MHz, DMSO-d_6) δ 171.47, 155.09, 143.76, 140.75, 127.62, 127.07, 125.03, 120.12, 83.45, 74.53, 65.55, 49.10, 46.63. HRMS (ESI+): m/z calcd for $C_{19}H_{17}NO_5Na$ [M + Na^+], 362.1004; found, 362.1008.

Activation of (2*S*,3*S*)-3-(((9*H*-fluoren-9-yl)methoxy)carbonylamino)oxetane-2-carboxylic acid (**55a**) as pentafluorophenyl ester

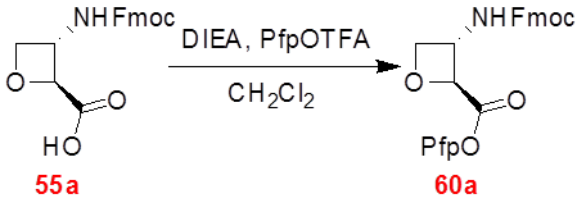

Fmoc-*epi*-oxetin **55a** (0.1134 g, 0.33 mmol) was suspended in CH_2Cl_2 (1 mL). DIEA (58 μL) and pentafluorophenyl trifluoroacetate (PfpOTfa, 57 μL) were added into the solution. The reaction was monitored by TLC (hexanes:ethyl acetate 1:1; UV light, R_f = 0.63). After the completion, the reaction mixture was diluted with CH_2Cl_2 and washed twice with 2N HCl, followed by water and saturated $NaHCO_3$ (twice each). Organic phase was evaporated and the residue was washed with hexanes to obtain compound **60a** as a pink solid in 0.0461 g (28% yield) which was used in PNA synthesis without further purification.

2.6. Synthesis of methyl 3-(((9*H*-fluoren-9-yl)methoxy)carbonylamino)oxetane-2-carboxylate (61) for determination of enantiomeric purity of 55a

The enantiomeric purity of **55a** was determined by chiral HPLC. However, since the available chiral column (OJ-H) operates in normal phase mode, conversion of the carboxylic acid **55a** to the less polar methyl ester **61a** is required. This was achieved by methylation with diazomethane.

Methylation of racemic-3-(((9*H*-fluoren-9-yl)methoxy)carbonylamino)oxetane-2-carboxylic acid (**55a** and **55b**)

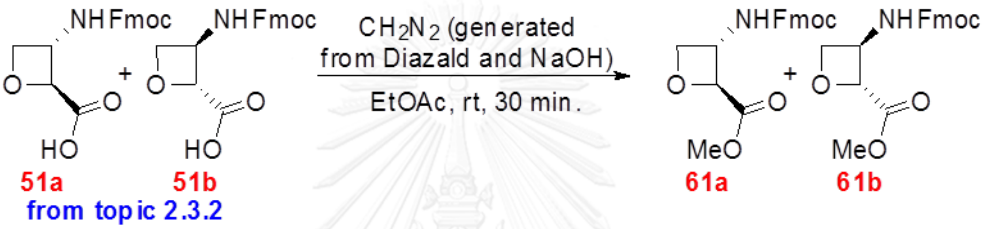

Racemic **55** (0.0972 g, 0.29 mmol, from 2.3.2) was suspended into ethyl acetate (5 mL). In a separated container, a solution of Diazald™ (0.1894 g, 0.88 mmol) in EtOH (2 mL) was mixed with 5 M NaOH (2 mL) resulting in generation of diazomethane, which was bubbled into the solution of **55** with the aid of N_2 stream at ambient temperature for 30 minutes. After the reaction was completed as monitored by TLC (hexanes: ethyl acetate 1:1; UV light, R_f = 0.34), the solution was evaporated to dryness by flushing with N_2 and purified by column chromatography on silica gel using hexanes:ethyl acetate 7:3 as isocratic mobile phase to obtain racemic-methyl 3-(((9*H*-fluoren-9-yl)methoxy)carbonylamino)oxetane-2-carboxylate (**61a** and **61b**) as white solid in 0.0480 g (28% yield over 3 steps, hexanes:ethyl acetate 1:1; UV light, R_f = 0.34). Mp: 127-129 $^{\circ}$C, IR (ATR): 3302, 3100-2850, 1735, 1697, 1542, 1262 cm^{-1}. ^{1}H NMR (400 MHz, $CDCl_3$) δ 7.68 (d, *J* = 7.5 Hz, 2H, Fmoc aromatic C*H*), 7.49 (d, *J* = 6.5 Hz, 2H, Fmoc aromatic C*H*), 7.32 (t, *J* = 7.4 Hz, 2H, Fmoc aromatic C*H*), 7.23 (t, *J* = 7.4 Hz, 2H, Fmoc aromatic C*H*), 5.34 (d, *J* = 6.1 Hz, 1H, -N*H*-Fmoc), 4.94 (s, 1H, oxetane proton C*H*CO_2H), 4.74 (s, 2H, oxetane protons C*H*NH and C*H*HO), 4.52 – 4.27 (m, 3H, oxetane proton CH*H*O and Fmoc aliphatic CH_2), 4.12 (t, *J* = 6.3 Hz, 1H, Fmoc aliphatic C*H*), 3.72 (s, 3H, -CO_2CH_3). ^{13}C NMR (100 MHz, $CDCl_3$) δ 170.32, 155.11, 143.66, 141.39, 127.83, 127.12, 124.87, 120.08, 84.38, 76.07, 67.00, 52.46, 49.73, 47.16. HRMS (ESI+): m/z calcd for $C_{19}H_{17}NO_5Na$ [M + Na^+], 376.1161; found, 376.1167.

Methylation of (2*S*,3*S*)-3-(((9*H*-fluoren-9-yl)methoxy)carbonylamino)oxetane-2-carboxylic acid (**55a**)

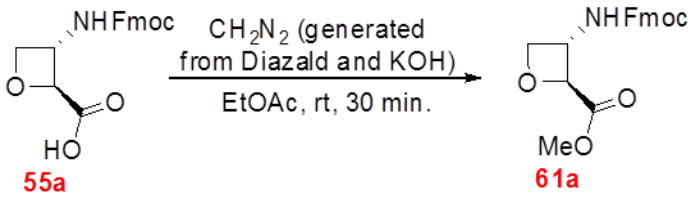

Following the same protocol for methylation of racemic-3-(((9*H*-fluoren-9-yl)methoxy)carbonylamino)oxetane-2-carboxylic acid (**55a** and **55b**) using compound **55a** (0.0150 g, 0.044 mmol), ethyl acetate (0.5 mL), Diazald™ (0.0287 g, 0.13 mmol), 5 M NaOH in water (0.5 mL) and EtOH (2 mL) to obtain (2*S*,3*S*)-methyl 3-(((9*H*-fluoren-9-yl)methoxy)carbonylamino)oxetane-2-carboxylate (**61a**) as white solid in 0.0154 g (99% yield, hexanes:ethyl acetate 1:1; UV light, R_f = 0.34). Mp: 157-159 °C, 94%ee was determine by chiral HPLC (column:OJ-H chiral column, mobile phase:70% ^{i}PrOH in *n*-hexane, flow rate: 1.0 mL/min @ 270 nm, t_R minor:23.13 min, t_R major:26.85 min). $[\alpha]_D^{23}$ +10.8° (c 0.5, $CHCl_3$). IR (ATR): 3303, 3100-2850, 1737, 1695, 1540, 1264 cm^{-1}. ^{1}H NMR (400 MHz, $CDCl_3$) δ 7.69 (d, *J* = 7.5 Hz, 2H, Fmoc aromatic C*H*), 7.49 (d, *J* = 6.5 Hz, 2H, Fmoc aromatic C*H*), 7.33 (t, *J* = 7.4 Hz, 2H, Fmoc aromatic C*H*), 7.24 (t, *J* = 7.3 Hz, 2H, Fmoc aromatic C*H*), 5.34 (s, 1H, -N*H*-Fmoc), 4.95 (s, 1H, oxetane proton C*H*CO_2H), 4.75 (s, 2H, oxetane protons C*H*NH and C*H*HO), 4.35-4.50 (m, 3H, oxetane proton CH*H*O and Fmoc aliphatic CH_2), 4.13 (t, *J* = 6.3 Hz, 1H, Fmoc aliphatic C*H*), 3.73 (s, 3H, -CO_2CH_3). ^{13}C NMR (100 MHz, $CDCl_3$) δ 170.28, 155.07, 143.65, 141.39, 127.83, 127.12, 124.87, 120.08, 84.40, 76.08, 67.03, 52.46, 49.74, 47.16. HRMS (ESI+): m/z calcd for $C_{19}H_{17}NO_5Na$ [M + Na^+], 376.1161; found, 376.1176.

2.7. Synthesis of racemic-3-benzamidooxetane-2-carboxylic acid (63) for mechanistic study

Synthesis of racemic-3-benzamidooxetane-2-carboxylic acid (**63a** and **63b**) was accomplished by following the procedure as shown in Figure 2.7, starting from racemic-*tert*-butyl-2-(hydroxymethyl)oxetan-3-ylcarbamate (**32a** and **32b**).

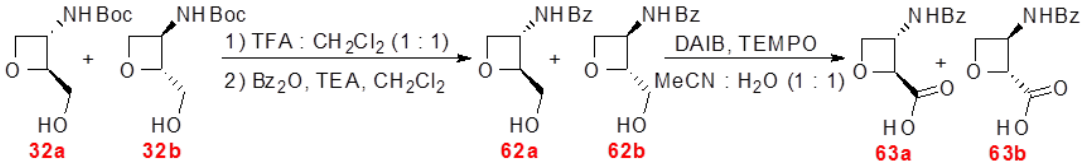

Figure 2.7 Synthesis of racemic **63** from racemic **32** through intermediate **62**

Benzoyl protection of racemic-*tert*-butyl (2*S*,3*S*)-2-(hydroxymethyl)oxetan-3-ylcarbamate (**32a** and **32b**)

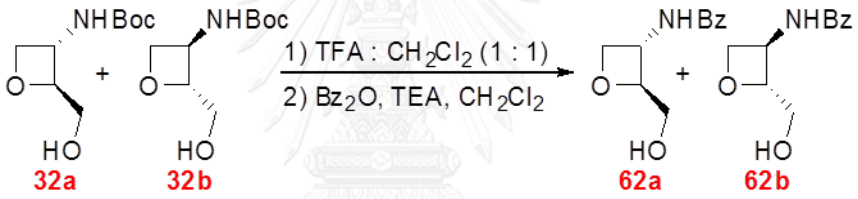

Racemic **32** (0.1002 g, 0.49 mmol) was dissolved in 50% v/v TFA:CH_2Cl_2 (1 mL) and stirred for 15 minutes. The reaction was neutralized with TEA, and the solvent was removed under a stream of N_2. The crude reaction product was dissolved in CH_2Cl_2 (5 mL), containing TEA (70 μL, 0.49 mmol). The solution was treated with Bz_2O (0.1115 g, 0.49 mmol). The reaction was stirred at ambient temperature for 2 hours and monitored by TLC (CH_2Cl_2:ethyl acetate 1:1, R_f = 0.17). Then, crude reaction product was obtained by evaporation and purified by column chromatography on silica gel using CH_2Cl_2:ethyl acetate 1:1 as isocratic mobile phase to obtain racemic-*N*-(2-(hydroxymethyl)oxetan-3-yl)benzamide (**62a** and **62b**) as syrup in 0.0636 g (45% yield). IR (ATR): 3377, 3307, 3100-2900, 1632, 1531, 1027, 952 cm^{-1}. ^{1}H NMR (400 MHz, $CDCl_3$) δ 7.82 (d, *J* = 7.5 Hz, 2H, C(O)$C_5H_2H_3$), 7.54 (t, *J* = 7.2 Hz, 1H, C(O)C_5H_4H), 7.44 (t, *J* = 7.5 Hz, 2H, C(O)$C_5H_2H_2H$), 7.20 (d, *J* = 4.4 Hz, 1H, -N*H*-Bz), 5.05 – 4.89 (m, 1H, oxetane proton C*H*-CH_2OH), 4.88 – 4.71 (m, 2H, oxetane protons C*H*NH and C*H*HO), 4.64 (t, *J* = 6.5 Hz, 1H, oxetane proton CH*H*O), 3.85 (qd, *J* = 12.1, 3.9 Hz, 2H, -CH_2-OH). ^{13}C NMR (100 MHz, $CDCl_3$) δ 167.77, 133.28, 132.12, 128.71, 127.13, 89.62, 73.74, 63.80, 47.44. HRMS (ESI+): m/z calcd for $C_{11}H_{14}NO_3$ [M + H^+], 208.0974; found, 208.0998.

Oxidation of racemic-*N*-(2-(hydroxymethyl)oxetan-3-yl)benzamide (**62a** and **62b**) to carboxylic acid

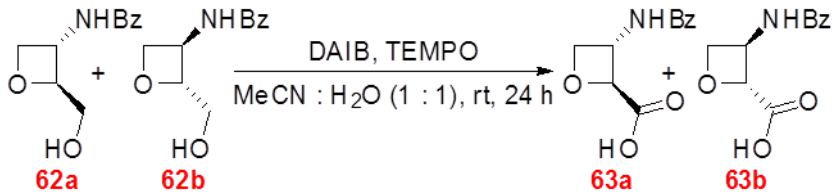

Following the same protocol for oxidation of racemic *tert*-butyl (2*S*,3*S*)-2-(hydroxymethyl)oxetan-3-ylcarbamate (**32a** and **32b**) to carboxylic acid using racemate **62** (0.0470 g, 0.23 mmol), and DAIB (0.1778 g, 0.55 mmol), and TEMPO (0.0125 g, 0.35 mmol) in 50% v/v acetonitrile in water (4 mL) to obtain racemic-3-benzamidooxetane-2-carboxylic acid (**63a** and **63b**) as syrub in 0.0160 g (44% yield, MeOH:CH_2Cl_2 3:17; UV light, R_f = 0.07). IR (ATR): 3320, 3100-2800, 1777, 1645, 1536, 970 cm^{-1}. ^{1}H NMR (400 MHz, DMSO-d_6) δ 9.31 (d, *J* = 7.3 Hz, 1H, -N*H*-Bz), 7.90 (d, *J* = 7.4 Hz, 2H, C(O)$C_5H_2H_3$), 7.58 (t, *J* = 7.2 Hz, 1H, C(O)C_5H_4H), 7.51 (t, *J* = 7.4 Hz, 2H, C(O)$C_5H_2H_2$H), 5.12 (d, *J* = 6.5 Hz, 1H, oxetane proton C*H*CO_2H), 5.08 – 4.99 (m, 1H, oxetane proton C*H*NH), 4.69 (t, *J* = 6.8 Hz, 1H, oxetane proton C*H*HO), 4.57 (t, *J* = 6.3 Hz, 1H, oxetane proton CH*H*O). ^{13}C NMR (100 MHz, DMSO-d_6) δ 171.52, 165.92, 133.54, 131.63, 128.36, 127.34, 83.06, 74.50, 47.80. HRMS (ESI+): m/z calcd for $C_{11}H_{12}NO_4$ [M + H^+], 222.0766; found, 222.0782.

2.8. Synthesis and characterization of aocPNA

2.8.1. Synthesis of aocPNA

The aocPNA was synthesized on Tentagel S-RAM resin (0.24 mmol/g loading) by Fmoc-solid phase peptide synthesis (Fmoc-SPSS) at 1.5 μmol scale from the four Fmoc-protected pyrrolidinyl PNA monomers (Fmoc-A^{Bz}-Opfp, Fmoc-T-Opfp, Fmoc-C^{Bz}-Opfp and Fmoc-G^{Ibu}-OH)[5] and Pfp-activated *epi*-oxetin spacer **60a**. The PNA synthesis followed the protocols previously developed for acpcPNA,[26] which consisted of three reaction 3 steps, namely 1. Fmoc deprotection 2.coupling 3.capping.

First, Fmoc-L-Lys(Mtt)-OH was coupled to the solid support as the starting point on the *C*-terminal to improve water solubility. The synthesis began with Fmoc deprotection by treating the solid support with 100 μL of 20% (v/v) piperidine and 2% (v/v) DBU in DMF for 5 minutes. Then, the coupling of Fmoc-L-Lys(Mtt)-OH (3.9 equiv.) was performed by activation with *O*-(7-azabenzotriazol-1-yl)-*N*,*N*,*N*',*N*'-tetramethyluronium hexafluorophosphate (HATU) (4 equiv.) and

DIEA (8 equiv.) in 30 μL of DMF for 40 minutes. Next, the capping step was performed using a mixture of 5 μL of acetic anhydride and 30 μL of 7% (v/v) DIEA in DMF for 5 minutes.

The cycle of deprotection-coupling-capping was repeated with the PNA monomer instead of lysine. For coupling of activated PNA monomers including Fmoc-A^{Bz}-OPfp, Fmoc-T-OPfp and Fmoc-C^{Bz}-OPfp, the Fmoc-deprotected solid support was treated with 4 equiv. of PNA monomers, 4 equiv. of 1-hydroxy-7-azabenzotriazole (HOAt) and 4 equiv. of DIEA in 30 μL of DMF for 40 minutes. For free acid-PNA monomer (Fmoc-G^{Ibu}-OH), activation by HATU was required. This was carried out exactly the same way as for the coupling of lysine monomer.

The next step was coupling of activated *epi*-oxetin spacer **60a** following the same deprotection-coupling-capping cycle and using the same coupling condition as activated PNA monomers. The coupling of PNA monomers and *epi*-oxetin spacer **60a** were performed sequcncially until the desired sequence of PNA was obtained. The remaining Fmoc was removed, and the amino group of the PNA was optionally capped by acetylation or benzoylation as shown in Figure 2.8 using the same procedure for corresponding pyrrolidinyl PNAs.[5]

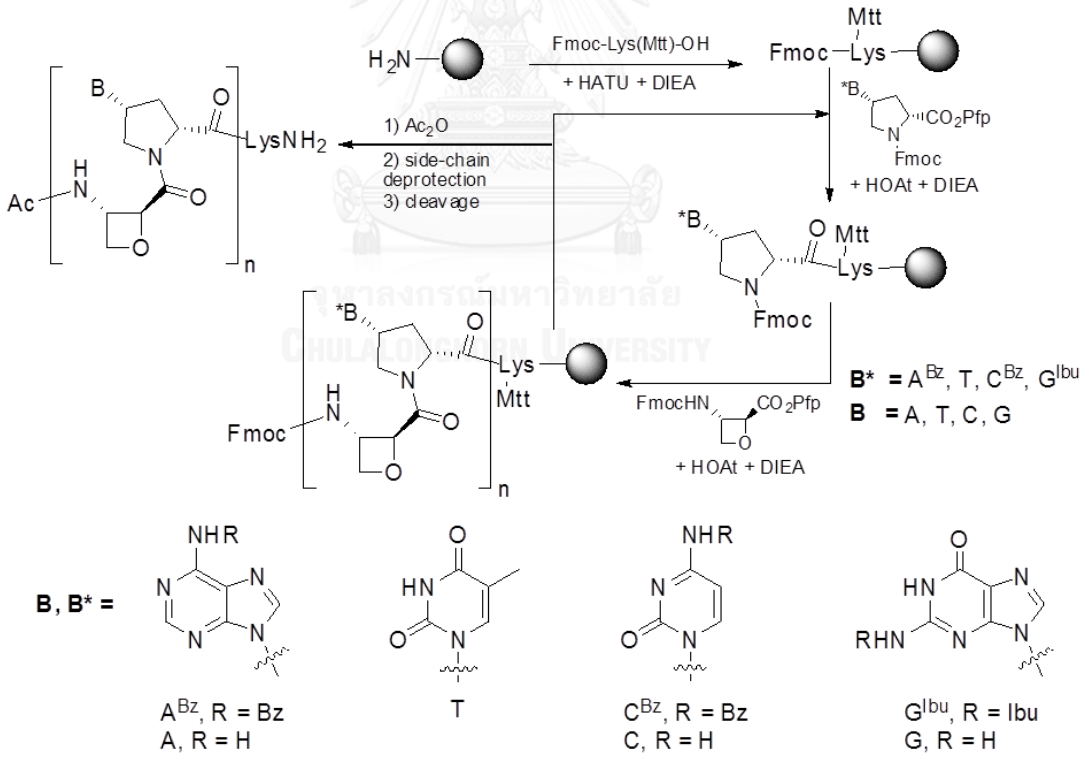

Note: Bz = benzoyl and Ibu = isobutyryl

Figure 2.8 Synthesis of aocPNA *via* Fmoc-SPPS

For monitoring the progress of the reaction, the nucleobase was deprotected by treatment with 1:1:2 *tert*-butylamine:MeOH:H_2O at 60 $^{\circ}C$ for 2 hours followed by cleavage of the PNA from the solid support by treatment with TFA for 10 minutes and MALDI-TOF mass spectrometric analysis as described in 2.8.5.2.

2.8.2. Studying of coupling efficiency in synthesis of aocPNA

Coupling efficiency of aocPNA synthesis was determined spectrophotometrically after completion of aocPNA sequence by measuring the amount of deprotected Fmoc group in the final deprotection reaction. The measured absorbance at 264 nm converted into the amount of free amino group at *N*-terminal according to equation 1.[27] This was further calculated to the total amount of PNA, which after division by the synthesis scale, the synthesis efficiency can be estimated.

concentration of free NH_2 group (μmol/L) = $\frac{(OD_{264} + 0.016)}{0.0182}$ (1)

2.8.3. Cleavage of protecting group on aocPNA's nucleobase

The side chain deprotection on aocPNA was investigated in aocPNA with benzoyl protection at the *N*-terminus. In order to figure the suitable deprotection condition, two conditions were studied:

1. deprotection with 1:1 35% (w/v) aqueous ammonia:dioxane at 60 $^{\circ}$C overnight[5]

2. deprotection with 1:1:2 *tert*-butylamine:MeOH:H_2O at 60 $^{\circ}$C at 1, 2 and 2.5 hours[28]

After the completion of side chain deprotection, the aocPNA on solid support was washed with DMF, MeOH and dried by flushing with nitrogen gas. Then, the aocPNA was cleaved from the solid support by treating with 10 μL of TFA for 10 minutes and characterization by MALDI-TOF mass spectrometry (section 2.8.5.2)

2.8.4. Cleavage of aocPNA from solid support

After the studying of side chain deprotection condition, the conditions for cleavage of aocPNA from the solid support were investigated. Four reaction conditions were studied:

1. TFA at ambient temperature for 10 minutes

2. TFA at ambient temperature for 3 hours

3. TFA with 1% (v/v) triisopropylsilane (TIPS) at ambient temperature for 3 hours

4. 50% (v/v) TFA in CH_2Cl_2 at ambient temperature (every 2 minutes followed by immediate precipitation of PNA with Et_2O)

The cleavage reaction was monitored by MALDI-TOF mass spectrometry (section 2.8.5.2)

2.8.5. Purification and characterization of aocPNA

2.8.5.1. Purification of aocPNA by reverse phase HPLC

The crude aocPNA obtained from side chain deprotection and cleavage from solid support was dissolved in water and purified by reverse phase HPLC using ACE 5 A71197, C18-AR, 150 x 4.6 mm, 5 μm particle size column with a mobile phase consisting of 0.1% (v/v) TFA in Milli-Q water (solvent A) and 0.1% (v/v) TFA in methanol (solvent B) as eluent (A:B 90:10 for 5 minutes, followed by linear gradient to 10:90 over 60 minutes). HPLC fractions were collected manually by observation of real-time HPLC chromatogram at 270 nm. The purity of each fraction was determined by MALDI-TOF mass spectrometry as described in section 2.8.5.2. Fractions were combined and neutralized by ammonium bicarbonate in order to reduce decomposition of aocPNA under acidic condition and the combined fraction was freeze-dried.

2.8.5.2. aocPNA characterization by MALDI-TOF mass spectrometry

All PNAs were characterized by MALDI-TOF mass spectrometry using α-cyano-4-hydroxycinnamic acid (CCA) as matrix. Samples were prepared by mixing 2 μL of PNA solution with 8 μL of CCA solution, fixed to target plate and run under linear positive ion mode, using LSI laser and electro potential 19.00, 9.00 and 20.00 kV on ion source, lens and reflector respectively at 6.4 x 10^{-7} mbar.

2.8.5.3. Analysis of aocPNA purity by reverse phase HPLC

The purity of the aocPNA was analyzed by reverse phase HPLC on Vertisep UPS, 50 x 4.6 mm, 3 μm particle size HPLC column with a mobile phase consisting of 0.1% (v/v) TFA in Milli-Q water (solvent A) and 0.1% (v/v) TFA in methanol (solvent B) as eluent (A:B 90:10 for 5 minutes, followed by linear gradient to 10:90 over 35 minutes). The composition of the mixed solvent was returned to 90:10 solvent A:B again at 40 minutes with constant rate declining and retained in this proportion until completion of analysis.

2.8.6. Determination of aocPNA concentration

The concentration of aocPNA was determined spectrophotometrically at 260 nm using a Nanodrop 2000 spectrophotometer. According to Beer's law, the concentration was calculated from the absorbance at 260 nm according to equation 2. Extinction coefficients of aocPNA (ε) was calculated from summation of extinction coefficients (ε) of all nucleobases :8.8 mL μmol^{-1} cm^{-1} (T), 10.8 mL μmol^{-1} cm^{-1} (A), 7.4 mL μmol^{-1} cm^{-1} (C) and 11.5 mL μmol^{-1} cm^{-1} (G). (Reference from http://www.chemistry.sc.chula.ac.th/pna/pna.asp)

$$A = \varepsilon cl \qquad (2)$$

when A = absorbance

ε = extinction coefficients (L mol^{-1} cm^{-1})

l = path length (cm)

c = concentration of PNA sample in solution (M)

2.9. Investigation of aocPNA binding properties to DNA/RNA

Thermal denaturation was performed using cuvette with path length = 1 cm under 1000 μL of solution 1 μM aocPNA and DNA/RNA in aqueous 10 mM sodium phosphate buffer pH 7 and 100 mM NaCl. UV absorbtion at 260 nm was collected every 1 $^{\circ}$C between 20-90 $^{\circ}$C with 1

°C/min heating rate. Each observed absorbance at each temperature was normalized by dividing with the initial absorbance as shown in equation 3. The observed temperature was corrected by equation 4 to obtain corrected temperature plotting to normalized absorbance.[29] The obtained melting curve was processed using KaliedaGraph 4.0 (Synergy software) and Microsoft Excel (Microsoft Corporation), smoothed by a five-point adjacent averaging algorithm and indicated melting temperature (T_m) by calculating maxima of the first derivative plot.

$$\text{Normalized absorbance} = abs_{observe}/abs_{initial} \quad (3)$$

$$\text{Correct temperature} = (0.9696 \times T_{observe}) - 0.6068 \quad (4)$$

2.10. Computational calculation

All calculations of model **64** and **65** (the structures as shown in Figure 2.9) were performed by Associate Professor Dr. Viwat Vchirawongkwin with the Gaussian 09 program package using Pople basis set with a diffuse and polarization function on the heavy atoms (6-31+G(d)) at the density-functional theory with Becke three-parameter hybrid exchange functional and the Lee-Yang-Parr correlation functional (B3LYP). The implicit solvent model of conductor-like polarizable continuum model (CPCM) was also included, accounting the effect of water molecules surrounding these structures.

Figure 2.9 Structures of (1*S*,2*S*)-*N*-methoxycarbonyl-2-aminocyclobutanecarboxylic acid dimethylamide (**64**) and (2*S*,3*S*)-*N*-methoxycarbonyl-2-aminooxetanecarboxylic acid dimethylamide (**65**) used as models for the conformational analysis of acbc and (2*S*,3*S*)-*epi*-oxetin, respectively.

Chapter 3

Results and Discussion

In this work, a novel synthesis of the (2*S*,3*S*)-*epi*-oxetin derivative is proposed in order to reduce the complexity and multiple-step synthesis of previous reports. Retrosynthetic analysis of the target molecule (**55a**) pointed to an obvious oxetane intermediate **53a**, which could be converted to **55a** by few steps of functional group interconversion. The oxetane intermediate **53a** was obtained by selective activation of hydroxyl and then cyclization of compound **51a**. The compound **51a** could be prepared by azide ring opening of epoxide **50a** which in turn can be obtained by enantioselective epoxidation of allylic alcohol **42** as shown in Figure 3.1.

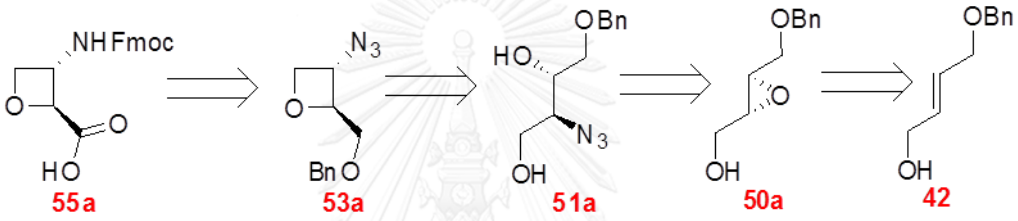

Figure 3.1 Retrosynthetic analysis of (2*S*,3*S*)-*epi*-oxetin derivative (**55a**)

3.1. Synthesis of (*E*)-4-(benzyloxy)but-2-en-1-ol (42)

Allylic alcohol **42** is commercially available.[19] However, the price is considerably high up to 8,640 baht per gram (LabSeeker, http://www.labseeker.com/goods.php?id=16310). Different synthetic pathways for **38** were evaluated to find the most convenient synthesis that can be scaled up.

3.1.1. Synthesis of (*E*)-4-(benzyloxy)but-2-en-1-ol (42) starting from (*Z*)-but-2-ene-1,4-diol (38)

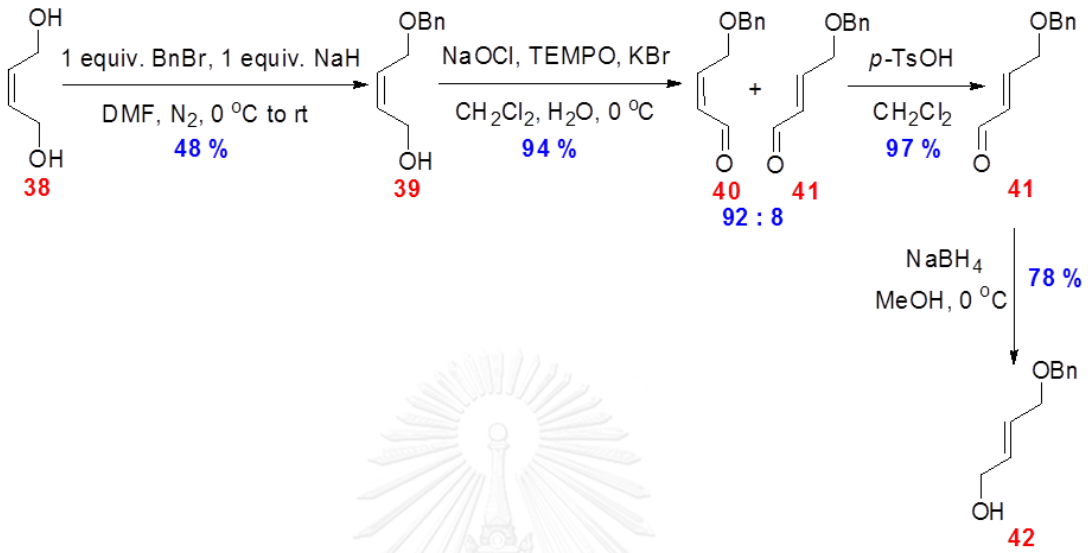

Figure 3.2 Synthetic of allylic alcohol **42** starting from compound **38**

The most straightforward pathway to synthesize **42** is mono-benzylation of *trans*-2-butene-1,4-diol to obtain the desired allylic alcohol **42**.[30] However, the *trans*-2-butene-1,4-diol was not commercially available, therefore *cis*-2-butene-1,4-diol (**38**) was used as a starting material instead.[17-19, 31] Commercially available *cis*-2-butene-1,4-diol (**38**) was first subjected to mono-benzylation by using one equivalent of BnBr[17] and provided compound **39** in 48 % yield. Next, oxidation of the remaining hydroxyl to aldehyde followed by isomerization under acidic condition yield the *trans*-aldehyde **41**.[18-19, 31] Pyridinium chlorochromate (PCC) oxidation of compound **39** was previously reported to efficiently generate the *trans*-aldehyde directly.[32] In this work, Anelli's oxidation[31] (NaOCl, cat.TEMPO, and KBr) was a method of choice since it was more environmental friendly. A mixture of *cis*- and *trans*-aldehyde **40** and **41** was thus obtained in 94% yield.

The ratio between *cis*-aldehyde **40** to *trans*-aldehyde **41** was analyzed by ^{1}H NMR, which clearly showed two sets of sp^{2}-aldehyde proton signals: major product (10.05 ppm, J = 6.79 Hz) and minor product (9.69 ppm, J = 7.92 Hz) as shown in Figure 3.3.

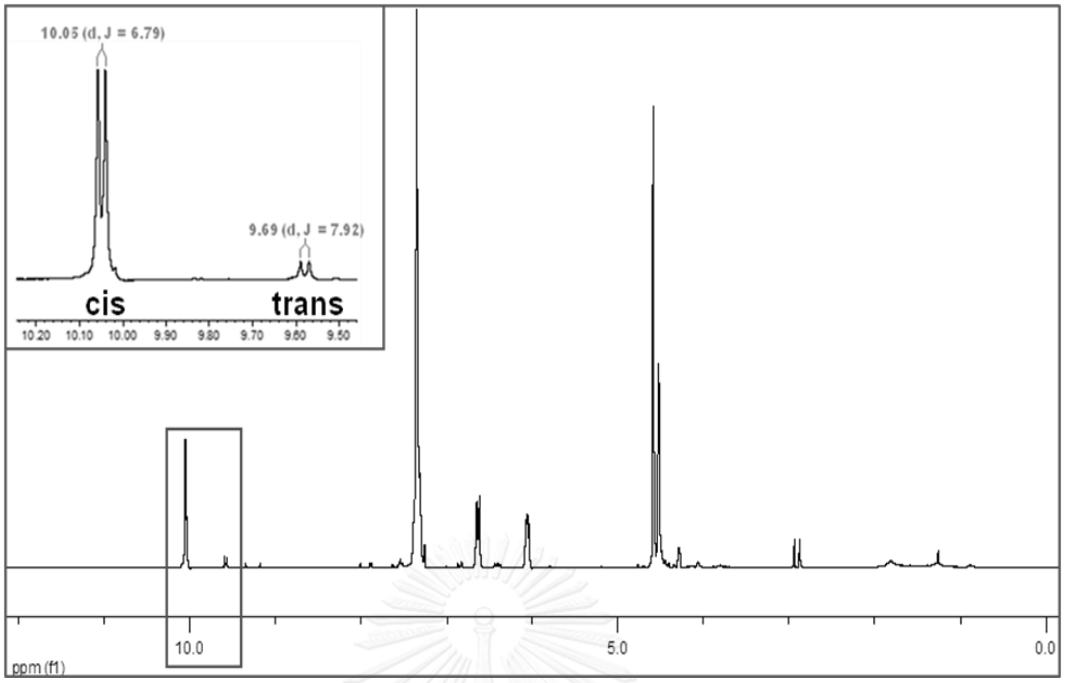

Figure 3.3 ^{1}H NMR spectrum from Anelli's oxidation of compound **39**

By comparison the chemical shift of each signal to the literature,[18] the major and minor products were determined as *cis*-aldehyde **40** (9.69 ppm) and *trans*-aldehyde **41** (10.05 ppm) respectively. The ratio of **40**:**41** was determined by integration to be 12:1 or roughly 92:8.

The mechanism of Anelli's oxidation is discussed below (Figure 3.4).[31] Oxidation of KBr by sodium hypochlorite generated hypobromous acid (HOBr) which then further oxidized TEMPO to *N*-oxoammonium intermediate **A**. Nucleophilic addition of compound **39** on nitrogen atom of **A** generates intermediate **B**. Then, aldehyde **40** was formed by elimination of **B**. Finally, product **C** was oxidized in order to regenerate TEMPO back to the system.

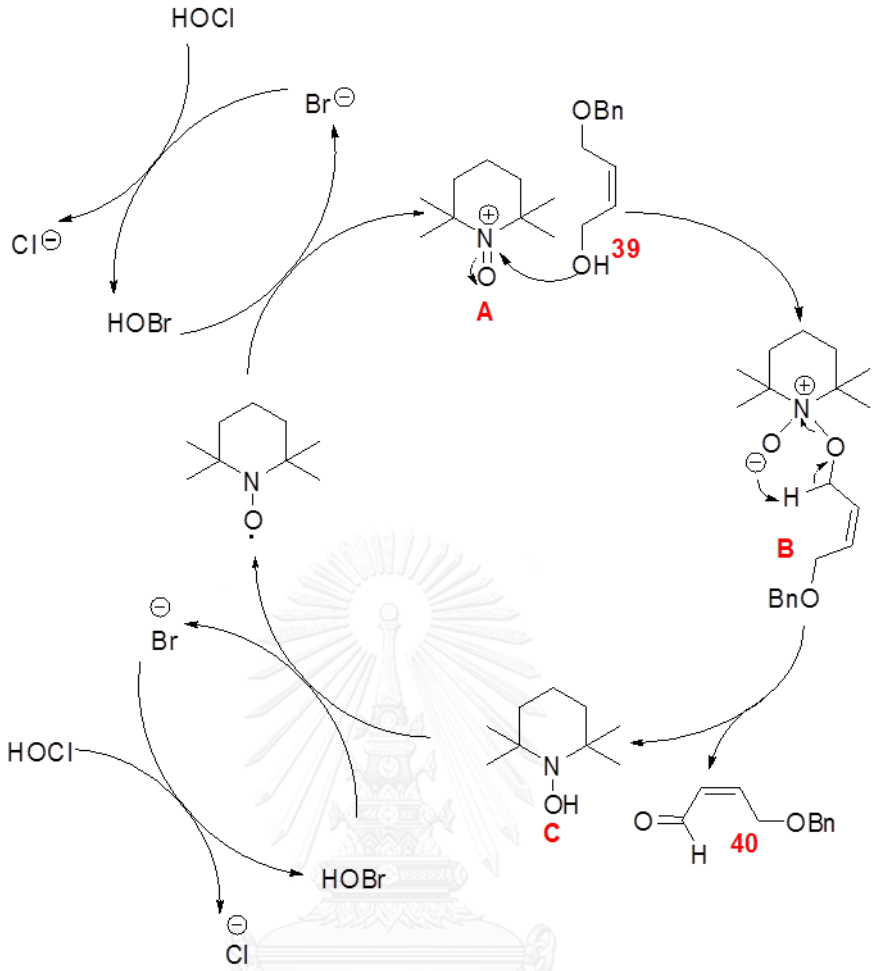

Figure 3.4 Anelli's oxidation mechanism of compound **39**

Isomerization of *cis*-aldehyde **40** by treatment with an acid catalyst (TsOH) following a known procedure gave *trans*-aldehyde **41** in 97% yield (Figure 3.2).[22] Finally, the *trans*-aldehyde **41** was converted to the *trans*-alcohol **42** by $NaBH_4$ reduction at 0 °C[19] in 78% yield. To sum up, this oxidation-isomerization-reduction sequence created the desired *trans*-allylic alcohol **42** from *cis*-2-butene-1,4-diol (**38**) in 34% overall yield over 4 steps. Further discussion about reduction of aldehyde **41** was reported in 3.1.3.

3.1.2. Synthesis of (*E*)-4-(benzyloxy)but-2-en-1-ol (42) from but-2-yne-1,4-diol (43)

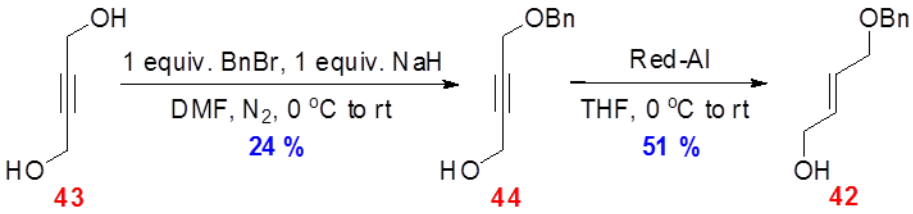

Figure 3.5 Synthetic results of **42** starting from **43**

The second pathway for the synthesis of **42** from alkyne diol **43** was reported earlier.[17, 20] Treatment of alkyne diol **43** with 1 equivalent of BnBr/NaH resulted in mono-benzyl protected **44** in 24% yield (Figure 3.5). Reduction of the intermediate **44** with Red-Al afforded the *trans*-alcohol **42**[20] in 51% yield. Due to the low yield of the first benzylation step, this synthetic route produced desired **42** in 12% yield over 2 steps.

3.1.3. Synthesis of (*E*)-4-(benzyloxy)but-2-en-1-ol (42) from benzyl glycidyl ether (45)

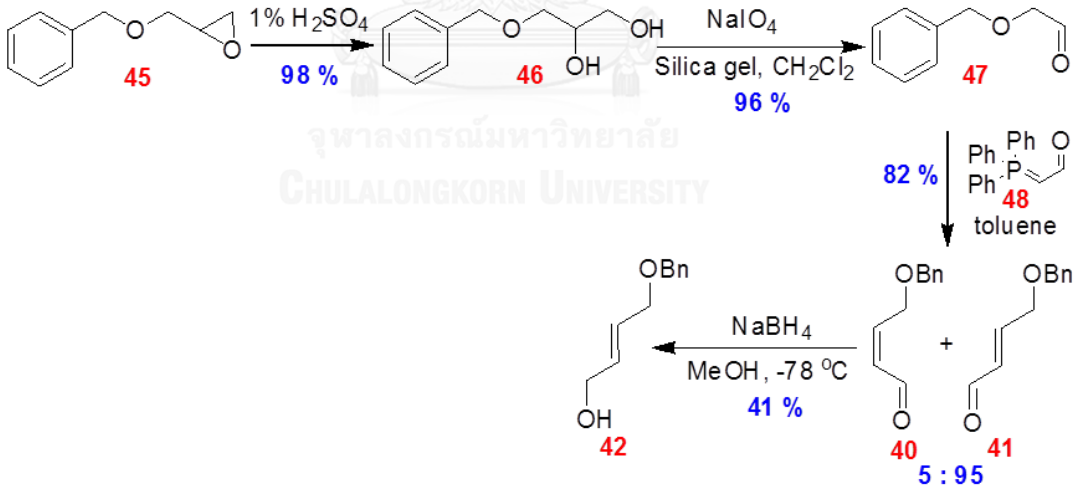

Figure 3.6 Synthetic results of **42** starting from **45**

The third pathway for the synthesis of **42** was depicted in Figure 3.6. This strategy relies on Wittig olefination starting from benzyl glycidyl ether (**45**) precursor in 4 steps. Acidic hydrolysis of epoxide **45** proceeded to generate diol **46** in 98% yield.[21] Oxidative cleavage of the diol **46** gave the aldehyde **47** in 96% yield. Wittig reaction between the aldehyde **47** and a

stabilized ylide **48** produced a 5:95 mixture of *cis:trans* aldehyde in 82% yield. This result is consistent to theory that Wittig reaction involving stabilized ylide generates *trans*-alkene as a major product. Finally, the aldehyde was reduced using $NaBH_4$ at -78 °C to produce compound **42** in 41% yield as shown in Figure 3.6. In conclusion, this 4-step reaction sequence generated *trans*-alkene **42** in 32% overall yield starting from compound **45**.

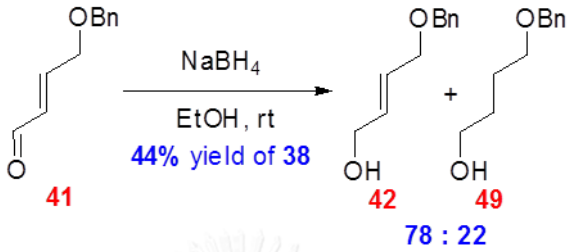

Figure 3.7 $NaBH_4$ reduction of compound **41** at ambient temperature

It's worth noting that success of the $NaBH_4$ reduction of aldehyde **40** and **41** depended on the reaction temperature. The reduction at ambient temperature provided only 44% yield of **42** accompanied with saturated alcohol byproduct from 1,4-reduction (Figure 3.7). In order to avoid this byproduct, the reaction was performed at -78 °C which resulted in incompletion and gave the desired alkene **42** only in 41% yield (Figure 3.6). Thus, the reaction was processed at 0 °C to afford compound **42** in 78% yield (Figure 3.2).

The generation of saturated alcohol byproduct **49** can be rationalized in Figure 3.8. Borohydride reduction of α,β-unsaturated aldehyde **41** produced enol **A**, which tautomerized to the aldehyde intermediate **B**. Finally, normal 1,2-reduction of the aldehyde **B** furnished compound **49**.

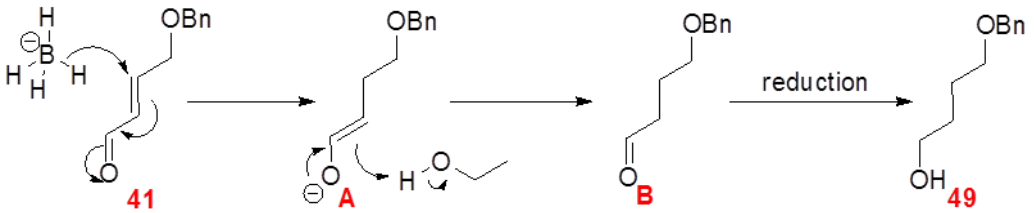

Figure 3.8 Mechanism of conjugate reduction of compound **41**

The first synthetic pathway was a 4-step reaction sequence starting from (*Z*)-but-2-ene-1,4-diol (**38**). This procedure gave 34% overall yield of **42** and required the shortest reaction time. For example, oxidation and isomerization underwent to completion only within 10 and 30 minutes respectively.

The second route was very short and used a very cheap but-2-yne-1,4-diol (**43**) as precursor, which costs only 3.5 baht per gram (http://www.sigmaaldrich.com/catalog/product/aldrich/b103209?lang=en&region=TH). In our hands, only 12% yield of product **42** was obtained which was possibly due to moisture sensitive nature of the Red-Al reduction. The third pathway starting from benzyl glycidyl ether (**45**) yielded the allylic alcohol **42** in 32% overall yield. Although the reduction yield should be improvable (compared between Figure 3.2 and 3.6), the Wittig olefination required a considerably expensive ylide **48** (384 baht per gram, http://www.sigmaaldrich.com/catalog/product/aldrich/280933?lang=en&region=TH) Therefore, we decided to choose the first synthetic method to produce (*E*)-4-(benzyloxy)but-2-en-1-ol (**42**) due to lower cost and efficiency of all transformations.

3.2. Preliminary results of racemic model for synthesis of 3-(((9*H*-fluoren-9-yl)methoxy)carbonylamino)oxetane-2-carboxylic acid (55)

3.2.1. Synthesis of racemic-3-(((9*H*-fluoren-9-yl)methoxy)carbonylamino)oxetane-2-carboxylic acid (55)

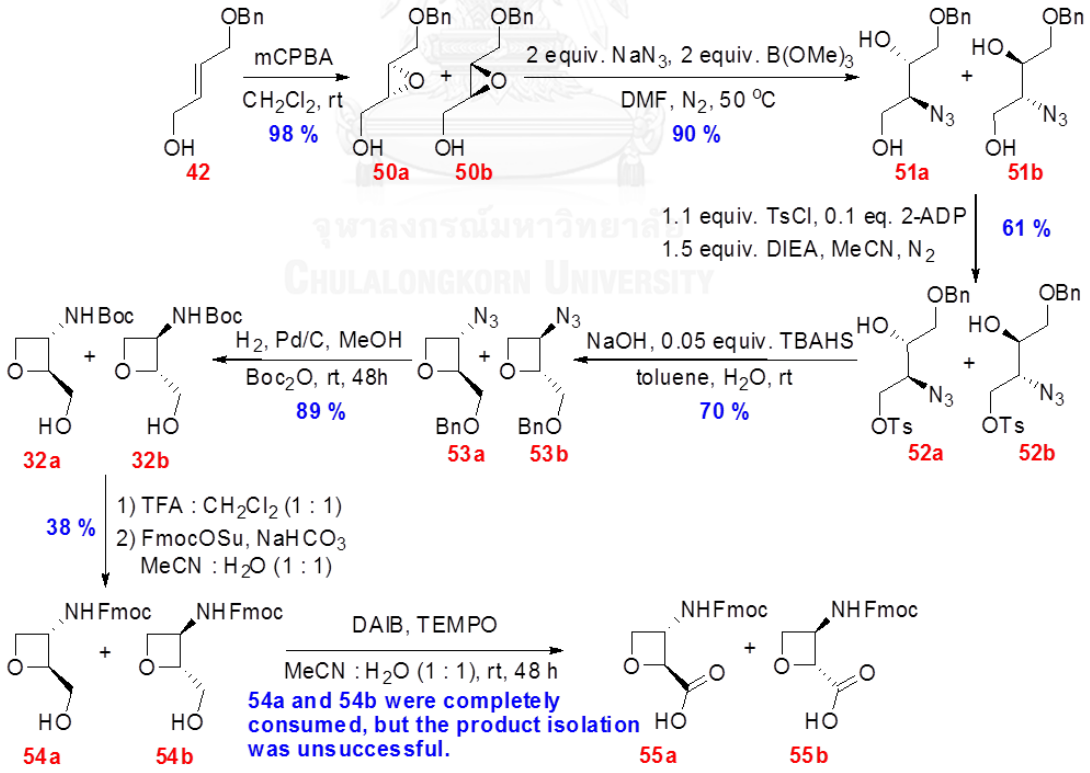

Figure 3.9 Synthetic results of racemic mixture **55** starting from **42**

The preliminary study on the synthesis of racemic **55a** and **55b** was first investigated to ensure the viability the synthetic route. The racemic mixture **55a** and **55b** will be also useful as reference standard for subsequent determination of enantiomeric excess of Fmoc-protected *epi*-oxetin **55a**. Allylic alcohol **42**[13] underwent mCPBA epoxidation to afford racemic epoxides **50a** and **50b** in 98% yield. The epoxides were treated with sodium azide and $B(OMe)_3$ to undergo regioselective epoxide ring-opening.[23] The racemic azide **51a** and **51b** were obtained as major regioisomer in 90% yield (Figure 3.10).

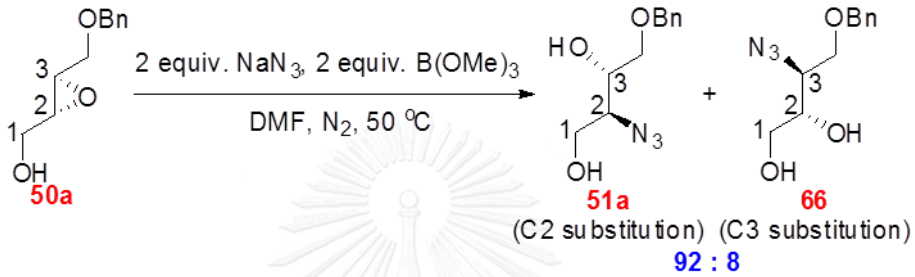

Figure 3.10 Epoxide ring opening with azide ion from reference[23]

In principle, there are 2 possibilities for azide anion to undergo epoxide ring-opening. The substitution can occur at either C2 or C3 carbon as shown in Figure 3.10. However, Sasaki and coworkers reported that regioselective substitution on C2 position was achieved by addition of $B(OMe)_3$ as a Lewis acid.[23] The mechanism for the selective C2 substitution begins with addition of hydroxyl in racemic **50a** or **50b** to $B(OMe)_3$ generating the tetracoordinate intermediate **A**. Elimination of the methoxy leaving group, followed by intramolecular coordination between oxygen atom of the epoxide and boron Lewis acid to form intermediate **B**. Azide substitution at the more electrophilic carbon atom (C2) yielded the borate ester intermediate **C**. By $NaHCO_3$ working up, borate ester **C** was hydrolyzed and gave racemic **51a** and **51b** as shown in Figure 3.11.[23]

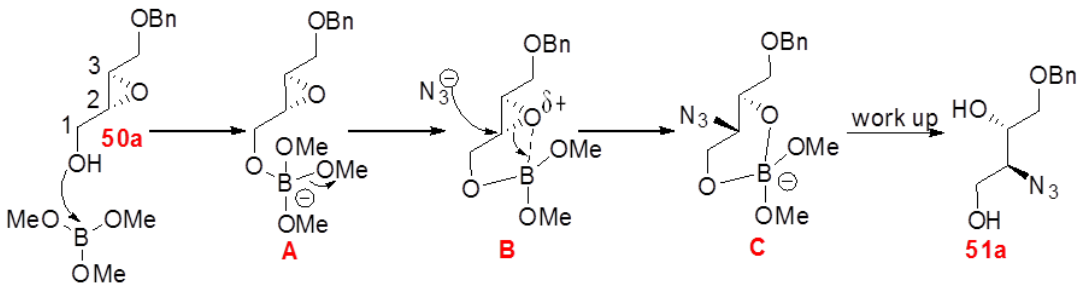

Figure 3.11 Mechanism of regioselective epoxide ring opening with azide ion on C2 position of **50a**

Our result was consistent with earlier report by Sasaki group as we observed the C2 substitution product **51** as the major product.[23] The ^{1}H NMR analysis of this compound was complicated due to overlapping of proton signals. However, by comparing with previous report,[23] we estimated the ratio of C2 substitution **51** and C3 substitution **66** to be 92:8.

Next, tosylation of the racemic azidoalcohol **51a** and **51b** under standard condition (1 equiv. TsCl, 2.2 equiv. Et_3N and cat. DMAP) was carried out.[33] Racemic **52a** and **52b** was obtained in only 38% yield along with ditosylated by-product **56** in 13% yield. The starting material **51** was also recovered in 23% yield. Despite only one equivalent of TsCl was used, selective monotosyaltion was difficult. Therefore, several conditions were investigated to achieve the desired monotosylation. Recently, Miller and coworkers achieved selective monofunctionalization for protection and tosylation of 1,2 and 1,3-diols by using borinate catalyst.[34] The borinate first coordinates to both hydroxyls groups and exaggerated the difference in nucleophilicity of both alcohols. In this case, the terminal hydroxyl is greater in nucleophilicity thus underwent tosylation faster than the internal hydroxyl group.[34] The condition was applied to our substrate racemic **51** and we were pleased to obtain racemic **52** in 61% yield, which is much better than previous standard condition. This condition will be used in the enantioselective synthesis of **55a**.

The mechanism of selective monotosylation of racemic **51** is depicted in Figure 3.12. Ligand exchange between borinate catalyst and substrate **51** followed by tosylation of 2-aminoethanol ligand were proposed. The terminal hydroxyl group of the newly generated intermediate **A** undergoes addition to TsCl to obtain intermediate **B**. Finally, ligand exchange to starting material **51a** releases the monotosylated product **52a** as shown in Figure 3.12.[34]

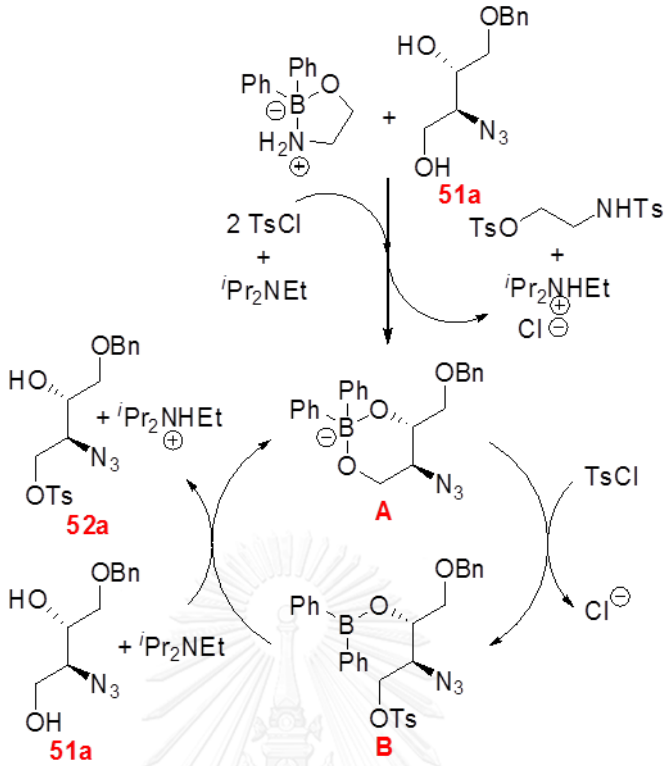

Figure 3.12 Mechanism of selective monotosylation of **51a** through borinate intermediate

Cyclization of racemic **52** was performed under phase-transfer condition[35] to furnish the oxetane intermediate **53** in 70% yield. Since this reaction is a key step on the synthetic route of racemic **55**, careful characterization of racemic oxetane **53** was required.

^{1}H NMR spectra of racemic **52** starting material and oxetane **53** are shown in Figure 3.13. Methyl signal of tosyl group at 2.38 ppm (i) and 7.74 ppm (g) of aromatic protons disappeared after the cyclization, indicating substitution of tosyl group. The signals of aliphatic protons in **52** around 3.60-4.50 ppm moved downfield to 4.50-4.80 ppm, correlating to cyclic pattern of oxetane intermediate **53**. Moreover, the number and signal shape of two methylene protons at 4.51 ppm (b), two methylene protons at 3.66 ppm (c), and other highly overlaped signals between 4.55-4.90 ppm (4H, which were too complex to assign for individual signal) are consistent with the structure of the oxetane intermediate **53**.

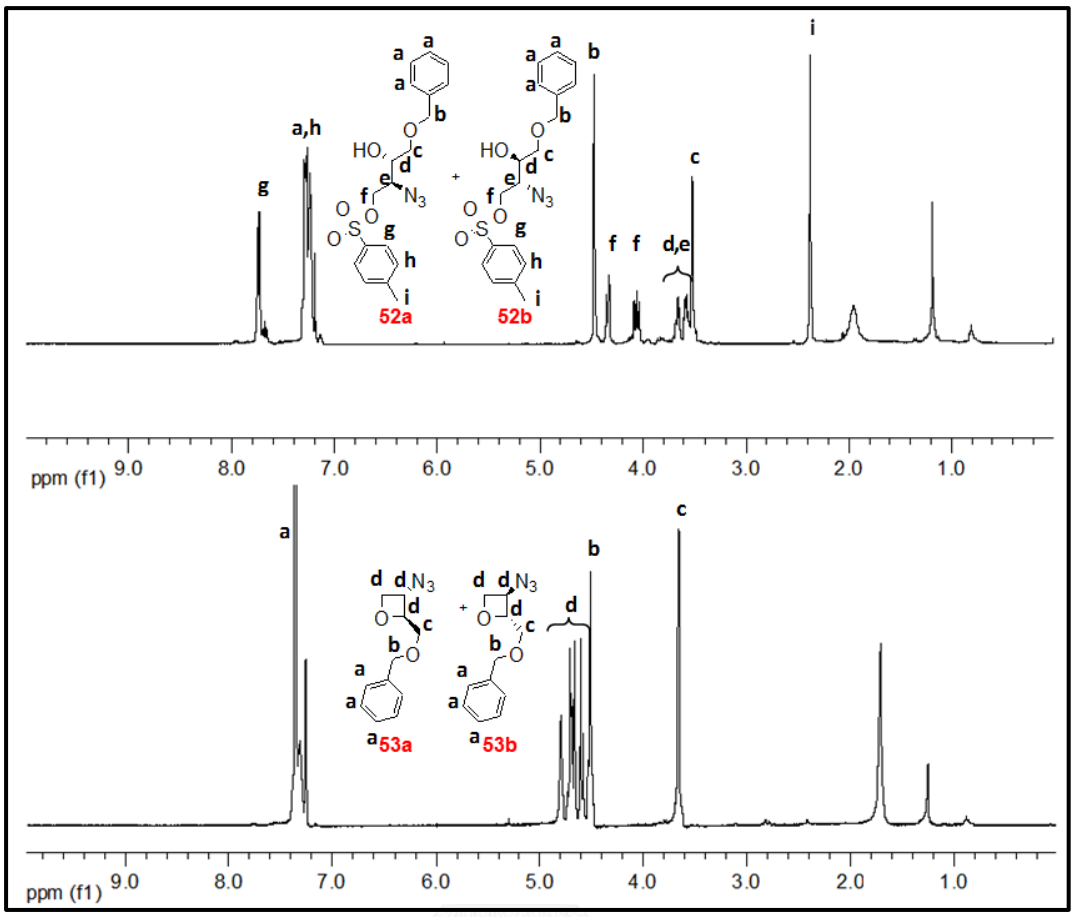

Figure 3.13 Comparison of ^{1}H NMR (400 MHz, $CDCl_3$) spectra between racemic **52** and **53**

The next 3 steps of functional group interconversion and protecting group manipulation were illustrated in Figure 3.9. Azide reduction and debenzylation of racemic oxetane **53** were carried out under hydrogen atmosphere over $Pd(OH)_2/C$ catalyst[13] and the newly formed amino group was protected *in situ* with Boc_2O. The racemic **32** was obtained in 89% yield. ^{1}H and ^{13}C NMR of racemic **32** matched with the spectroscopic data of (2*S*,3*S*)-Boc-oxetane alcohol **32a** reported earlier by Howell's group.[15] Again, this was an evidence to confirm the achievement of the previous cyclization step.

The Boc protecting group was then exchanged to Fmoc by acidic cleavage and standard Fmoc protection[8] to afford racemic **54** in 38% yield. Lastly, oxidation of primary alcohol in racemate **54** with DAIB and catalytic TEMPO was performed.[36] Although the Fmoc-oxetane alcohol **54** was completely consumed, none of the expected product was obtained.

Mechanism of DAIB oxidation is similar to Anelli's oxidation (Figure 3.4). However, DAIB is used as stoichiometric oxidant instead of NaOCl. To begin with disproportionation of TEMPO 2 molecules under catalyzed by acetic acid from DAIB, the intermediate **A** and **B** were generated.

Then, oxoammonium intermediate **A** oxidizes primary alcohol to aldehyde **C**, releasing intermediate **B** which is then oxidized back to TEMPO by DAIB. The addition of water into aldehyde moiety of intermediate **C** is under equilibrium to furnish hemiacetal **D**. Finally, the intermediate **D** is oxidized again with **A** to yield carboxylic acid **55a** as shown in Figure 3.14.[37]

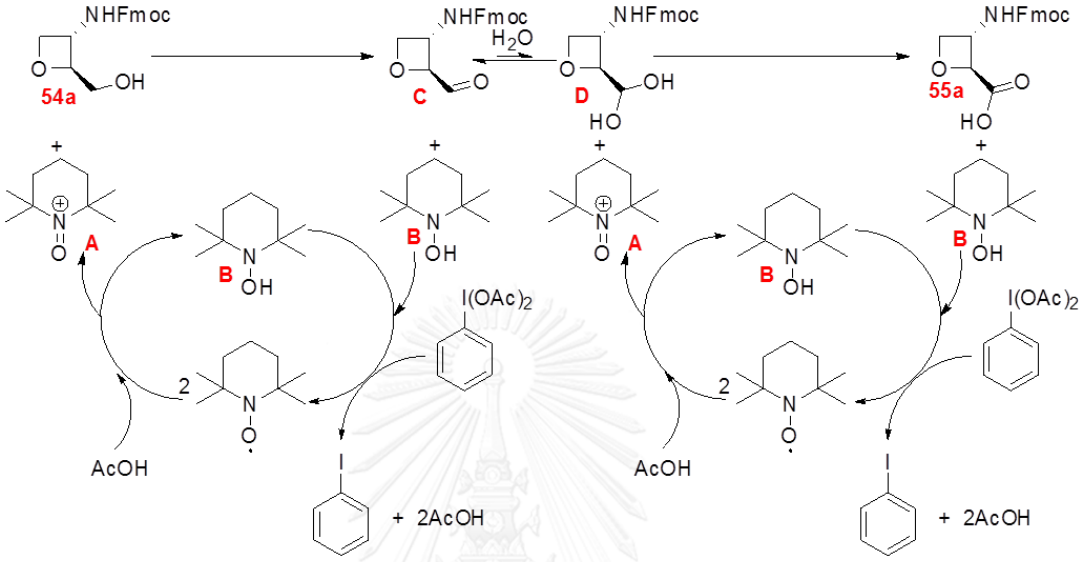

Figure 3.14 Mechanism of DAIB oxidation catalyzed by TEMPO of **55a**

We propose that the failure of previous oxidation might come from poor water solubility of Fmoc-protected alcohol **54a**. As one can see from the mechanism above, addition of water to intermediate **C** and generation of hemiacetal **D** is an essential step before oxidation of **D**.

3.2.2. Alternative pathway to improve the synthesis of 3-(((9*H*-fluoren-9-yl)methoxy)carbonylamino)-oxetane-2-carboxylic acid (55)

From the hypothesis in the previous section, the problem of poor solubility Fmoc-protected alcohol **54** in water was circumvented by performing the oxidation on the Boc alcohol **32**[32] before changing the protecting group to Fmoc[8] as shown in Figure 3.15.

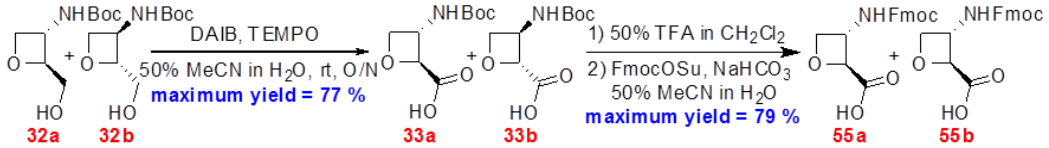

Figure 3.15 Synthetic scheme of racemic **55** starting from racemic **32** toward intermediate **33**

Gratifyingly, the DAIB oxidation using TEMPO as a catalyst[36] converted the racemic Boc-alcohol **32** to racemic Boc-carboxylic acid **33** in 77% maximum yield. The achievement in synthesis of racemic **33** was confirmed by comparison of ^{1}H NMR spectrum with enantiopure **33a** from previous report.[15] After switching Boc into Fmoc group,[8] the desired racemic product **55** was afforded in 79% yield. Structural elucidation of racemic **55** was assured by comparing between ^{1}H NMR spectrum of **33** and racemate **55** as shown in Figure 3.16. The methyl proton from the *tert*-butyl group at 1.47 ppm in **33** disappeared and four aromatic signals (two protons each) between 7.20-8.00 ppm were replaced correlating to aromatic pattern of Fmoc. The signals between 4.20-5.00 ppm (seven protons) could be assigned as protons on oxetane ring, methylene protons and a proton on tertiary carbon of Fmoc group. However, there were still some impurities contaminated in the final product since there were unaccountable ^{1}H NMR signals at 3.67 and 3.97 ppm. At this point, we believe that optimization and improvement of work up method should gain higher purity of desired compound **55.** In conclusion, the racemic synthesis of compound **55** was successful as planned.

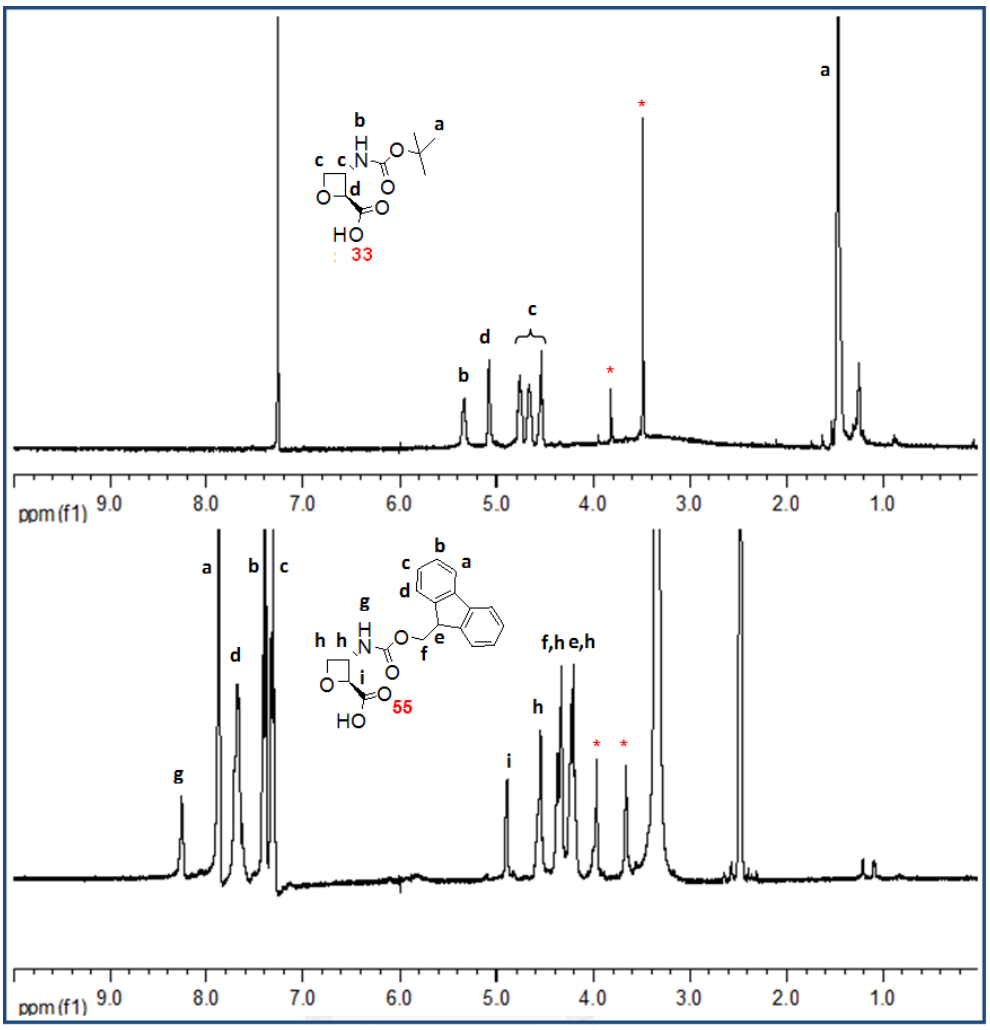

Figure 3.16 Comparison between ^{1}H NMR spectra of recemic **33** (400 MHz, $CDCl_3$) and racemic **55** (400 MHz, DMSO-d_6)

Next, we applied a similar synthetic strategy (Figure 3.17) for enantioselective synthesis of (2*S*,3*S*)-isomer **55a**. The most challenging task of this work was to perform enantioselective epoxidation to the allylic alcohol **42** to introduce the chirality, which will be carried all the way through the final product *epi*-oxetin **55a**

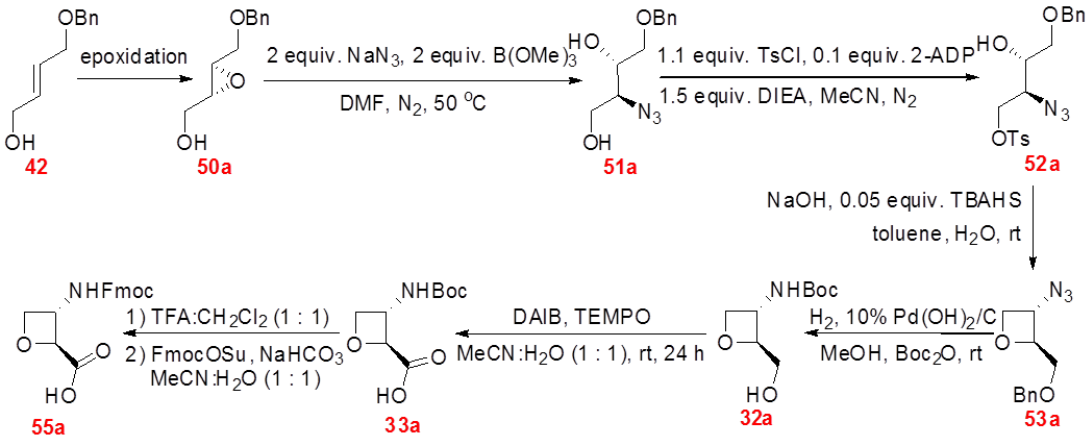

Figure 3.17 Improved synthetic pathway to synthesize **55a**

3.3. Investigation on synthesis of (2*R*,3*R*)-3-(benzyloxymethyl)oxiran-2-yl)methanol (50a) with enantioselective epoxidation

3.3.1. Sharpless epoxidation[24]

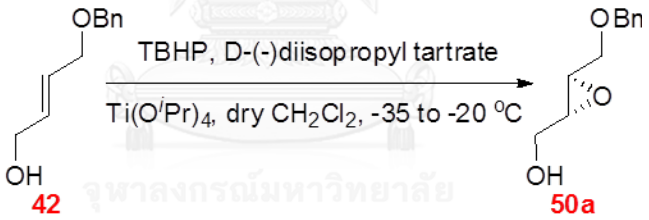

Figure 3.18 Synthesis of **50a** *via* Sharpless epoxidation of alkene **42**

This section focused on study of enantioselective epoxidation to generate chiral epoxide **50a** (Figure 3.18). Several works have been reported on the synthesis of optically active epoxy alcohol **50**, either by Sharpless epoxidation of the allylic alcohol **42**[24] or enzymatic resolution of racemic epoxy alcohol **50**.[19] Initially, Sharpless epoxidation was selected in this study because this reaction has reliable reputation in asymmetric epoxidation of allylic alcohol.[24] In this work, two conditions were investigated as shown in Table 3.1.

Table 3.1 Results of Sharpless epoxidation

entry	**42** (mmol)	TBHP (equiv.)	D-(-)diisopropyl tartrate (equiv.)	$Ti(O^iPr)_4$ (equiv.)	%yield	%ee[c]
1	7.58	2.5	0.38	0.25	78	66
2[a]	4.92	3.8	2.3	1.5	52[b]	40

Note

[a] allylic alcohol **42** with 4-(benzyloxy)butan-1-ol (**49**) contaminant in proportion of **42**:**49** = 68:32

[b] %yield calculating from 4.92 mmol of **42** from 7.57 mmol of mixture between **42** and **49**

[c] observation of %ee by chiral HPLC (column:OJ-H chairal column, mobile phase:15% ^{i}PrOH in *n*-hexane, flow rate:0.6 mL/min @ 210 nm, t_R major:36.21 min, t_R minor:41.68 min)

Sharpless epoxidation results are summarized in Table 3.1. We obtained the desired (*R*,*R*)-epoxide, as confirmed by optical rotation. However, only moderate yield and enantioselectivity of **50a** was obtained in our hands despite the reported high above 90% ee for the same substrate.[24] The main difficulty was to several reaction parameters such as moisture, proportion of reagent, temperature, and purity of the starting material **42**. Thus, this method was not further attempted, and other enantioselective epoxidations were investigated.

3.3.2. Shi epoxidation

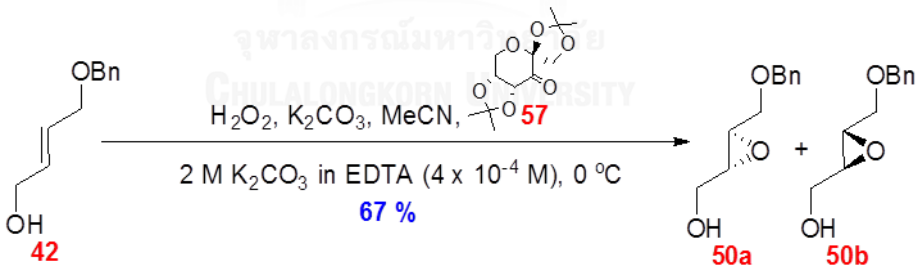

Figure 3.19 Synthesis of **50a** *via* Shi epoxidation of alkene **42**

Shi epoxidation under aqueous media was another attractive method. Examples of epoxidation of allylic alcohol substrates such as (*E*)-3-phenylprop-2-en-1-ol are known to generate (*R*,*R*) enantiomer of epoxide in 94% ee.[38] Although Shi epoxidation of the allylic alcohol **42** has not been reported, we hope to achieve some enantioselectivities. The general conditions for Shi epoxidation uses oxone under aqueous acetonitrile media, however, we selected a modified Shi reaction using H_2O_2 as oxidant instead (Figure 3.19),[39] because the modified Shi

reaction can be done at ambient temperature without strict temperature control. In the presence of 4.0 equivalents of H_2O_2 and 30 mol% **57** as catalyst, the allylic alcohol **42** was converted to the epoxide **50** in only 4% yield, and the starting material **42** was also recovered in 76%. Increasing H_2O_2 up to 40 equivalents improved the yield of the epoxide product **50** to 67% yield. Unfortunately, completely racemic mixture epoxide **50** was obtained in both cases (4.0 equiv. and 40 equiv. H_2O_2) as confirmed by chiral HPLC (column: OJ-H chiral column, mobile phase: 15% ^{i}PrOH in *n*-hexane, flow rate: 0.6 mL/min @ 210 nm).

3.3.3. Jorgensen epoxidation[25]

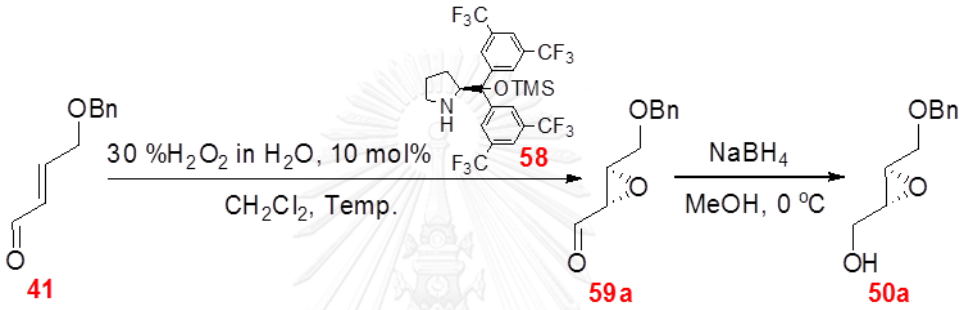

Figure 3.20 Synthesis of **50a** *via* Jorgensen epoxidation of aldehyde **41**

Jorgensen enantioselective epoxidation was next studied. Jorgensen epoxidation of α,β-unsaturated aldehydes using pyrrolidine **58** as organocatalyst was recently reported.[25] According to the literature, epoxidation of **41** was performed in aqueous media and afforded the epoxy aldehyde **59a** in 84% yield and 94% ee.[25] In our work, the Jorgensen epoxidation was set under the same conditions as report in the reference,[25] and the epoxyaldehyde **59a** was immediately reduced by $NaBH_4$ at 0 $^{\circ}$C without isolation as shown in Figure 3.20. The epoxy alcohol **50a** was obtained in moderate yield (46-69% yield) but high enantioselectivity (91-95% ee). Absolute stereochemistry of **50a** was determined to be the desired (2*R*,3*R*) by comparison of the sign of specific rotation (between +17.48 to +18.01 versus +22.0 from the literature[40]). The results from four different runs are compared in Table 3.2.

Table 3.2 Summary of Jorgensen epoxidation results

entry	**41** (mmol)	$NaBH_4$ (equiv.)	Temp. (^oC)	%yield	specific rotation at 23 ^oC[c]	%ee[e]
1	1.01	1.14	rt	55	+18.01	92
2	1.01	1.04	10-20	56	+17.48[d]	94
3	5.86	1.01	10-20	48	+17.70	95
4[b]	4.0	1.12	10-20	69	+17.70	91

Notes

[a] condition: **41** 1 equiv., 30% w/v H_2O_2 13.0 equiv. and **58** 10 mol%

[b] changing equiv. of 30% w/v H_2O_2 to be 1.3

[c] c = 0.5 g/100 mL in chloroform

[d] specific rotation at 22 ^oC

[e] %Ee was measured by chiral HPLC (column:OJ-H chairal column, mobile phase:15% ^{i}PrOH in *n*-hexane, flow rate:0.6 mL/min @ 210 nm, t_R major:36.21 min, t_R minor:41.68 min).

From Table 3.2, the synthesis of **50a** in high %ees (above 90%) and high yield was accomplished under various reaction scales and conditions, indicating the robustness of the reaction. Mechanism of enantioselective Jorgensen epoxidation is illustrated in Figure 3.21. Condensation between organocatalyst **58** and aldehyde **41** provided imine intermediate **A**. Nucleophilic addition of H_2O_2 on electrophilic C3 position resulted in delocalization of electrons to the N atom forming enamine intermediate **B**. By nucleophilic attack of C2 position to O atom, the enamine was converted to the epoxide-imine intermediate **C**. Finally, hydrolysis of the imine returns the catalyst **58** to the catalytic cycle and yields epoxy aldehyde **59a**.[25]

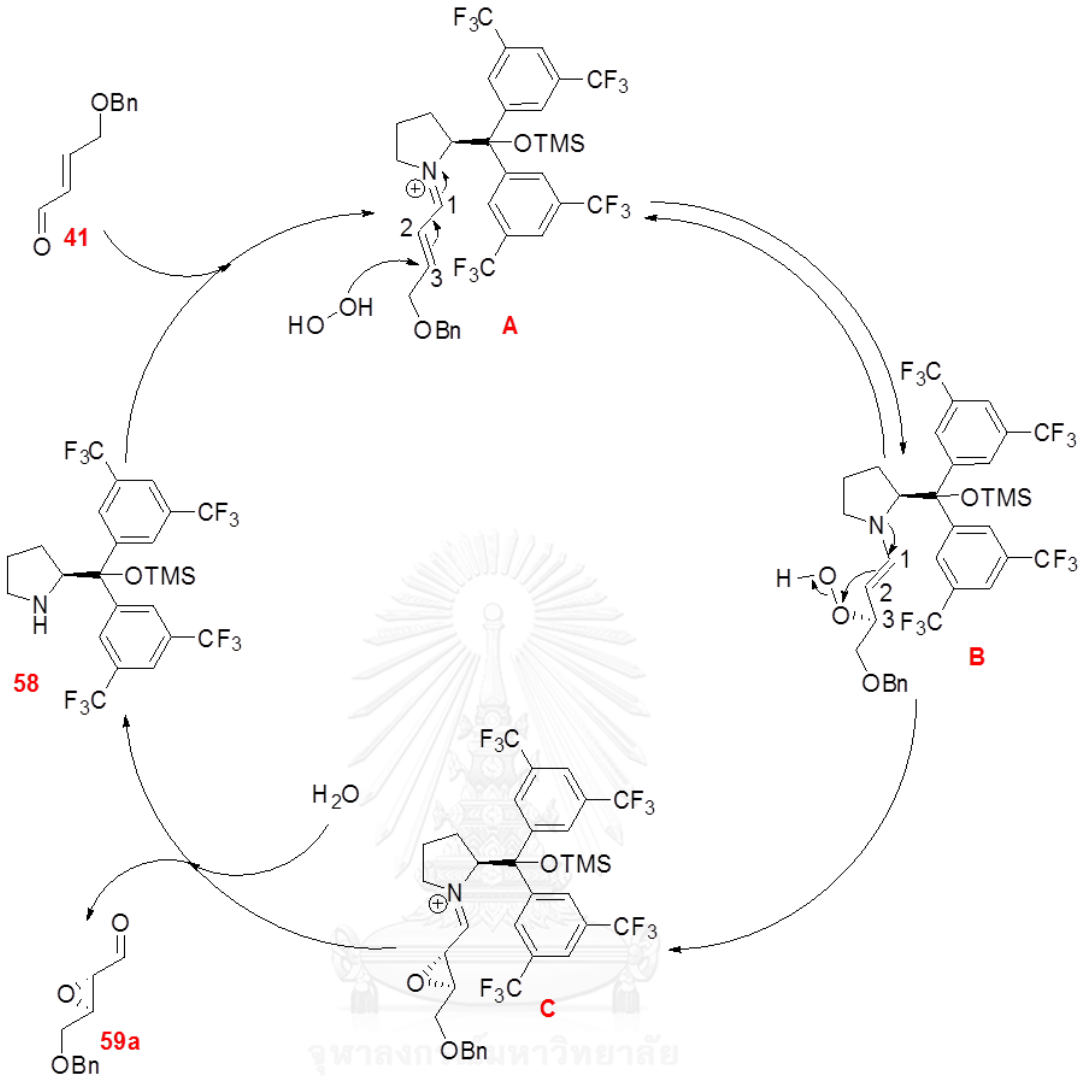

Figure 3.21 Mechanism of Jorgensen epoxidation of compound **41**

3.4. Synthesis of (2*S*,3*S*)-3-(((9*H*-fluoren-9-yl)methoxy)carbonylamino)oxetane-2-carboxylic acid (55a) from ((2*R*,3*R*)-3-(benzyloxymethyl)oxiran-2-yl)methanol (50a)

The synthesis of optically pure **55a** was essentially the same route as previous racemic model and was summarized in Figure 3.22. The enantiomerically pure epoxide **50a** from Jorgensen epoxidation was used in place of the racemic epoxide **50**. The synthesis began with regioselective epoxide ring-opening of highly enantiomerically enriched **50a** (%ee >90%) with azide to obtain **51a** in 91% yield. This was followed by selective tosylation[34] at primary alcohol to generate **52a** in 62% yield. Phase transfer cyclization[35] was performed to afford the oxetane intermediate **53a** in 69% yield. The remaining steps involved straightforward functional group manipulations including hydrogenation[13] and Boc_2O protection of azide provided **32a** in 81% yield. The remaining primary alcohol was then oxidized[34] to carboxylic acid **33a** in 87% yield.

Lastly, the Boc protecting group was switched to Fmoc[8] to furnish the desired compound **55a** in 64% yield as shown in Figure 3.22.

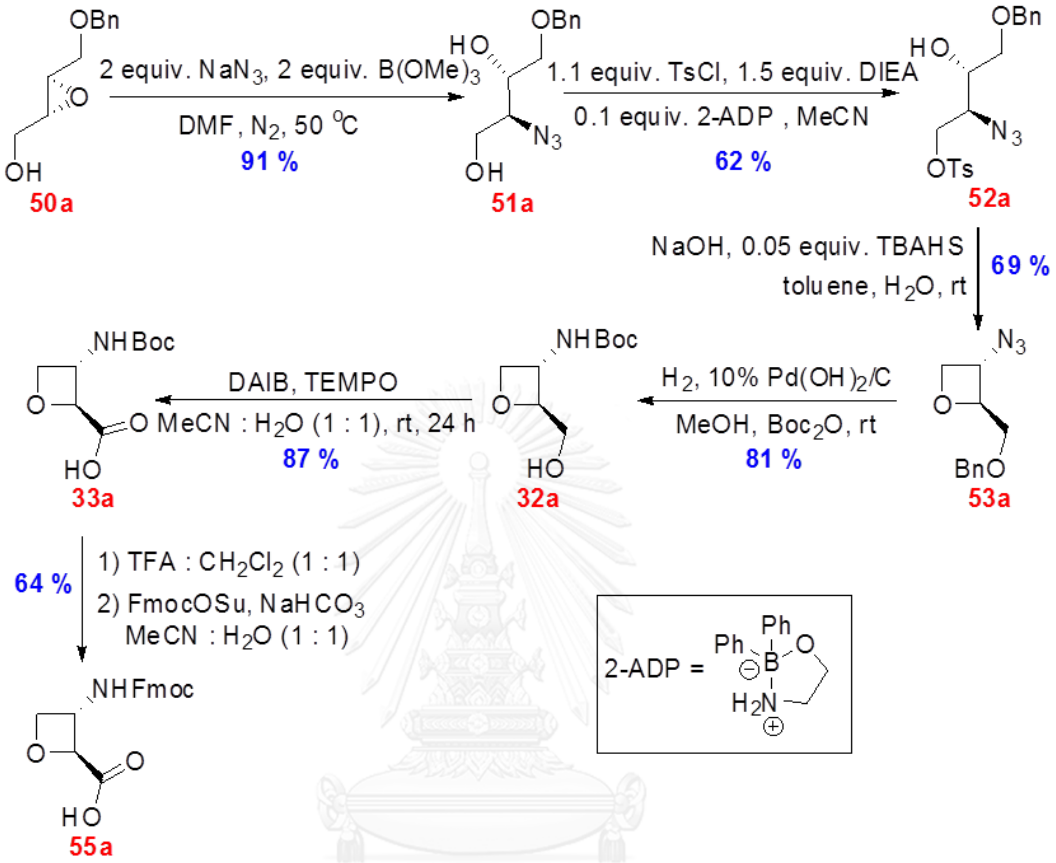

Figure 3.22 Synthetic scheme for single enantiomer **55a** starting from **50a**

3.5. Determination of enantiomeric purity of enantiomeric pure 55a

The enantiomeric purity of the obtained **55a** was determined by chiral HPLC and expressed in term of % ee. However, the carboxylic acid functional group was too polar, and thus both the racemate **55** and compound **55a** was first converted to the corresponding methyl esters **61** and **61a** as shown in Figure 3.23.

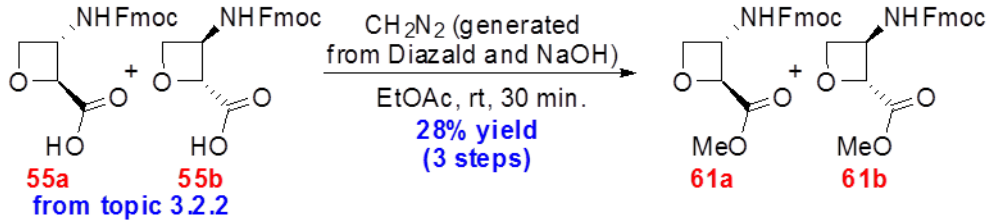

Figure 3.23 Synthesis of racemic **61** from methylation of racemic **55** using diazomethane

A suspension of racemic **55** (from topic 3.2.2) was treated with freshly prepared diazomethane to obtain racemate **61** in 28% yield over 3 steps as shown in Figure 3.23. The same reaction was applied to **55a** to generate the methyl ester **61a** in 99% yield. The enantioselectivity was determined to be 94% by chiral HPLC as shown in Figure 3.24.

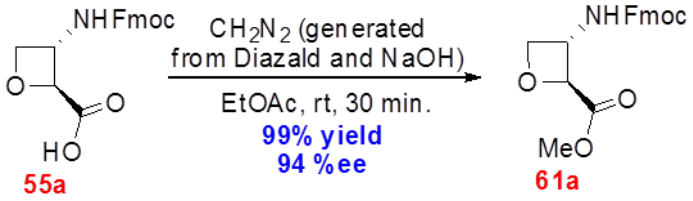

Figure 3.24 Synthesis of **61a** from methylation of **55a** using diazomethane

3.6. Preactivation of aoc spacer

Pre-activation of carboxylic acid **55a** was necessary for amide coupling between *epi*-oxetin spacer and pyrrolidinyl PNA monomer on aocPNA synthesis. Treatment of acid **55a** with PfpOTFA provided pentafluorophenyl (Pfp) ester[10] **60a** in 28% yield as shown in Figure 3.25. This unstable activated ester was used for the next step without characterization and purification.

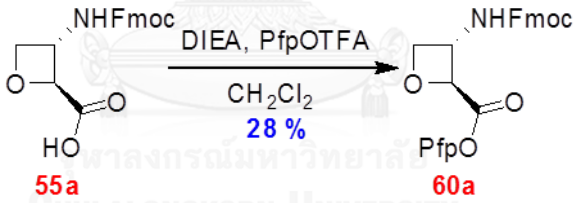

Figure 3.25 Activation of *epi*-oxetin **55a** toward synthesis of pentafluorophenyl ester **60a**

3.7. Synthesis of aocPNA

The aocPNA was synthesized by standard Fmoc solid phase peptide synthesis (SPPS) starting from the four Fmoc-protected pyrrolidinyl PNA monomers (A^{Bz}, T, C^{Bz}, and G^{Ibu}) and Pfp-activated *epi*-oxetin spacer **60a** according to the previously developed protocol.[26] A mix-base 10mer aocPNA with a sequence of X-GTAGATCACT-LysNH_2 (X = Ac or H) was chosen as a model. The synthetic protocol was described in section 2.6.1. The synthesis proceeded smoothly, with 23% overall coupling yield, which translated into 93% for each coupling cycle which was quite similar to other PNA synthesis. However, unlike other pyrrolidinyl PNAs, nucleobase deprotection of aocPNA under standard condition (1:1 aqueous ammonia:dioxane, 60 $^{\circ}C$, overnight) on H-GTAGATCACT-LysNH_2 followed by TFA cleavage of aocPNA from solid support (10 minutes

duration) provided unexpected degradation products as shown by MALDI-TOF mass spectrum of the crude aocPNA after cleavage from the solid support (Figure 3.26).

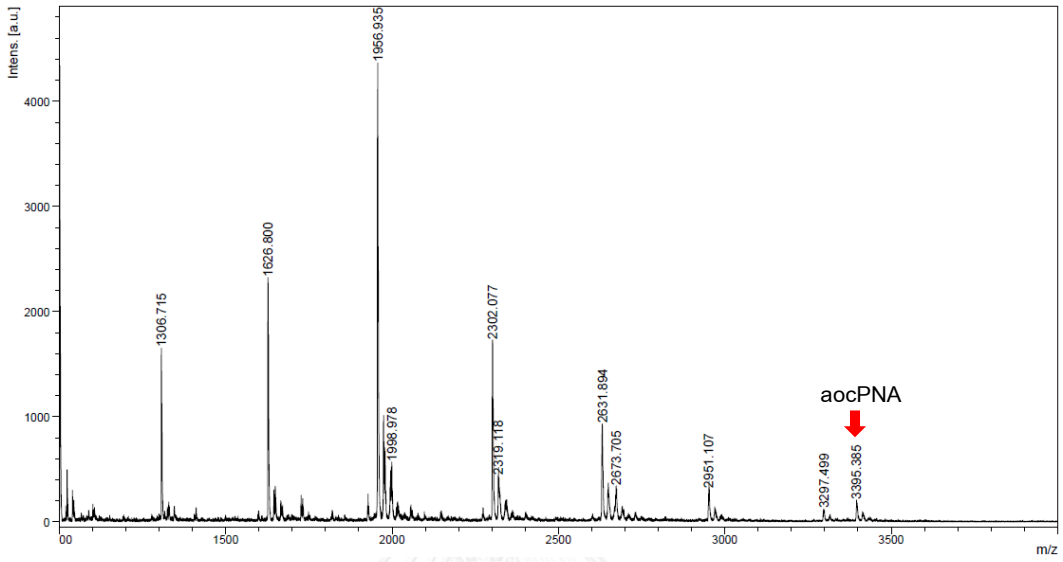

Figure 3.26 MALDI-TOF mass spectrum of aocPNA nucleobase deprotection under 1:1 aqueous ammonia:dioxane at 60 °C for overnight following by TFA cleavage for 10 minutes

According to the mass spectrum in Figure 3.26, the molecular ion peak of aocPNA at *m/z* = 3395.4 confirmed the success of the synthesis of the mix-sequence 10mer aocPNA (H-GTAGATCACT-LysNH_2). Nevertheless, the signal was relatively weak and a series of fragmented products were observed. Analysis of each molecular ion peaks suggest the degradation pattern as shown in Table 3.3.

Table 3.3 Analysis of MALDI-TOF mass spectrum of aocPNA fragmentation from Figure 3.26

Fragment[a]	m/z (calcd)[b]	m/z (observed)[c]
H-CYAYCYT-LysNH_2	1308.3	1306.7
H-TYCYAYCYT-LysNH_2	1628.6	1626.8
H-AYTYCYAYCYT-LysNH_2	1957.9	1956.9
H-GYAYTYCYAYCYT-LysNH_2	2303.2	2302.1
H-AYGYAYTYCYAYCYT-LysNH_2	2632.5	2631.9
H-TYAYGYAYTYCYAYCYT-LysNH_2	2952.8	2951.1
H-GYTYAYGYAYTYCYAYCYT-LysNH_2	3298.2	3297.5
H-YGYTYAYGYAYTYCYAYCYT-LysNH_2	3397.2	3395.4

[a] Y represents oxetane spacer

[b] average mass of $M + H^+$

[c] MALDI-TOF mass spectrometry in linear positive mode using α-cyano-4-hydroxycinnamic acid (CCA) as matrix

The fragmentation analysis in Table 3.3 revealed that the smaller fragments were not originated from incomplete peptide coupling. If these smaller fragments were to derive from such incomplete coupling, they should carry a 43 Da higher in mass due to acetylation during the capping step (Figure 3.27). We proposed that aocPNA underwent decomposition by amide bond cleavage between *epi*-oxetin spacer and proline as shown in Figure 3.27. The degradation was facilitated under basic condition (1:1 aqueous ammonia:dioxane, 60 °C) required for the nucleobase deprotection.

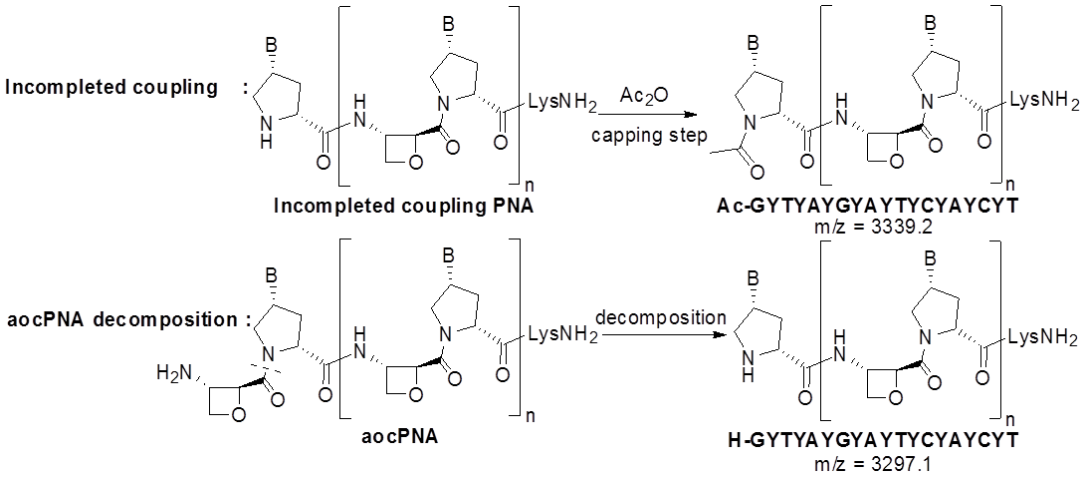

Figure 3.27 Comparison between expected products of aocPNA incompleted coupling and aocPNA degradation

Initially, we believed that the free amino functional group on *N*-terminal of aocPNA plays a crucial role in the degradation by acting as internal nucleophile. Free NH_2-terminus accelerated amide bond cleavage to smaller fragments has been previously reported and this problem was solved by capping at the *N*-terminus of the PNA molecule.[41] This prompted us to investigate the stability of *N*-benzoylated aocPNA (Bz-aocPNA, M + H^+ calcd. *m/z* = 3501.4). MALDI-TOF mass spectra of Bz-aocPNA under different deprotections are summarized in Figure 3.28.

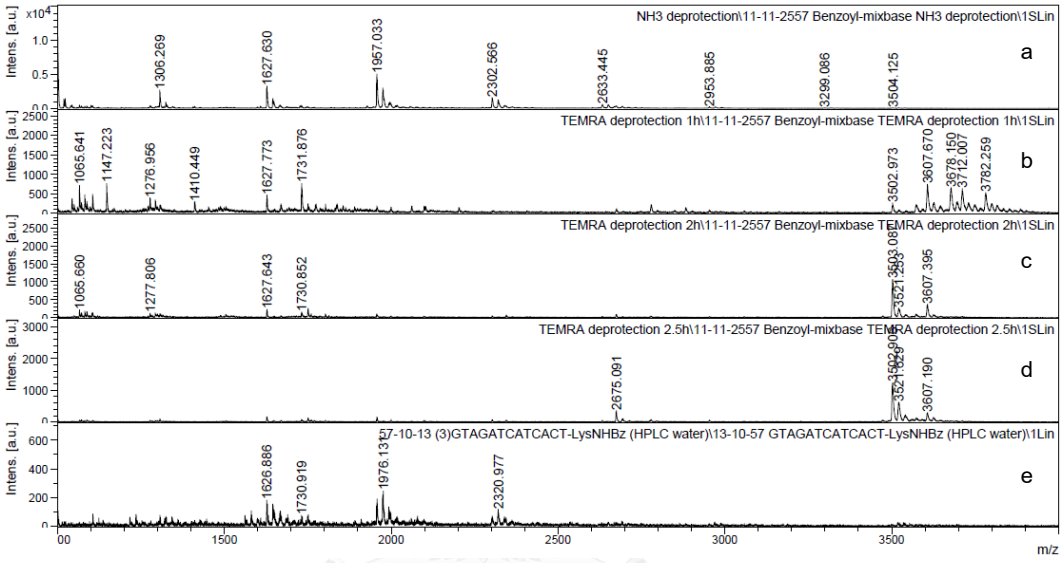

Figure 3.28 MALDI-TOF mass spectra of Bz-aocPNA under various basic deprotections and TFA cleavage **a)** mass spectrum of Bz-aocPNA from deprotection under 1:1 aqueous ammonia:dioxane at 60 °C for overnight **b)** mass spectrum of Bz-aocPNA from deprotection under 1:1:2 *tert*-butylamine:MeOH:H_2O at 60 °C for 1 hour **c)** mass spectrum Bz-aocPNA from of deprotection under 1:1:2 *tert*-butylamine:MeOH:H_2O at 60 °C for 2 hours **d)** mass spectrum Bz-aocPNA from of deprotection under 1:1:2 *tert*-butylamine:MeOH:H_2O at 60 °C for 2.5 hours. All of PNAs from investigation of side chain deprotection conditions (**a-d**) were cleaved from solid support under treated by TFA at room temperature for 10 minutes. **e)** mass spectrum of Bz-aocPNA from condition **d** following by TFA cleavage at room temperature for 3 hours

Treatment of Bz-aocPNA under the standard deprotection condition (1:1 aqueous ammonia:dioxane at 60 °C for overnight, **a**) still resulted in fragmentation similar to that of uncapped aocPNA system (H-aocPNA). Thus, decomposition of aocPNAs (for both H-aocPNA and Bz-aocPNA) must proceed through a different mechanism. Fortunately, less degradation was observed under milder deprotection conditions (1:1:2 *tert*-butylamine:MeOH:H_2O, 60 °C), which is commonly used to deprotect oligonucleotides carrying base-sensitive groups.[28] At short deprotection time (1 hour, **b**) incomplete deprotection was observed as shown by the signals with *m/z* larger than expected for Bz-aocPNA ($M + H^+$ of Bz-aocPNA, calcd. *m/z* = 3501.4). Prolonging the reaction time to 2 hours (**c**) led to a more complete deprotection but some fragmentation was observed (*m/z* = 2575.1) when the reaction time was increased to 2.5 hours (**d**). These results suggest that the harsh conditions and prolonged reaction times could promote the degradation of aoc-PNA. Therefore, 1:1:2 *tert*-butylamine:MeOH:H_2O at 60 °C for 2 hours was selected as the optimal deprotection condition.

Having the optimized side chain deprotection in hands, we moved to investigate the cleavage of aocPNA from solid support with TFA. For small scale, the cleavage time was keep relatively short (<10 minutes), and no apparent side reactions were observed. However, cleavage for larger scale synthesis (0.5 μmol) required up to 3 hours to ensure completion, and in this case, several smaller fragments are visible as shown in Figure 3.28e. Thus, aocPNA does not only degrade under basic conditions, but it is also sensitive under acidic cleavage from solid support with TFA.

Optimization of the conditions for cleavage of aocPNA from the solid support in order to avoid decomposition of aocPNA was next studied (Figure 3.29). Since benzoyl protection on *N*-terminal of aocPNA (Bz-aocPNA) did not improve the stability of aocPNA, *N*-terminally unprotected aocPNA (H-aocPNA) was used in this and the remaining studies.

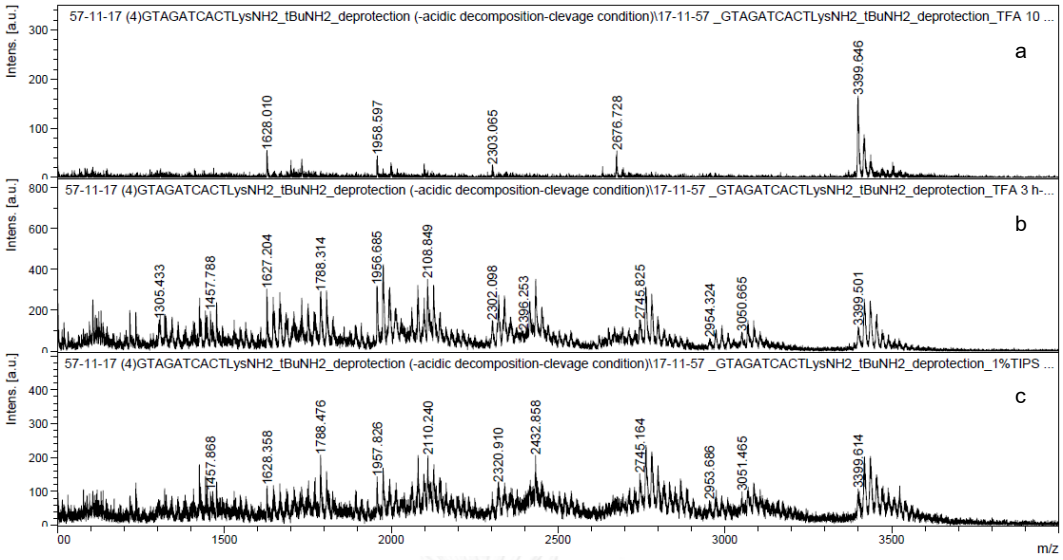

Figure 3.29 MALDI-TOF mass spectra of H-aocPNA under various cleavage conditions **a)** mass spectrum of H-aocPNA from cleavage with TFA at ambient temperature for 10 minutes **b)** mass spectrum of H-aocPNA from cleavage with TFA at ambient temperature for 3 hours **c)** mass spectrum of H-aocPNA from cleavage with 1% triisopropylsilane (TIPS) in TFA at ambient temperature for 3 hours. All of PNAs (**a-c**) were side-chain deprotected by treatment with 1:1:2 *tert*-butylamine:MeOH:H_2O at 60 $^{\circ}$C for 2 hours

When the cleavage time was short (10 minutes, **a**), the mass peak of the desired H-aocPNA (*m/z* H-aocPNA = 3396.2) was observed as the major peak. However, increasing the reaction time to 3 hours (**b**) resulted in degradation to smaller fragments having a pattern that was quite similar to that obtained from the nucleobase degradation (Table 3.3). However, both *N*-terminal and *C*-terminal fragments were also observed as shown in Table 3.4. This was different from the basic degradation that only solid support-bound *C*-terminal fragments were observed since the *N*-terminal fragments were washed away.

Table 3.4 Analysis of fragment identities from MALDI-TOF MS spectrum from Figure 3.26b

Terminal Fragment	Fragment[a]	m/z (calcd)[b]	m/z (observed)[c]
C-terminal Fragments	H-CYAYCYT-LysNH_2	1308.3	1305.4
	H-TYCYAYCYT-LysNH_2	1628.6	1627.2
	H-AYTYCYAYCYT-LysNH_2	1957.9	1956.7
	H-GYAYTYCYAYCYT- LysNH_2	2303.2	2302.1
	H-TYAYGYAYTYCYAYCYT- LysNH_2	2952.8	2954.3
	H-YGYTYAYGYAYTYCYAYCYT- LysNH_2	3397.2	3399.5
N-terminal Fragments	H-YGYTYAYG-Z	1458.3	1457.8
	H-YGYTYAYGYA-Z	1787.7	1788.3
	H-YGYTYAYGYAYT-Z	2108.0	2108.8
	H-YGYTYAYGYAYTYC-Z	2413.2	2415.5
	H-YGYTYAYGYAYTYCYA-Z	2742.6	2745.8
	H-YGYTYAYGYAYTYCYAYC-Z	3047.8	3050.7

[a] Y represents oxetane spacer, Z represents end terminal of lactone moiety from degradation (m/z = 116, as shown in Figure 3.35)

[b] average mass of $M + H^+$

[c] MALDI-TOF mass spectrometry in linear positive mode using α-cyano-4-hydroxycinnamic acid (CCA) as matrix

In addition to the degradation products, a series of M+18 peaks were observed in all fragments. For example, considering the peak at *m/z* 1956.7, series of peaks at *m/z* 1975.1, 1992.7 and 2011.2 were also found. The results suggest that degradation of aocPNA involved initial hydrolysis of the oxetane ring, probably catalyzed by TFA. Initially we suspected that acidic decomposition might be induced by the 4-methyltrityl carbocation generated during the lysine(Mtt) deprotection. Thus, addition of triisopropylsilane (TIPS) as a carbocation scavenger could diminish the degradation.[40] However, the decomposition was still present in the presence of 1% triisopropylsilane (TIPS) (**c**).

To suppress the decomposition by reduce a possibility of aocPNA to contact with acid, it was necessary to decrease the reaction time and to use lower concentration of acid (Figure 3.30). H-aocPNA on the solid support (0.25 μmol scale) was cleaved by brief treatment with 50% TFA in CH_2Cl_2 for 2 minutes. Each fraction was evaporated and precipitated in Et_2O immediately to reduce the contact of the aocPNA and the acid. The cleavage was repeated until no more PNA

was cleaved from the resin or until degradation was observed, according to MALDI-TOF analysis. The results are shown in Figure 3.30.

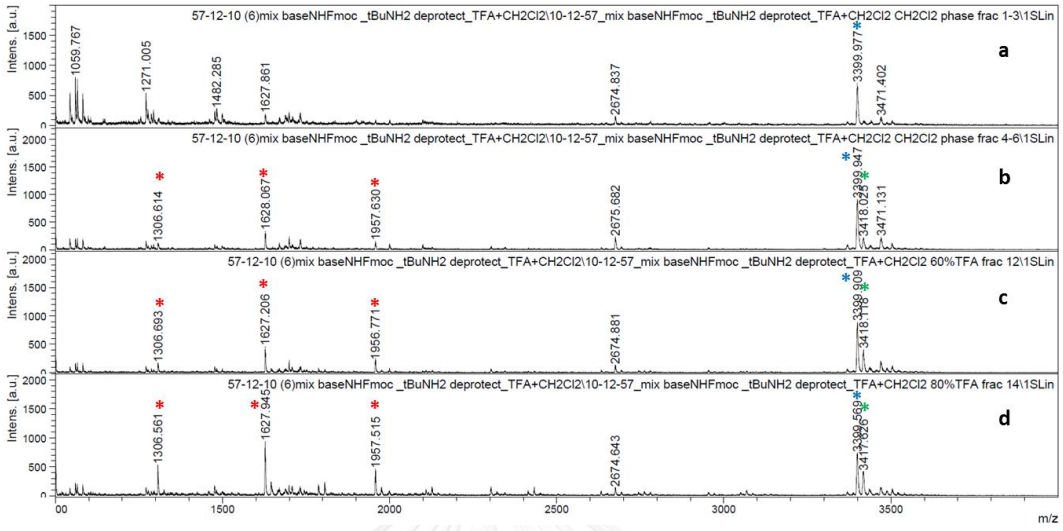

Figure 3.30 MALDI-TOF mass spectra of H-aocPNA cleavage from solid support under treated with 50% TFA in CH_2Cl_2 **a)** mass spectrum of aocPNA within first 6 minutes **b)** mass spectrum between 6-12 minutes **c)** mass spectrum of aocPNA under treatment with 60% TFA in CH_2Cl_2 at 24 minutes **d)** mass spectrum of aocPNA under treatment with 80% TFA in CH_2Cl_2 at 28 minutes. H-aocPNA was nucleobase deprotected under 1:1:2 *tert*-butylamine:MeOH:H_2O at 60 $^{\circ}C$ for 2 hours

During the first 6 minutes, the cleavage in solution of 50 % TFA in CH_2Cl_2 (**a**) provided desired H-aocPNA at *m/z* 3400.0 ($M + H^+$ of H-aocPNA, calcd. *m/z* = 3397.2, peaks labled with blue star) as a major product. However, the hydrolysis and fragmentation start to appear during 6-12 minutes, **b** since +18 signal (*m/z* = 3418.0, peaks labled with green star) and 3 fragment peaks (*m/z* = 1306.7.0, 1628.1 and 1957.6, peaks labled with red star) were observed. The *m/z* peak of a single water adduct (*m/z* = 3418.0) became apparent after leaving the reaction for longer period, especially at higher acid concentration (60% and 80% TFA in CH_2Cl_2). In these cases, obvious fragment peaks were also observed (labeled with red stars) (**c-d**).

For obtaining H-aocPNA product, each cleavage fractions obtained during the first 12 minutes were immediately dried and precipitated with diethyl ether to reduce the acid contact as much as possible. The residue were dissolved in water and neutralized by addition of ammonium bicarbonate before being freeze dried and then purified by reverse phase HPLC. The aocPNAs were synthesized in two versions, non-acetylated (H-aocPNA) and acetylated (Ac-aocPNA). These were characterized by MALDI-TOF mass spectrometry (Table 3.5) and the purity

was determined to be >90% by reverse phase HPLC. Despite the decent overall coupling efficiency of 23%, the isolated yields were quite low (1.2 and 1.3% yield for H-aocPNA and Ac-aocPNA, respectively, compared to 10-30% of corresponding pyrrolidinyl PNAs[26]). This could be attributed to the sensitivity of the aocPNA under acidic and basic conditions, and also partly to loss during HPLC purification. Nevertheless, the aocPNAs were obtained in sufficient quantities for some preliminary DNA/RNA binding studies.

Table 3.5 Efficiency on synthesis and characterization of aocPNAs

PNA sequences	Coupling efficiency[a]	Isolated yield (%)[a]	t_R (min.)[b]	m/z (calcd)[c]	m/z (observed)[d]
H-GTAGATCACT-$LysNH_2$	23 %	1.2	25.9	3397.2	3397.1
Ac-GTAGATCACT-$LysNH_2$		1.3	30.1	3439.3	3440.9

[a] Coupling efficiency and isolated yield, spectrophotometrically determined

[b] HPLC conditions: C18 column, 4.6 × 50 mm, 3 μ, gradient 0.1% TFA in H_2O:MeOH 90:10 for 5 minutes then linear gradient to 10:90 over 30 minutes, flow rate: 0.5 mL/min, 260 nm.

[c] average mass of $M + H^+$

[d] MALDI-TOF mass spectrometry in linear positive mode using α-cyano-4-hydroxycinnamic acid (CCA) as matrix

3.8. Mechanistic investigation of aocPNA degradation

According to the results acidic cleavage of aocPNA from solid support, MALDI-TOF spectra indicated addition of water to aocPNA followed by cleavage of amide bond between proline and the *epi*-oxetin spacer. We hypothesized that the aocPNAs degradation began with hydrolysis of the oxetane ring because this *epi*-oxetin moiety is the only significant difference from other previous pyrrolidinyl PNAs which are stable under both standard side chain deprotection (1:1 aqueous ammonia:dioxane) and cleavage from the solid support (TFA).

Kanoh and coworkers reported that 3-phenyl-3-(phthalimidomethyl)oxetane (**67**) which is an oxetane having a carbonyl as a neighboring group, underwent ring-expansion through neighboring group participation (NGP) of carbonyl group under Lewis acid catalysis[42] as shown in Figure 3.31.

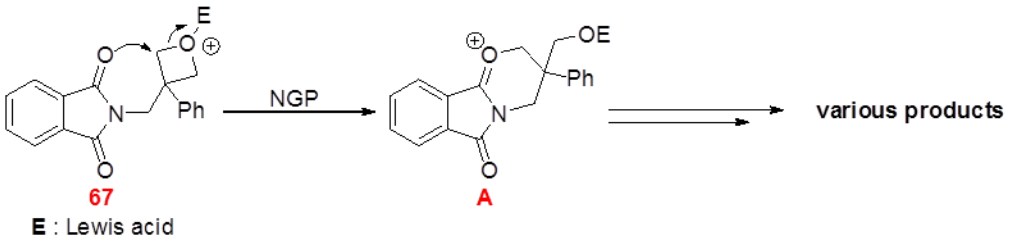

Figure 3.31 Mechanism of the amide-assisted oxetane ring opening of 3-phenyl-3-(phthalimidomethyl)oxetane (**67**)

Further investigation on NGP of amide carbonyl towards hydrolysis of *epi*-oxetin was examined by using *N*-benzoyl *epi*-oxetin (**63**) and *epi*-oxetin (**6**) as model substrates (Figure 3.32).

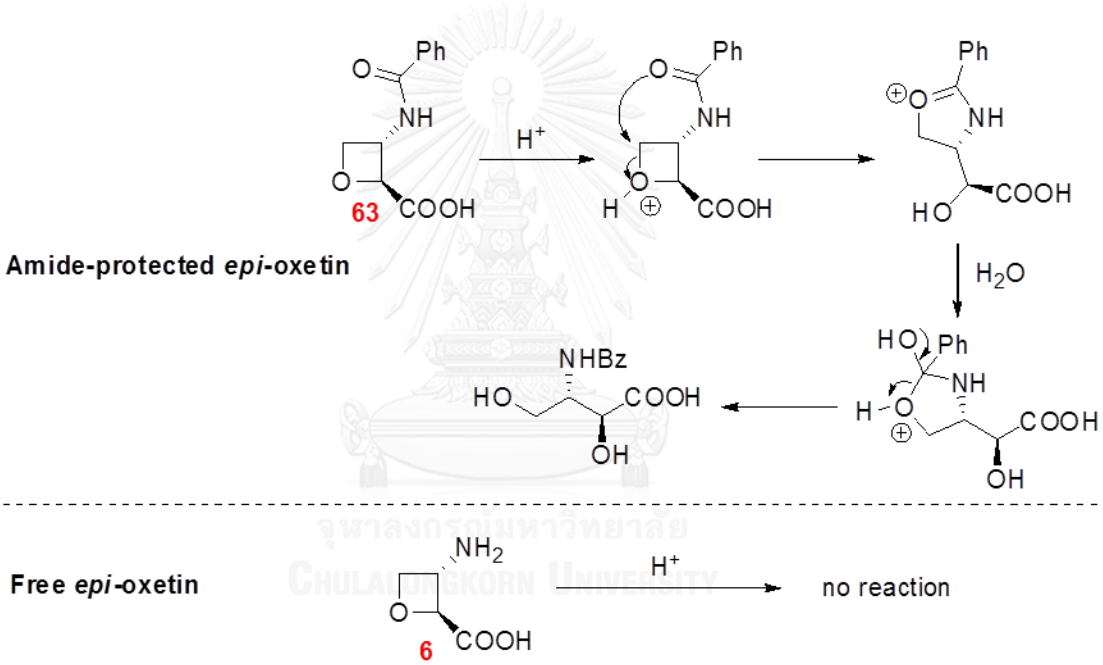

Figure 3.32 proposed decomposition mechanism of amide-protected *epi*-oxetin and general *epi*-oxetin

Racemic *N*-benzoyl *epi*-oxetin (**63**) was synthesized according to Figure 3.33. Protecting group manipulation of the Boc-oxetane alcohol (**32**) furnished the *N*-benzoylamino-oxetane alcohol (**62**) in 45% yield. The alcohol intermediate **62** was oxidized to the acid **63** in 30% yield. The free *epi*-oxetin (**6**) was prepared by Boc deprotection of racemic **33** with 1:1 TFA:CH_2Cl_2.

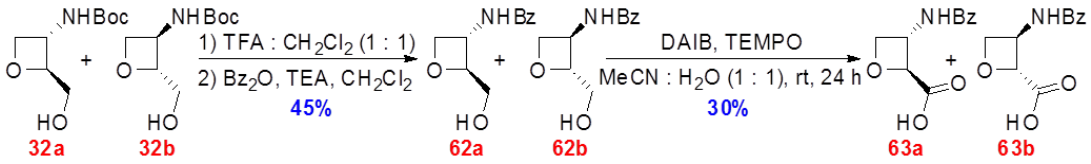

Figure 3.33 synthesis of benzoyl amide-protected *epi*-oxetin (**63**) starting from Boc-oxetane **32**

Compound **63** and *epi*-oxetin (**6**) were both treated with 0.1 M TFA in D_2O. ^1H NMR spectra of the free *epi*-oxetin (**6**) showed no appreciable change throughout the reaction period (time = 0 to 7 days). The stability of *epi*-oxetin was also supported by ESI-MS analysis ($C_4H_9NO_3$; *m/z* calcd. for M + H^+ 118.11; found 118.08). This indicated the oxetane ring itself is stable under acidic condition. However, ^1H NMR signals of *N*-benzoyl-*epi*-oxetin (**63**) changed over time and the starting material was completely consumed after 2 days as shown in Figure 3.34. ESI-MS analyses confirmed hydrolysis by detection of m/z +18 in molecular weight of **63** ($C_{11}H_{15}NO_5$; *m/z* calcd. for M + H^+ 240.23; found 240.20). Moreover, MALDI-TOF mass spectrometry studies also confirmed the hydrolytic ring opening of compound **63** and the stability of *epi*-oxetin (**6**) in 0.1 M TFA in H_2O (Figure A73). The result implies that the presence of the amide group is necessary for the hydrolysis of *N*-acyl *epi*-oxetin, and presumably aocPNAs, under acidic conditions.

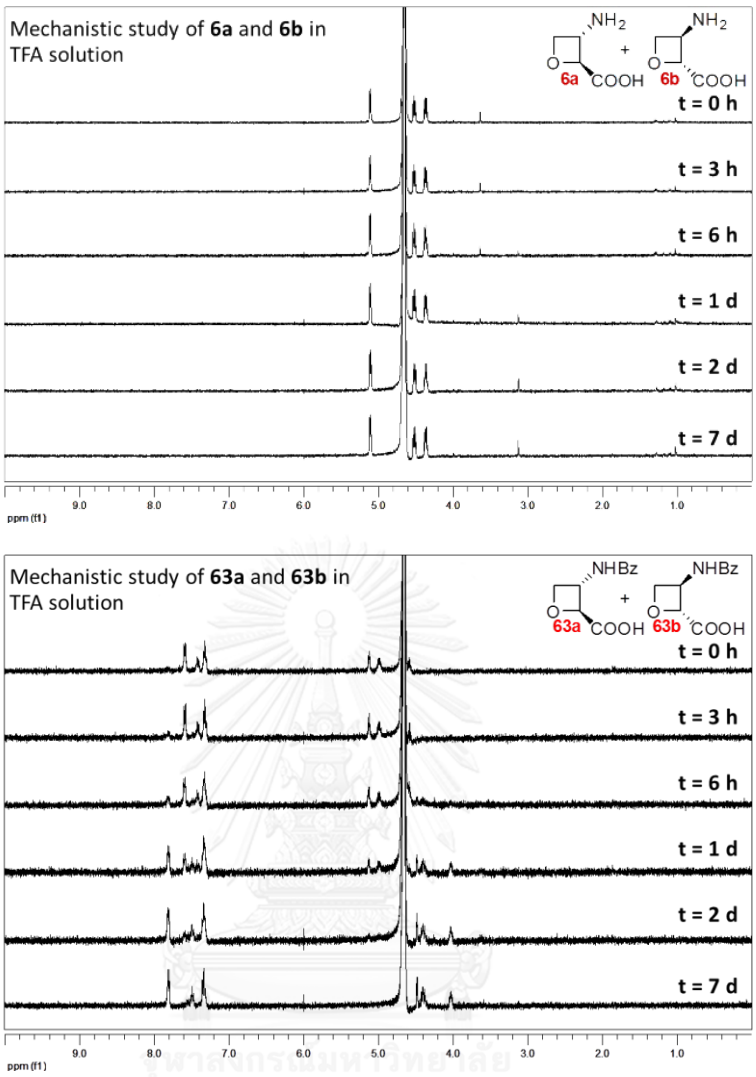

Figure 3.34 Mechanistic insight of *epi*-oxetin ring hydrolysis by comparison of ^{1}H NMR signals between *epi*-oxetin (**6**) and benzoyl amide-protected *epi*-oxetin (**63**) at various reaction times (0-7 d); condition:0.02 mM compound **6**/**63**, 0.1 M TFA in D_2O at ambient temperature

The mechanism of degradation of aocPNAs under acidic conditions was therefore proposed based on the susceptibility of degradation of oxetane ring *via* NGP of the amide group and the analysis of degradation fragments (Table 3.4) as shown in Figure 3.35. First, the oxetane ring was hydrolyzed *via* NGP through a five-membered ring intermediate **A**. Addition of a water molecule at the most electrophilic carbonyl followed by elimination generated a diol intermediate **B**, which could be detected as a series of M+18 peaks as shown in Figure 3.29. After that, the hydroxyl group attacked the carbonyl of the amide bond at the *C*-terminal side of the proline, generating 5-membered ring intermediate which underwent further degradation, resulting in cleavage of the amide bond between proline and oxetane spacer.

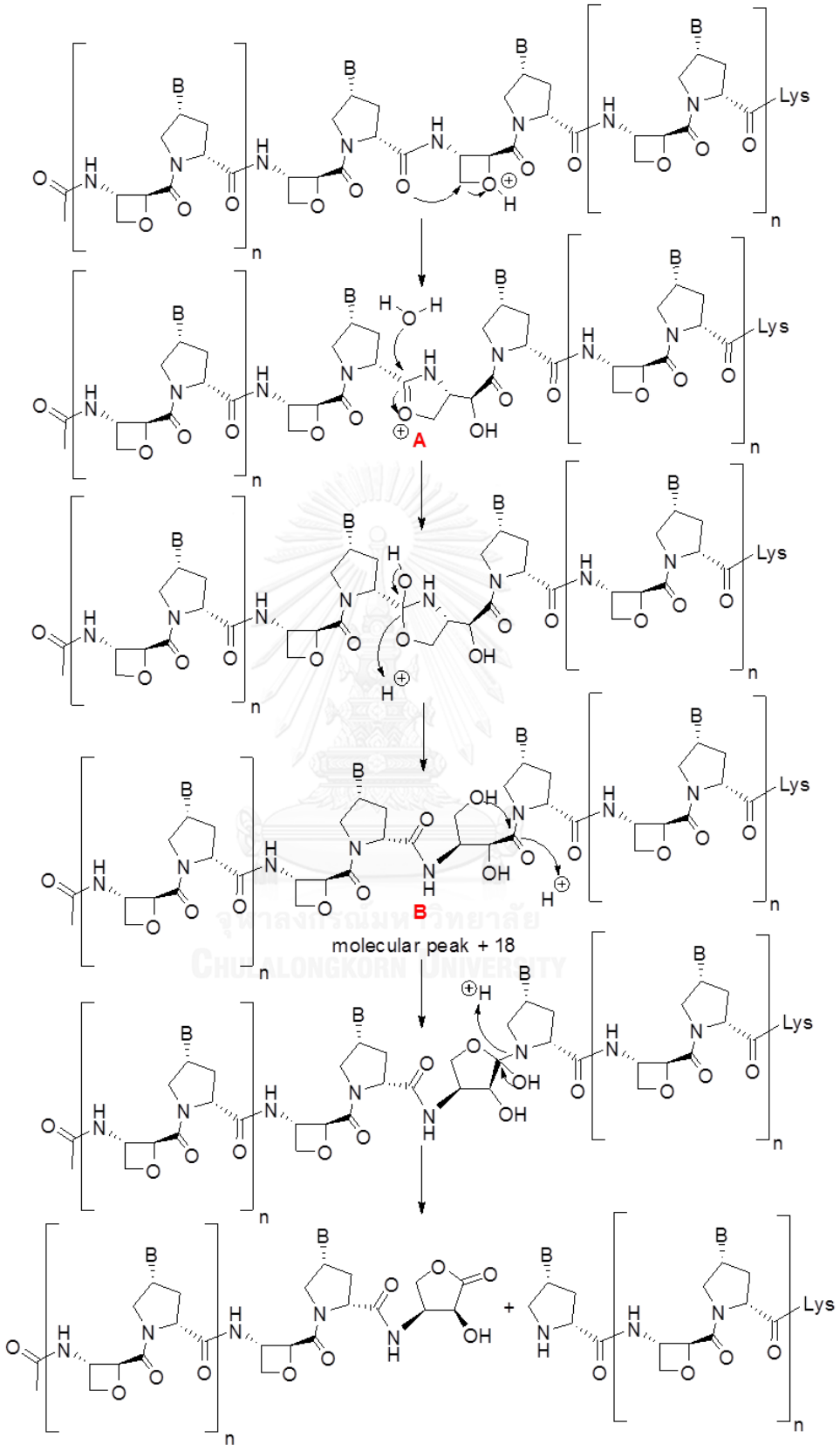

Figure 3.35 A proposed mechanism of aocPNAs decomposition under acidic condition (TFA)

For the mechanistic investigation of aocPNA degradation under basic conditions, racemic *epi*-oxetin (**6**) and *N*-Benzoyl *epi*-oxetin (**63**) were treated with NaOH in D_2O. ^1H NMR monitoring indicated good stability of both compounds under basic conditions at ambient temperature as shown in Figure 3.36. According to the available data, it is therefore not possible to conclude about the mechanistic pathway leading to the degradation of aocPNA under basic conditions. It should be noted that the actual conditions was performed with hot and concentrated aqueous ammonia, which could not be exactly mimicked in this model study.

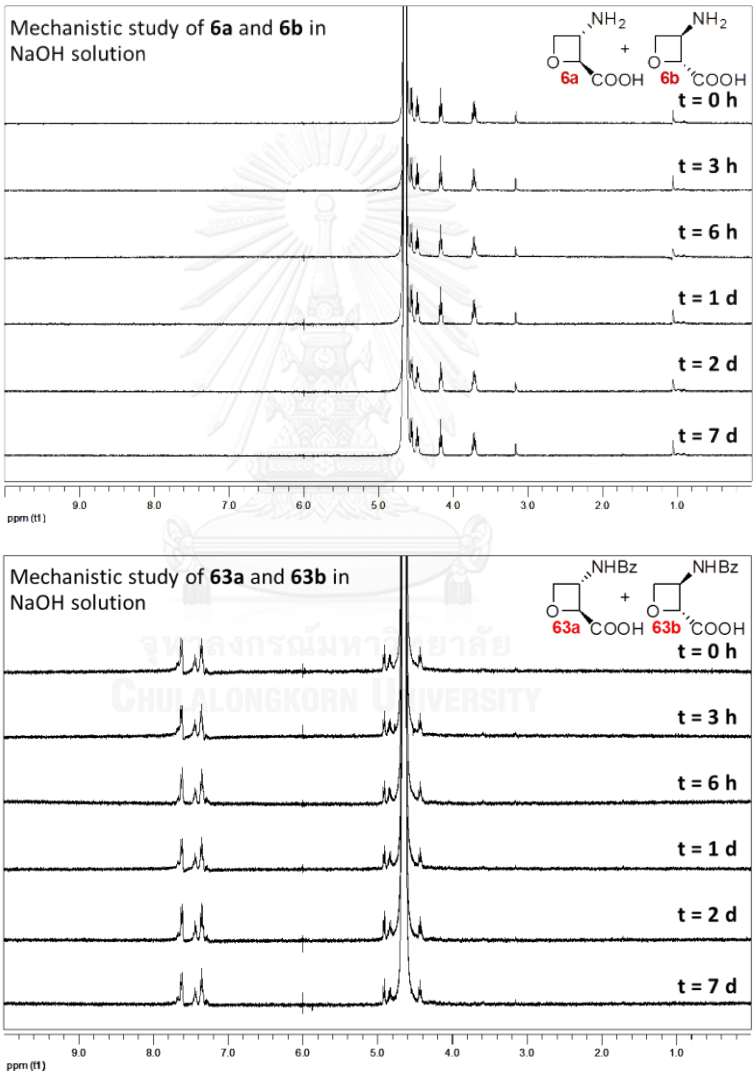

Figure 3.36 Mechanistic insight of *epi*-oxetin spacer by comparison of ^1H NMR signals between *epi*-oxetin (**6**) and benzoyl amide-protected *epi*-oxetin (**63**) at various reaction times (0-7 d); condition:0.02 mM compound **6**/**63**, 0.1 M NaOH in D_2O at ambient temperature

3.9. Investigation on binding affinities between aocPNAs and DNAs/RNAs

Stabilities of the hybrids formed between aocPNA and DNA or RNA were determined by thermal denaturation experiments by measuring the UV absorption at 260 nm in the temperature range between 20-90 ^{o}C. Initially, binding of the non-acetylated aocPNA (H-aocPNA; H-GTAGATCACT-LysNH_2) and acetylated aocPNA (Ac-aocPNA; Ac-GTAGATCACT-LysNH_2) to complementary DNA and RNA were evaluated as shown in Table 3.6.

Table 3.6 Thermal stabilities of hybrids between aocPNAs and complementary DNA/RNA.

Entry	*N*-terminal capping(X)[a]	DNA/RNA sequence	T_m (^{o}C) aocPNA[b]	T_m (^{o}C) acbcPNA[c]	T_m (^{o}C) acpcPNA[c]	T_m (^{o}C) atfcPNA[c]
1	Ac	5'-dAGTGATCTAC-3'	46.3	66.1	53.3	52.5
2	H	5'-dAGTGATCTAC-3'	46.1	-	-	-
3	Ac	5'-rAGUGAUCUAC-3'	31.3	58.2	42.3	36.0
4	H	5'-rAGUGAUCUAC-3'	30.3	-	-	-

[a] aocPNA sequence is X-GTAGATCACT-LysNH_2

[b] condition: 1.0 μM PNA, 1.0 μM DNA/RNA, 10 mM sodium phosphate buffer pH 7.0, 100 mM NaCl. Heating rate 1 ^{o}C/ 1 min.

[c] Literature data[8, 10] under the same conditions; all PNA sequences involved were acetyl-capped.

According to the results in Table 3.6, aocPNAs showed the ability to bind with both complementary DNA and RNA. Melting temperatures (T_m) of the non-acetylated and *N*-acetylated aocPNAs were found to be in the same range (temperature difference < 1.0 ^{o}C) (entry 1 versus 2 / entry 3 versus 4). However, when the melting temperatures (T_m) of aocPNA were compared to three other previously reported pyrrolidinyl PNAs;[8, 10] acpcPNA (with 2-aminocyclopentanecarboxylic acid spacer), acbcPNA (with 2-aminocyclobutanecarboxylic acid spacer), and atfcPNA (with 3-aminotetrahydrofuran-2-carboxylic acid spacer), the thermal stability of aocPNA-DNA and aocPNA-RNA hybrids were significantly decreased. The T_m of aocPNA with DNA was lowered by -7.0, -19.8 and -6.2 ^{o}C respectively when compared with acpcPNA, acbcPNA and atfcPNA. In the case of aocPNA-RNA binding, the T_m values were decreased by -11.0, -26.9, -4.7 ^{o}C (acpcPNA, acbcPNA and atfcPNA) as shown in entry 3.

The binding specificity between aocPNA and DNA was also investigated by comparing T_m values between the aocPNA-complementary DNA hybrid and three single mismatches at the middle position of the DNA sequence. Since the thermal stability difference between H-aocPNA and Ac-aocPNA was not significant as previously discussed (Table 3.6), only H-aocPNA was included in the study as shown in Table 3.7.

Table 3.7 Binding specificity by comparison between H-aocPNA-complementary DNA and mismatch DNAs.

Entry	DNA code[a]	T_m (°C) aocPNA[b, c]	T_m (°C) acbcPNA[d]	T_m (°C) acpcPNA[d]	T_m (°C) atfcPNA[d]
1	Dcom	46.1	66.1	53.3	52.5
2[e]	DsmC	<20 (>26.1)	39.8 (26.3)	23.8 (29.4)	23.4 (29.1)
3[e]	DsmG	<20 (>26.1)	36.4 (29.7)	23.9 (29.3)	23.4 (29.1)
4[e]	DsmT	28.1 (18.0)	46.6 (19.5)	29.4 (23.8)	25.4 (27.1)

[a] DNA sequence:5'-dAGTGXTCTAC-3'; X = A (Dcom), C (DsmC), G (DsmG), T (DsmT)

[b] aocPNA sequence was H-GTAGATCACT-$LysNH_2$

[c] condition: 1.0 μM PNA, 1.0 μM DNA/RNA, 10 mM sodium phosphate buffer pH 7.0, 100 mM NaCl. Heating rate 1 °C/ min.

[d] Literature data[8, 10] under the same conditions; all PNA sequences were acetyl-capped

[e] value in parentheses are $\Delta T_m = T_m$ (complementary) - T_m (mismatch)

Even if the aocPNA exhibited lower binding affinity to DNA than acpcPNA, acbcPNA and atfcPNA, good specificity of the binding was still observed as shown by ΔT_m between complementary and mismatched DNA hybrids in the range of 18.0-26.1 °C. This range is similar to acbcPNA (ΔT_m between 19.5-29.7 °C) and not much different from both acpcPNA (ΔT_m between 23.8-29.4 °C) and atfcPNA (ΔT_m between 27.1-29.1 °C). Interestingly, for all pyrrolidinyl PNAs, the pT-dT mismatch showed the lowest specificity (smallest ΔT_m) by comparison to other mismatches.

3.10. Theoretical calculation

The excellent binding of acpcPNA to DNA has been investigated by molecular dynamics (MD) simulations.[8] The model suggested that the optimal torsional angle between the C(O)-C-C-NH in the β-amino acid in the DNA binding conformation of acpcPNA was close to 100°. This value agrees well with the value obtained from an X-ray structure of acbc-derived oligomer (95–100°).[8, 43] It was proposed that the low binding affinity between aocPNA and DNA might be originated from the deviation of the torsional angle from this optimal value due to the shorted C-O compare to C-C bonds, leading to flattening of the ring and widening of the torsional angle.

Computational calculation (performed by Assoc. Prof. Viwat Vchirawongkwin) was applied to optimize the geometries and find the optimal torsional angles of two model compounds, namely (1*S*,2*S*)-*N*-methoxycarbonyl-2-aminocyclobutanecarboxylic acid dimethylamide (**64**) to represent acbc in acbcPNA and (2*S*,3*S*)-*N*-methoxycarbonyl-2-aminooxetanecarboxylic acid dimethylamide (**65**) to represent aoc in aocPNA (Figure 3.37). The ab initio method was employed to scan and calculate the lowest relative energy between torsional angles from 80 to 140°. The optimized structures of the model compounds **64** and **65** are shown in Figure 3.38a. The minimum in relative energy was observed at 95.3 and 110.3°, respectively as shown in Figure 3.38b.

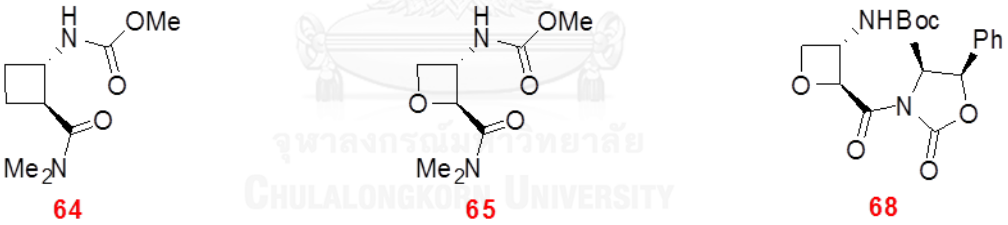

Figure 3.37 Structures of (1*S*,2*S*)-*N*-methoxycarbonyl-2-aminocyclobutanecarboxylic acid dimethylamide (**64**), (2*S*,3*S*)-*N*-methoxycarbonyl-2-aminooxetanecarboxylic acid dimethylamide (**65**) (models of acbcPNA and aocPNA, respectively) and *tert*-butyl (2*S*,3*S*)-2-((4*S*,5*R*)-4-methyl-2-oxo-5-phenyloxazolidine-3-carbonyl)oxetan-3-ylcarbamate (**68**)

According to the model, the optimal torsional angle of compound **58** (acbc model) was 95.3°, which is quite close to the angle from X-ray structure of acbc-derived oligomer between 95-100°,[43] and fits well with the torsional angle of 99-102° required for acpcPNA-DNA duplex.[8] However, the much wider torsional angle of **59** (aoc model) at 110.3° are quite deviated from the optimal torsional angle of pyrrolidinyl PNA-DNA duplex.[8] Furthermore, the torsional angle of oxetane β-amino acid **68** was recently experimentally determined by X-ray crystallography to be 123.5°,[16] which confirm that the torsional angle in *epi*-oxetin is indeed very far from the optimum

value. Therefore, more conformational adjustment is required for the aoc spacer in aocPNA than the acbc spacer in acbcPNA upon binding with DNA. This should explain the relatively low thermal stability of aocPNA-DNA hybrid compared to acbcPNA-DNA hybrid.

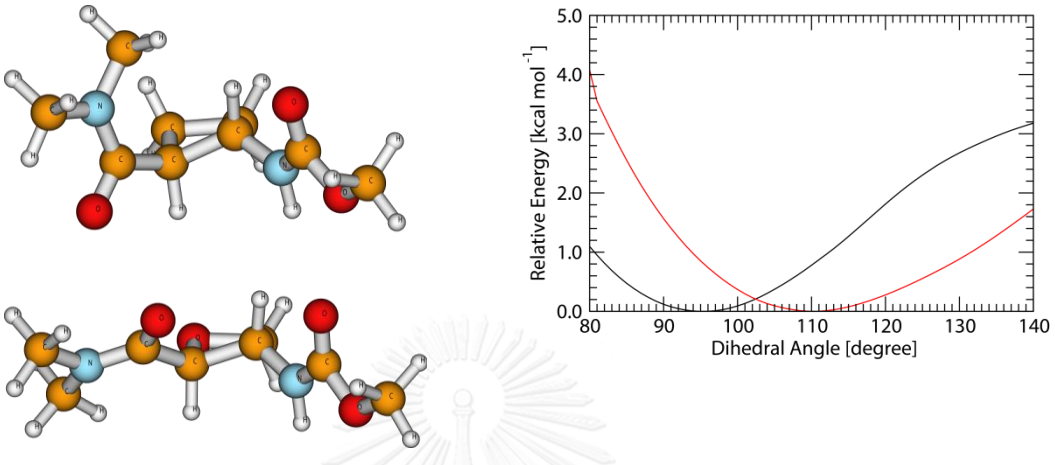

(a) (b)

Figure 3.38 The optimized geometries and the torsional energy profiles of compound **64** and **65** using as the model for linker of acbcPNA and aocPNA respectively; (a) the structures of (top) **64** and (bottom) **65**, (b) the torsional energy profiles of (black line) **64** and (red line) **65**

Chapter 4
Conclusion

Successful enantioselective synthesis of Fmoc-protected (2*S*,3*S*)-*epi*-oxetin (**55a**) [(2*S*,3*S*)-3-(((9*H*-fluoren-9-yl)methoxy)carbonylamino)oxetane-2-carboxylic acid] was reported. The synthesis was accomplished through an 11 step-sequence reaction developed from previous work by Ōmura's research group. Our synthetic strategy provided a straightforward, concise and highly atom-economical route (Figure 4.1). The synthesis started with monobenzylation of the commercially available diol **38** followed by Anelli's oxidation and isomerization to *trans*-aldehyde **41** under acidic condition. Enantioselective Jorgensen's organocatalytic epoxidation was carried out to afford the epoxide **59a**, which was subsequently reduced by $NaBH_4$ to provide the epoxyalcohol **50a** in high yield and enantioselectivity (91-95% ee). Next, regioselective epoxide ring-opening by sodium azide yielded **51a** in high yield. The azidoalcohol **51a** was treated with catalytic 2-ADP boron catalyst and TsCl to give monotosylate intermediate **52a** which was subsequently cyclized under phase-transfer condition to provide (2*S*,3*S*)-3-azido-2-(benzyloxymethyl)oxetane (**53a**). Functional group interconversion and protecting group manipulation of intermediate **53a** were proceeded as follow. Hydrogenation to remove benzyl ether and reduction of azide to amine with concomitant Boc-protection in the presence of Boc_2O yielded oxetane **32a**. Primary alcohol oxidation of **32a** by using DAIB-TEMPO provided **33a** in good yield. Finally, conversion of the protecting group from Boc to Fmoc furnished the desired (2*S*,3*S*)-*epi*-oxetin (**55a**) in 5.1% overall yield and 94% ee over 11 steps from the precursor **38** as shown in Figure 4.1.

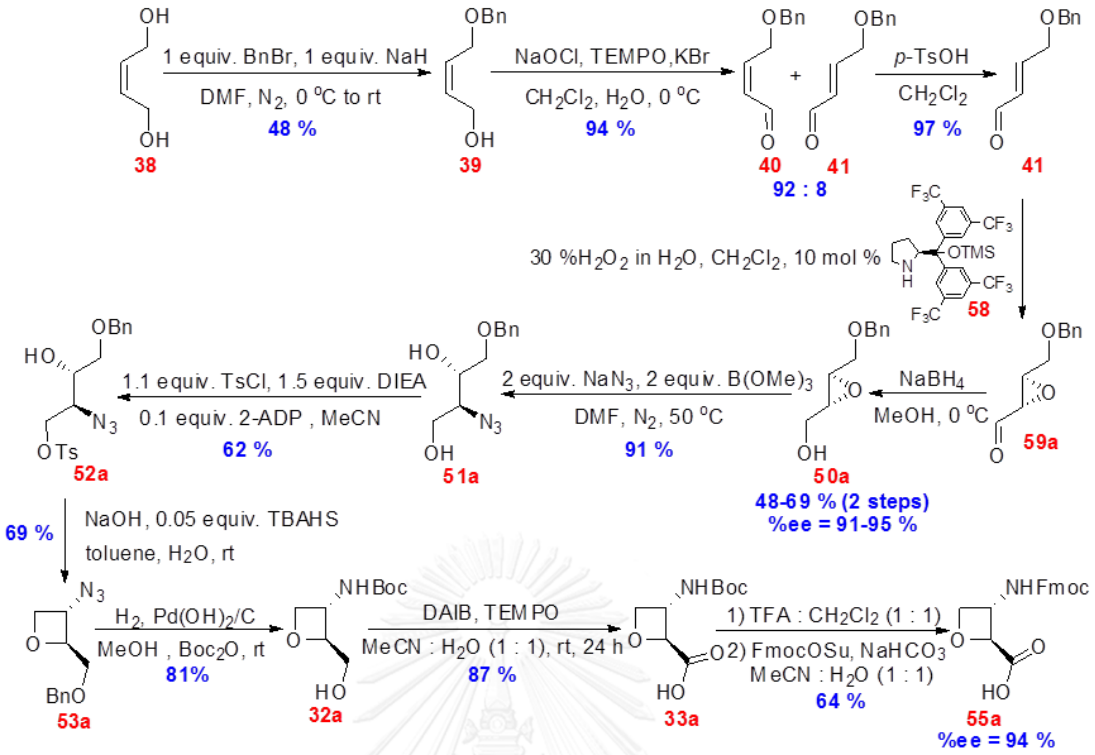

Figure 4.1 Synthesis of target molecule **55a** from **38**

Next, two of aocPNAs 10mer mix-base sequences differing at only the *N*-terminal capping (H- vs Ac-) were successfully synthesized *via* Fmoc-solid phase peptide synthesis starting from (2'*R*,4'*R*)-pyrrolidinyl PNA monomers and **55a** (pre-activated with pentafluorophenyl ester). The overall coupling efficiency as measured spectroscopically was 23%, which translated to 93% per each coupling cycle. However, aocPNAs exhibited unexpected sensitivity under both basic condition of nucleobase deprotection and acidic condition required for cleavage of the aocPNA from the solid support. After careful optimization of deprotection and cleavage conditions, aocPNAs were obtained in low yield between 1.2-1.3% after reverse phase HPLC purification. The decomposition mechanism of the aocPNA under acidic condition proposed to initially begin with hydrolysis of oxetane ring by acceleration with neighboring group participation from oxygen atom of the amide carbonyl group. The initially formed oxetane hydrolysis product further cyclized to a five-membered ring lactone, resulting in cleavage of the amide bond. Thermal denaturation experiments indicated that aocPNA binds specifically to both complementary DNA and RNA. However, binding affinities were lower than other pyrrolidinyl PNAs (acpcPNA, acbcPNA and atfcPNA) bearing the same sequence. This relatively low thermal stability of aocPNA-DNA hybrid is explained by the different torsional angle C(O)-C-C-N of acbc and aoc. Computational simulation indicated that the angle of aoc model (110.3°) is quite different to the optimal torsional angle required in pyrrolidinyl PNA-DNA duplexes (99-102°) compared to that of acbc model (95.3°). This

implied that aocPNA would require more conformational adjustment than acbcPNA for binding to DNA, thus explained in lower binding affinity. Due to the low yield, as well as the poor binding affinity towards DNA and RNA, the solubility and non-specific binding properties of aocPNA has not been investigated further.

REFERENCES

1. Nielsen, P. E.; Haaima, G., Peptide nucleic acid (PNA). A DNA mimic with a pseudopeptide backbone. *Chemical Society Reviews* **1997,** *26* (2), 73-78.

2. Egholm, M.; Buchardt, O.; Christensen, L.; Behrens, C.; Freier, S. M.; Driver, D. A.; Berg, R. H.; Kim, S. K.; Norden, B.; Nielsen, P. E., PNA Hybridizes to Complementary Oligonucleotides Obeying the Watson-crick Hydrogen-bonding Rules. *Nature* **1993,** *365* (6446), 566-568.

3. Demidov, V. V.; Potaman, V. N.; Frank-Kamenetskil, M. D.; Egholm, M.; Buchard, O.; Sönnichsen, S. H.; Nielsen, P. E., Stability of peptide nucleic acids in human serum and cellular extracts. *Biochemical Pharmacology* **1994,** *48* (6), 1310-1313.

4. Nielsen, P. E., Peptide nucleic acid: a versatile tool in genetic diagnostics and molecular biology. *Current Opinion in Biotechnology* **2001,** *12* (1), 16-20.

5. Vilaivan, T.; Srisuwannaket, C., Hybridization of Pyrrolidinyl Peptide Nucleic Acids and DNA: Selectivity, Base-Pairing Specificity, and Direction of Binding. *Organic Letters* **2006,** *8* (9), 1897-1900.

6. Ananthanawat, C.; Vilaivan, T.; Hoven, V. P.; Su, X., Comparison of DNA, aminoethylglycyl PNA and pyrrolidinyl PNA as probes for detection of DNA hybridization using surface plasmon resonance technique. *Biosensors and Bioelectronics* **2010,** *25* (5), 1064-1069.

7. Vilaivan, C.; Srisuwannaket, C.; Ananthanawat, C.; Suparpprom, C.; Kawakami, J.; Yamaguchi, Y.; Tanaka, Y.; Vilaivan, T., Pyrrolidinyl peptide nucleic acid with alpha/beta-peptide backbone: A conformationally constrained PNA with unusual hybridization properties. *Artificial DNA, PNA & XNA* **2011,** *2* (2), 50-59.

8. Mansawat, W.; Vilaivan, C.; Balázs, Á.; Aitken, D. J.; Vilaivan, T., Pyrrolidinyl Peptide Nucleic Acid Homologues: Effect of Ring Size on Hybridization Properties. *Organic Letters* **2012,** *14* (6), 1440-1443.

9. Sahu, B.; Sacui, I.; Rapireddy, S.; Zanotti, K. J.; Bahal, R.; Armitage, B. A.; Ly, D. H., Synthesis and characterization of conformationally preorganized, (R)-diethylene glycol-containing gamma-peptide nucleic acids with superior hybridization properties and water solubility. *Journal of organic chemistry* **2011,** *76* (14), 5614-5627.

10. Sriwarom, P.; Padungros, P.; Vilaivan, T., Synthesis and DNA/RNA Binding Properties of Conformationally Constrained Pyrrolidinyl PNA with a Tetrahydrofuran Backbone Deriving from Deoxyribose. *Journal of organic chemistry* **2015,** *80* (14), 7058-7065.

11. Bach, T.; Schröder, J., A Short Synthesis of (±)-Oxetin. *Liebigs Annalen* **1997,** *1997* (11), 2265-2267.

12. Kitamatsu, M.; Takahashi, A.; Ohtsuki, T.; Sisido, M., Synthesis of pyrrolidine-based oxy-peptide nucleic acids carrying four types of nucleobases and their transport into cytoplasm. *Tetrahedron* **2010,** *66* (51), 9659-9666.

13. Kawahata, Y.; Takatsuto, S.; Ikekawa, N.; Murata, M.; Omura, S., Synthesis of a new amino acid-antibiotic, oxetin and its three stereoisomers. *Chemical & pharmaceutical bulletin* **1986,** *34* (8), 3102-10.

14. Adelwöhrer, C.; Takano, T.; Nakatsubo, F.; Rosenau, T., Synthesis of 13C-Perlabeled Cellulose with more than 99% Isotopic Enrichment by a Cationic Ring-Opening Polymerization Approach. *Biomacromolecules* **2009,** *10* (10), 2817-2822.

15. Blauvelt, M. L.; Howell, A. R., Synthesis of epi-Oxetin via a Serine-Derived 2-Methyleneoxetane. *Journal of organic chemistry* **2008,** *73* (2), 517-521.

16. Kassir, A. F.; Ragab, S. S.; Nguyen, T. A. M.; Charnay-Pouget, F.; Guillot, R.; Scherrmann, M.-C.; Boddaert, T.; Aitken, D. J., Synthetic Access to All Four Stereoisomers of Oxetin. *Journal of organic chemistry* **2016,** *81* (20), 9983-9991.

17. Thurner, A.; Faigl, F.; Toke, L.; Mordini, A.; Valacchi, M.; Reginato, G.; Czira, G., Useful base promoted elaborations of oxiranyl ethers. *Tetrahedron* **2001,** *57* (38), 8173-8180.

18. Fournier, J. F.; Mathieu, S.; Charette, A. B., Diastereoselective Zinco-Cyclopropanation of Chiral Allylic Alcohols with gem-Dizinc Carbenoids. *Journal of the American Chemical Society* **2005,** *127* (38), 13140-13141.

19. Shen, L. L.; Wang, F.; Mun, H. S.; Suh, M.; Jeong, J. H., Solvent-dependent reactivity in porcine pancreatic lipase (PPL)-catalyzed hydrolysis. *Tetrahedron: Asymmetry* **2008,** *19* (14), 1647-1653.

20. Marshall, J. A.; Fitzgerald, R. N., Synthesis of a syn,syn,syn,syn-Stereopentad Precursor of the Marine Sponge Polyketide Callystatin A. *Journal of organic chemistry* **1999,** *64* (12), 4477-4481.

21. Tsujigami, T.; Sugai, T.; Ohta, H., Microbial asymmetric reduction of α-hydroxyketones in the anti-Prelog selectivity. *Tetrahedron: Asymmetry* **2001,** *12* (18), 2543-2549.

22. Krueger, E. B.; Hopkins, T. P.; Keaney, M. T.; Walters, M. A.; Boldi, A. M., Solution-Phase Library Synthesis of Furanoses. *Journal of combinatorial chemistry* **2002,** *4* (3), 229-238.

23. Sasaki, M.; Tanino, K.; Hirai, A.; Miyashita, M., The C2 Selective Nucleophilic Substitution Reactions of 2,3-Epoxy Alcohols Mediated by Trialkyl Borates: The First endo-Mode Epoxide-Opening Reaction through an Intramolecular Metal Chelate. *Organic Letters* **2003,** *5* (10), 1789-1791.

24. Hayes, M. P.; Hatala, P. J.; Sherer, B. A.; Tong, X.; Zanatta, N.; Borer, P. N.; Kallmerten, J., Regioselective synthesis of ^{13}C1-labeled 2-deoxyribonolactones. *Tetrahedron* **2001,** *57* (8), 1515-1524.

25. Marigo, M.; Franzén, J.; Poulsen, T. B.; Zhuang, W.; Jørgensen, K. A., Asymmetric Organocatalytic Epoxidation of α,β-Unsaturated Aldehydes with Hydrogen Peroxide. *Journal of the American Chemical Society* **2005,** *127* (19), 6964-6965.

26. Vilaivan, T., Pyrrolidinyl PNA with α/β-Dipeptide Backbone: From Development to Applications. *Accounts of Chemical Research* **2015,** *48* (6), 1645-1656.

27. Vilaivan, T. Synthesis and Properties of Novel Nucleopeptide. University of Oxford, United Kingdom, 1996.

28. Vinayak, R. S.; Lee, L. G.; Mullah, K. B.; Rosenblum, B. B., Labelled oligonucleotides synthesized on solid-supports. Google Patents: 2004.

29. Ngamviriyavong, P. Synthesis of Peptide Nucleic Acid Containing Aminoethyl Linkers. Chulalongkorn University, Thailand, 2004.

30. Nelson, B.; Hiller, W.; Pollex, A.; Hiersemann, M., Palladium(II)-Catalyzed Cycloisomerization of Functionalized 1,5-Hexadienes. *Organic Letters* **2011,** *13* (16), 4438-4441.

31. Lucio Anelli, P.; Biffi, C.; Montanari, F.; Quici, S., Fast and selective oxidation of primary alcohols to aldehydes or to carboxylic acids and of secondary alcohols to ketones mediated by oxoammonium salts under two-phase conditions. *Journal of organic chemistry* **1987,** *52* (12), 2559-2562.

32. Danishefsky, S.; Berman, E. M.; Ciufolini, M.; Etheredge, S. J.; Segmuller, B. E., A stereospecific route to aziridinomitosanes: the synthesis of novel mitomycin congeners. *Journal of the American Chemical Society* **1985,** *107* (13), 3891-3898.

33. Miller, J. J.; Rajaram, S.; Pfaffenroth, C.; Sigman, M. S., Synthesis of amine functionalized oxazolines with applications in asymmetric catalysis. *Tetrahedron* **2009,** *65* (16), 3110-3119.

34. Lee, D.; Williamson, C. L.; Chan, L.; Taylor, M. S., Regioselective, Borinic Acid-Catalyzed Monoacylation, Sulfonylation and Alkylation of Diols and Carbohydrates: Expansion of Substrate Scope and Mechanistic Studies. *Journal of the American Chemical Society* **2012,** *134* (19), 8260-8267.

35. Rao, H. S. P.; Senthilkumar, S. P., A convenient procedure for the synthesis of allyl and benzyl ethers from alcohols and phenols. *Journal of Chemical Sciences* **2001,** *113* (3), 191-196.

36. Epp, J. B.; Widlanski, T. S., Facile Preparation of Nucleoside-5‘-carboxylic Acids. *Journal of organic chemistry* **1999,** *64* (1), 293-295.

37. De Mico, A.; Margarita, R.; Parlanti, L.; Vescovi, A.; Piancatelli, G., A Versatile and Highly Selective Hypervalent Iodine (III)/2,2,6,6-Tetramethyl-1-piperidinyloxyl-Mediated Oxidation of Alcohols to Carbonyl Compounds. *Journal of organic chemistry* **1997,** *62* (20), 6974-6977.

38. Wong, O. A.; Shi, Y., Organocatalytic Oxidation. Asymmetric Epoxidation of Olefins Catalyzed by Chiral Ketones and Iminium Salts. *Chemical Reviews* **2008,** *108* (9), 3958-3987.

39. Shu, L.; Shi, Y., An efficient ketone-catalyzed asymmetric epoxidation using hydrogen peroxide (H_2O_2) as primary oxidant. *Tetrahedron* **2001,** *57* (24), 5213-5218.

40. Pearson, D. A.; Blanchette, M.; Baker, M. L.; Guindon, C. A., Trialkylsilanes as scavengers for the trifluoroacetic acid deblocking of protecting groups in peptide synthesis. *Tetrahedron Letters* **1989,** *30* (21), 2739-2742.

41. Lowe, G.; Vilaivan, T., Solid-phase synthesis of novel peptide nucleic acids. *Journal of the Chemical Society, Perkin Transactions 1* **1997,** (4), 555-560.

42. Kanoh, S.; Nishimura, T.; Ando, K.; Senda, H.; Ogawa, H.; Motoi, M.; Tanaka, T., Anomalous cyclodimerization of 3-phenyl-3-(phthalimidomethyl)oxetane via monomer isomerization and consecutive cation transfer. *Macromolecules* **1998,** *31* (22), 7988-7991.

43. Fernandes, C.; Faure, S.; Pereira, E.; Théry, V.; Declerck, V.; Guillot, R.; Aitken, D. J., 12-Helix folding of cyclobutane β-Amino acid oligomers. *Organic Letters* **2010,** *12* (16), 3606-3609.

APPENDIX

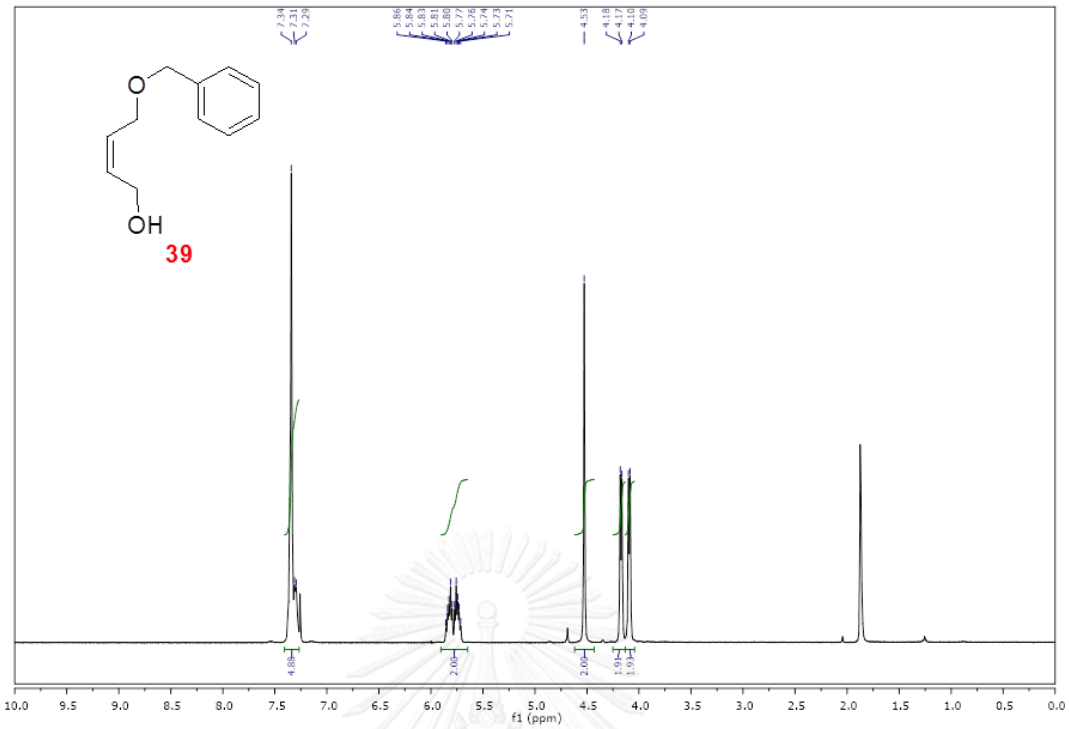

Figure A1 ^{1}H NMR spectrum (400 MHz, $CDCl_3$) of (*Z*)-4-(benzyloxy)but-2-en-1-ol (**39**)

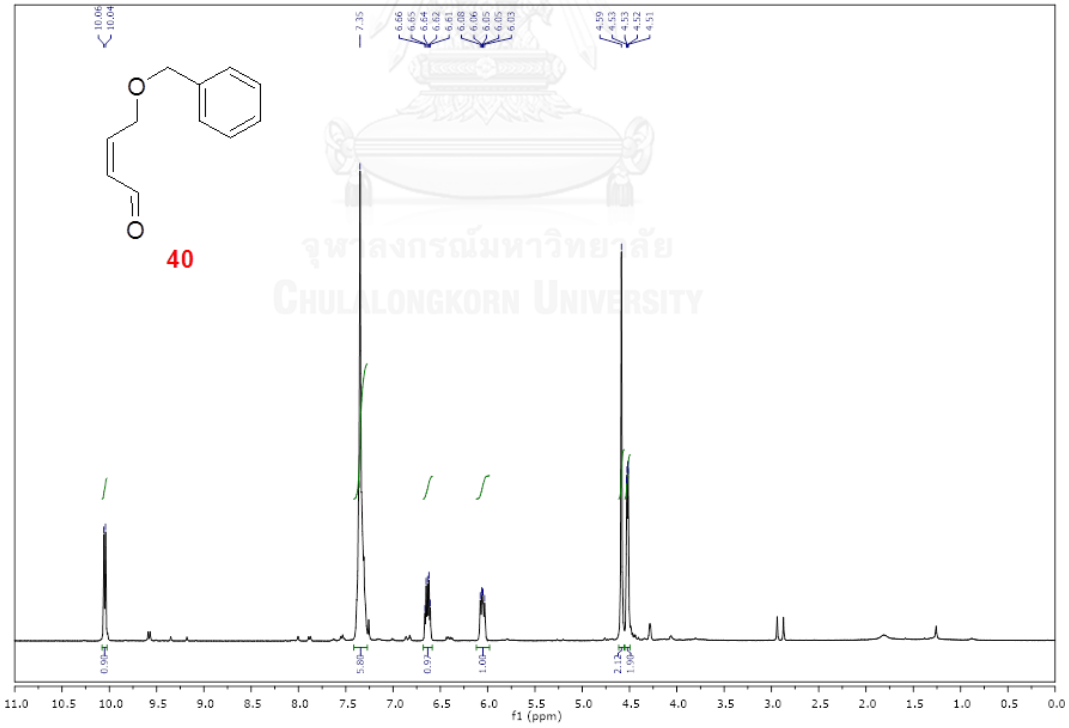

Figure A2 ^{1}H NMR spectrum (400 MHz, $CDCl_3$) of (*Z*)-4-(benzyloxy)but-2-enal (**40**)

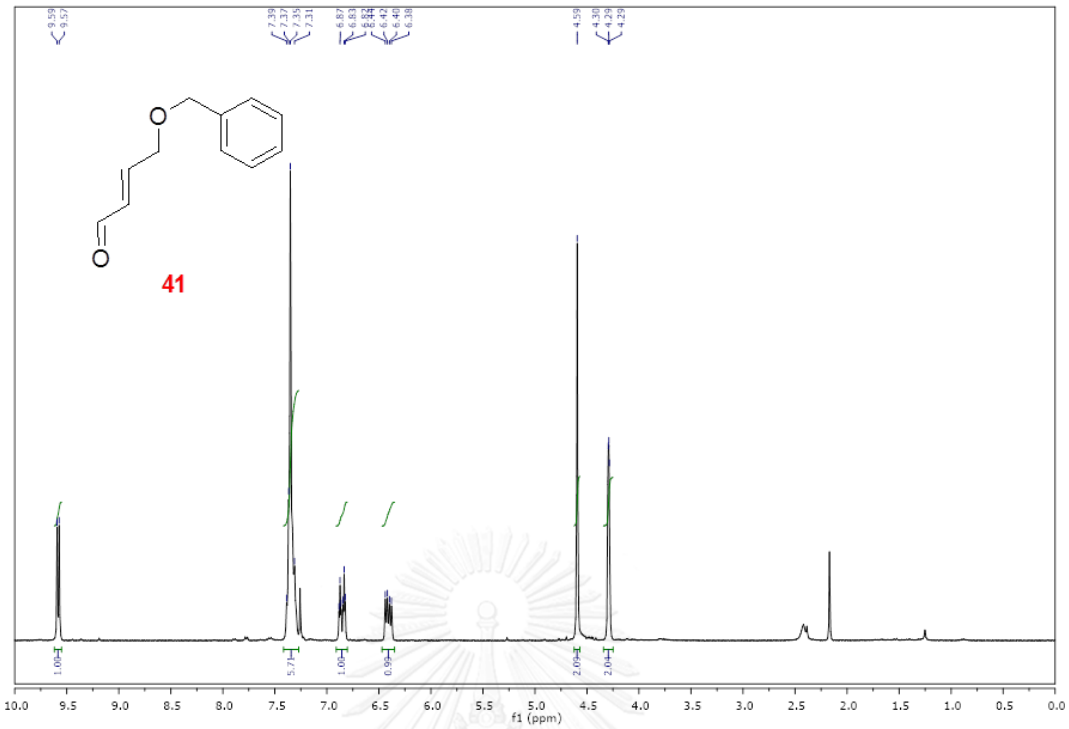

Figure A3 ^{1}H NMR spectrum (400 MHz, $CDCl_3$) of (*E*)-4-(benzyloxy)but-2-enal (**41**)

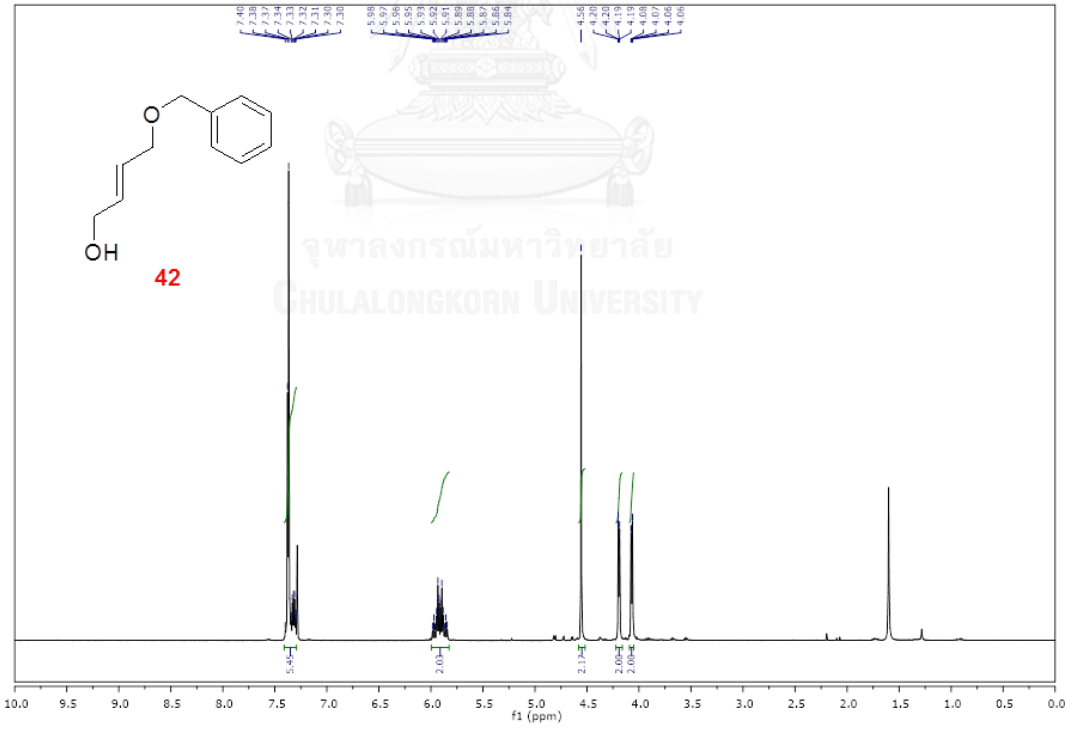

Figure A4 ^{1}H NMR spectrum (400 MHz, $CDCl_3$) of (*E*)-4-(benzyloxy)but-2-en-1-ol (**42**)

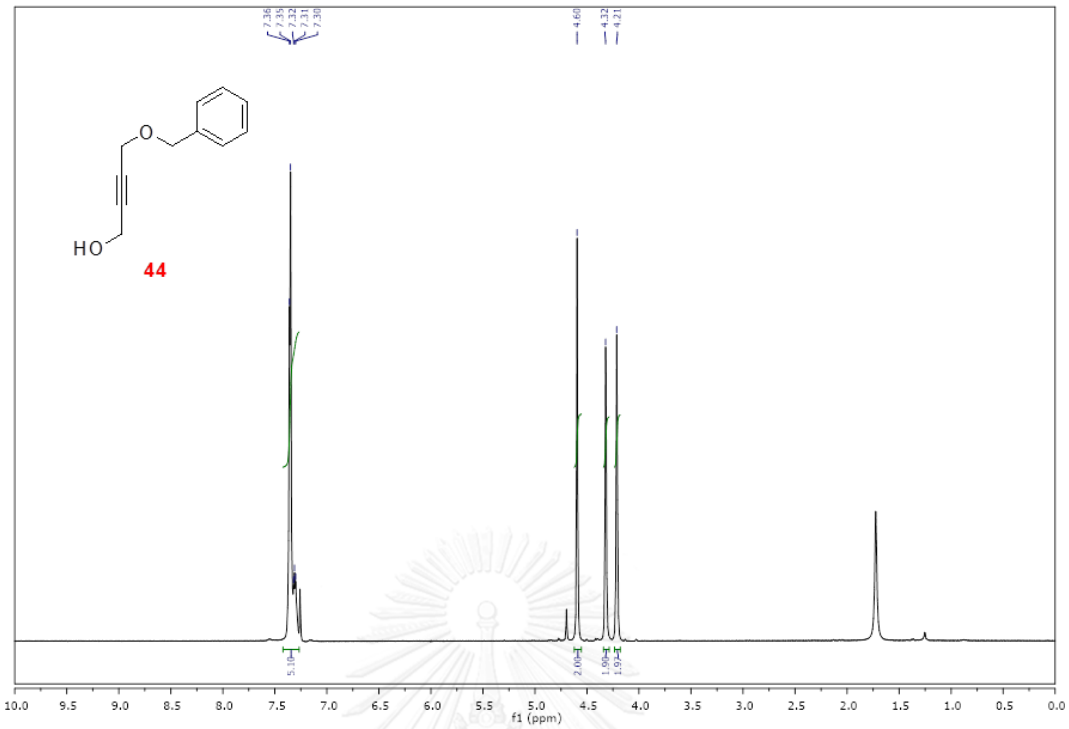

Figure A5 ^{1}H NMR spectrum (400 MHz, $CDCl_3$) of 4-(benzyloxy)but-2-yn-1-ol (**44**)

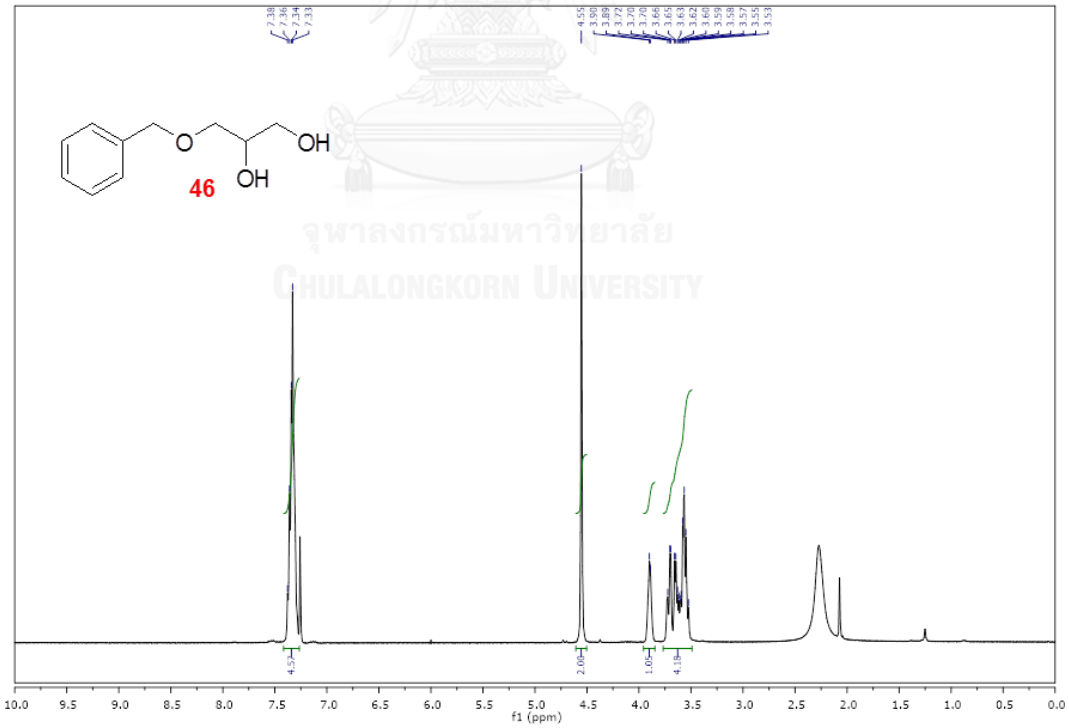

Figure A6 ^{1}H NMR spectrum (400 MHz, $CDCl_3$) of 3-(benzyloxy)propane-1,2-diol (**46**)

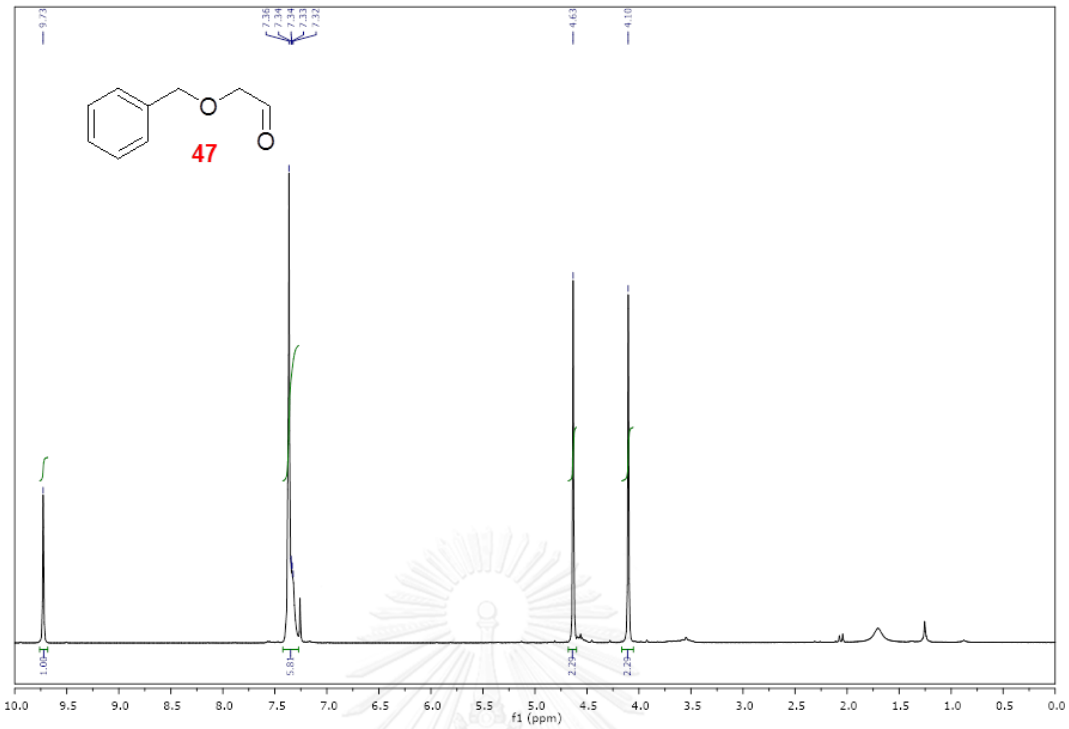

Figure A7 ^{1}H NMR spectrum (400 MHz, $CDCl_3$) of 2-(benzyloxy)acetaldehyde (**47**)

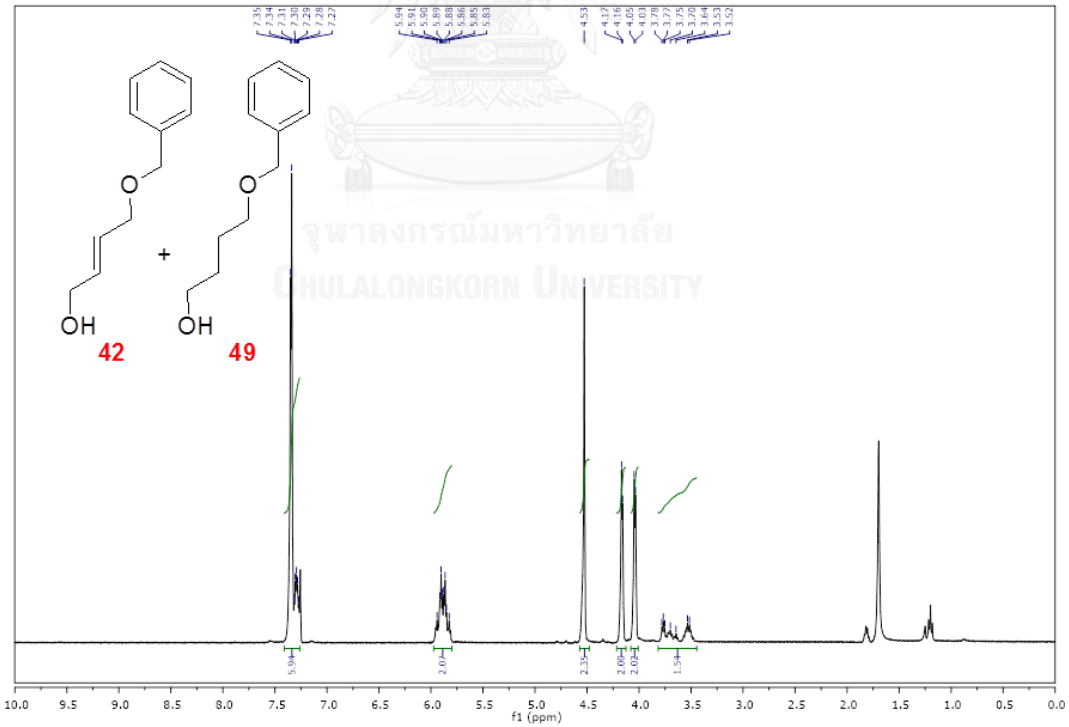

Figure A8 ^{1}H NMR spectrum (400 MHz, $CDCl_3$) of (*E*)-4-(benzyloxy)but-2-en-1-ol (**42**) from $NaBH_4$ reduction of (*E*)-4-(benzyloxy)but-2-en-1-ol (**41**) at room temperature

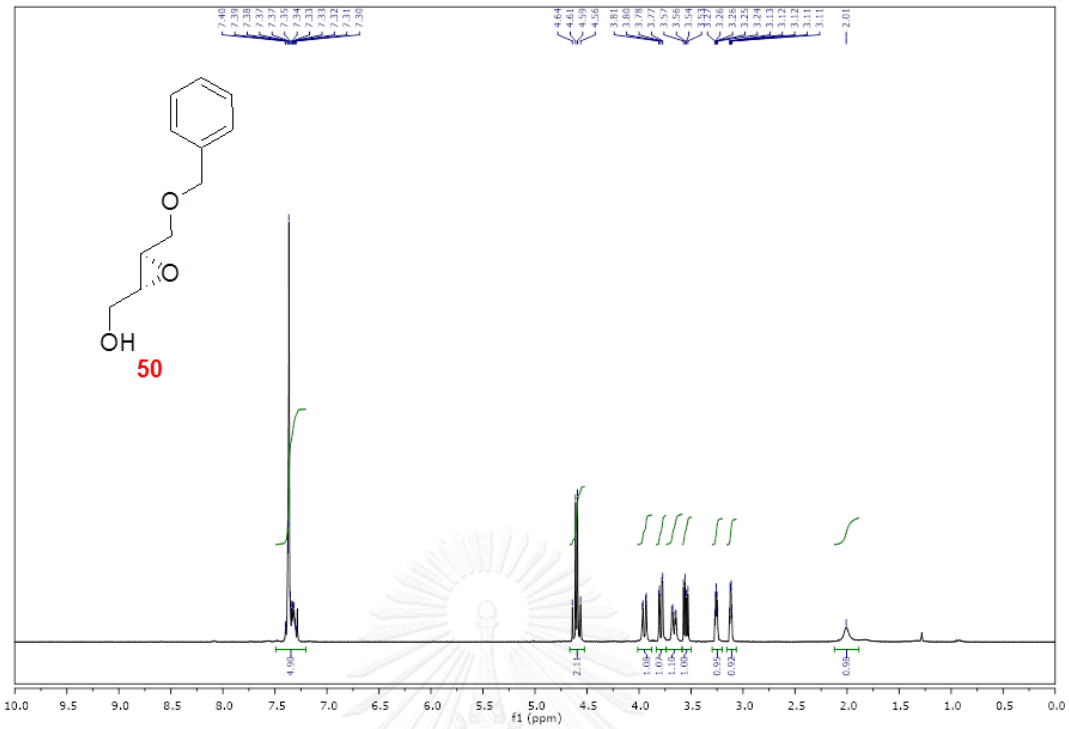

Figure A9 ^{1}H NMR spectrum (400 MHz, $CDCl_3$) of racemic (3-(benzyloxymethyl)oxiran-2-yl)methanol (**50**)

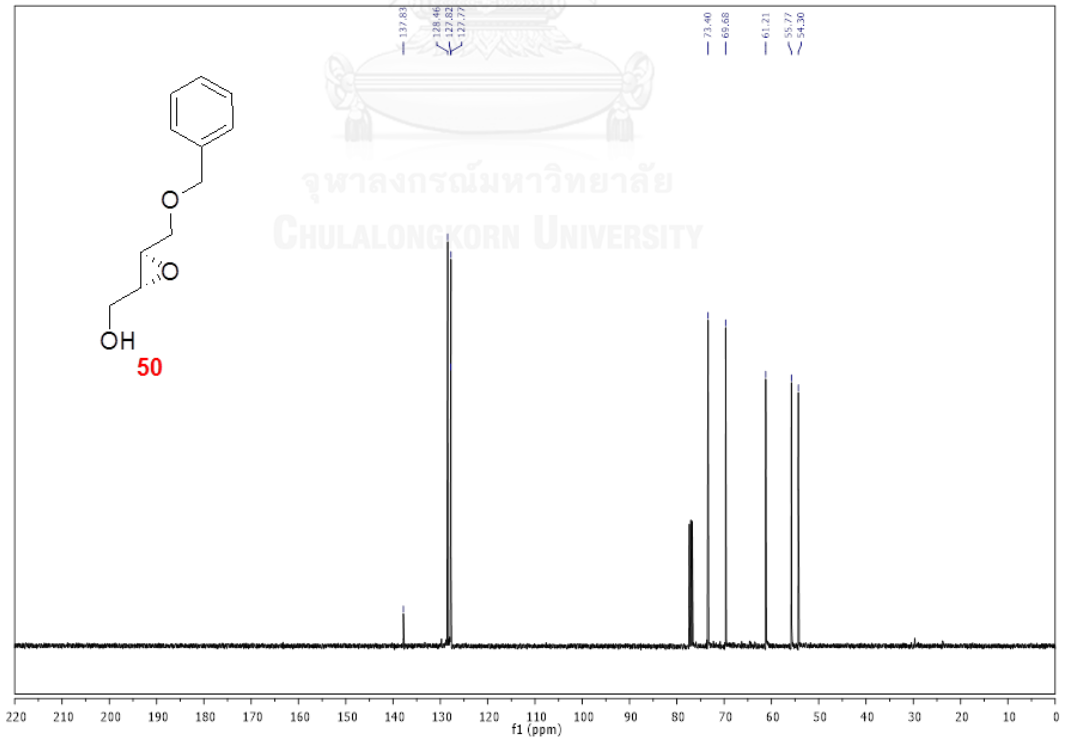

Figure A10 ^{13}C NMR spectrum (100 MHz, $CDCl_3$) of racemic (3-(benzyloxymethyl)oxiran-2-yl)methanol (**50**)

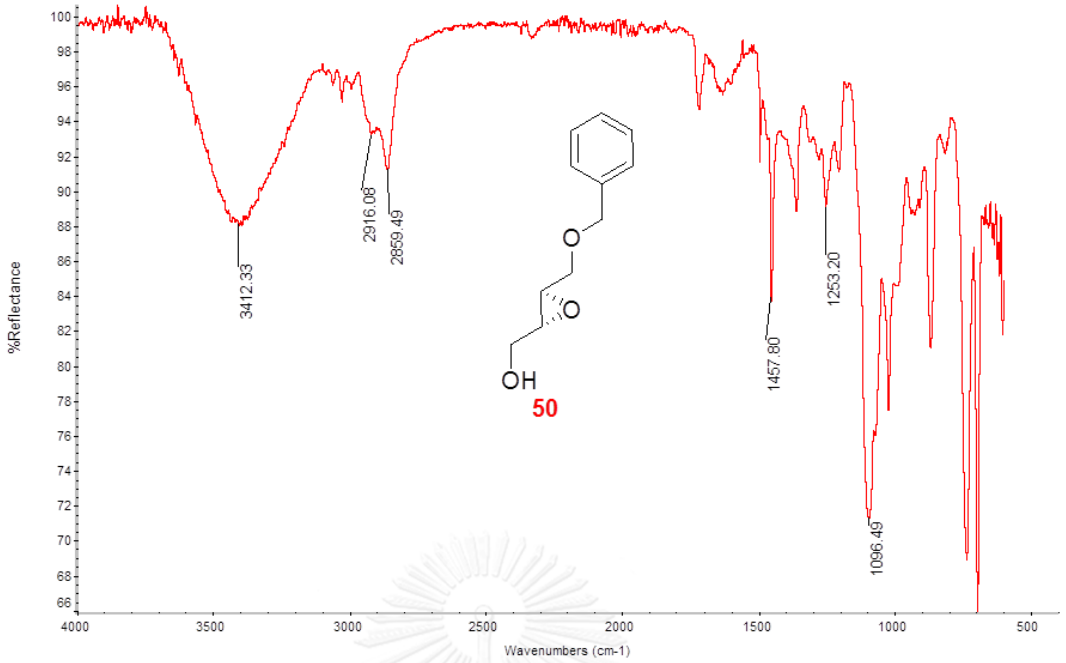

Figure A11 IR spectrum (ATR) of racemic (3-(benzyloxymethyl)oxiran-2-yl)methanol (**50**)

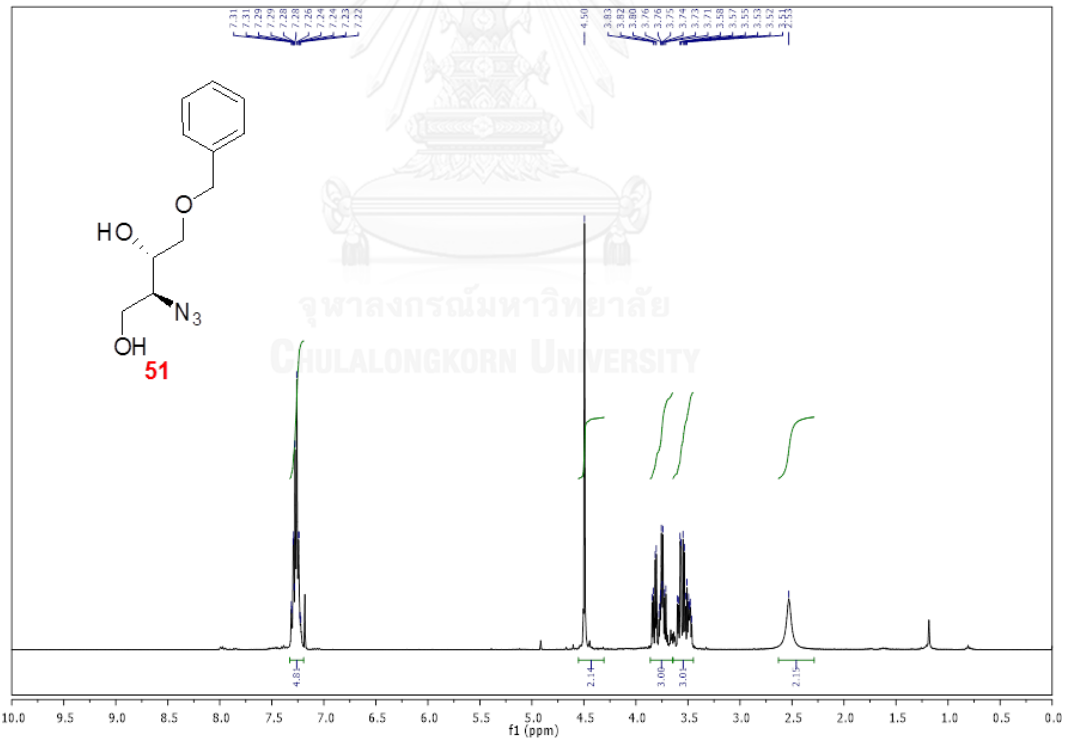

Figure A12 ^{1}H NMR spectrum (400 MHz, $CDCl_3$) of racemic 2-azido-4-(benzyloxy)butane-1,3-diol (**51**)

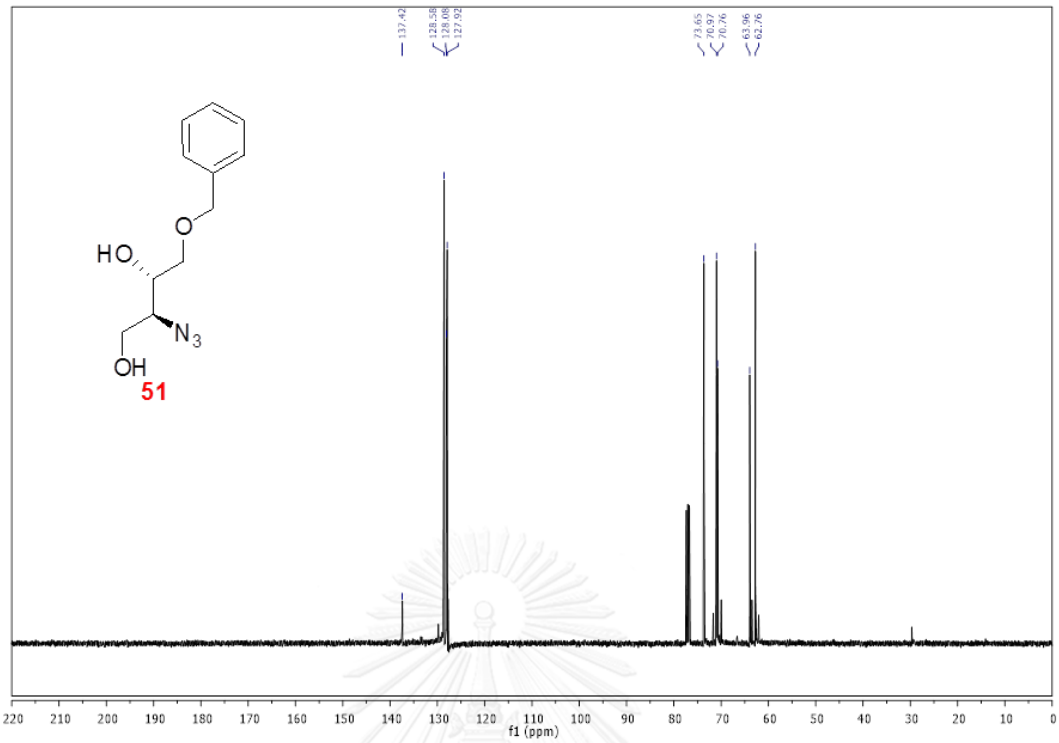

Figure A13 ^{13}C NMR spectrum (100 MHz, $CDCl_3$) of racemic 2-azido-4-(benzyloxy)butane-1,3-diol (**51**)

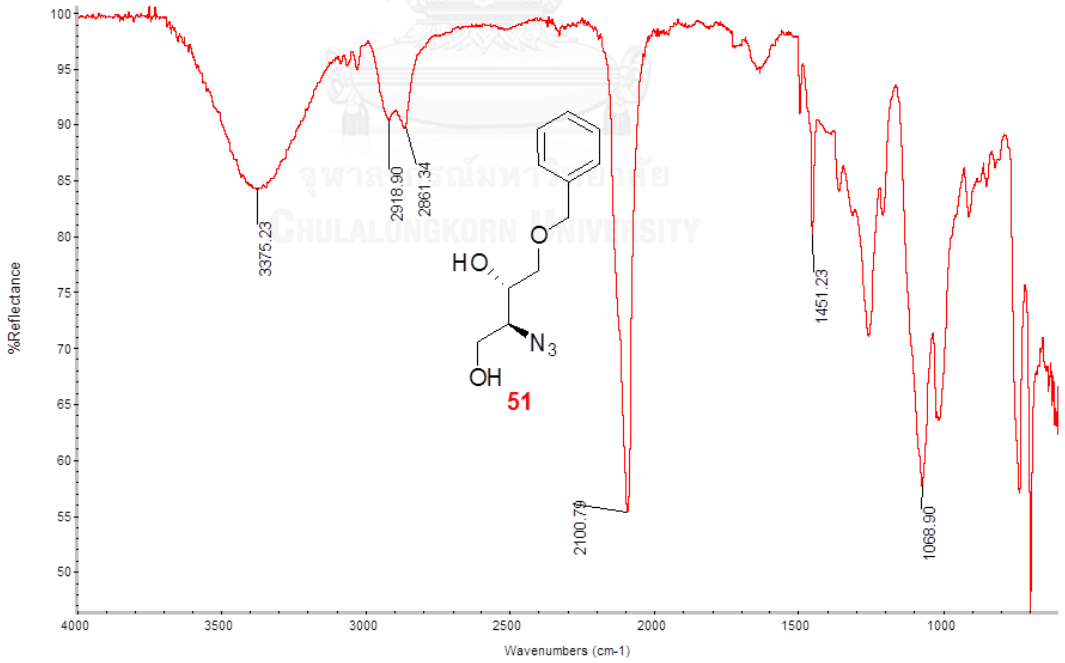

Figure A14 IR spectrum (ATR) of racemic 2-azido-4-(benzyloxy)butane-1,3-diol (**51**)

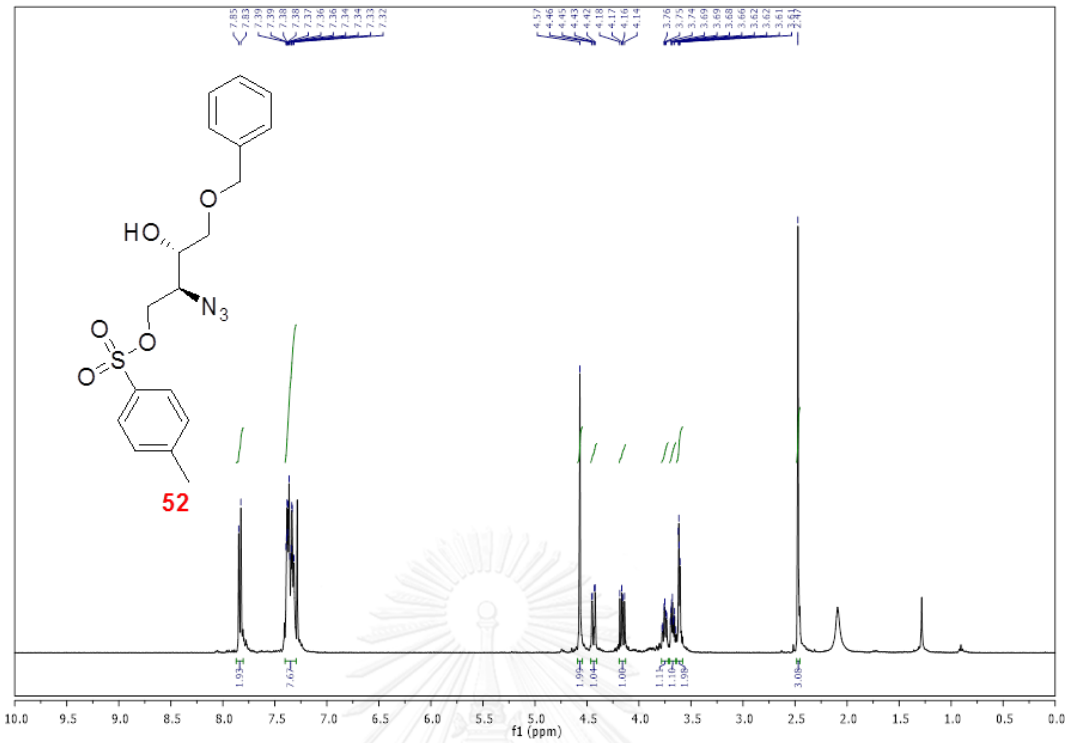

Figure A15 ^{1}H NMR spectrum (400 MHz, $CDCl_3$) of racemic 2-azido-4-(benzyloxy)-3-hydroxybutyl 4-methylbenzenesulfonate (**52**)

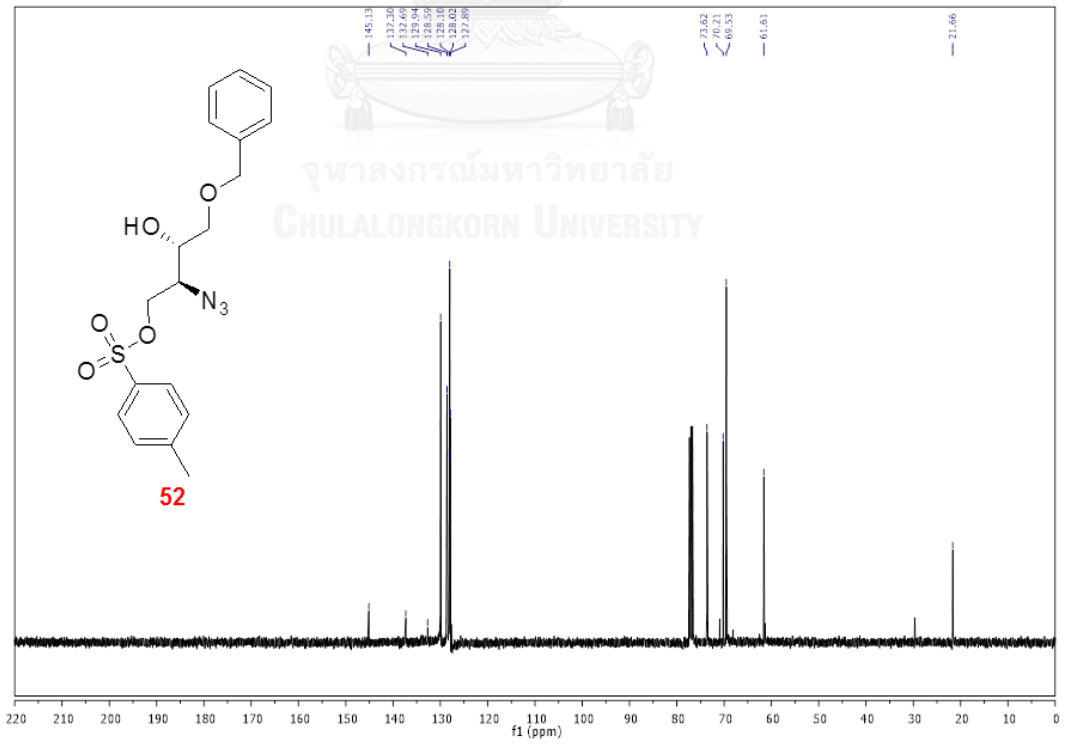

Figure A16 ^{13}C NMR spectrum (100 MHz, $CDCl_3$) of racemic 2-azido-4-(benzyloxy)-3-hydroxybutyl 4-methylbenzenesulfonate (**52**)

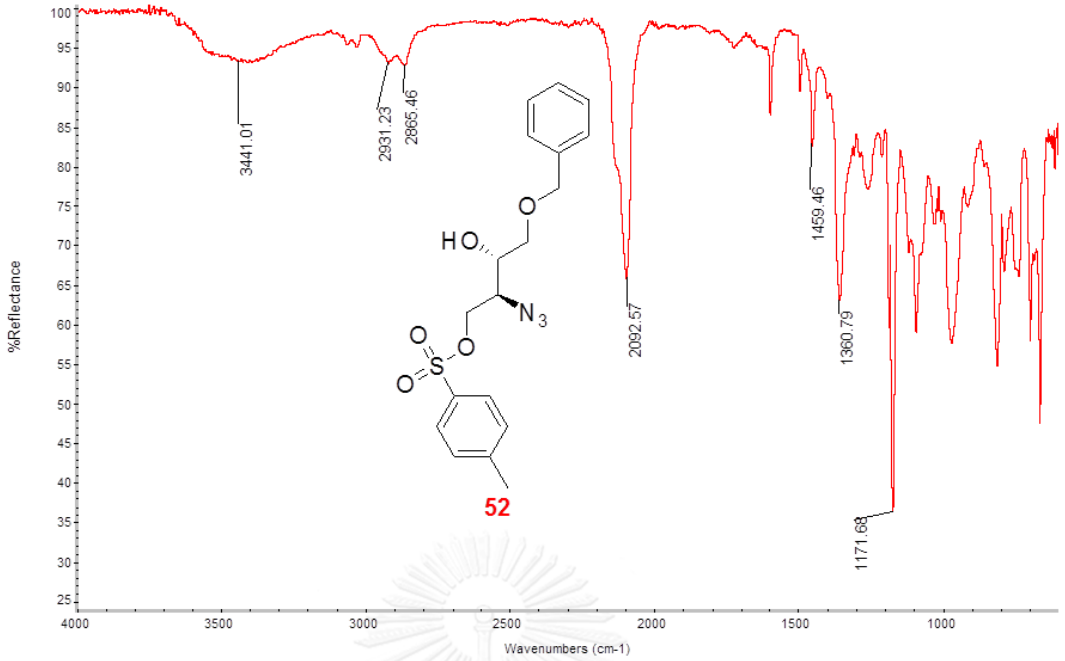

Figure A17 IR spectrum (ATR) of racemic 2-azido-4-(benzyloxy)-3-hydroxybutyl 4-methylbenzenesulfonate (**52**)

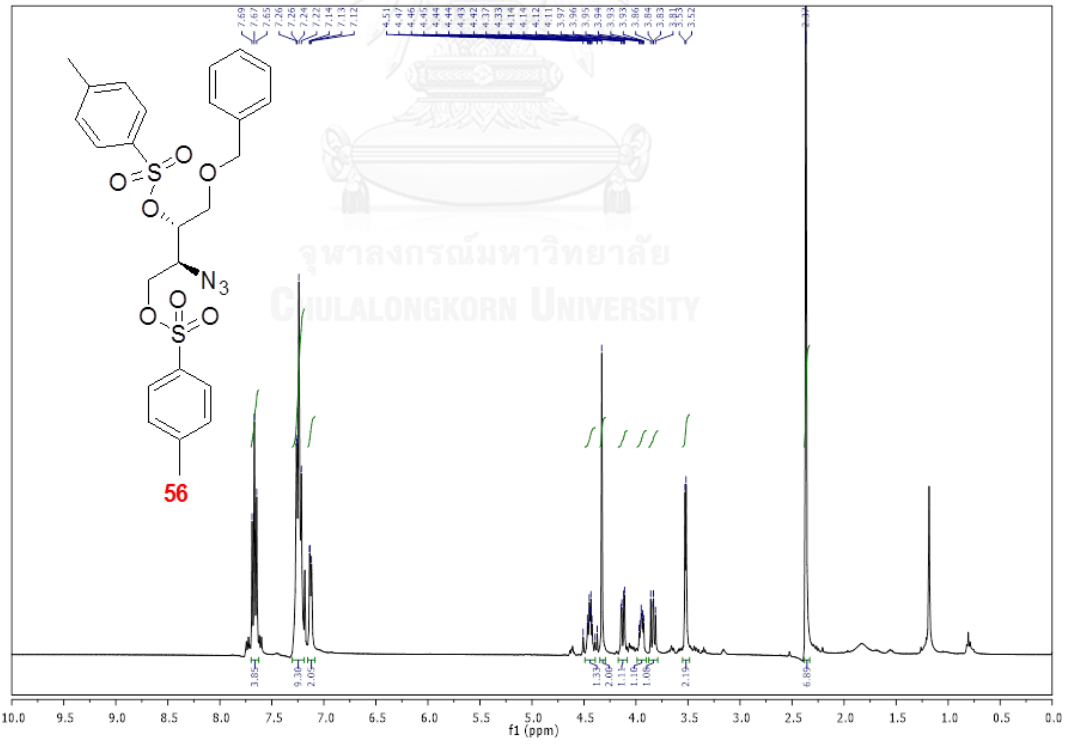

Figure A18 ^{1}H NMR spectrum (400 MHz, $CDCl_3$) of racemic-2-azido-4-(benzyloxy)butane-1,3-diyl bis(4-methylbenzenesulfonate) (**56**)

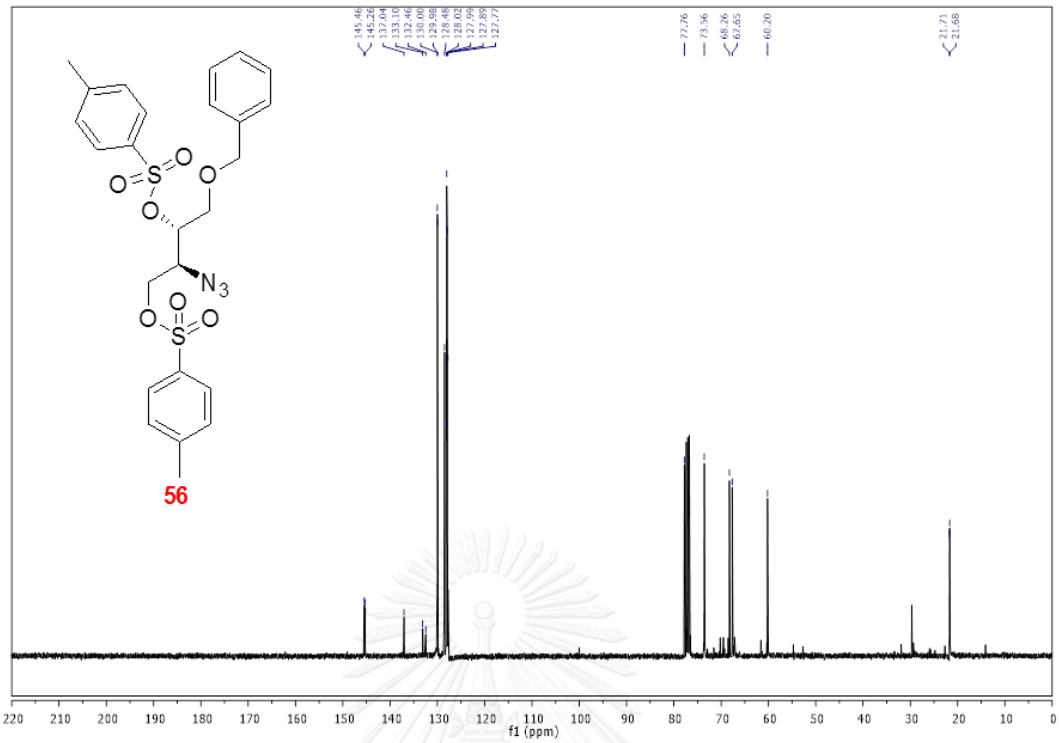

Figure A19 ^{13}C NMR spectrum (100 MHz, $CDCl_3$) of racemic-2-azido-4-(benzyloxy)butane-1,3-diyl bis(4-methylbenzenesulfonate) (**56**)

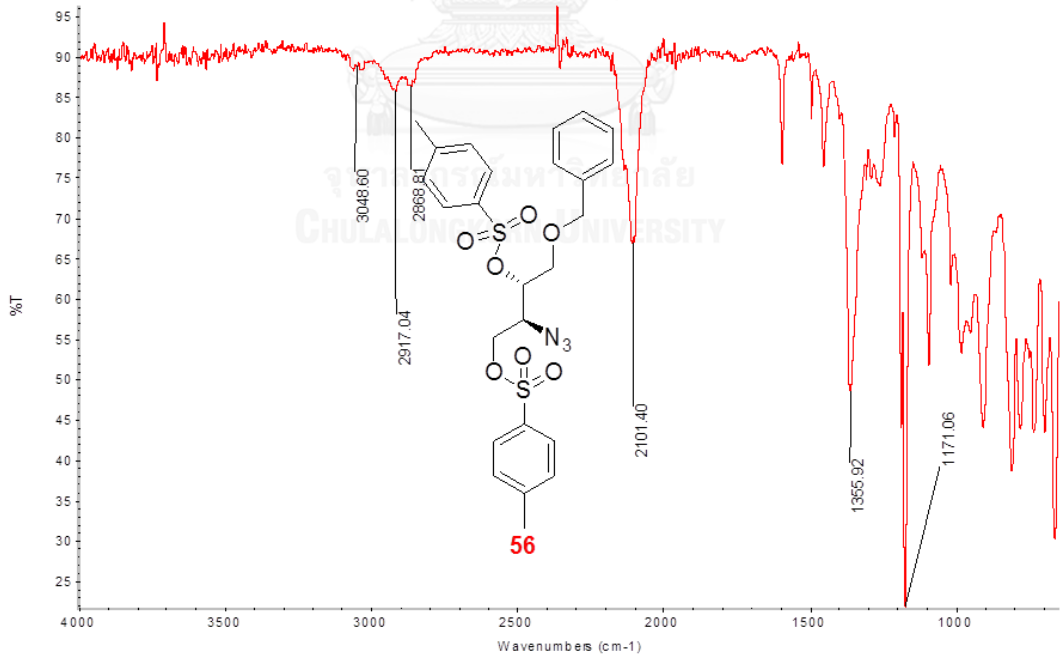

Figure A20 IR spectrum (ATR) of racemic-2-azido-4-(benzyloxy)butane-1,3-diyl bis(4-methylbenzenesulfonate) (**56**)

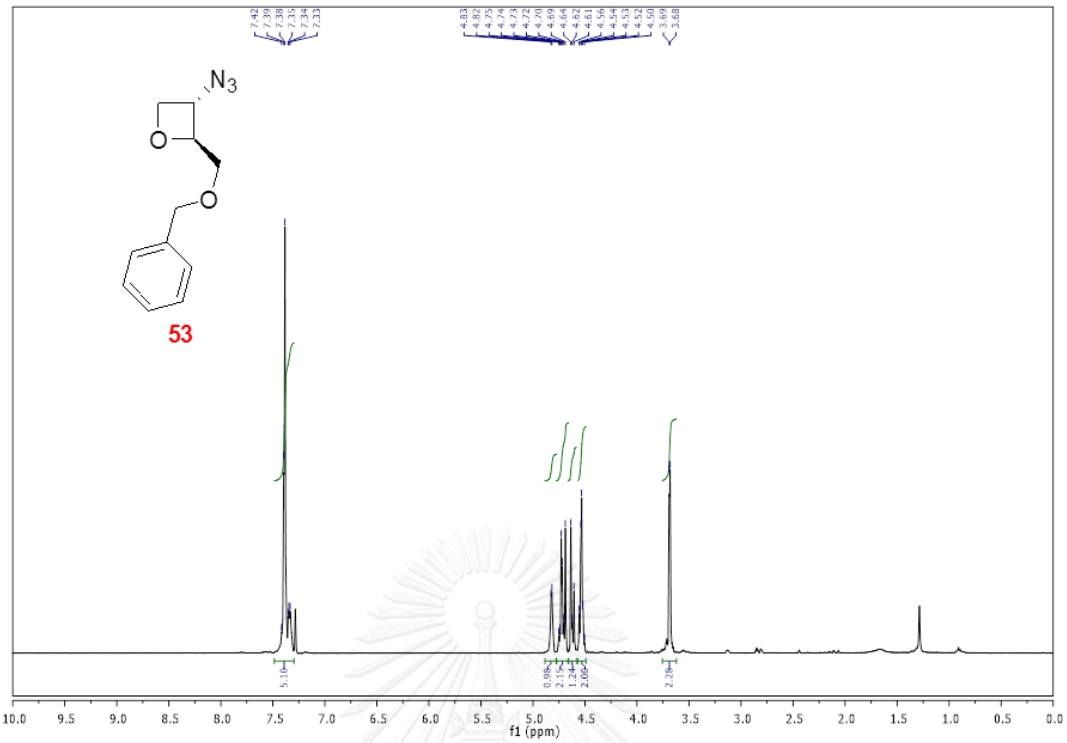

Figure A21 ^{1}H NMR spectrum (400 MHz, $CDCl_3$) of racemic-3-azido-2-(benzyloxymethyl)oxetane (**53**)

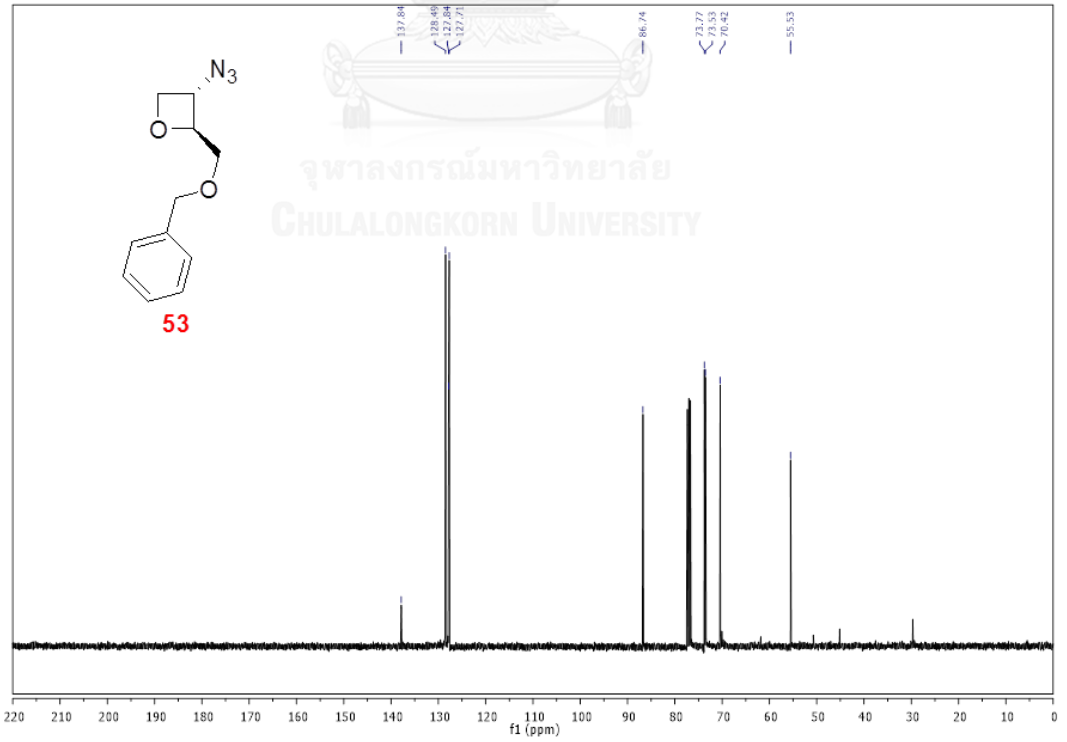

Figure A22 ^{13}C NMR spectrum (100 MHz, $CDCl_3$) of racemic-3-azido-2-(benzyloxymethyl)oxetane (**53**)

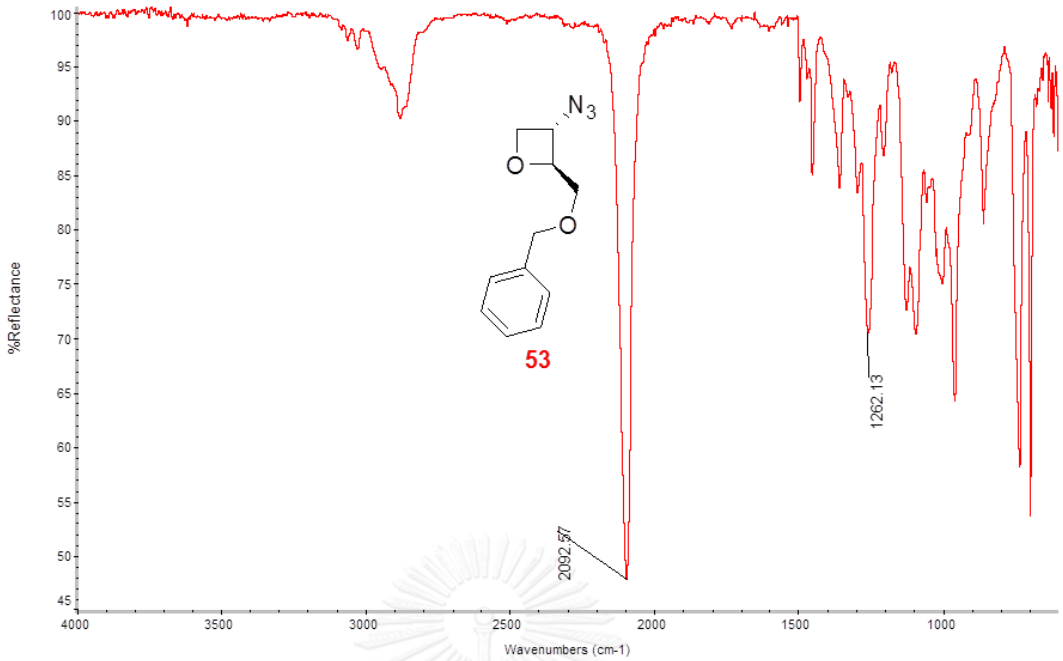

Figure A23 IR spectrum (ATR) of racemic-3-azido-2-(benzyloxymethyl)oxetane (**53**)

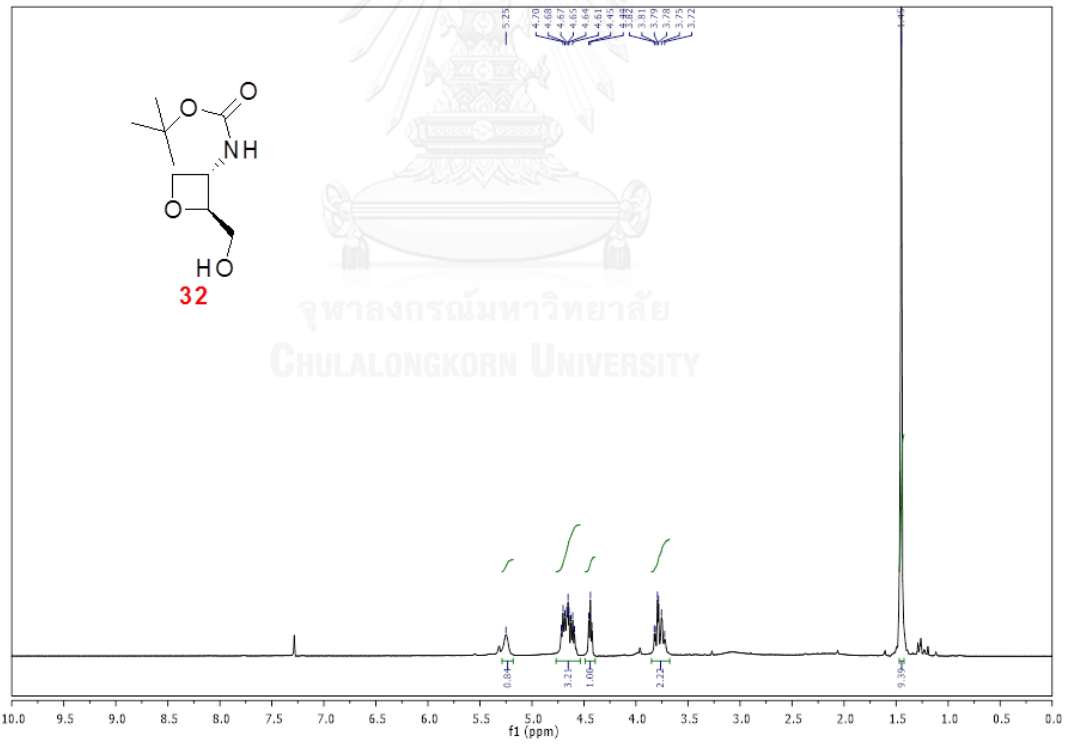

Figure A24 ^{1}H NMR spectrum (400 MHz, $CDCl_3$) of racemic-*tert*-butyl-2-(hydroxymethyl)oxetan-3-ylcarbamate (**32**)

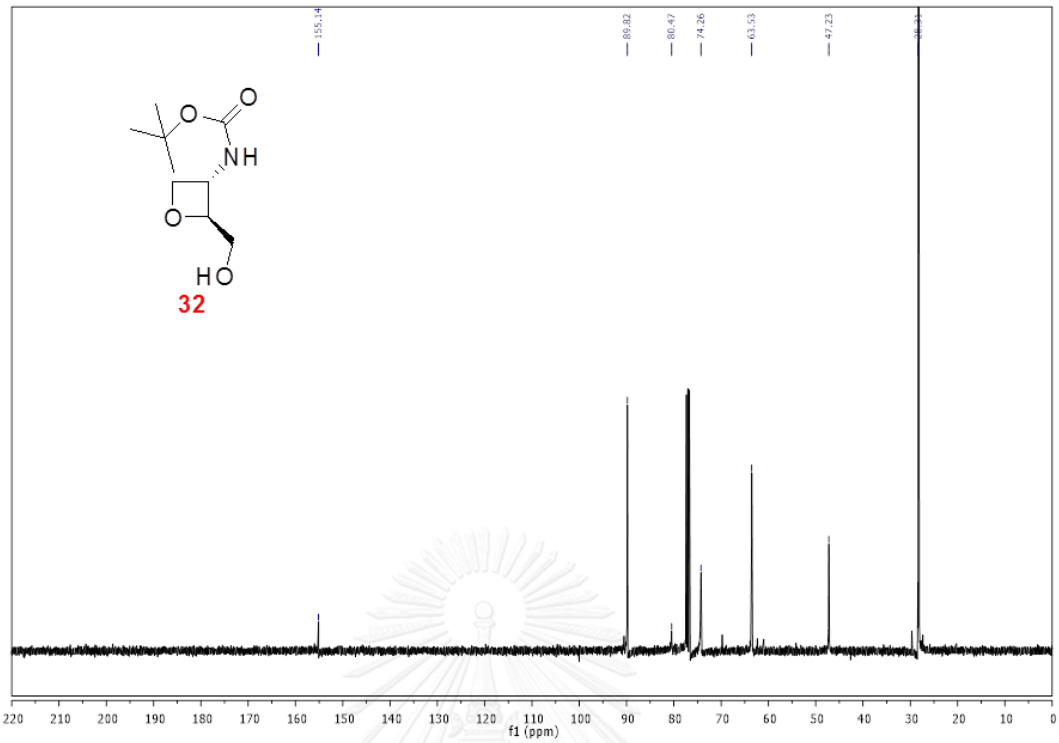

Figure A25 ^{13}C NMR spectrum (100 MHz, $CDCl_3$) of racemic-*tert*-butyl-2-(hydroxymethyl)oxetan-3-ylcarbamate (**32**)

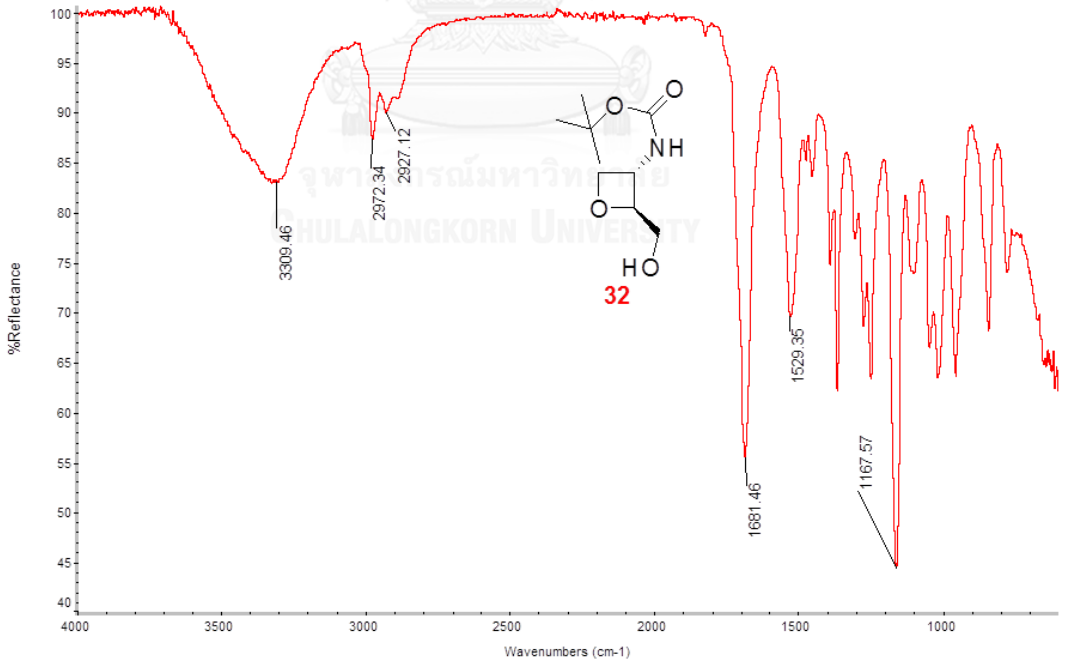

Figure A26 IR spectrum (ATR) of racemic-*tert*-butyl-2-(hydroxymethyl)oxetan-3-ylcarbamate (**32**)

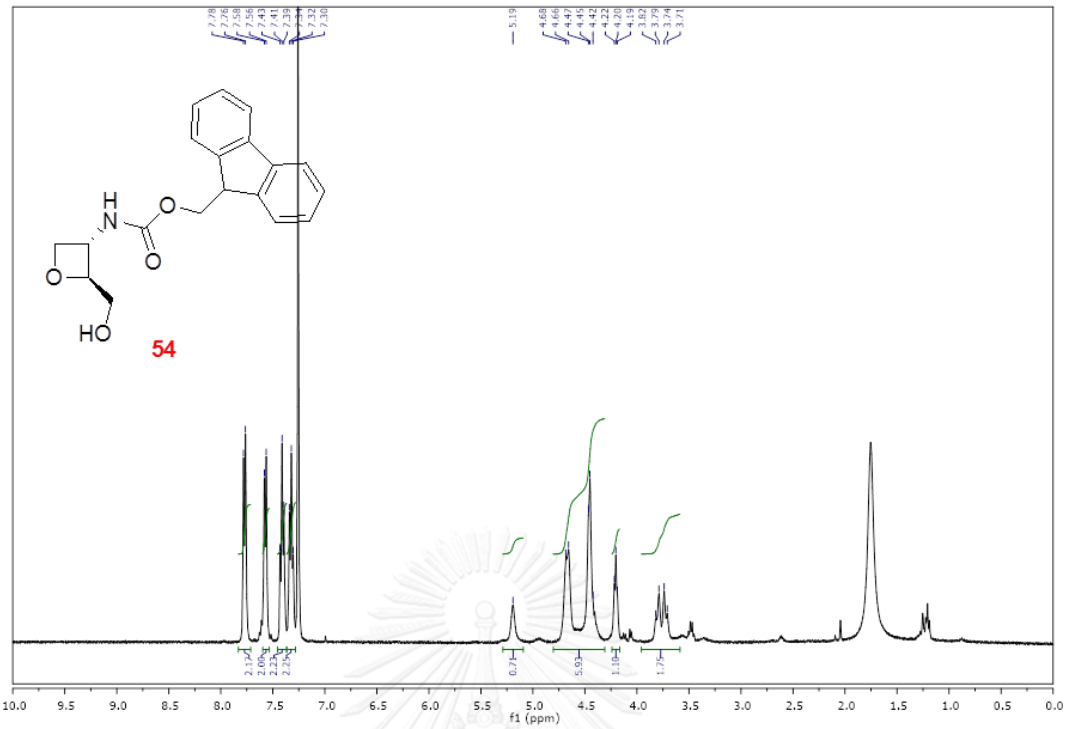

Figure A27 ^{1}H NMR spectrum (400 MHz, $CDCl_3$) of racemic-(9*H*-fluoren-9-yl)methyl 2-(hydroxymethyl)oxetan-3-ylcarbamate (**54**)

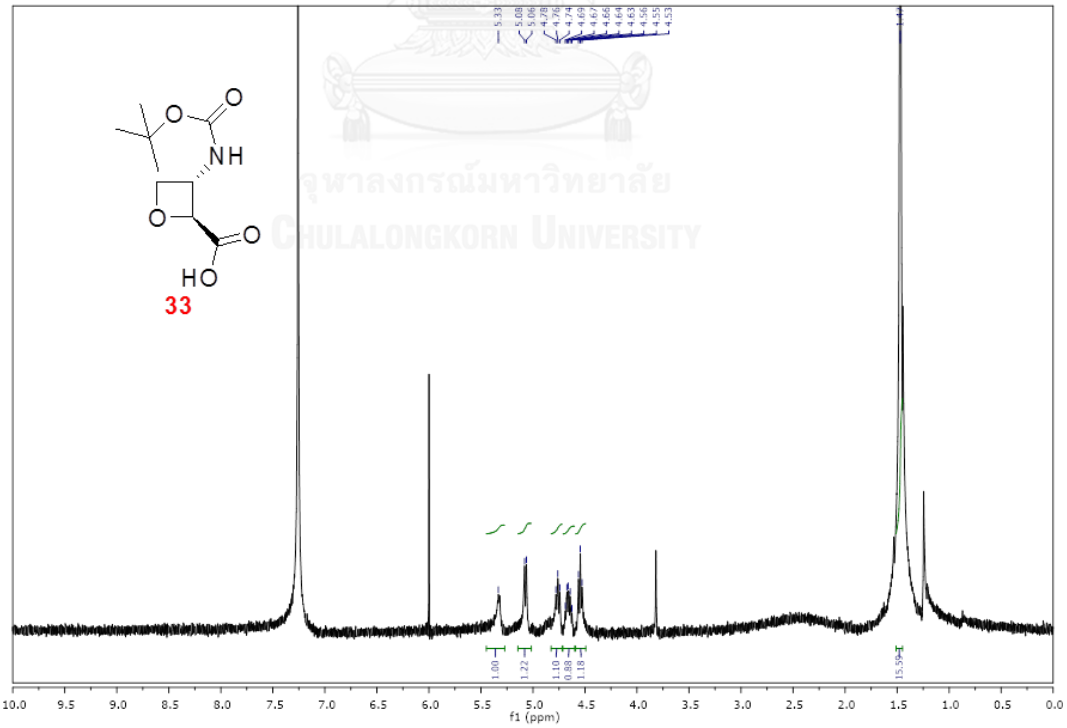

Figure A28 ^{1}H NMR spectrum (400 MHz, $CDCl_3$) of racemic-3-(*tert*-butoxycarbonylamino)oxetane-2-carboxylic acid (**33**)

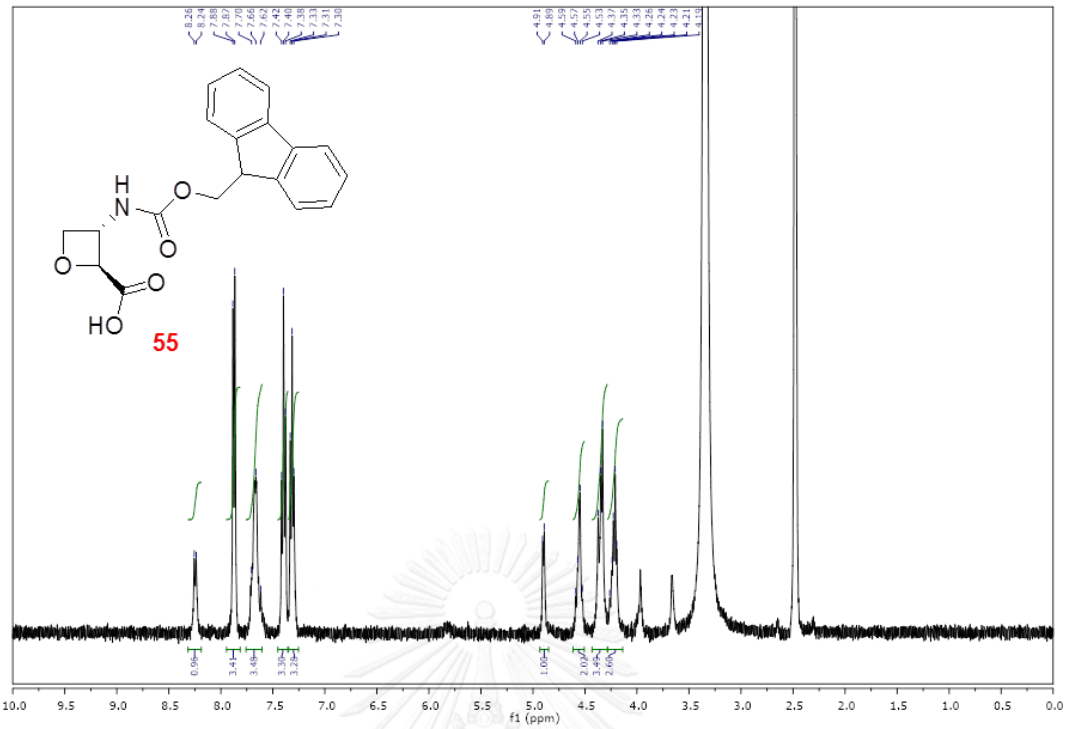

Figure A29 ^{1}H NMR spectrum (400 MHz, DMSO-d_6) of racemic-3-(((9*H*-fluoren-9-yl)methoxy)carbonylamino)oxetane-2-carboxylic acid (**55**)

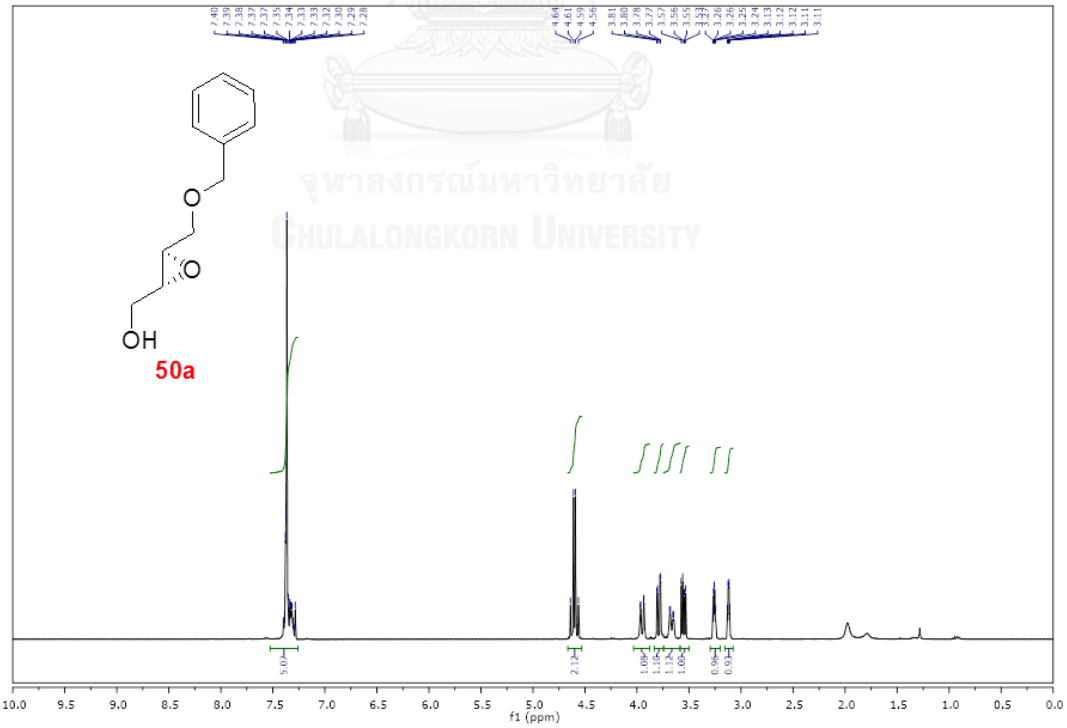

Figure A30 ^{1}H NMR spectrum (400 MHz, $CDCl_3$) of ((2*R*,3*R*)-3-(benzyloxymethyl)oxiran-2-yl)methanol (**50a**)

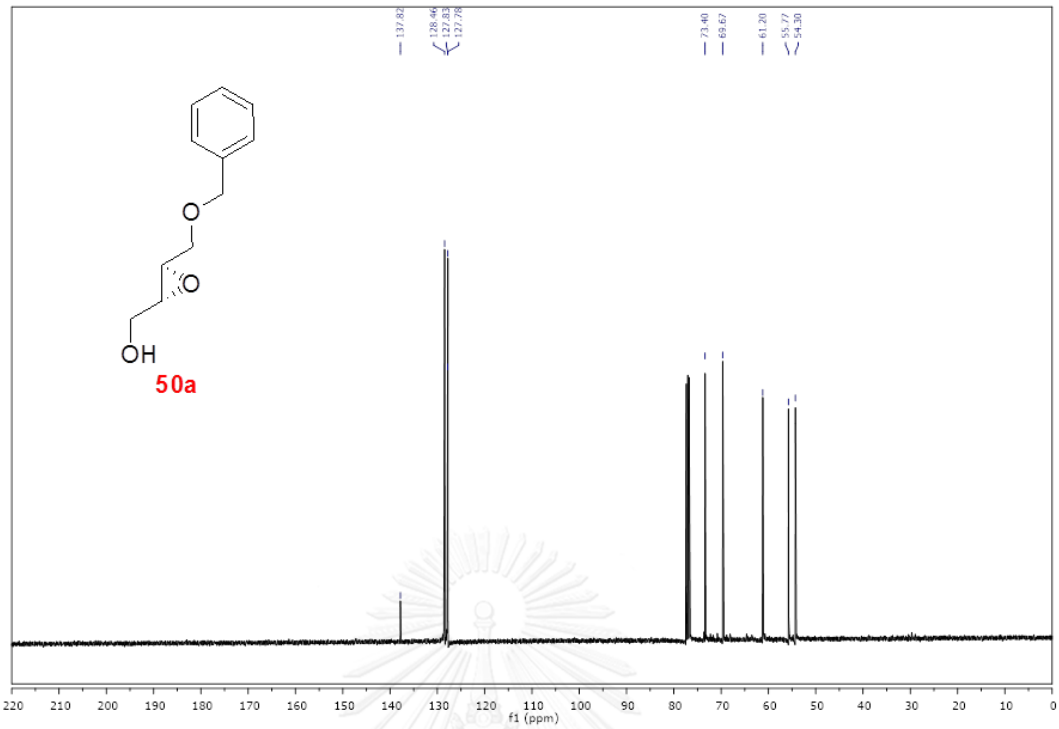

Figure A31 ^{13}C NMR spectrum (100 MHz, $CDCl_3$) of ((2*R*,3*R*)-3-(benzyloxymethyl)oxiran-2-yl)methanol (**50a**)

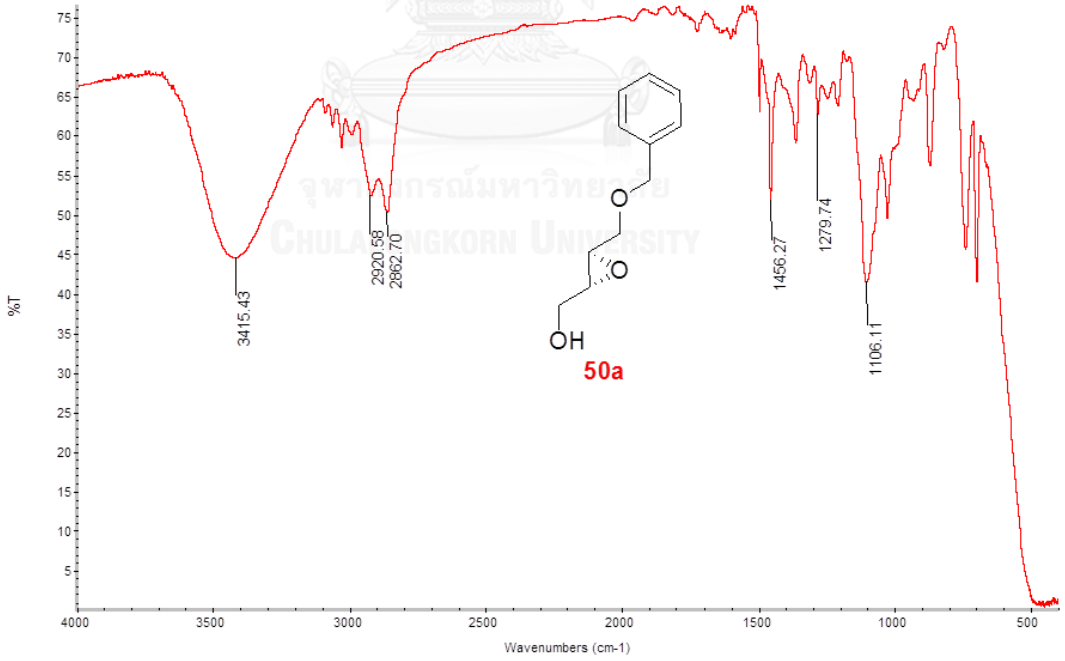

Figure A32 IR spectrum (thin film) of ((2*R*,3*R*)-3-(benzyloxymethyl)oxiran-2-yl)methanol (**50a**)

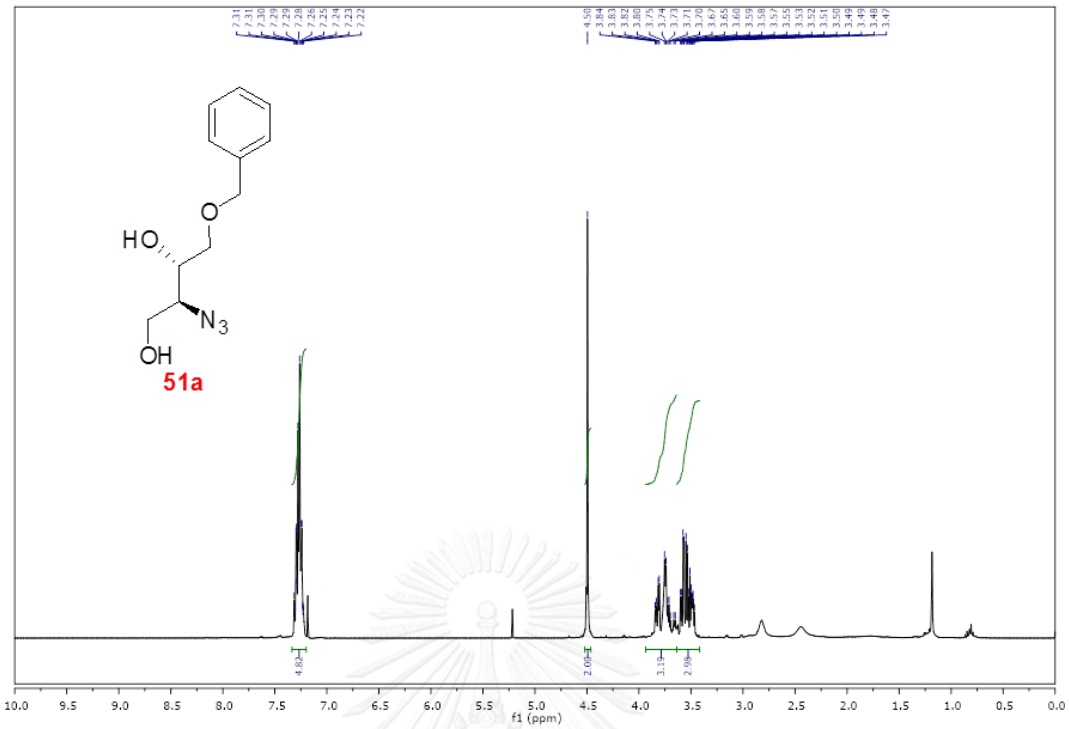

Figure A33 ^{1}H NMR spectrum (400 MHz, $CDCl_3$) of (2*S*,3*S*)-2-azido-4-(benzyloxy)butane-1,3-diol (**51a**)

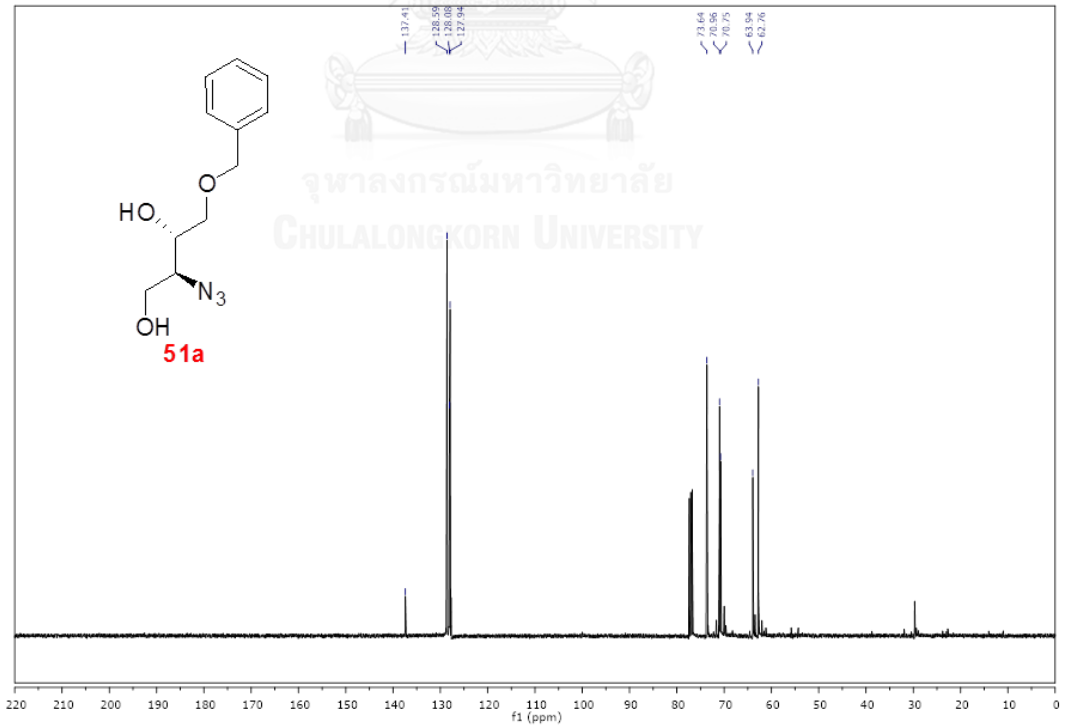

Figure A34 ^{13}C NMR spectrum (100 MHz, $CDCl_3$) of (2*S*,3*S*)-2-azido-4-(benzyloxy)butane-1,3-diol (**51a**)

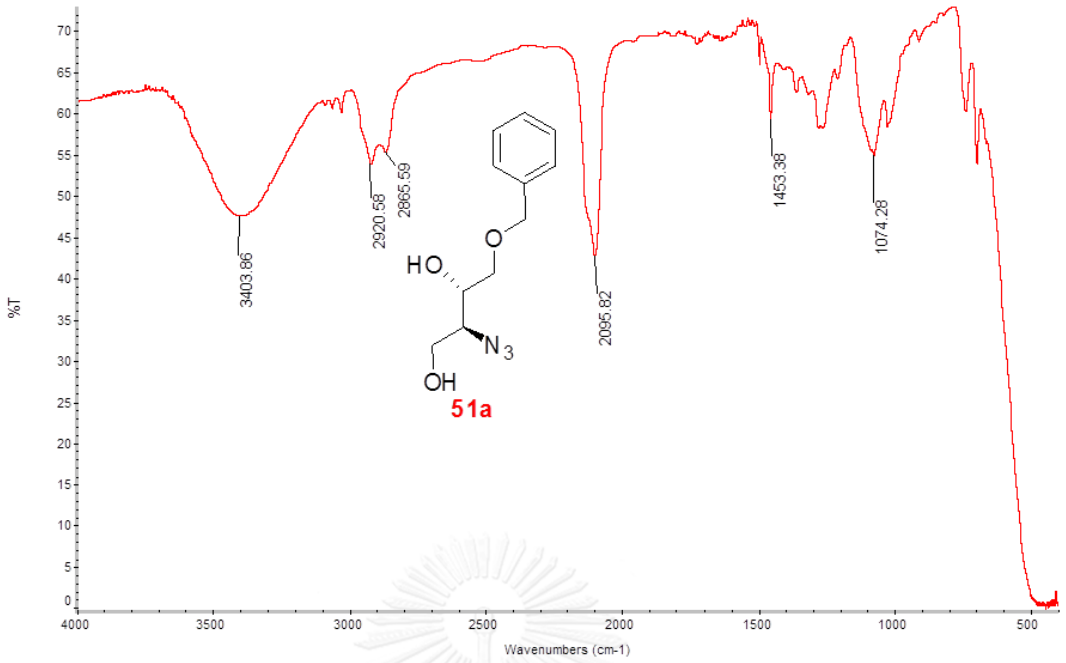

Figure A35 IR spectrum (thin film) of (2*S*,3*S*)-2-azido-4-(benzyloxy)butane-1,3-diol (**51a**)

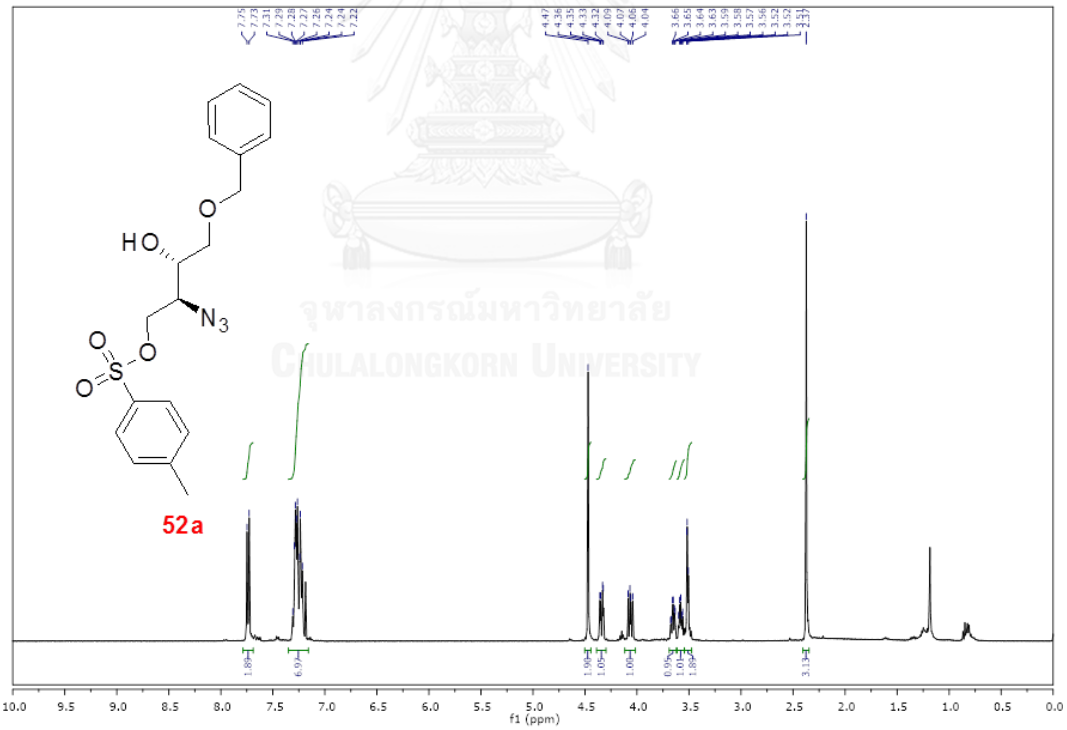

Figure A36 ^{1}H NMR spectrum (400 MHz, $CDCl_3$) of (2*S*,3*S*)-2-azido-4-(benzyloxy)-3-hydroxybutyl 4-methylbenzenesulfonate (**52a**)

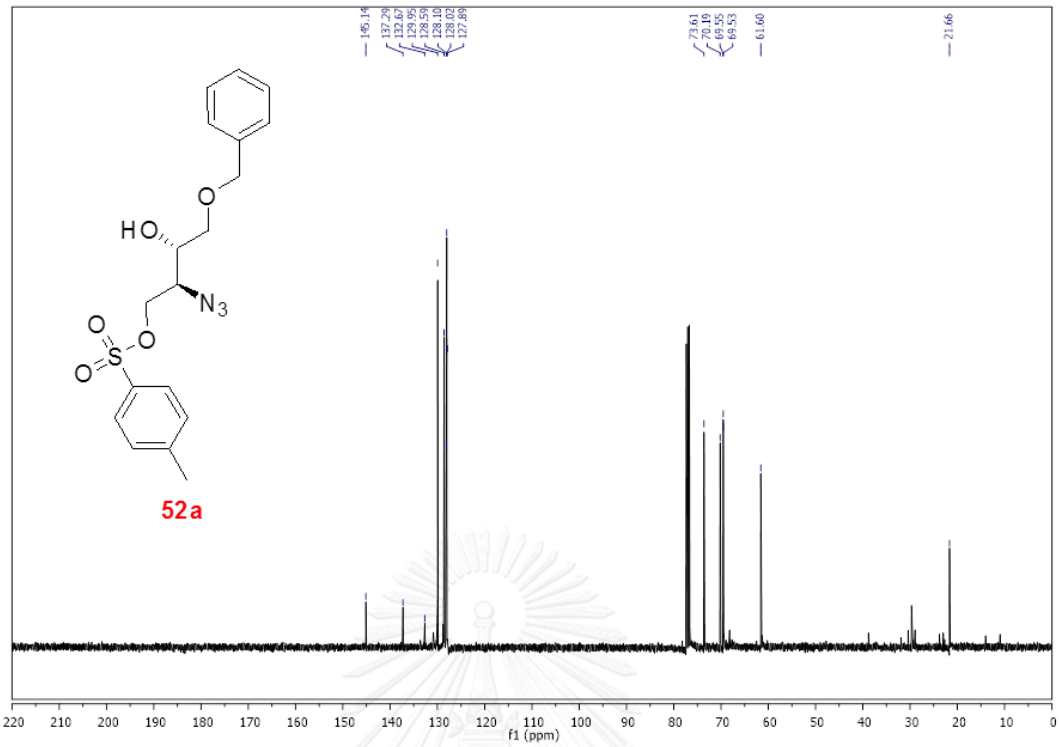

Figure A37 ^{13}C NMR spectrum (100 MHz, $CDCl_3$) of (2*S*,3*S*)-2-azido-4-(benzyloxy)-3-hydroxybutyl 4-methylbenzenesulfonate (**52a**)

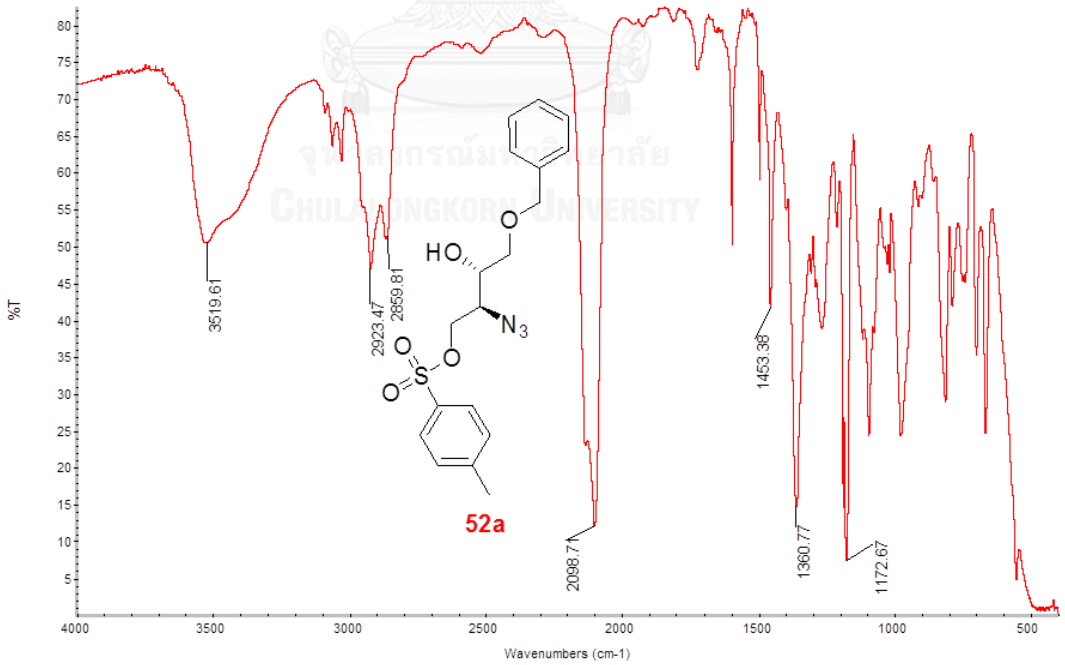

Figure A38 IR spectrum (thin film) of (2*S*,3*S*)-2-azido-4-(benzyloxy)-3-hydroxybutyl 4-methylbenzenesulfonate (**52a**)

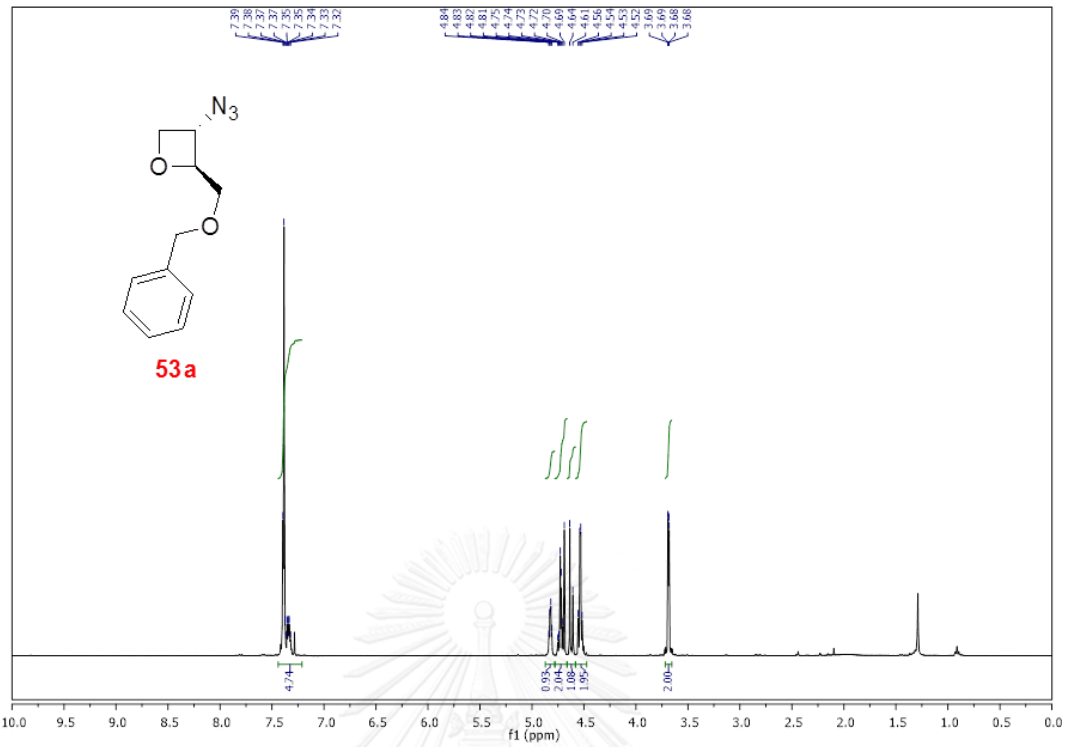

Figure A39 ^{1}H NMR spectrum (400 MHz, $CDCl_3$) of (2*S*,3*S*)-3-azido-2-(benzyloxymethyl)oxetane (**53a**)

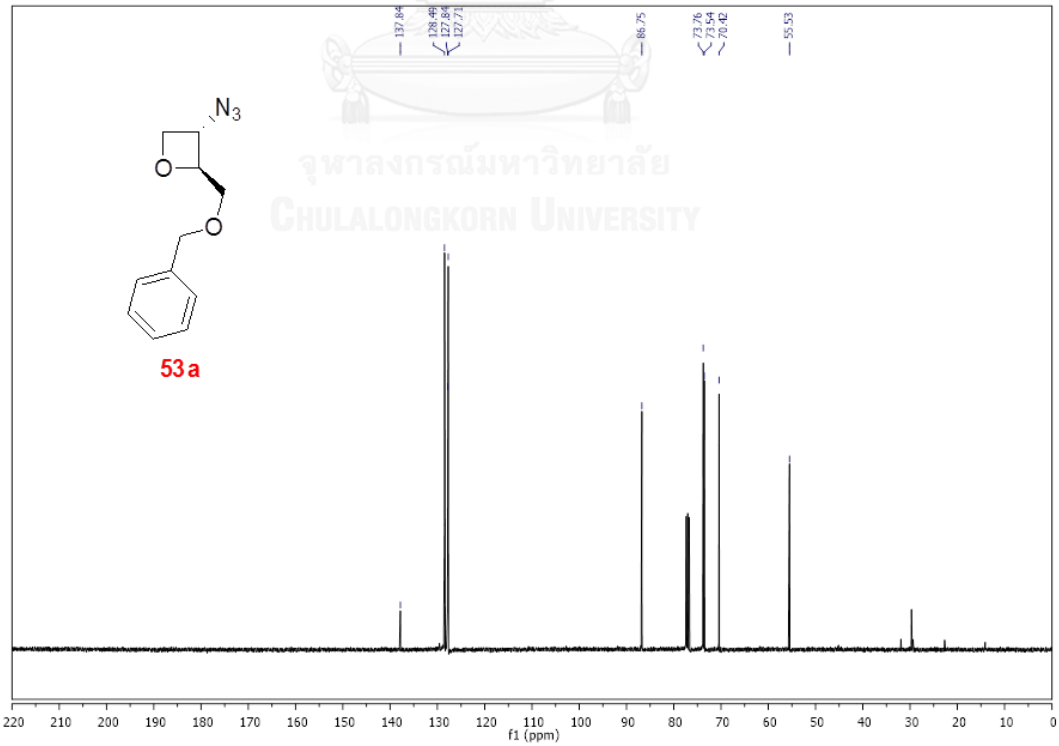

Figure A40 ^{13}C NMR spectrum (100 MHz, $CDCl_3$) of (2*S*,3*S*)-3-azido-2-(benzyloxymethyl)oxetane (**53a**)

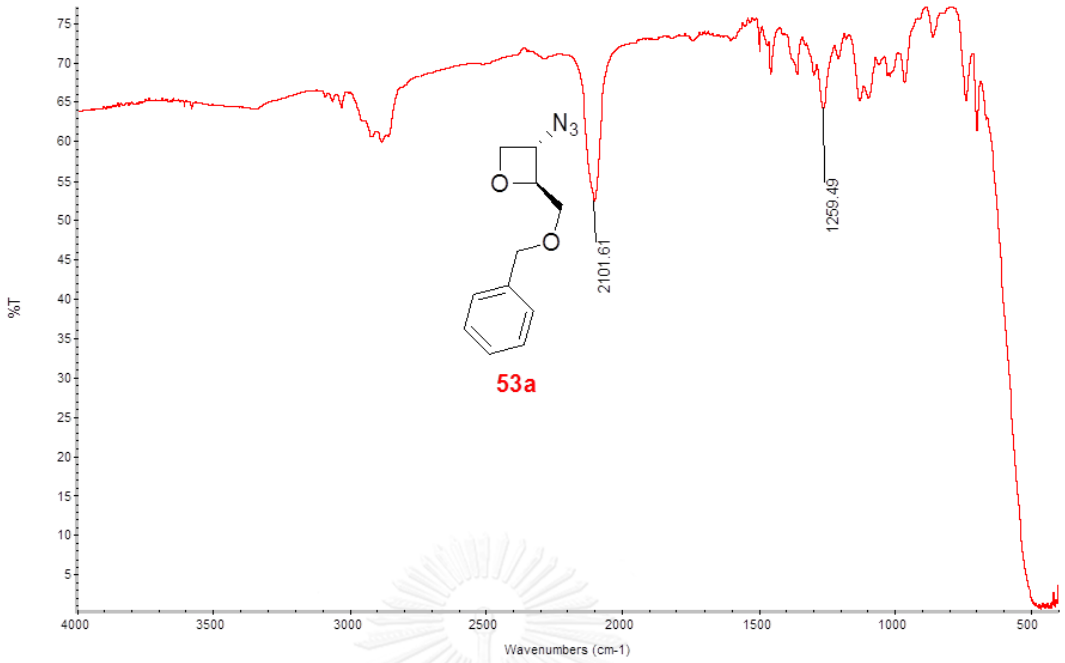

Figure A41 IR spectrum (thin film) of (2*S*,3*S*)-3-azido-2-(benzyloxymethyl)oxetane (**53a**)

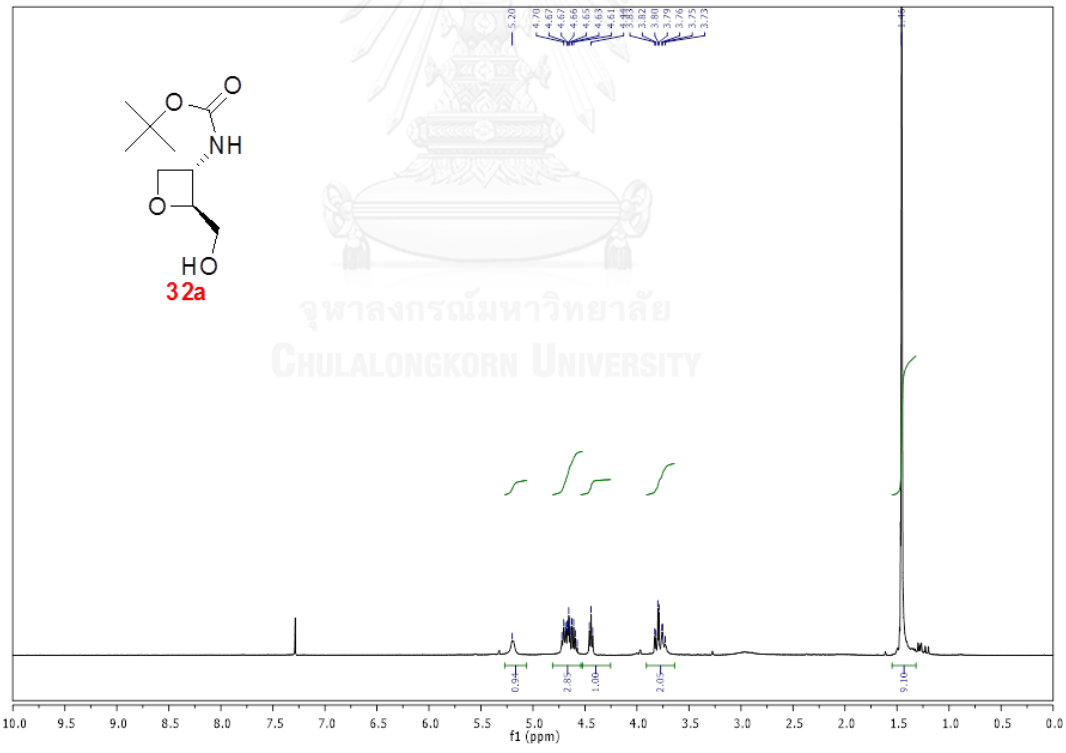

Figure A42 ^{1}H NMR spectrum (400 MHz, $CDCl_3$) of *tert*-butyl (2*S*,3*S*)-2-(hydroxymethyl)oxetan-3-ylcarbamate (**32a**)

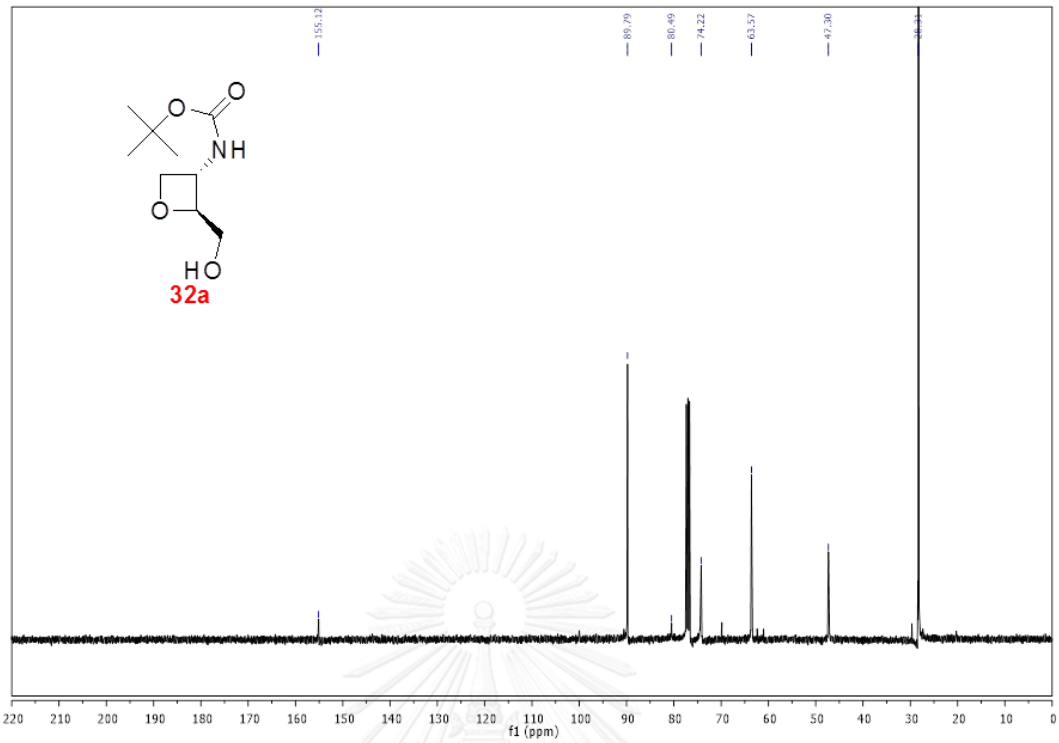

Figure A43 ^{13}C NMR spectrum (400 MHz, $CDCl_3$) of *tert*-butyl (2*S*,3*S*)-2-(hydroxymethyl)oxetan-3-ylcarbamate (**32a**)

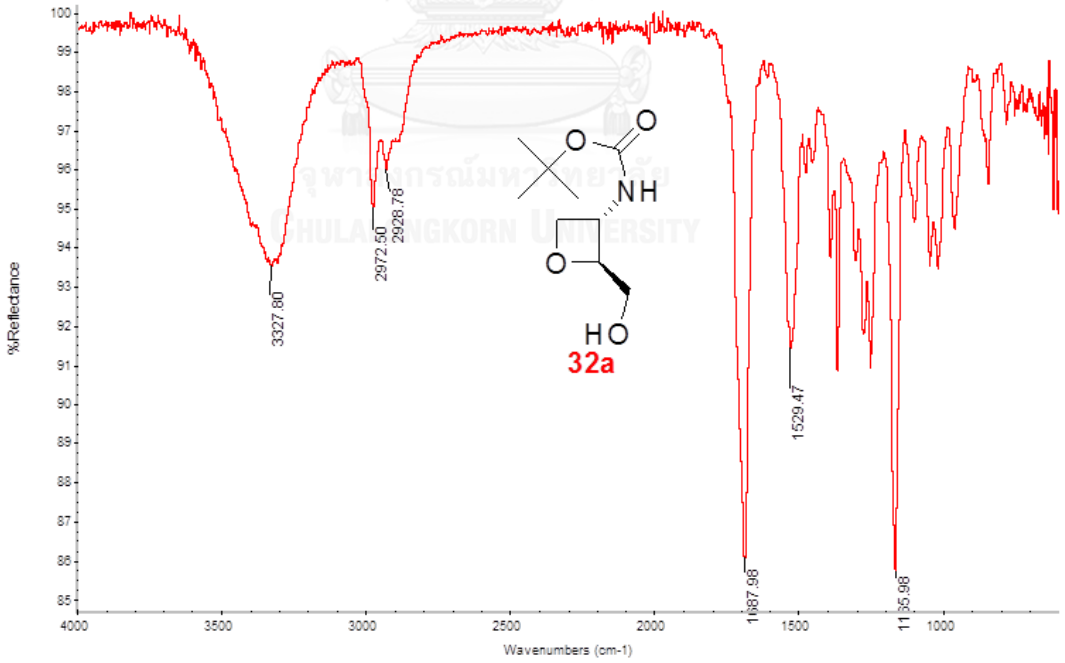

Figure A44 IR spectrum (ATR) of *tert*-butyl (2*S*,3*S*)-2-(hydroxymethyl)oxetan-3-ylcarbamate (**32a**)

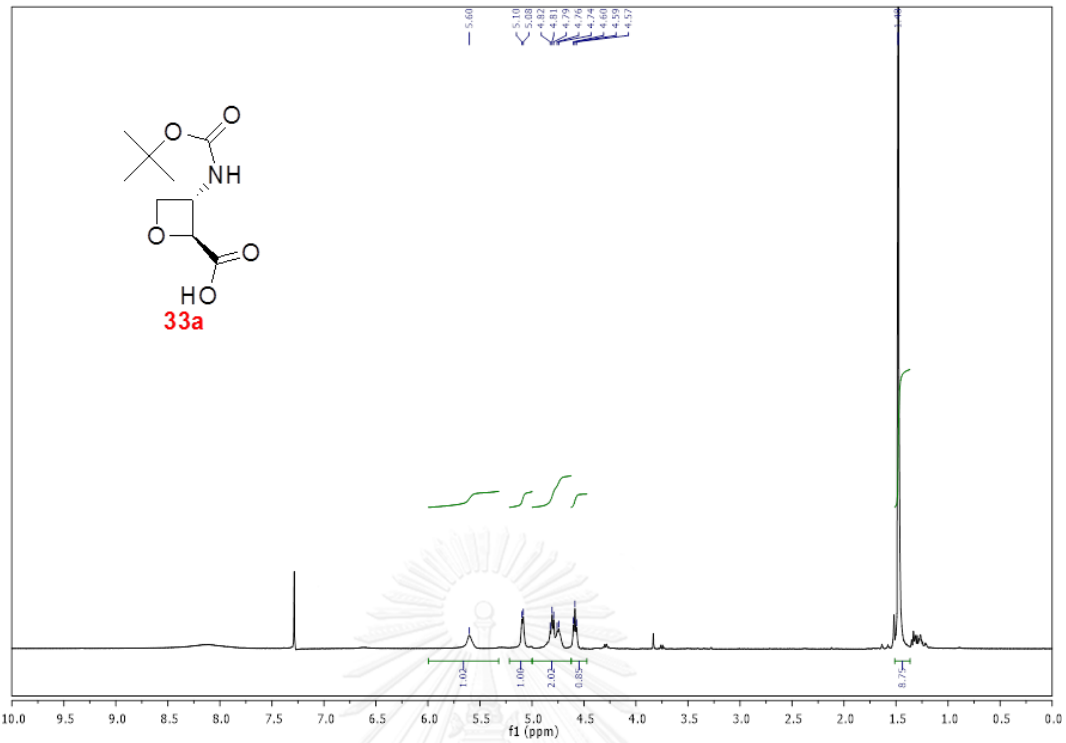

Figure A45 ^{1}H NMR spectrum (400 MHz, $CDCl_3$) of (2*S*,3*S*)-3-(*tert*-butoxycarbonylamino)oxetane-2-carboxylic acid (**33a**)

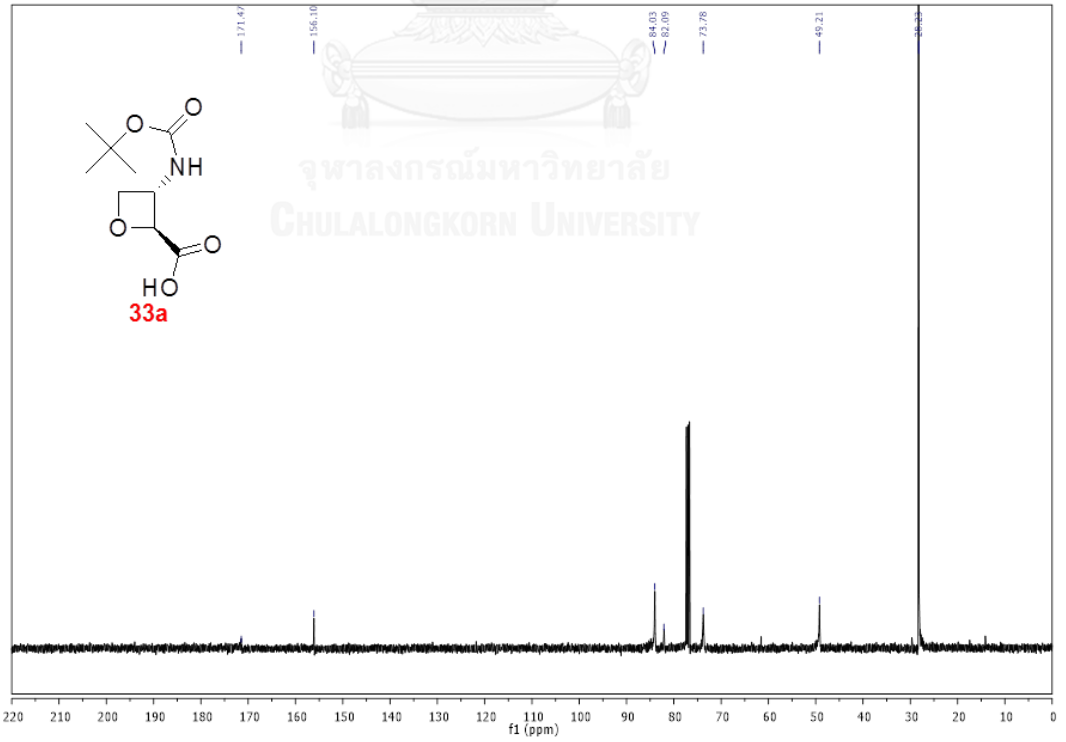

Figure A46 ^{13}C NMR spectrum (100 MHz, $CDCl_3$) of (2*S*,3*S*)-3-(*tert*-butoxycarbonylamino)oxetane-2-carboxylic acid (**33a**)

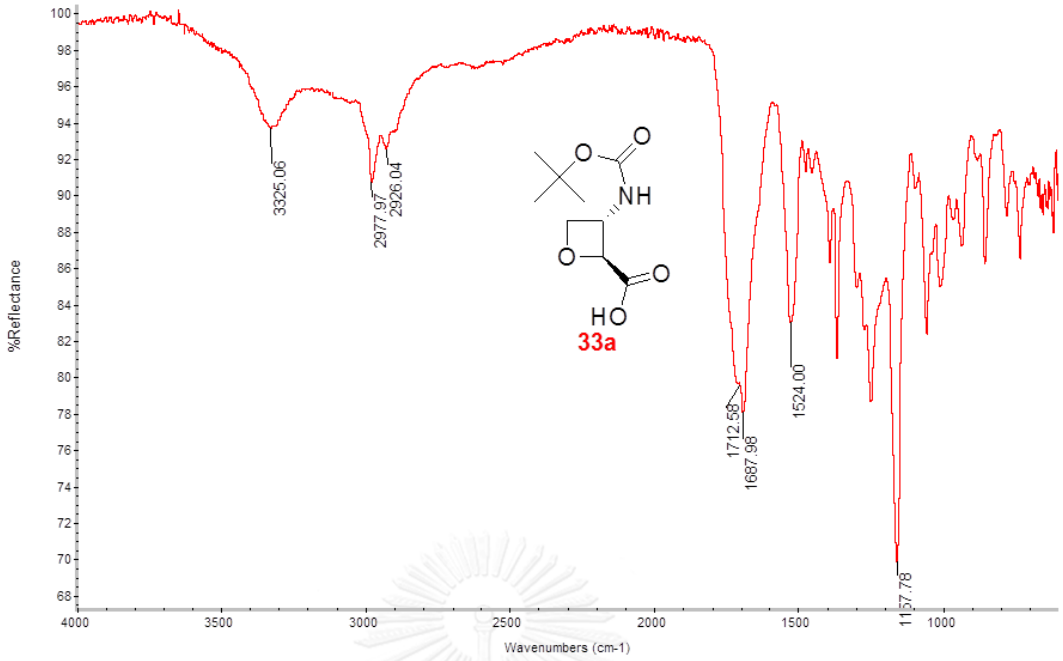

Figure A47 IR spectrum (ATR) of (2*S*,3*S*)-3-(*tert*-butoxycarbonylamino)oxetane-2-carboxylic acid (**33a**)

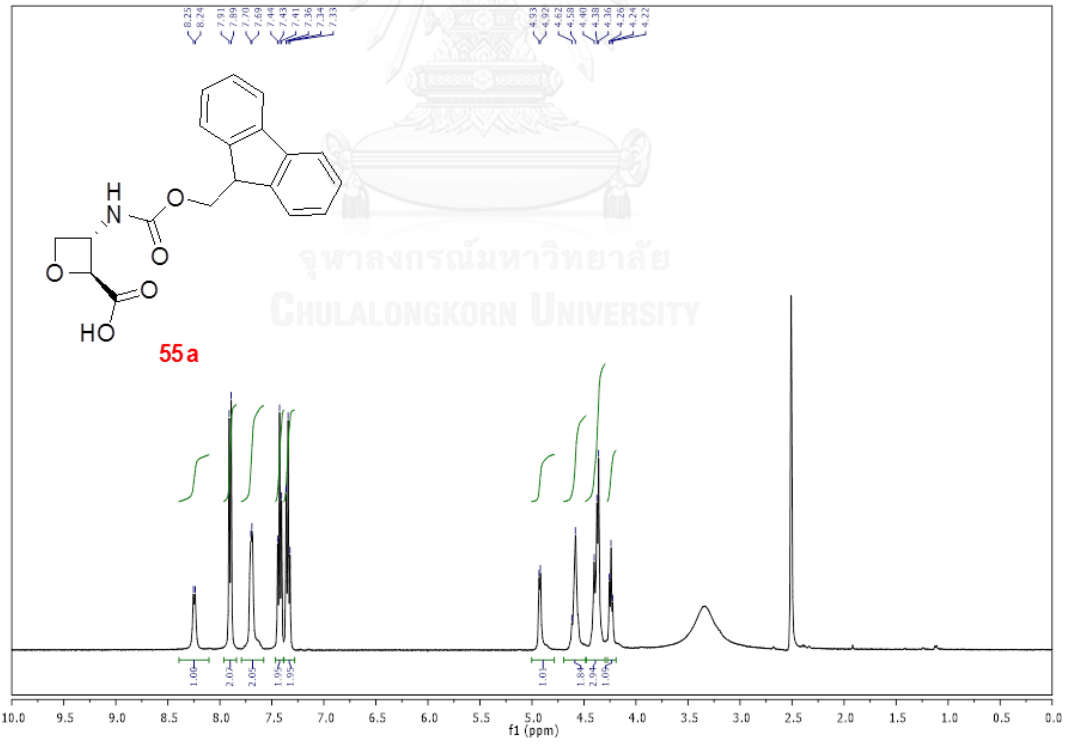

Figure A48 ^{1}H NMR spectrum (400 MHz, DMSO-d_6) of (2*S*,3*S*)-3-(((9*H*-fluoren-9-yl)methoxy)carbonylamino)oxetane-2-carboxylic acid (**55a**)

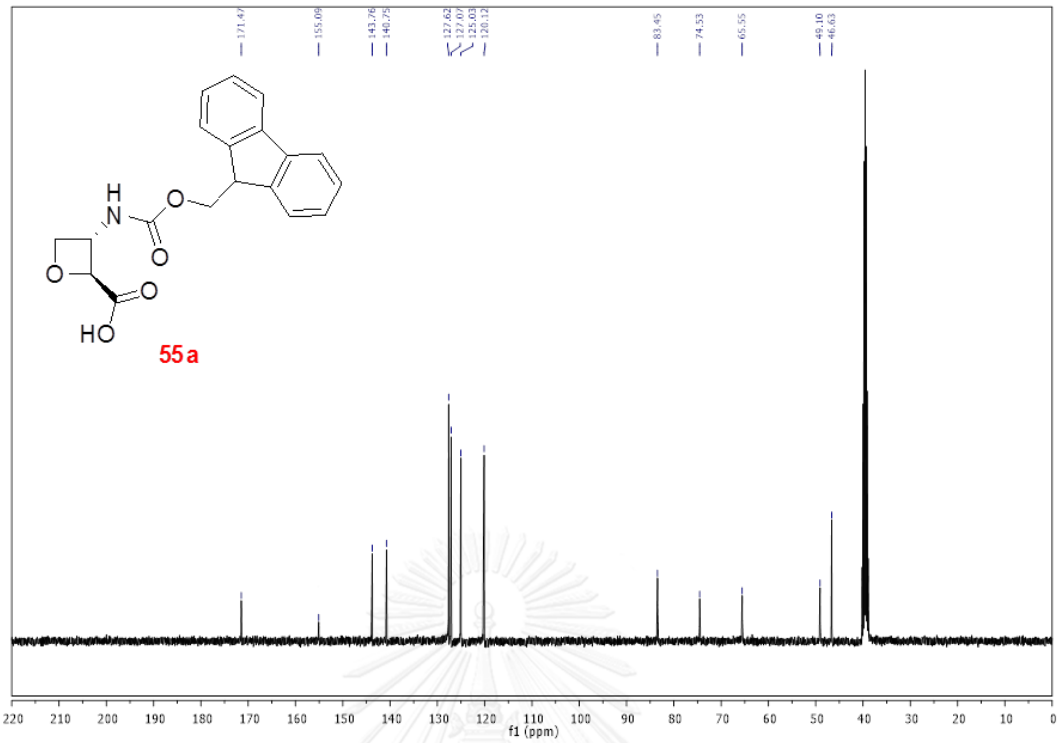

Figure A49 ^{13}C NMR spectrum (100 MHz, DMSO-d_6) of (2*S*,3*S*)-3-(((9*H*-fluoren-9-yl)methoxy)carbonylamino)oxetane-2-carboxylic acid (**55a**)

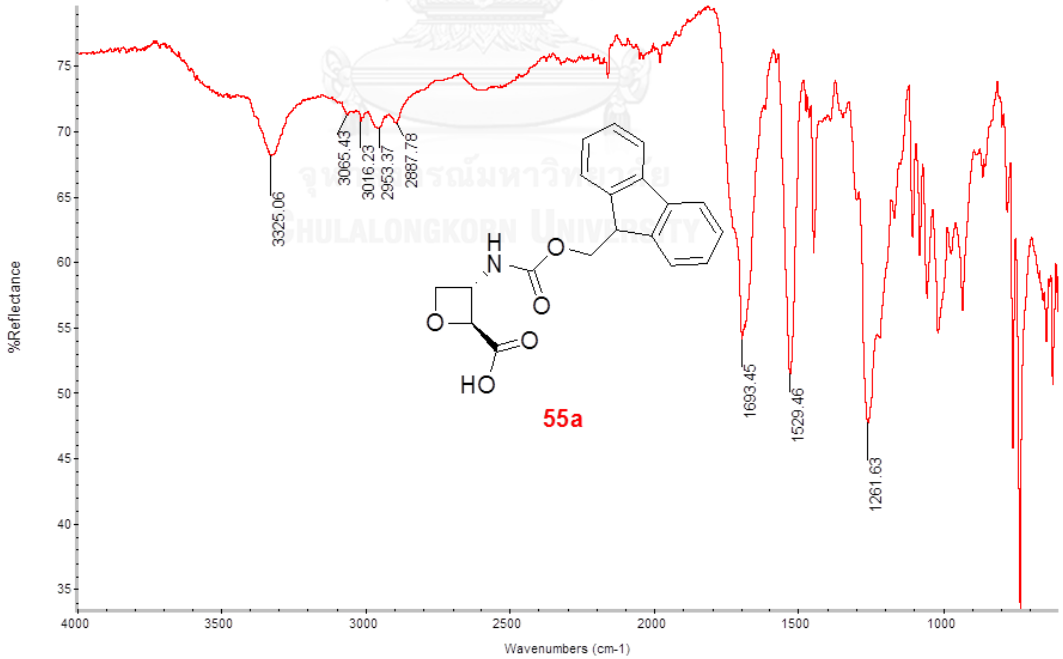

Figure A50 IR spectrum (ATR) of (2*S*,3*S*)-3-(((9*H*-fluoren-9-yl)methoxy)carbonylamino)oxetane-2-carboxylic acid (**55a**)

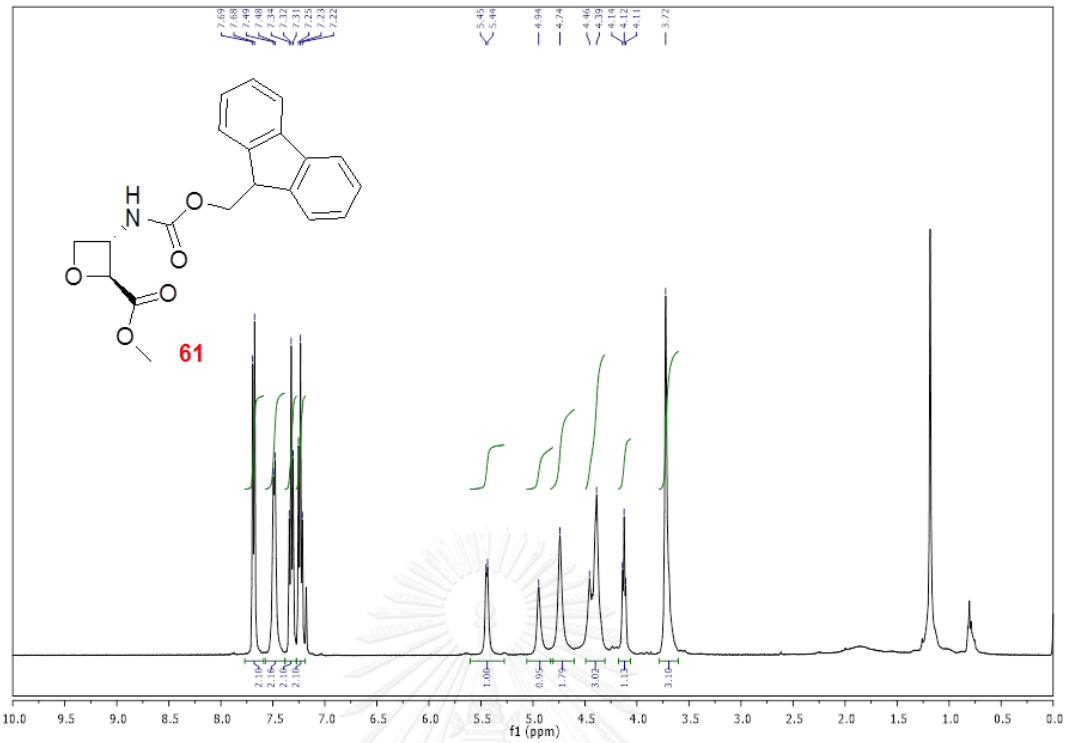

Figure A51 ^{1}H NMR spectrum (400 MHz, $CDCl_3$) of racemic-methyl 3-(((9*H*-fluoren-9-yl)methoxy)carbonylamino)oxetane-2-carboxylate (**61**)

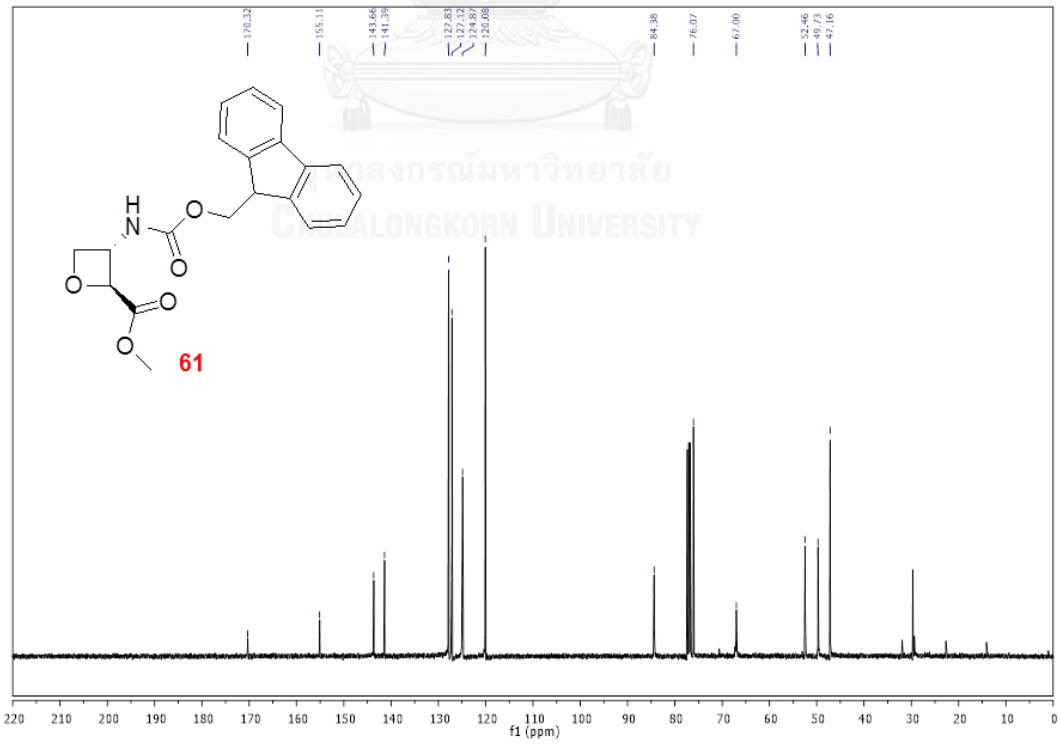

Figure A52 ^{13}C NMR spectrum (100 MHz, $CDCl_3$) of racemic-methyl 3-(((9*H*-fluoren-9-yl)methoxy)carbonylamino)oxetane-2-carboxylate (**61**)

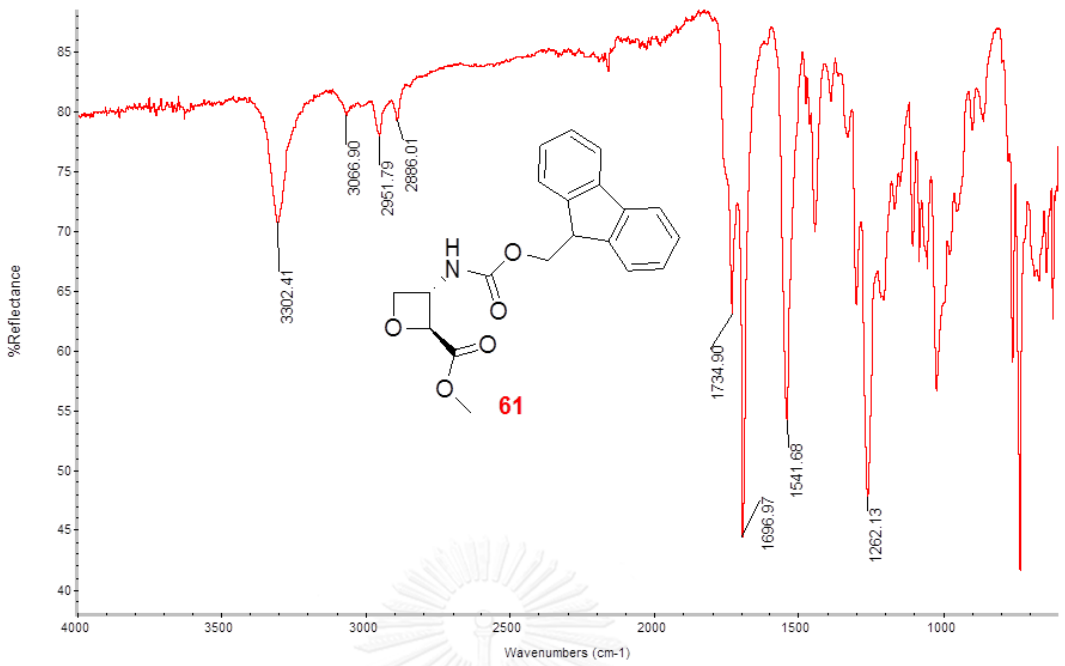

Figure A53 IR spectrum (ATR) of racemic-methyl 3-(((9*H*-fluoren-9-yl)methoxy)carbonylamino)oxetane-2-carboxylate (**61**)

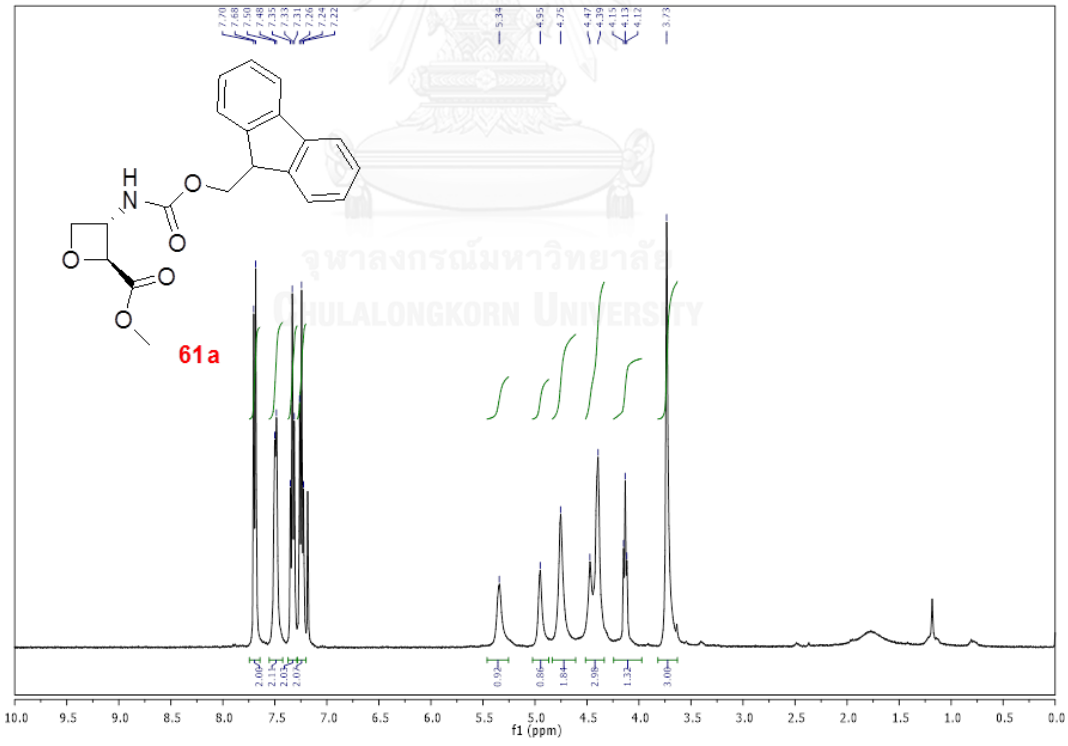

Figure A54 ^{1}H NMR spectrum (400 MHz, $CDCl_3$) of (2*S*,3*S*)-methyl 3-(((9*H*-fluoren-9-yl)methoxy)carbonylamino)oxetane-2-carboxylate (**61a**)

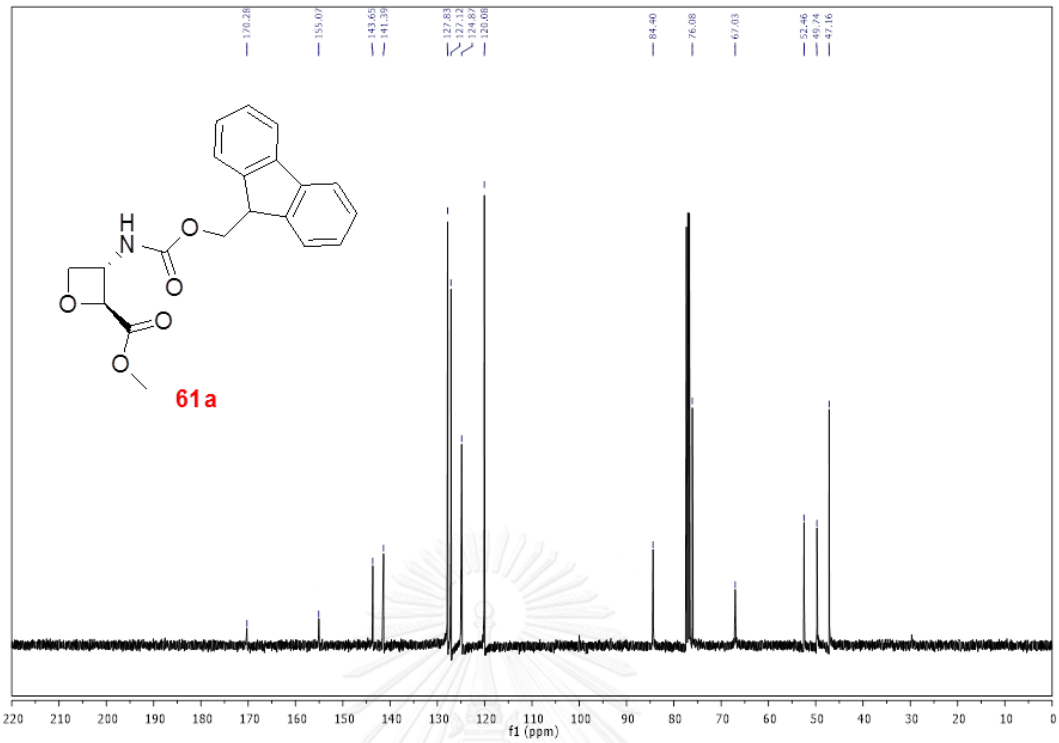

Figure A55 ^{13}C NMR spectrum (100 MHz, $CDCl_3$) of (2*S*,3*S*)-methyl 3-(((9*H*-fluoren-9-yl)methoxy)carbonylamino)oxetane-2-carboxylate (**61a**)

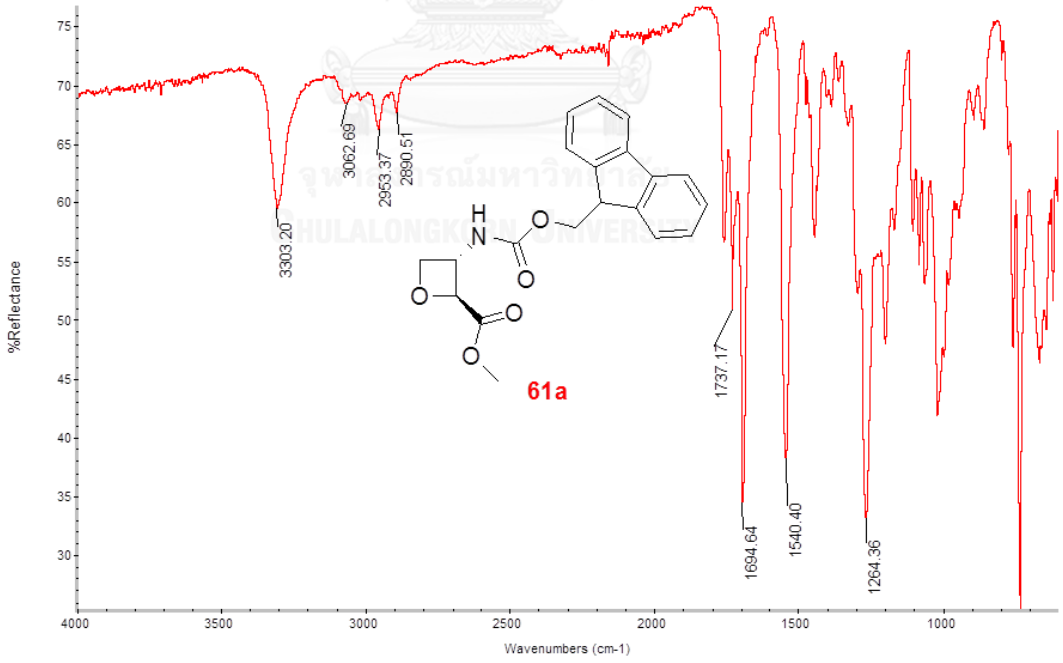

Figure A56 IR spectrum (ATR) of (2*S*,3*S*)-methyl 3-(((9*H*-fluoren-9-yl)methoxy)carbonylamino)oxetane-2-carboxylate (**61a**)

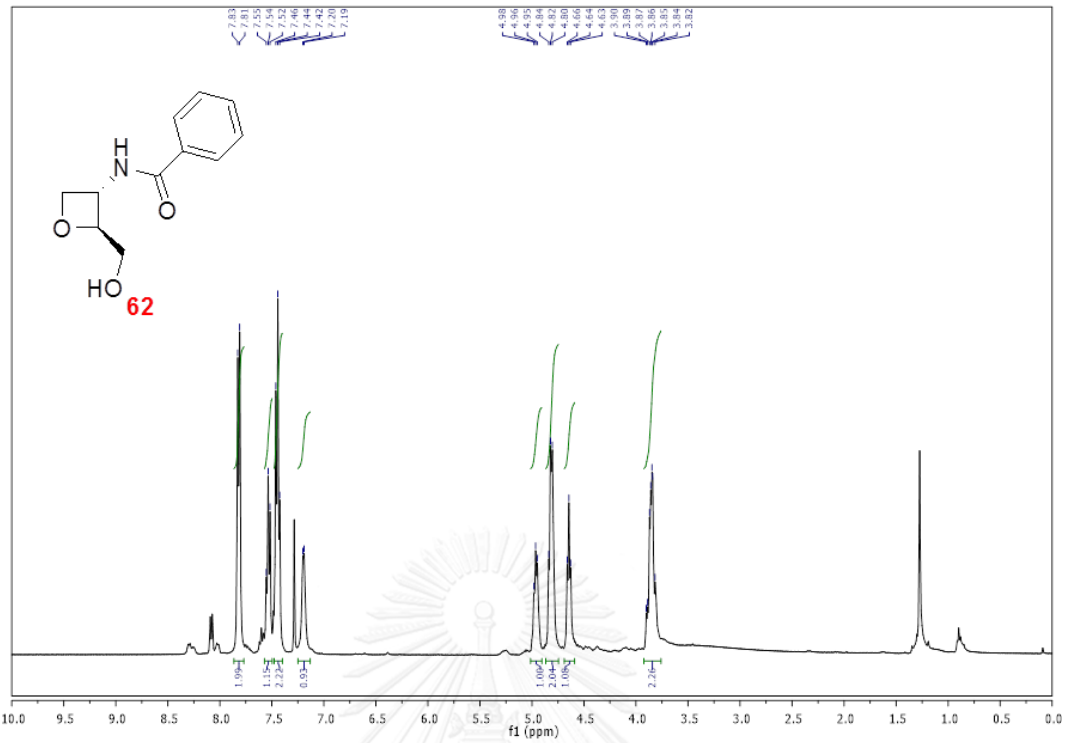

Figure A57 ^{1}H NMR spectrum (400 MHz, $CDCl_3$) of racemic-*N*-(2-(hydroxymethyl)oxetan-3-yl)benzamide (**62**)

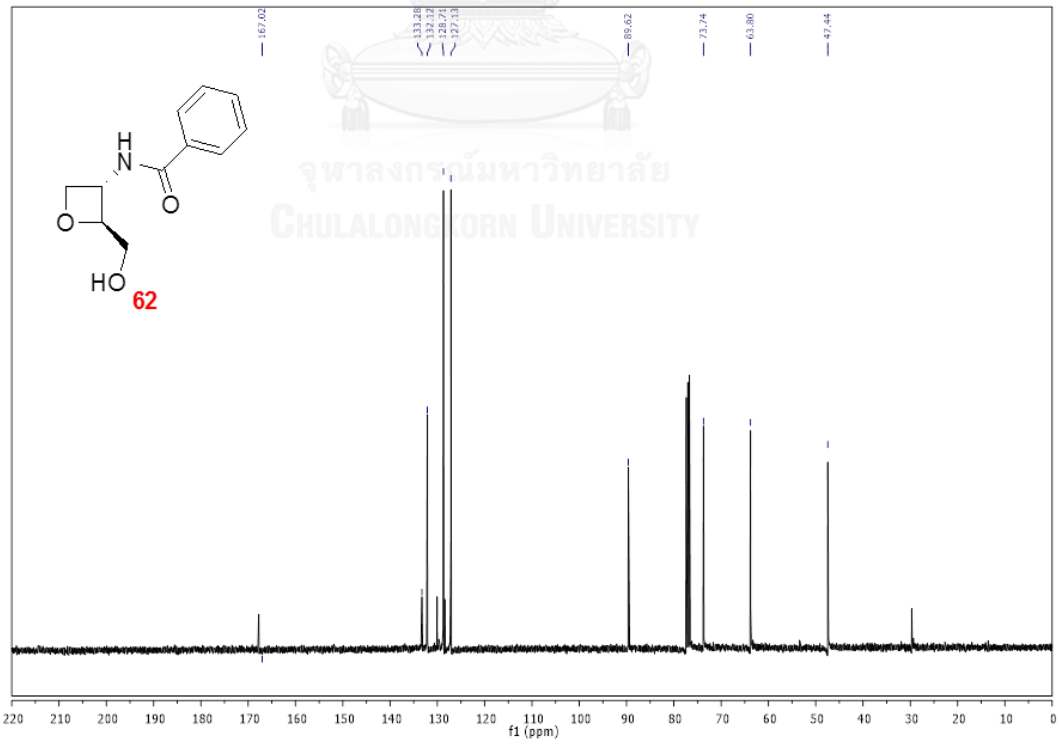

Figure A58 ^{13}C NMR spectrum (100 MHz, $CDCl_3$) of racemic-*N*-(2-(hydroxymethyl)oxetan-3-yl)benzamide (**62**)

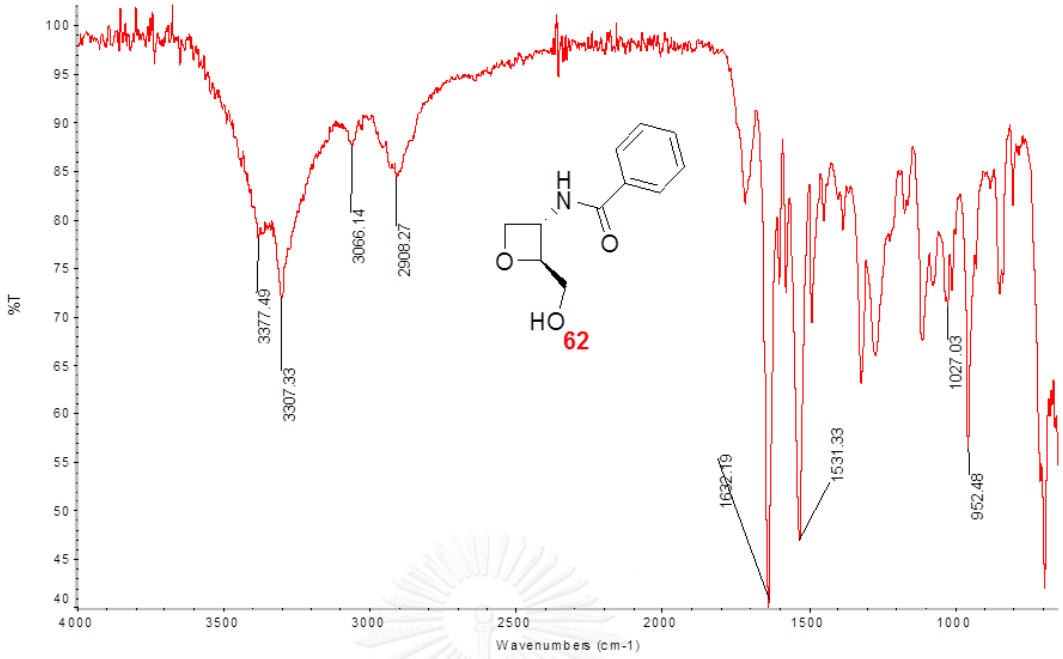

Figure A59 IR spectrum (ATR) of racemic-*N*-(2-(hydroxymethyl)oxetan-3-yl)benzamide (**62**)

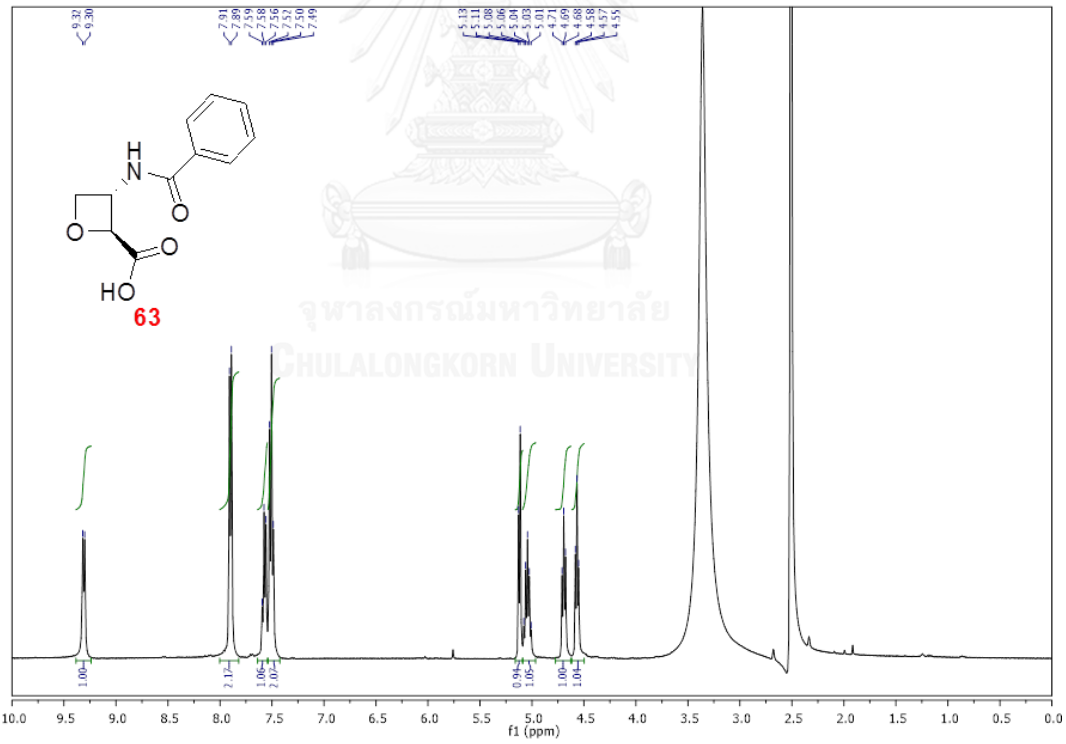

Figure A60 ^{1}H NMR spectrum (400 MHz, $CDCl_3$) of racemic-3-benzamidooxetane-2-carboxylic acid (**63**)

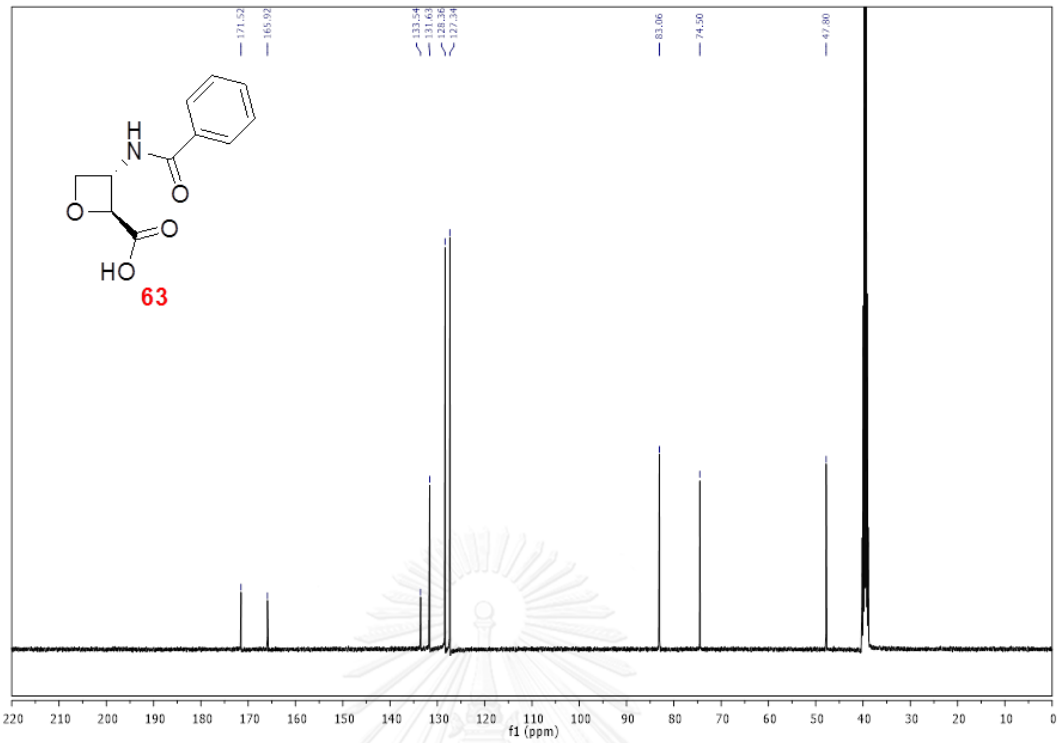

Figure A61 ^{13}C NMR spectrum (100 MHz, $CDCl_3$) of racemic-3-benzamidooxetane-2-carboxylic acid (**63**)

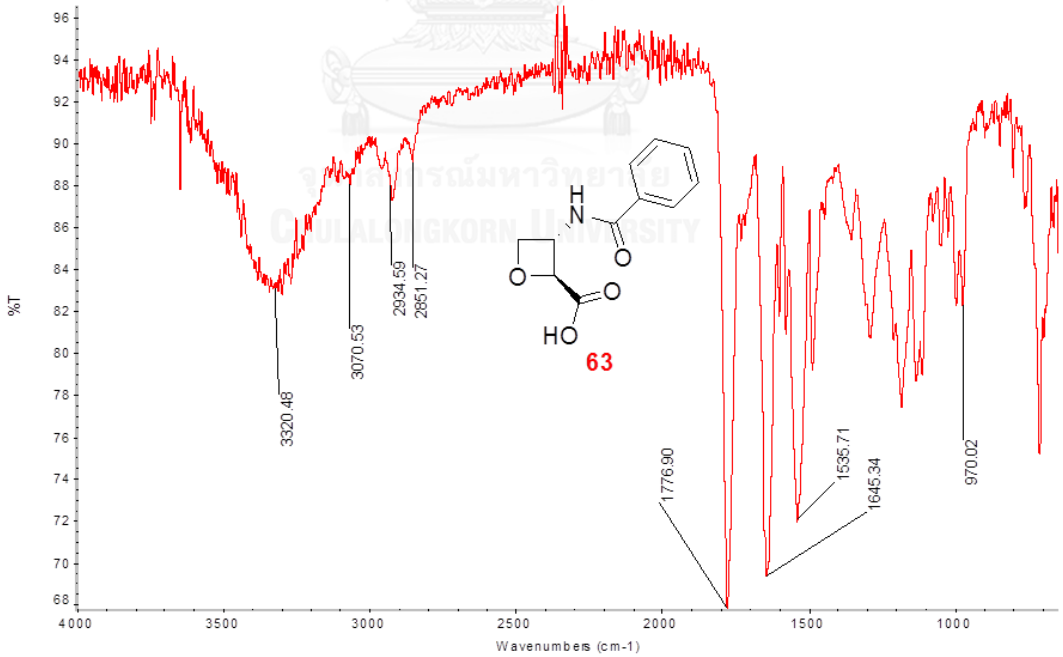

Figure A62 IR spectrum (ATR) of racemic-3-benzamidooxetane-2-carboxylic acid (**63**)

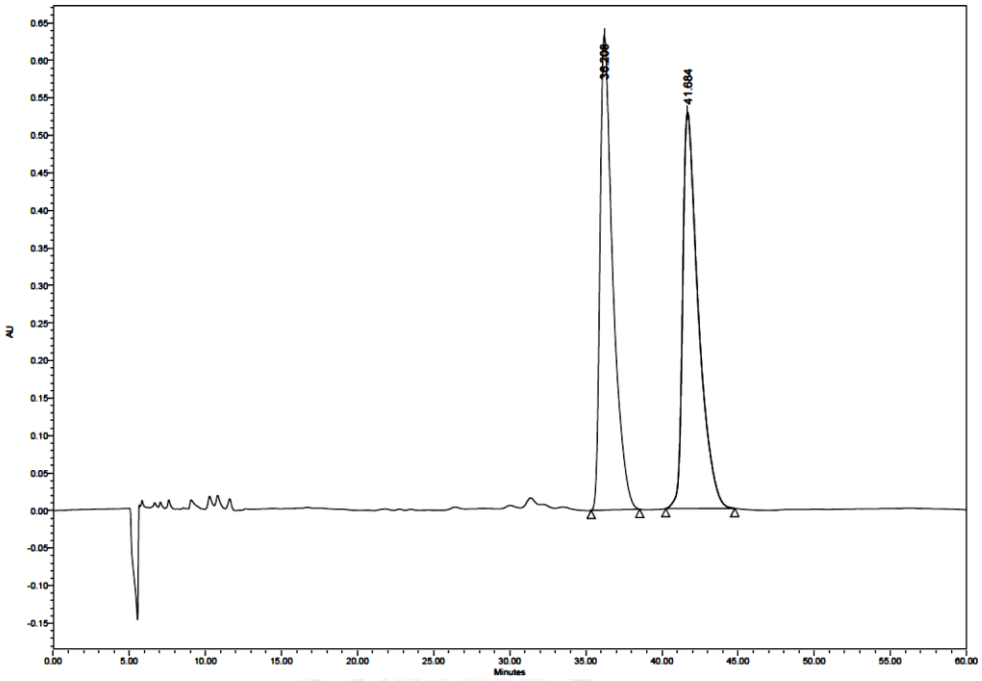

Figure A63 HPLC chromatogram of racemic-(3-(benzyloxymethyl)oxiran-2-yl)methanol (**50a** and **50b**) from mCPBA epoxidation

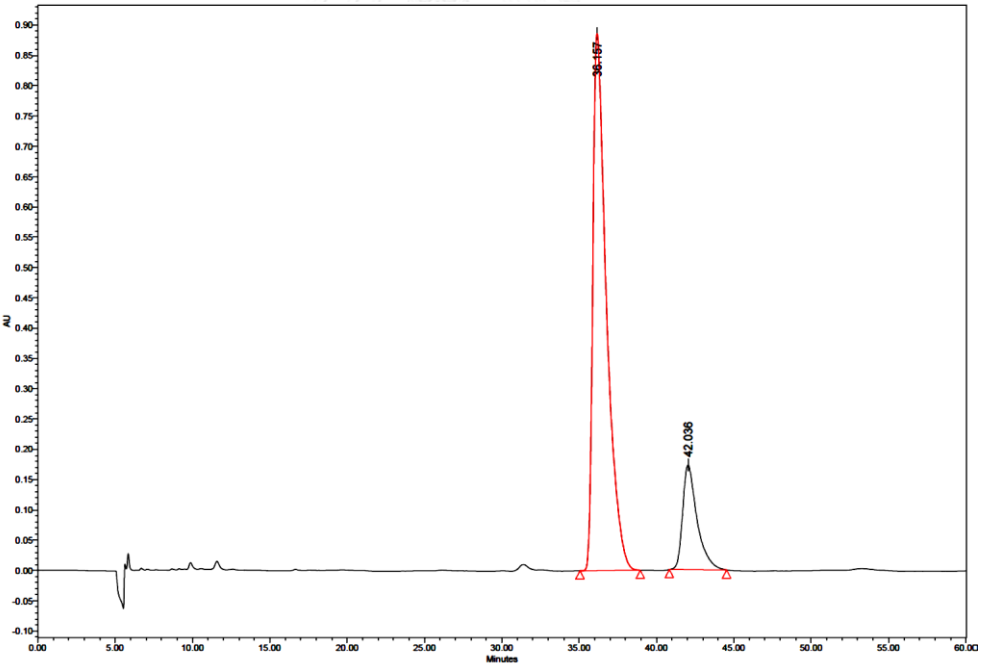

Figure A64 HPLC chromatogram of ((2*R*,3*R*)-3-(benzyloxymethyl)oxiran-2-yl)methanol (**50a**) from Sharpless epoxidation; condition: **42** (7.58 mmol), 2.5 equiv. TBHP, 0.38 equiv. D-(-)diisopropyl tartrate and 0.25 equiv. $Ti(O^{i}Pr)_4$

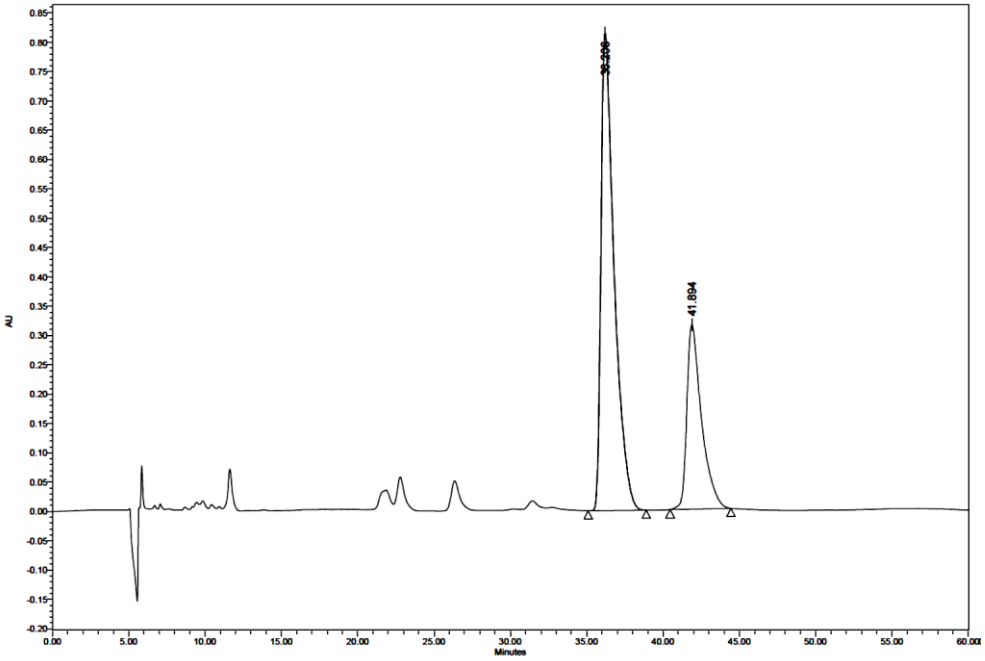

Figure A65 HPLC chromatogram of ((2*R*,3*R*)-3-(benzyloxymethyl)oxiran-2-yl)methanol (**50a**) from Sharpless epoxidation; condition: **42** (4.92 mmol) contraminated with **49** (**42**:**49** = 68:32), 3.8 equiv. TBHP, 2.3 equiv. D-(-)diisopropyl tartrate and 1.5 equiv. $Ti(O^{i}Pr)_4$

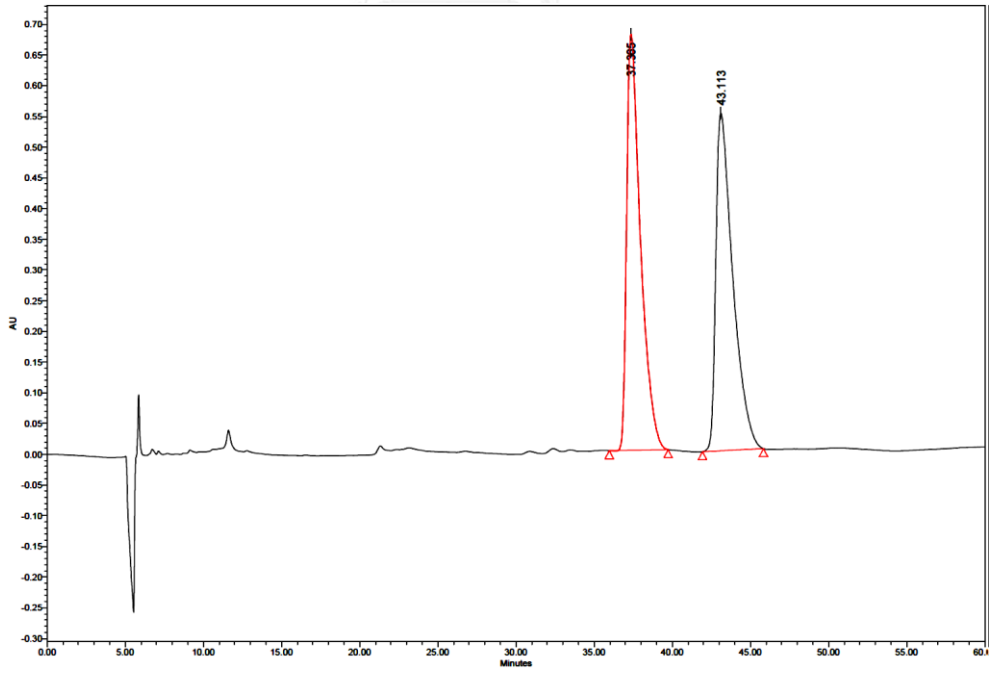

Figure A66 HPLC chromatogram of ((2*R*,3*R*)-3-(benzyloxymethyl)oxiran-2-yl)methanol (**50a**) from Shi epoxidation using H_2O_2 as oxidant

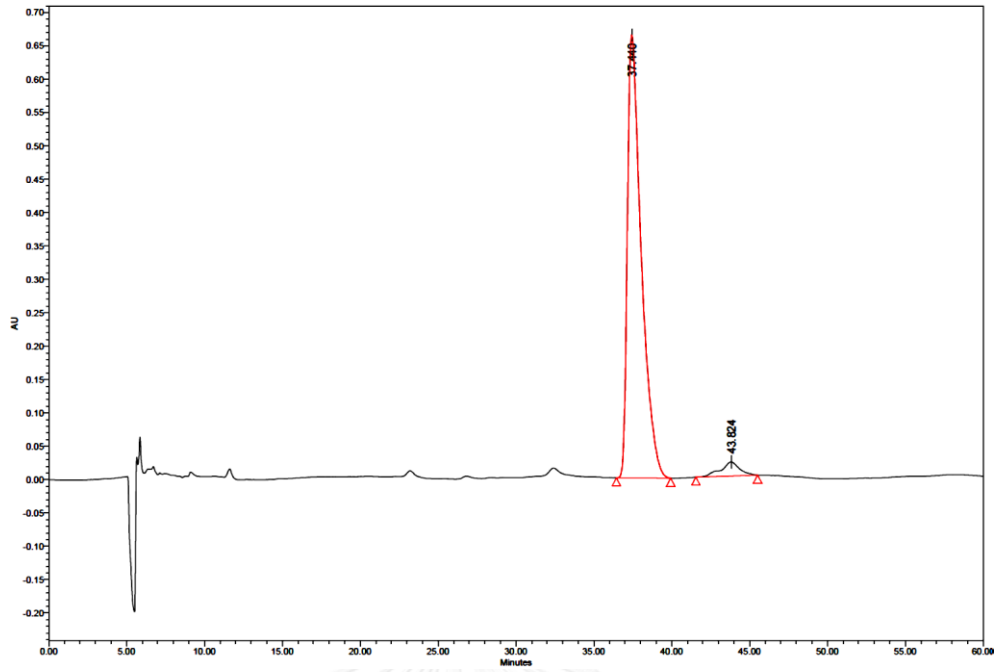

Figure A67 HPLC chromatogram of ((2*R*,3*R*)-3-(benzyloxymethyl)oxiran-2-yl)methanol (**50a**) from Jorgensen epoxidation; condition: **41** (1 mmol) and 13 equiv. H_2O_2 at ambient temperature

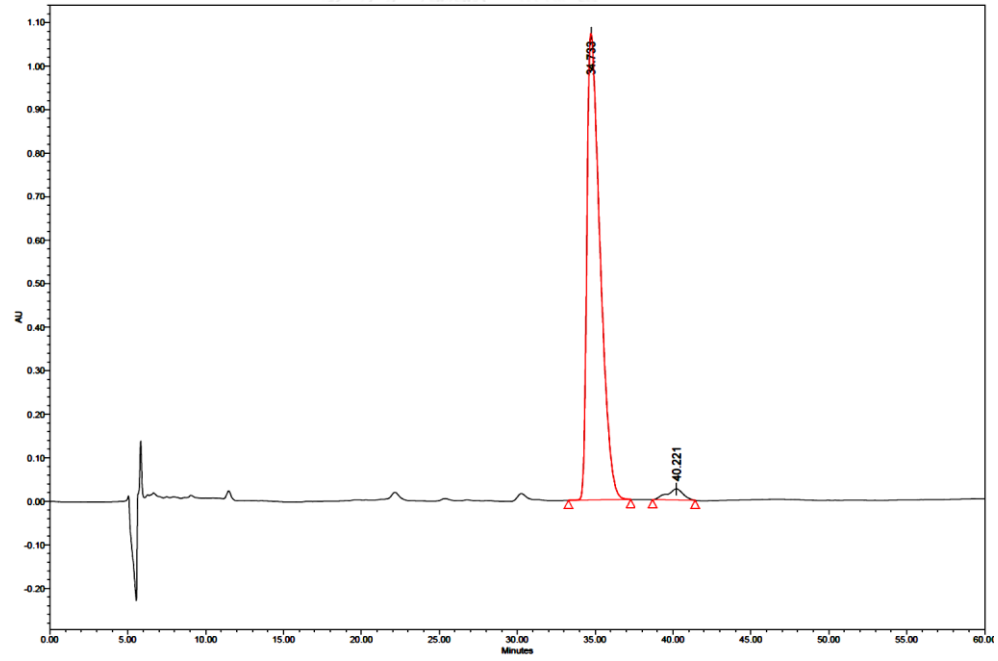

Figure A68 HPLC chromatogram of ((2*R*,3*R*)-3-(benzyloxymethyl)oxiran-2-yl)methanol (**50a**) from Jorgensen epoxidation; condition: **41** (1 mmol) and 13 equiv. H_2O_2 at 10-20 $^{\circ}$C

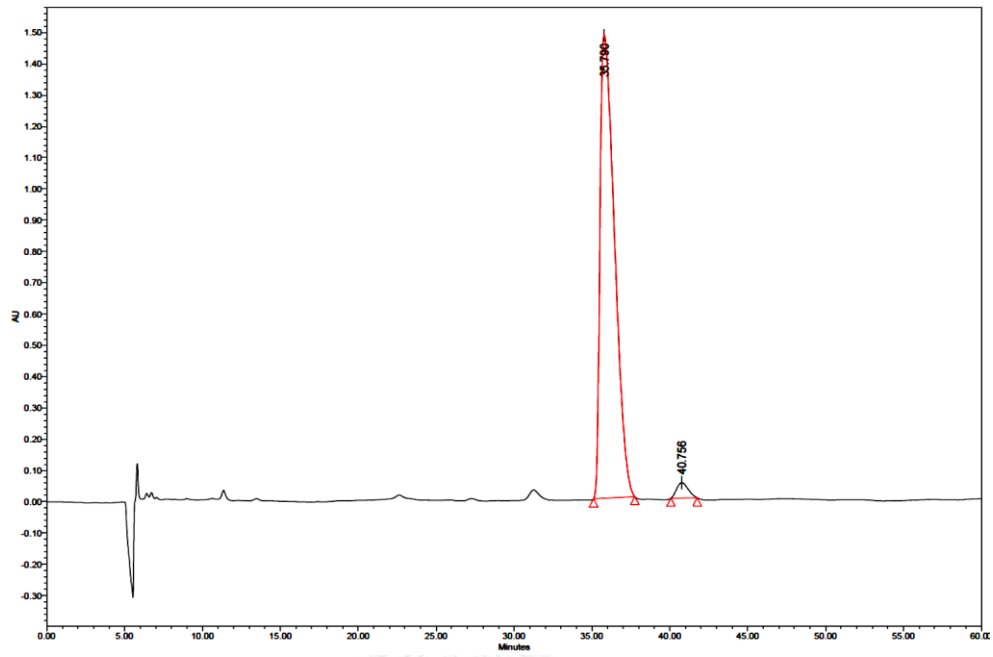

Figure A69 HPLC chromatogram of ((2*R*,3*R*)-3-(benzyloxymethyl)oxiran-2-yl)methanol (**50a**) from Jorgensen epoxidation; condition: **41** (5.86 mmol) and 13 equiv. H_2O_2 at 10-20 °C

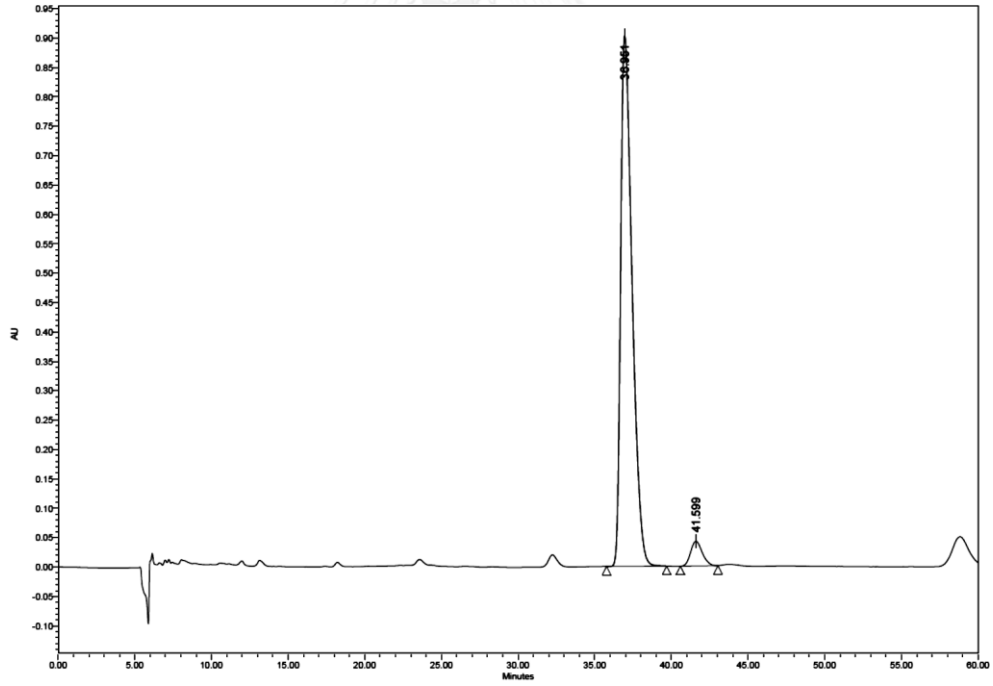

Figure A70 HPLC chromatogram of ((2*R*,3*R*)-3-(benzyloxymethyl)oxiran-2-yl)methanol (**50a**) from Jorgensen epoxidation; condition: **41** (4.0 mmol) and 1.3 equiv. H_2O_2 at 10-20 °C

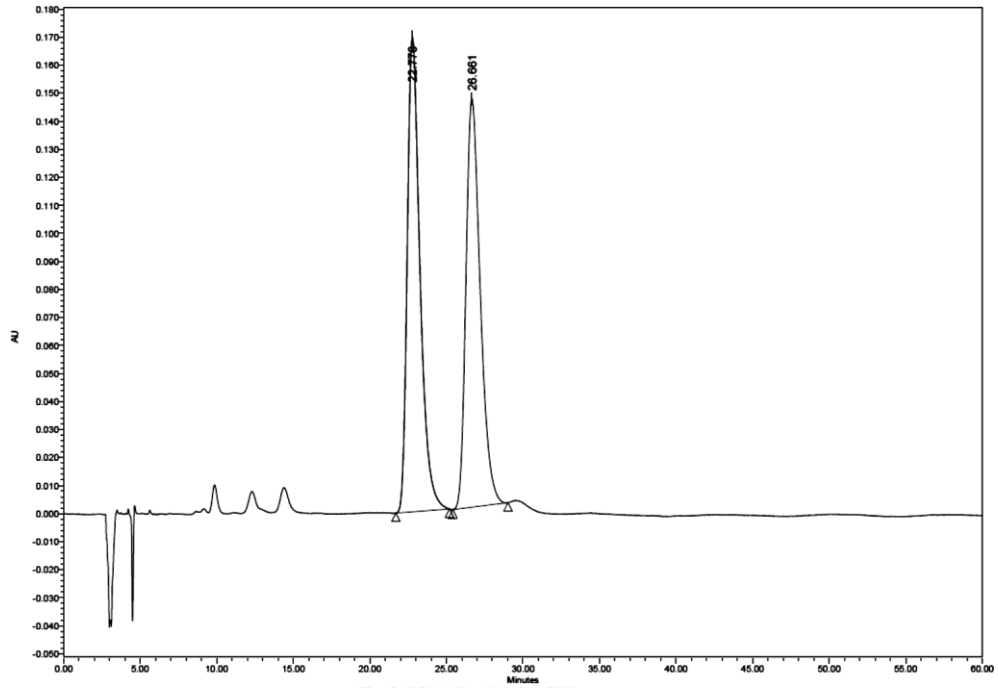

Figure A71 HPLC chromatogram of racemic-methyl 3-(((9*H*-fluoren-9-yl)methoxy)carbonylamino)oxetane-2-carboxylate (**61a** and **61b**)

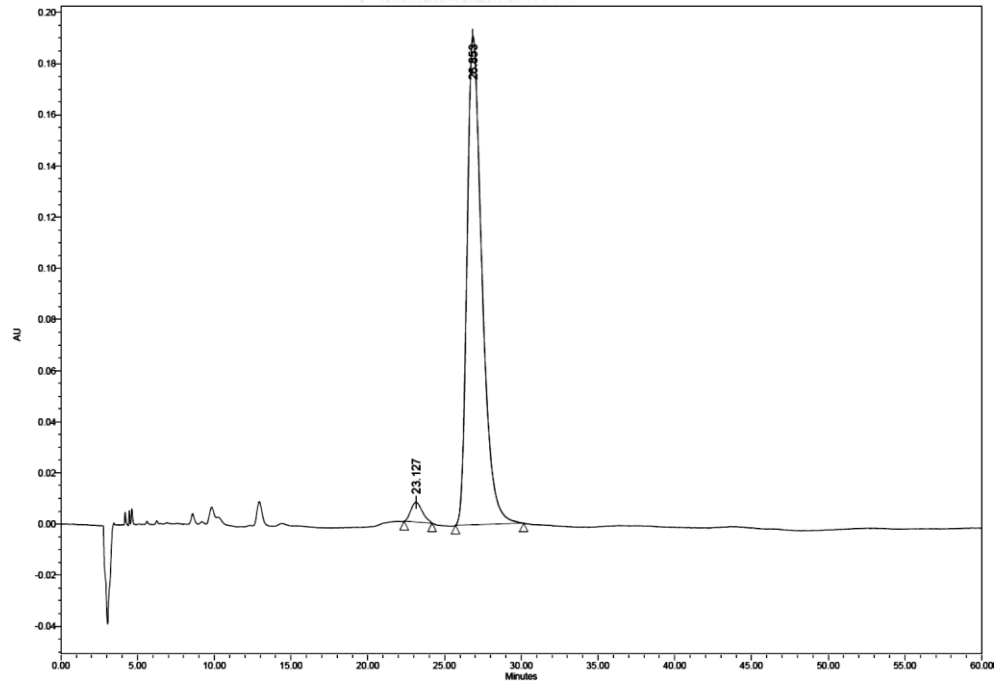

Figure A72 HPLC chromatogram of (2*S*,3*S*)-methyl 3-(((9*H*-fluoren-9-yl)methoxy)carbonylamino)oxetane-2-carboxylate (**61a**)

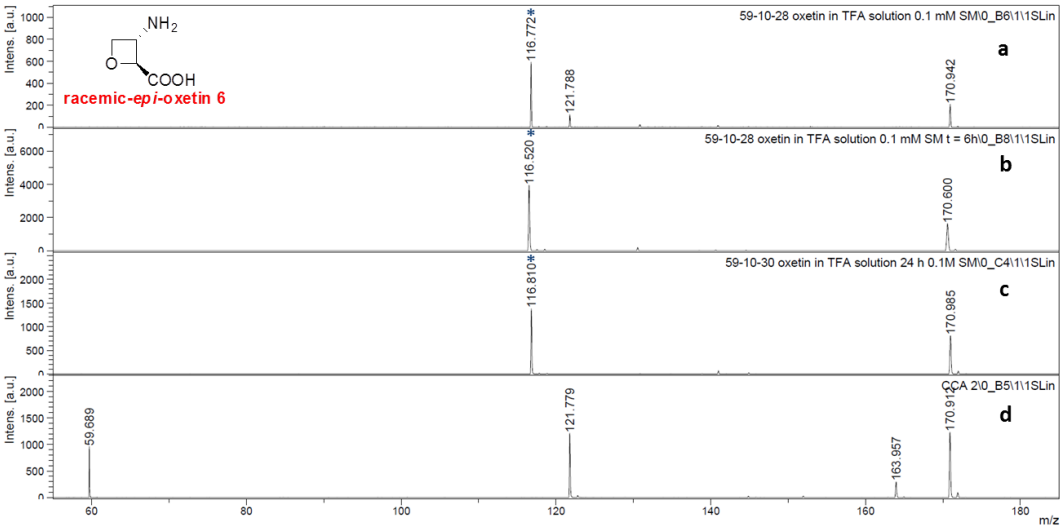

(a)

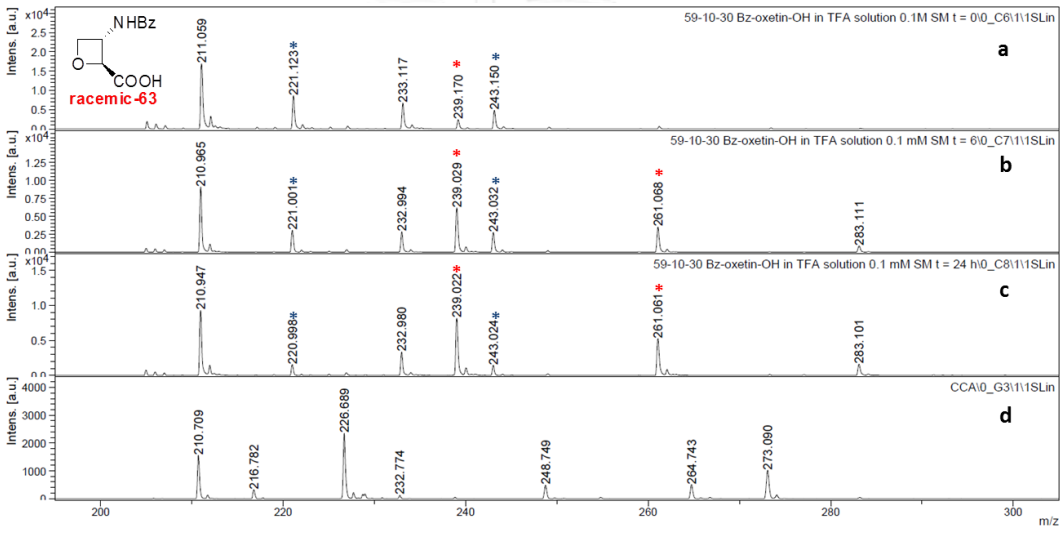

(b)

Figure A73 MALDI-TOF mass spectra of (a) racemic-*epi*-oxetin **6** and (b) racemic-*N*-benzoyl *epi*-oxetin **63** before and after treatment with 0.1 M TFA in H_2O at 0 (**a**), 6 (**b**) and 24 h (**c**). The spectra of CCA matrix are shown in panel (**d**). The relevant peaks are labeled by stars (blue = starting materials and Na^+ adducts, red = decomposition product and its Na^+ adduct).

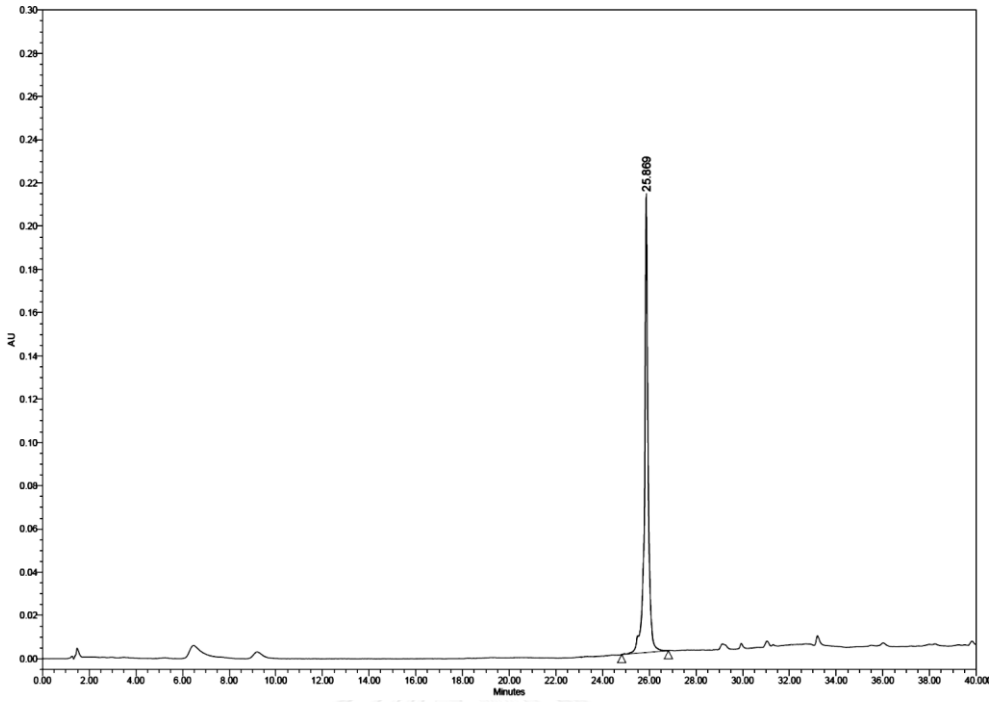

Figure A74 Analytical HPLC chromatogram of of H-aocPNA, H-GTAGATCACT-LysNH$_2$

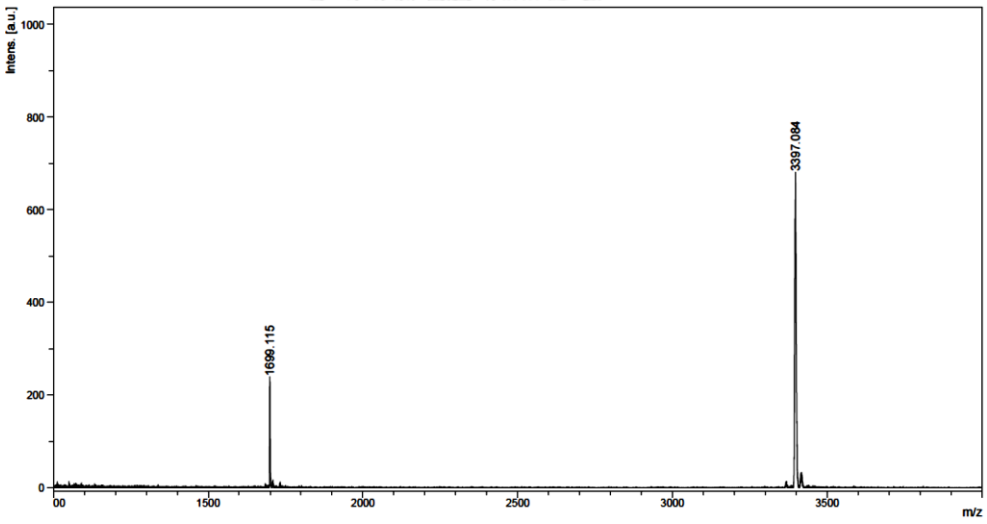

Figure A75 MALDI-TOF mass spectrum (CCA, linear positive ion mode) of H-aocPNA, H-GTAGATCACT-LysNH$_2$ (calcd for [M + H$^+$] m/z = 3397.2)

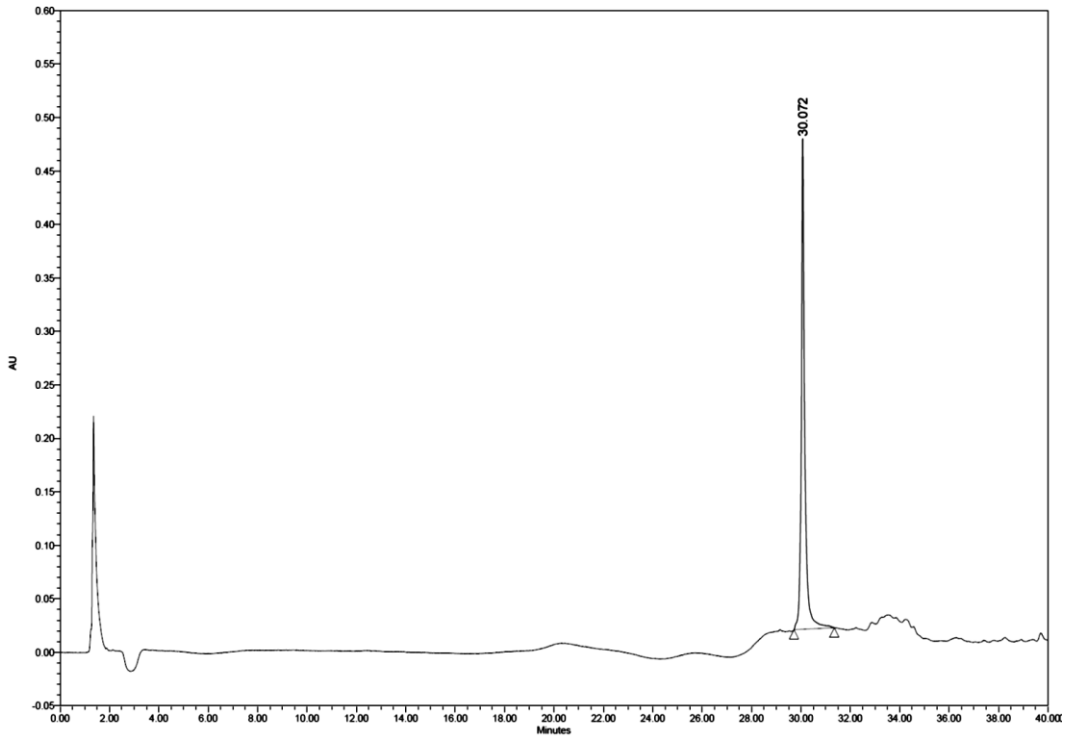

Figure A76 Analytical HPLC chromatogram of of Ac-aocPNA, Ac-GTAGATCACT-LysNH$_2$

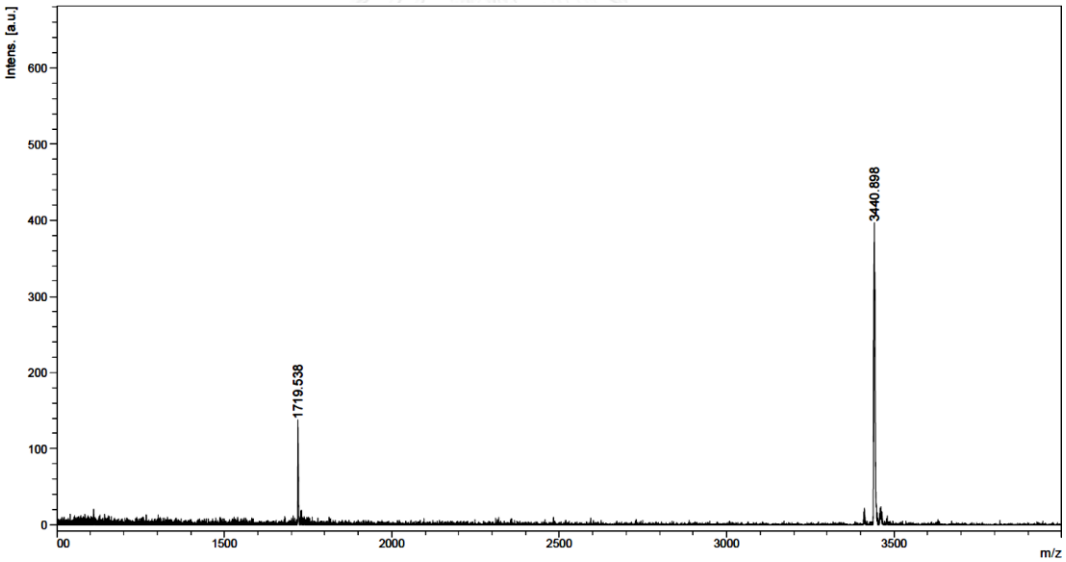

Figure A77 MALDI-TOF mass spectrum (CCA, linear positive ion mode) of Ac-aocPNA, Ac-GTAGATCACT-LysNH$_2$ (calcd for [M + H$^+$] m/z = 3439.3)

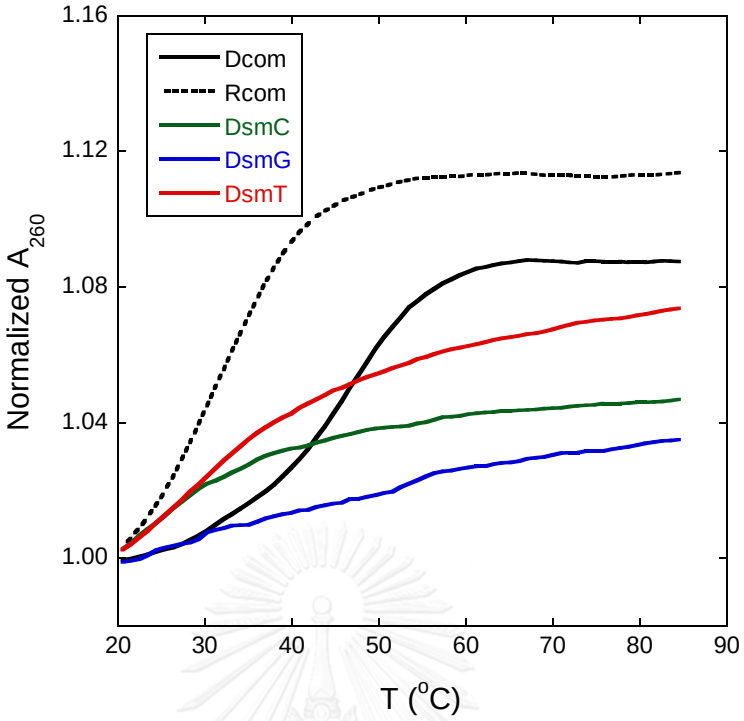

(a)

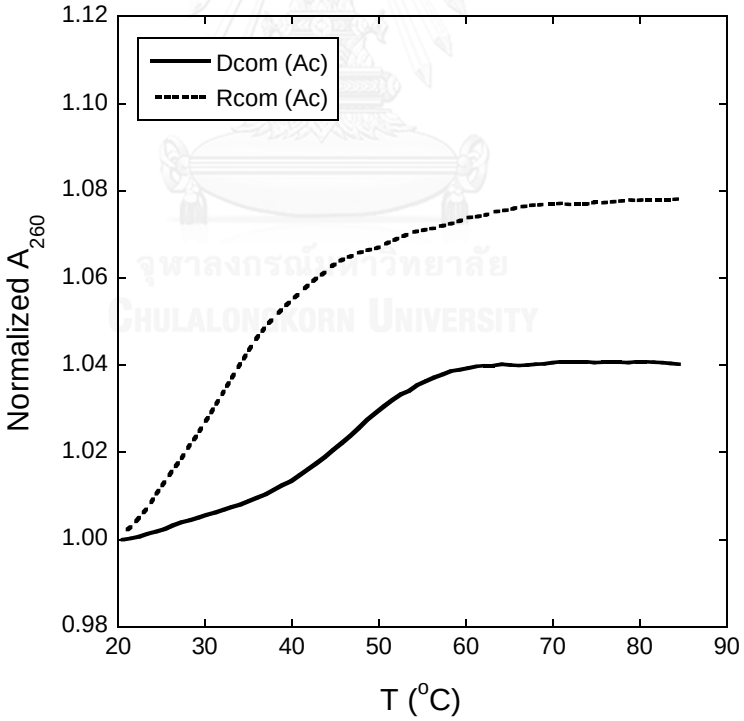

(b)

Figure A78 UV melting curves of aocPNA, (a) H-GTAGATCACT-LysNH_2 and (b) Ac-GTAGATCACT-LysNH_2 binding to various DNA and RNA. Conditions:1.0 μM PNA, 1.0 μM DNA/RNA, 10 mM sodium phosphate buffer pH 7.0, 100 mM NaCl. Heating rate 1 ^{o}C/min, 260 nm.

VITA

Pattarakiat Seankongsuk was born on August 14, 1991 in Bangkok, Thailand. He was selected to receive a Junior Science Talent Project (JSTP) grant from National Science and Technology Development Agency (NSTDA) since 2009. He graduated with Bachelor's Degree of Science (Honor program) with first class honors from Department of Chemistry, Faculty of Science, Chulalongkorn University in 2013. Since then he has been a graduate student (organic chemistry) studying towards Master's degree at Department of Chemistry, Chulalongkorn University.

Contact information: Pattarakiat.S@hotmail.com